

Development of CRISPR-Cas genome and epigenome engineering tools towards retinal degenerations

A thesis submitted for the degree of Doctor of Philosophy

Ariel Kantor

St. John's College

Nuffield Department of Clinical Neurosciences

University of Oxford

Supervisors:

Professor Robert E MacLaren

Dr Michelle E McClements

Michaelmas Term 2022







DECLARATION

The work presented in this thesis was undertaken in the laboratory of Professor Robert MacLaren at the University of Oxford, between 2019 and 2022. This thesis is entirely my own work except where otherwise stated. All figures are original; where adapted from another source, this has been clearly attributed. Experimental data from Dr Sònia Trigueros contributed to Chapter 3. Karyotyping analysis for the cell lines was completed by Dr Daniela Moralli from the Wellcome Centre for Human Genetics. DNA sequencing was commercially outsourced to Source Bioscience (UK) and Eurofins Genomics (Germany). Sources for all material from commercial manufacturers or provided as kind gifts from other researchers are acknowledged throughout and fully summarized in the Appendix.

At the time of submission, data from Chapter 3 had been published in *Pharmaceutics* (2022) and several major reviews and book chapters were published in *Human Gene Therapy* (2021), *Expert Opinion on Orphan Drugs* (2021), *Progress in Nucleic Acid Research and Molecular Biology* (2021), and *International Journal of Molecular Sciences* (2020). No other data has been submitted elsewhere.

The word count for this thesis is approximately 49,996 words (excluding table of contents, lists of figures, tables, and abbreviations, figure and table legends, references, and appendix). No materials presented in this thesis have been previously submitted to the University of Oxford, or to any other academic institution, for another degree or qualification.



--- Ariel Kantor, 2023

ACKNOWLEDGEMENTS

I would like to express my sincere gratitude to my supervisor Prof Robert MacLaren for his mentorship and encouragement, from weekly lab meetings to our data review sessions at the Nuffield Gym. The depth of his scientific and clinical acumen and passion for patient care have been deeply inspiring, and I consider myself extremely fortunate to have trained under his direction. I am also immensely grateful to my second supervisor, Dr Michelle McClements, for being a beacon of positivity and guiding my journey in the lab from the very beginning.

I am deeply grateful to The Rhodes Trust for funding this research and for welcoming me into a community of exceptionally talented and caring scholars. I would also like to thank the Nuffield Department of Clinical Neuroscience and St. John's College for providing financial support for travel to conferences to present my work.

I want to extend my gratitude to the MacLaren lab for their day-to-day support and guidance. From the lunchtime discussions (or 'Zoom coffees' for the first half of the DPhil) to the epic lab dinners, the lab has been a fantastic environment to foster science and friendships. A huge thank you to the full lab family for their time and effort, without whom this thesis would never have made it to the Bodleian. Thank you to Dr Kanmin Xue, Dr Jasmina Kapetanovic, Prof Susan Downes, Federica Staurenghi, Elena Piotter, Dr Jasleen Jolly, Dr Tom Buckley, Dr Connie Han, Dr Sophia Bellingrath, Dr Amandeep Josan, Laura Taylor, Joel Quinn, Dr Maria Kaukonen, Lauren Major, Ellen Rhodes, Dr Imran Yusuf, Molly John, Monica Hu, as well as Dr Solomon Merepa and Dr Ricardo Parolin Schnekenberg. A special thanks goes to Dr Ahmed Salman for the unbounded generosity with his time and knowledge. Thank you also to Dr Marco Bellini, for ensuring that my research (mostly) kept to budget and ran smoothly.

I would like to acknowledge the hard work of the animal technicians at the John Radcliffe BMS.

I am grateful for collaborators all around the world, who have contributed valuable ideas and reagents. Particularly, I would like to acknowledge Dr Sònia Trigueros and Dr Gemma Marfany from the University of Barcelona for their expertise and contributions to the gold nanoparticle pilot experiment. Thank you to Dr Daniela Moralli from the Wellcome Centre for Human Genetics for her contributions in karyotyping the cell lines.

Finally, I would like to thank my family and friends for their unconditional love and support. To Anna: I will always be grateful for your limitless love, patience, and understanding; from putting up with my midnight Zoom meetings to the weekend trips to the John Radcliffe. To mom: thank you for your unconditional support, for always encouraging me to aim high, and for your steadfast and everlasting confidence in my potential. From Ma'ale Adumim to Oxford University, this thesis is the culmination of your endless sacrifices. I hope that I have made you proud.

ABSTRACT

Inherited retinal diseases (IRDs) are a diverse family of disorders caused by genetic mutations that lead to dysfunction and death of cells in the outer retina. Together, they are the most common cause of untreatable blindness in the working age population. While gene supplementation therapies using adeno-associated viral (AAV) vectors have shown restoration of visual function in IRDs, they are limited to the treatment of recessively inherited diseases caused by small genes. The engineering of the clustered regularly interspaced short palindromic repeats (CRISPR)-CRISPR-associated (Cas) nuclease system has revolutionized the field of molecular biology and generated excitement for the potential of novel therapeutic approaches to treat retinal diseases. Here, I explore the development of CRISPR-Cas9 tools and their therapeutic adaptation towards the treatment of retinal disease.

This thesis firstly investigated the development and optimization of a CRISPR vector system towards *in vivo* application. I assessed different Cas9 orthologues and regulatory elements that permit minimalization of the construct size for efficient delivery. I demonstrated *in vitro* that a construct backbone comprised of the *Staphylococcus aureus* derived SaCas9 driven by elongation factor 1α short promoter mediated robust levels of gene knockdown. Subsequently, I investigated the use of DNA-wrapped gold nanoparticles as an alternative modality for non-viral gene delivery. I demonstrated the ability of gold nanoparticles to efficiently deliver genes *in vitro* and assessed aspects of their safety including effects on retinal structure and function, although I was not able to detect gene expression *in vivo.*

This thesis secondly investigated the development of a dCas9-epigenetic editing system for transcriptional repression. I characterized novel transcriptional repressor domains and demonstrated that a novel bipartite repressor comprised of SaCas9 fused to

the Krüppel-associated box (KRAB) repressor and the transcriptional repressor domain of Methyl-CpG Binding Protein 2 (MeCP2) facilitated high levels of transcriptional repression *in vitro*. I used AAV-delivered dCas9-repressors to successfully mediate robust and targeted gene repression in patient iPSC derived 3D retinal organoids. Finally, I evaluated the epigenetic editing system in a pilot *in vivo* experiment in an *Nrl.EGFP*$^{+/-}$ mouse model. This represents the first use of an all-in-one bipartite dCas9-repressor system to induce gene knockdown of photoreceptor genes.

The final set of work completed in this thesis focused on exploration of DNA base editing and prime editing technologies, with an eye towards their therapeutic translation for the treatment of IRDs. I demonstrated robust on-target adenine base editing in a novel reporter assay. Moreover, I engineered an enhanced minimal prime editor by truncating the Moloney Murine Leukemia Virus Reverse Transcriptase (M-MLV RT) and demonstrated efficient correction of the homologous *Ush2a* (p.W3947X) mouse mutation in a dual-luciferase assay.

CONTENTS

DECLARATION i

ACKNOWLEDGEMENTS ii

ABSTRACT iv

LIST OF FIGURES xvi

LIST OF TABLES xix

LIST OF ABBREVIATIONS xx

1. INTRODUCTION 1

1.1 The retina and inherited retinal disease 1

1.2 Current treatments for IRDs 5

1.2.1 Gene augmentation using AAV vectors 5

1.2.2 Other therapeutic strategies 8

1.3 Genome engineering in retinal diseases 11

1.3.1 Discovery of CRISPR-Cas 11

1.3.2 CRISPR genome editing 12

1.3.2.1 Repair of Cas-induced DSBs 13

1.3.3 HDR-independent DNA editing systems 19

1.3.3.1 Cytosine base editing 20

1.3.3.2 Adenine base editing 22

1.3.3.3 Prime editing 24

1.3.4 RNA editing 30

1.3.5 Epigenome editing 31

1.3.5.1 Transcriptional repression 32

1.3.5.2 Transcriptional activation 33

1.4 *In vivo* delivery of CRISPR agents 35

1.5 Thesis aims and overview 37

2. METHODS & MATERIALS 39

2.1 Molecular biology 39

2.1.1 Polymerase chain reaction 39

2.1.2 Plasmid cloning methodologies 40

2.1.3 Bacterial transformation 42

2.1.4 Colony selection, plasmid isolation & amplification 42

2.1.5 Restriction digestion 44

2.1.6 Agarose gel electrophoresis 44

2.1.7 Genomic DNA extraction 45

2.1.8 RNA extraction 45

2.1.9 cDNA synthesis 46

2.1.10 Real-time quantitative reverse transcription PCR 47

2.1.11 *In silico* design 49

2.1.12 TIDE analysis 49

2.1.13 Sanger sequencing 50

2.1.14 Protein extraction 50

2.1.15 Spectrophotometric quantification 51

2.1.16 Western blot 51
2.1.17 Fluorescence spectroscopy 52
2.2 Cell culture 53
2.2.1 Cell culture and maintenance 53
2.2.2 *In vitro* transfection and transduction 55
2.2.3 Microscopy imaging 59
2.3 AVV manufacture 59
2.3.1 HEK293T cell culture 61
2.3.2 Transfection 61
2.3.3 Cell harvesting & lysis 63
2.3.4 Isolation of AAV particles 63
2.3.5 Purification & concentration of AAV 65
2.3.6 Viral titration and capsid analysis 66
2.4 *In vivo* procedures 67
2.4.1 Anesthesia & pupil dilatation 68
2.4.2 Subretinal injection 68
2.4.3 Retinal imaging 70
2.4.4 Electroretinography 74
2.5 Cell & tissue processing 76
2.5.1 Retinal tissue collection 76
2.5.2 Immunohistochemistry 77
2.5.3 Confocal microscopy 79

2.6 Statistical analysis 80

3. DEVELOPMENT AND OPTIMIZATION OF CRISPR CONSTRUCTS TOWARDS *IN VIVO* ADAPTATION 81

3.1 Introduction 81

3.1.1 Developing an efficient system for AAV-directed delivery of CRISPR reagents 81

3.1.2 Non-viral delivery using DNA-wrapped gold nanoparticles 83

3.2 Chapter aims 85

3.3 Methods & materials 86

3.3.1 Plasmid cloning 86

3.3.2 Cell culture 89

3.3.3 Protein fluorescence assays 89

3.3.4 Analysis of editing efficiency (TIDE) 90

3.3.5 Gold nanoparticle production and nanotransfection 91

3.3.6 Animal procedures 91

3.3.7 Imaging and statistical analyses 92

3.4 Results 93

3.4.1 Design of an optimized all-in-one CRISPR vector 93

3.4.2 Evaluation of promoter elements and minimal PolyA sequences 93

3.4.3 Cas9 orthologue screening for gene suppression activity 96

3.4.3.1 Guide RNA design against transgenic HEK293-EGFP cell line 98

3.4.3.2 Effect of Cas9 orthologue on EGFP expression levels 99

3.4.3.3 Quantifying editing rates by TIDE analysis 104

3.4.4 Nanotransfection of HEK293 cells with DNA-wrapped gold nanoparticles 106

3.4.5 Pilot *in vivo* experiment with gold nanoparticles 108

3.4.5.1 Assessment of EGFP expression with cSLO autofluorescence imaging 108

3.4.5.2 SD-OCT and electroretinogram assessment of retinal structure and function following treatment 110

3.5 Discussion 114

3.5.1 Development of an all-in-one CRISPR construct for genome modification 114

3.5.1.1 Comparison of Cas9 orthologues 115

3.5.1.2 Evaluation of minimal regulatory elements 117

3.5.2 Assessment of gold nanoparticles for non-viral delivery 118

3.5.2.1 Insights from pilot gold nanoparticle study 120

3.5.2.2 Hurdles for nanoparticle delivery to the retina 121

3.5.2.3 Nuclear localization of DNA-wrapped gold nanoparticles 122

3.5.3 Conclusions 124

4. EVALUATION OF CRISPR-CAS9 REPRESSORS FOR TARGETED EPIGENOME EDITING 126

4.1 Introduction 126

4.2 Chapter aims 128

4.3 Methods & materials 129

4.3.1 Cloning of all-in-one repressor constructs 129

4.3.2 Dual luciferase assay design and cloning 131
4.3.3 Cell line generation for reporting transcriptional repression 132
4.3.4 Cell culture and transfections 133
4.3.5 Imaging and statistical analyses 134
4.4 Results 135
4.4.1 Designing and cloning all-in-one dCas9 repressor fusions 135
4.4.2 Pilot evaluation of dCas9-repressor effectors 138
4.4.3 Development of HEK293-dGFP cell line for repressor screening 140
4.4.4 Investigation of retinoblastoma-derived cell lines for screening of CRISPR agents 142
4.4.5 Testing of dCas9-KRAB-MeCP2 TRD epigenetic repressor construct targeting *NRL* 144
4.5 Discussion 149
4.5.1 Development of potent bipartite transcriptional repressor 149
4.5.2 Investigation of *in vitro* models for screening of dCas9 repressor fusions and gRNAs 151
4.5.2.1 Destabilized GFP cell line for screening of dCas9 repressor fusions 151
4.5.2.2 Dual luciferase assay for high throughput gRNA screening 151
4.5.3 Insights from guide RNA screening 152
4.5.4 Conclusion 153
5. EPIGENETIC REPRESSION IN IPSC-DERIVED RETINAL ORGANOIDS AND A PILOT STUDY IN AN *NRL.EGFP* MOUSE MODEL 154
5.1 Introduction 154

5.2 Chapter aims 156

5.3 Methods & materials 157

5.3.5 Animal models and procedures 159

5.3.9 Imaging and statistical analyses 165

5.4 Results 166

5.4.1 AAV vector production 166

5.4.2 Evaluation of AAV-directed bipartite repressors in patient iPSC derived retinal organoids 168

5.4.3 AAV-dCas9-KRAB-MeCP2 TRD mediates high levels of gene repression in patient iPSC derived retinal organoids 169

5.4.4 Pilot study of dCas9 repressor fusions in *NRL.EGFP* mouse model 171

5.4.4.1 Evaluation of AAV-GRK1-dCas9 bipartite repressor *in vivo* 171

5.4.4.2 Analysis of repression and retinal function in AAV-GRK1-dCas9 bipartite repressor pilot 175

5.5 Discussion 177

5.5.1 *Nrl* as a genetic target for epigenome editing 177

5.5.2 Off-target effects and toxicity 180

5.5.3 Immunogenic response 183

5.5.4 Translational considerations and challenges: Safety, efficiency, and precision 184

5.5.5 Conclusions 186

6. DEVELOPMENT OF HDR-INDEPENDENT BASE EDITING AND PRIME EDITING TECHNOLOGIES 187

6.1 Introduction 187

6.2 Chapter aims 190

6.3 Methods & materials 191

6.3.1 Plasmid construction 191

6.3.2 Cell line generation for reporting DNA base editing 191

6.3.3 Cloning for guide RNA screening 192

6.3.4 Protein modeling 192

6.3.5 Cell culture and transfections 193

6.3.6 Dual-Glo luciferase assay 193

6.3.7 Analysis of DNA editing with Dual-Glo luciferase assay 194

6.3.8 Analysis of on-target DNA editing 195

6.4 Results 196

6.4.1 Development of cell lines to report adenine and cytosine DNA base editing 196

6.4.2 Development and evaluation of DNA base editing constructs 200

6.4.2.1 Development of dual vector strategy for adenine base editing 200

6.4.2.2 Pilot adenine base editing study 201

6.4.2.3 Guide RNA and dose optimizations 203

6.4.2.4 Screening of adenine base editors 204

6.4.2.5 Quantifying adenine base editing by Sanger sequencing 207

6.4.2.6 Evaluating SaCas9-ABEs with altered PAM recognition 207

6.4.3 Development of an enhanced prime editing system 211

6.4.3.1 Generation of minimal prime editors 211
6.4.3.2 NgRNA and pegRNA screening 215
6.4.3.3 Evaluation of minimal prime editors using a dual luciferase assay 216
6.5 Discussion 221
6.5.1 Development of reporter cell lines 221
6.5.2 Screening of adenine base editors 222
6.5.3 Engineering of minimal prime editors 224
6.5.4 Therapeutic possibilities with base and prime editing systems 225
6.5.4.1 Editing large genes 226
6.5.4.2 Targeting autosomal dominant diseases 226
6.5.4.3 Editing premature stop codons 227
6.5.4.4 Editing splice-site variants 228
6.5.5 Conclusion 229
7. GENERAL DISCUSSION 230
7.1 Summary of thesis aims and outcomes 230
7.2 Translational considerations 232
7.2.1 Undesired genome editing 234
7.2.2 Immunogenicity concerns 236
7.2.3 Improving safety of CRISPR-Cas systems 237
7.2.4 Improving targeting scope of CRISPR-Cas systems 239
7.2.5 Forthcoming development of dCas-based epigenome editing 240
7.3 Future clinical application of precision editing in inherited retinal diseases 243

7.4 Final perspectives 245

7.5 Concluding remarks 246

8. REFERENCES 248

9. APPENDIX 295

i. List of key plasmids 295

ii. List of gRNA sequences 296

iii. Key sequencing and PCR primers 301

iv. Sequences of key plasmid elements 306

v. List of key resources 318

vi. Published manuscripts, book chapters, & presentations 321

LIST OF FIGURES

Figure 1.1 | Anatomy of the primate retina 3

Figure 1.2 | Retinal features of USH2A-related retinal degeneration 5

Figure 1.3 | AAV Vector biology 8

Figure 1.4 | Gene therapy approaches for retinal disease 10

Figure 1.5 | Summary of therapeutic CRISPR-based genome-editing strategies 34

Figure 2.1 | Adeno-associated virus production, purification, tittering 60

Figure 2.2 | Iodixanol gradients following ultracentrifugation 65

Figure 2.3 | Subretinal injection 70

Figure 2.4 | Retinal imaging by cSLO and OCT 73

Figure 3.1 | Representative full plasmid maps of all-in-one SaCas9 and CjCas9 plasmids 88

Figure 3.2 | Example output of TIDE analysis 91

Figure 3.3 | Cloning of regulatory elements for gene suppression 94

Figure 3.4 | Evaluation of minimal promoter and PolyA signals 95

Figure 3.5 | Cloning of an all-in-one vector harboring different Cas9 orthologues 97

Figure 3.6 | Guide RNA design for Cas9 orthologue comparison 99

Figure 3.7 | Comparison of SpCas9 and SaCas9 editing efficiency 102

Figure 3.8 | CjCas9 shows substantially lower levels of editing compared to SpCas9 and SaCas9 orthologues 104

Figure 3.9 | Quantifying cutting efficiency of Cas9 orthologues by TIDE analysis . 105

Figure 3.10 | Transfection of HEK293T cells with gold nanoparticles wrapped with EGFP and DsRed reporter plasmids 107

Figure 3.11 | En face cSLO imaging following subretinal injection 109

Figure 3.12 | Photoreceptor layer thickness following subretinal injection of gold nanoparticles 111

Figure 3.13 | Assessment of retinal function by electroretinography 113

Figure 4.1| Representative full plasmid map of all-in-one dCas9-repressor 131

Figure 4.2 | PsiCHECK-2 dual luciferase assay for Cas9 orthologue comparison 132

Figure 4.3 | Generation of a dCas9 bipartite repressor comprised of the Methyl-CpG Binding Protein 2 (MeCP2) transcriptional repression domain 137

Figure 4.4 | Evaluation of dCas9-repressor effectors using HEK293-EGFP transgenic cell line 139

Figure 4.5 | Screening of dCas9-repressor fusions using the HEK293-dGFP cell line 141

Figure 4.6 | Characterization and evaluation of Y79 human retinoblastoma cell line for screening of dCas9-repressor fusions 144

Figure 4.7 | Top-performing gRNAs against NRL cloned into the dCas9-KRAB-MeCP2 TRD vector and screened using a dual luciferase assay 147

Figure 5.1 | Cryosectioning of retinal organoids 161

Figure 5.2 | Production of dCas9 repressor AAV vectors 167

Figure 5.3 | Outer layer of patient iPSC derived retinal organoid 3D cultures represents photoreceptor-like cells 169

Figure 5.4 | AAV-directed dCas9-repressor fusions mediate robust gene silencing in human iPSC 3D retinal organoids 171

Figure 5.5 | Pilot study in the Nrl-EGFP mouse model 172

Figure 5.6 | En face cSLO imaging following subretinal injection with dCas9-KRAB-MeCP2 TRD non-targeting vector 174

Figure 5.7 | En face cSLO and OCT imaging following subretinal injection with dCas9-KRAB-MeCP2 TRD targeting vector 175

Figure 5.8 | Pilot evaluation of AAV-directed dCas9-repressor fusions in Nrl-EGFP mouse model 176

Figure 6.1 | Construction of cell line to report cytosine base editing 197

Figure 6.2 | Construction of cell line to report adenine base editing 198

Figure 6.3 | Representative karyotypes from HEK-CBE and HEK-ABE cell lines 199

Figure 6.4 | Development of a dual vector strategy 201

Figure 6.5 | Initial evaluation of adenine base editing in HEK-ABE reporter cell-line 203

Figure 6.6 | Screening of base editor architectures 206

Figure 6.7 | Quantifying adenine base editing by Sanger sequencing and evaluating ABEs with altered PAM recognition 209

Figure 6.8 | Protein modeling of the M-MLV Reverse Transcriptase 213

Figure 6.9 | Generation of a minimal prime editor by truncation of M-MLV reverse transcriptase 215

Figure 6.10 | The engineered minimal PE variant showed enhanced rates of prime editing in vitro 219

Figure 7.1 | Future clinical application of precision editing in IRDs 245

LIST OF TABLES

Table 1.1 | Summary of *in vivo* CRISPR studies targeting inherited retinal disease . 19

Table 1.2 | Evolution of CRISPR base editing and prime editing tools 30

Table 2.1 | Standard PCR conditions for cloning and sequencing applications..... 40

Table 2.2 | Cell seeding density for plasmid transfection..... 57

Table 2.3 | Calculations to determine plasmid concentrations for rAAV production 62

Table 2.4 | Preparation of iodixanol gradients..... 64

Table 2.5 | ERG recording protocol..... 76

Table 3.1 | Cloning of all-in-one AAV plasmids..... 88

Table 4.1 | Cloning of epigenetic repressors..... 130

Table 4.2 | Design and cloning of individual and bipartite dCas9-repressor fusions 136

Table 4.3 | Guide RNA design targeting NRL..... 146

Table 4.4 | MeCP2 interaction with molecular partners 150

Table 5.1 | AAV titers of dCas9-repressor vectors 158

Table 5.2 | Primary antibodies used for immunohistochemistry and western blot.. 163

Table 5.3 | TaqMan probe panel used for pRT-PCR analysis of rod- and cone-specific genes in retinal organoids transduced with AAV-dCas9-KRAB-MeCP2..... 165

Table 5.4 | Guide RNA sequence Nucleotide BLAST..... 182

Table 6.1 | Screening of adenine base editors..... 205

Table 6.2 | Prime editing ngRNA / pegRNA cloning 216

Table 6.3 | *mUsh2a*-W3947X dual luciferase reporter assay for prime editing reporting 217

LIST OF ABBREVIATIONS

AAG	Alkyl adenine DNA glycosylase
AAV	Adeno-associated virus
ABCA4	ATP-binding cassette transporter protein family members 4
ABE	Adenine base editor
AD	Autosomal dominant
$ADAR_{DD}$	Adenosine deaminase acting on RNA deaminase domain
AMD	Age-related macular degeneration
ANOVA	Analysis of variance
APOBEC1	Apolipoprotein B mRNA Editing Enzyme Catalytic Subunit 1
AR	Autosomal recessive
ATP	Adenosine triphosphate
AuNP	Gold nanoparticle
BAF	Blue autofluorescence
BER	Base excision repair
BEST1	Bestrophin 1
bGH	Bovine growth hormone polyA
BM	Bruch membrane
BSA	Bovine serum albumin
Cas	CRISPR-associated
CBE	Cytosine base editor
cDNA	Complementary DNA
CDS	Coding sequence
CEP290	Centrosomal protein 290
CjCas9	*Campylobacter jejuni* Cas9
CK30PEG	Polyethylene glycol-substituted polylysine
CNGA3	Cyclic nucleotide gated channel subunit alpha 3
CNGB3	Cyclic nucleotide gated channel subunit beta 3
CP-Cas9	Circularly permuted Cas9
CPP	Cell-penetrating peptide
CRB1	Crumbs cell polarity complex component 1
CRISPR	Clustered regularly interspaced short palindromic repeats

CRISPRa	CRISPR activation
CRISPRi	CRISPR interference
crRNA	CRISPR RNA
CRX	Cone-rod homeobox
cSLO	Confocal scanning laser ophthalmoscope
C_t	Cycle threshold
CTD	C-terminal domain
DAPI	4′,6-diamidino-2-phenylindole
DBP	DNA binding protein
dCas	Dead Cas
dGFP	Destabilized GFP
DMEM	Dulbecco's Modified Eagle Medium
DNMT3A	DNA (cytosine-5)-methyltransferase 3A
DR	Direct repeat
DSB	Double stranded break
DBD	DNA binding domain
dsDNA	Double stranded DNA
EcTadA	*Escherichia coli* tRNA adenosine deaminase
EditR	Edit deconvolution by inference of traces in R
EDTA	Ethylenediaminetetraacetic acid
EFS-1α	Elongation factor 1-alpha 1 short intron-less promoter
ELM	External limiting membrane
ELOVL4	Elongation of very long chain fatty acids
ERG	Electroretinogram
ESC	Embryonic stem cell
ESCS	Enhanced S-cone syndrome
EYS	Eyes shut homolog
EZ	Ellipsoid zone
FIPA	Fluorescence immunoprecipitation
GCL	Ganglion cell layer
GFP	Green florescent protein
GRK1	Human Rhodopsin Kinase Promoter
hCMV-MIE	Major immediate-early promoter and enhancer of the human cytomegalovirus promoter

HDR	Homology-directed repair
HEK293T	Human Embryonic Kidney 293 Cells Expressing Mutant SV40 T Antigen
HITI	Homology-independent targeted integration
ICGA	Indocyanine green angiography
ID	Intervening domain
IDP	Intrinsically disordered protein
IHC	Immunohistochemistry
INL	Inner nuclear layer
IPL	Inner plexiform layer
iPSC	Induced pluripotent stem cells
IRAF	Infrared autofluorescence
IRD	Inherited retinal degeneration
IS	Inner segment
ITR	Inverted terminal repeat
KRAB	Krüppel-associated box
LB	Luria Broth
LCA	Leber congenital amaurosis
LED	Light-emitting diode
LV	Lentiviral vector
MBD	Methyl binding domain
MeCP2	Methyl-CpG Binding Protein 2
MERTK	MER proto-oncogene tyrosine kinase
MGB	Mini groove binder
MMEJ	Microhomology-mediated end joining
M-MLV RT	Moloney murine leukemia virus reverse transcriptase
nCas9	Cas9 nickase
NF	Nuclear factor
NFQ	Non-florescent quencher
NGS	Normal Goat Serum
NGS	Next generation sequencing
NHEJ	Non-homologous end joining
NHP	Non-human primate
NP	Nanoparticle
NR2E3	Nuclear receptor subfamily 2 group E member 3

NRL	Neural leucine zipper
ns	Not significant
NTD	N-terminal domain
NTP	No template control
OCT	Optical coherence tomography
OCT	Optimal cutting temperature compound
ONL	Outer nuclear layer
OP	Optical density
OPL	Outer plexiform layer
ORF	Open reading frame
PACE	Phase assisted continuous evolution
PAGE	Polyacrylamide Gel Electrophoresis
PANCE	Phase assisted non-continuous evolution
PBS	Phosphate buffered saline
PBS	Primer binding site
PE	Prime editor
pegRNA	Prime-editing guide RNA
PEI	Polyethyleneimine
PF-68	Pluronic™ F-68 Surfactant
PFA	Paraformaldehyde
PI	Protease inhibitor
pmCDA1	*Petromyzon marinus* cytidine deaminase 1
PNK	Polynucleotide kinase
PR	Photoreceptor
PRL	Photoreceptor layer
PRPF31	Pre-mRNA processing factor 31
PRPH2	Peripherin 2
PTC	Premature termination codon
PVDF	Polyvinylidene difluoride
rAAV	Recombinant adeno-associated virus
RCS	Royal College of Surgeons rat
REP1	Rab escort protein 1
RIPA	Radioimmunoprecipitation
RNA	Ribonucleic acid

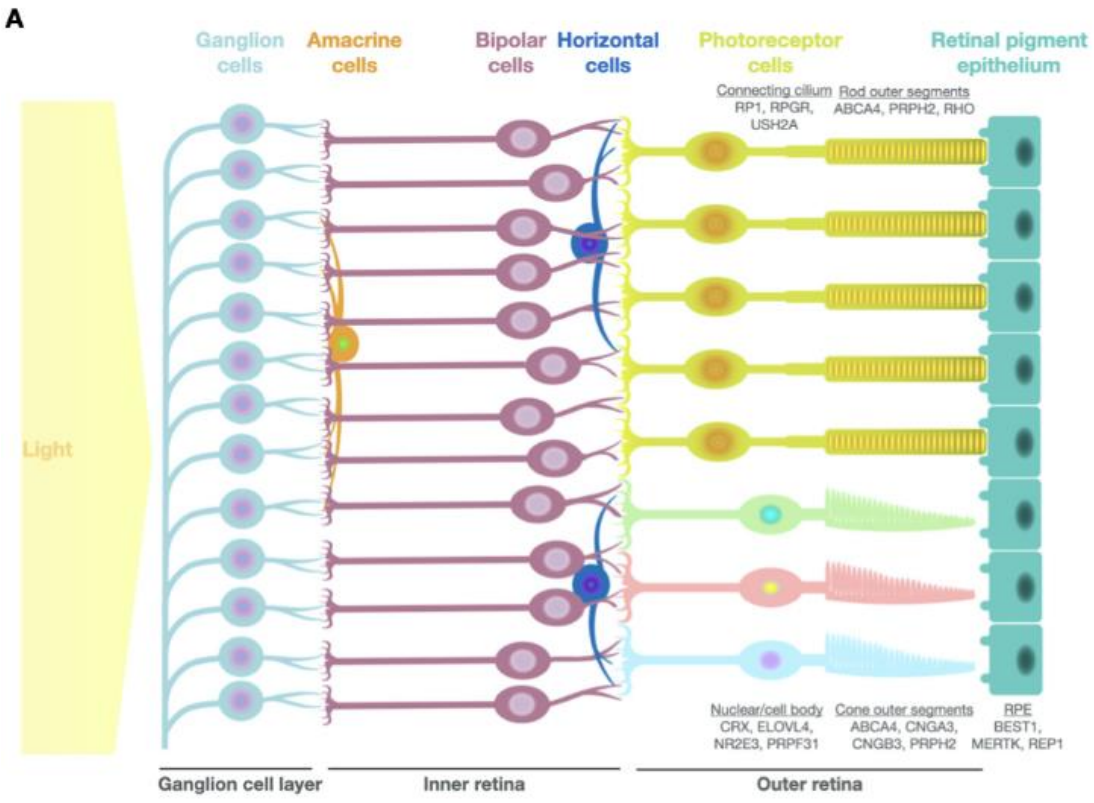
RNase H	Ribonuclease H
RNFL	Retinal nerve fiber layer
RNP	Ribonucleoprotein
RO	Retinal organoid
RP1	Retinitis pigmentosa 1
RPE	Retinal pigment epithelium
RS1	Retinoschisin 1
RT-qPCR	Real time quantitative PCR
SaCas9	*Staphylococcus aureus* Cas9
scFv	Single-chain fragment variable
SD	Standard deviation
SD-OCT	Spectral domain optical coherence tomography
secNluc	Secreted luciferase protein
SEM	Standard error of the mean
siRNA	Small interfering RNA
SNP	Single nucleotide polymorphism
SNRNP200	Small nuclear ribonucleoprotein U5 subunit 200
SOC	Super optimal broth with catabolite repression
SpCas9	*Streptococcus pyogenes* Cas9
SV40	Simian virus-40
TadA	tRNA adenosine deaminase
TAE	Tris/Acetate/EDTA
TALEN	Transcription activator-like effector nuclease
TBS	Tris-Buffered Saline
TBS-T	Tris-Buffered Saline with 0.01% Tween-20
TET1	Tet Methylcytosine Dioxygenase 1
TIDE	Tracking of Indels by Decomposition
tracrRNA	Trans-activating RNA
TRD	Transcriptional repression domain
UNG	Uracil N-glycosylate
USH2A	Usherin
UV	Ultraviolet
vg	Vector genomes
ZFN	Zinc finger nuclease

1. INTRODUCTION

1.1 The retina and inherited retinal disease

The retina is a specialized multi-layered structure that lines the inside surface of the eye (Figure 1.1). It is composed of numerous cell types that develop in a specific sequence, creating a neural tissue that is able to respond to visual stimuli.[1] Inherited retinal diseases are both genetically and clinically heterogeneous and arise from mutations in genes important to the functioning of the cells that form the retina.[2] Such diseases are currently known to be caused by mutations in over 300 genes / loci.[3] These mutations can lead to autosomal recessive, dominant and X-linked inherited forms that cause either dysfunction or loss of cells within the retina, ultimately preventing the retina from detecting or conveying responses to visual stimuli.

The light-sensitive rod and cone photoreceptor cells lie towards the back of the eye and form the outer retina (Figure 1.1). These cells have a highly specialized morphology, including an outer segment of stacked discs that increase the surface area of the cell. The membrane-bound discs contain light-sensitive pigments that absorb different wavelengths of light, the response to which initiates a transduction cascade that causes hyperpolarization of the photoreceptor cell. This in turn signals the cells of the inner retina, the bipolar cells, which subsequently transfer the signal on to the retinal ganglion cells. Cross-communication between these cell types occurs by way of horizontal and amacrine cells, with the resulting combined responses passing through the optic nerve to the brain for visual image processing.


A
Ganglion cells
Amacrine cells
Bipolar cells
Horizontal cells
Photoreceptor cells
Retinal pigment epithelium
Connecting cilium
RP1, RPGR, USH2A
Rod outer segments
ABCA4, PRPH2, RHO
Light
Nuclear/cell body
CRX, ELOVL4, NR2E3, PRPF31
Cone outer segments
ABCA4, CNGA3, CNGB3, PRPH2
RPE
BEST1, MERTK, REP1
Ganglion cell layer
Inner retina
Outer retina

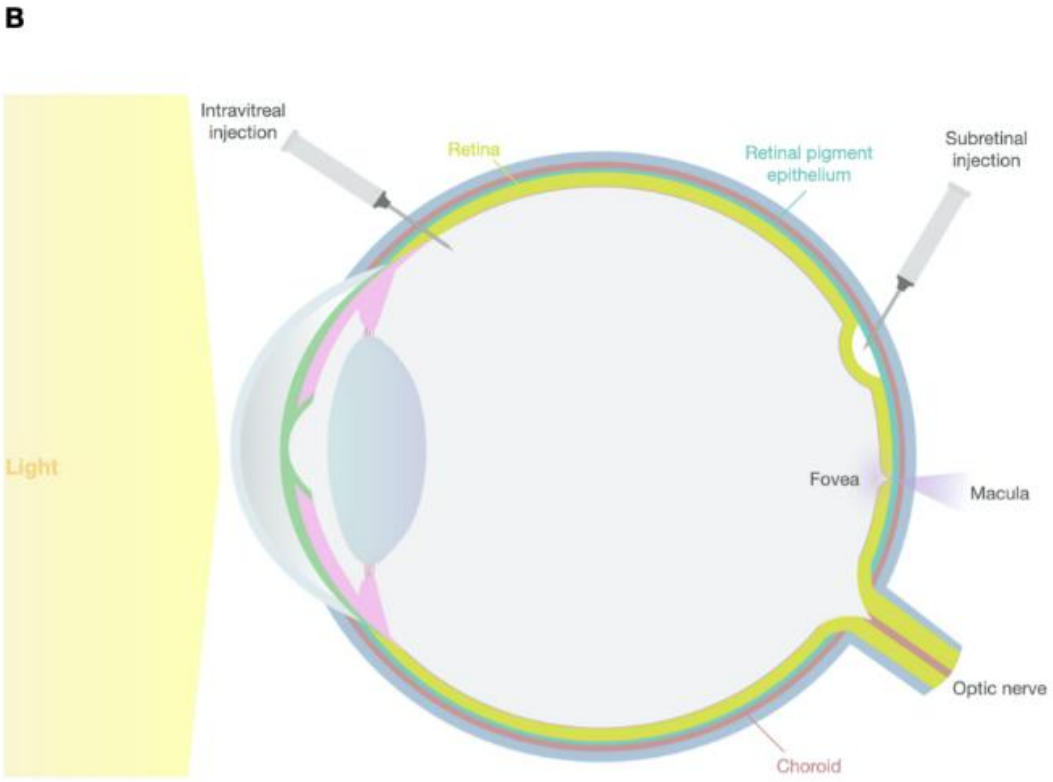

B
Intravitreal injection
Retina
Retinal pigment epithelium
Subretinal injection
Light
Fovea
Macula
Optic nerve
Choroid

Figure 1.1 | Anatomy of the primate retina

A. The retina is a highly structured neural tissue composed of multiple cell types. Light must pass through the retinal ganglion cell layer and inner retina to reach the outer segments of the rod- and cone-photoreceptors. These cells respond to the light and send the signal back through the bipolar cells and the ganglion cells, which converge into the optic nerve. Selected gene expression products in which mutations cause retinal disease are included: ATP-binding cassette transporter protein family members 4 (*ABCA4*), bestrophin 1 (*BEST1*), cyclic nucleotide gated channel subunit alpha 3 (*CNGA3*) and beta 3 (*CNGB3*), cone-rod homeobox (*CRX*), elongation of very long chain fatty acids (*ELOVL4*), MER proto-oncogene tyrosine kinase (*MERTK*), nuclear receptor subfamily 2 group E member 3 (*NR2E3*), peripherin 2 (*PRPH2*), pre-mRNA processing factor 31 (*PRPF31*), Rab escort protein 1 (*REP1*), rhodopsin (*RHO*), retinitis pigmentosa 1 (*RP1*), retinitis pigmentosa GTPase regulator (*RPGR*), usherin (*USH2A*). **B.** The retina forms the inner layer of the eye. The foveal depression occurs in the central region of the eye known as the macula, in which there is a high density of cone photoreceptor cells that enable color vision and higher visual acuity. The peripheral region beyond the macula is composed predominantly of rod photoreceptor cells. Gene therapy interventions can be provided by intravitreal or subretinal delivery routes.

Text, figures, and tables in this chapter have been adapted from: Kantor A, McClements ME, Peddle CF, *et al.* CRISPR genome engineering for retinal diseases. *Prog Mol Biol Transl Sci.* 2021;182:29-79. doi:10.1016/bs.pmbts.2021.01.024.

Given the complexity of the retinal structure and interaction among multiple cell types, it is clear how dysfunction in one or many of these cell populations might disrupt the important sequence of events that enables vision. Moreover, the functioning retina is dependent on the health of the retinal pigment epithelium (RPE), a layer of cells lining the outer retina that are critical in supporting photoreceptor cell survival. Genetic mutations can influence the function and survival of all these cell types, creating a wide variety of retinal phenotypes that vary in severity. The majority of known mutations

directly impact the photoreceptor and RPE cells, making these the primary targets of therapeutic interventions.[4]

In humans, the composition of photoreceptor cells is variable across the outer retina, with a concentrated area of cone photoreceptor cells in the central region, known as the macula, responsible for higher visual acuity and color vision. The density of cone photoreceptors then decreases outwardly from this zone, leaving the peripheral outer retina comprised largely of rod photoreceptor cells. The genetic origin of disease may lead to the dysfunction or death of one cell type of the retina, such as with cone dystrophies characterized by a predominant loss of central vision,[5] or it may affect multiple cell types within the retina, such as in the case of retinitis pigmentosa, where initial loss of peripheral cells is often followed by loss of photoreceptors in the outer retina.[6] Mutations in multiple different genes, including, *USH2A*, are associated with autosomal recessive retinitis pigmentosa (Figure 1.2). Similarly, in the severe condition Leber congenital amaurosis (LCA), patients suffer a rapid loss of photoreceptors in the outer retina at an early age.[7] Understanding the natural physiological progression that results from specific mutations provides a means to measure the success of a therapeutic intervention using non-invasive methods.[8]

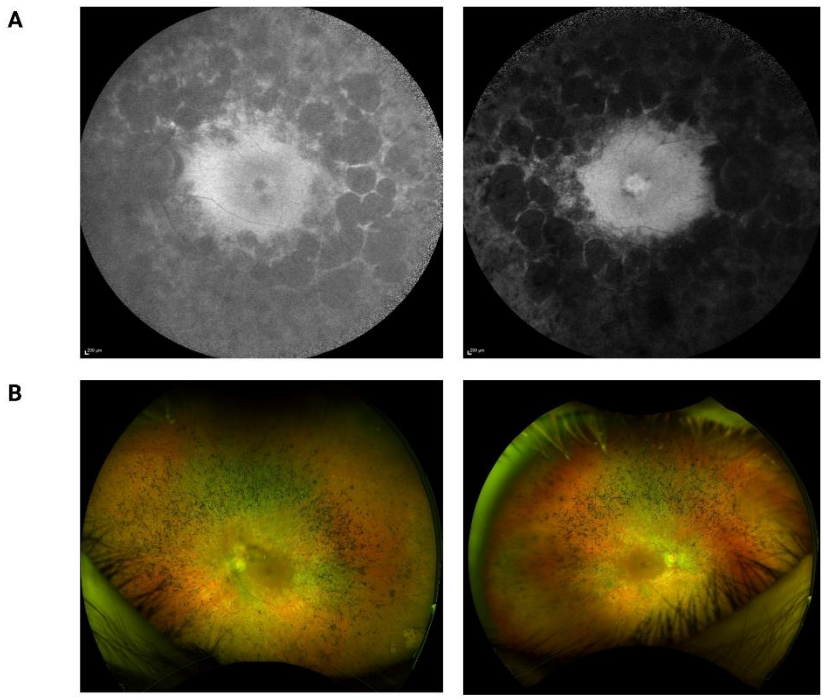


Figure 1.2 | Retinal features of *USH2A*-related retinal degeneration

Representative image of *USH2A*-associated retinal degeneration. **A.** Short wavelength fundus autofluorescence demonstrating peripheral hypo-autofluorescence and patches of RPE atrophy. **B.** Optos widefield color fundus image demonstrating peripheral pigmentary retinopathy and retinal thinning. Images provided by Laura Wood, Oxford Eye Hospital.

1.2 Current treatments for IRDs

1.2.1 Gene augmentation using AAV vectors

As a gene therapy target, the retina exhibits many benefits compared to other tissue types due its ease of accessibility, immune-privileged statues, and tight blood-retinal barriers.[9] Indeed, due in part to these key advantages, over the past decade the largest strides in gene therapy development have been achieved in the eye. Whilst lentiviral vectors have been used in clinical trials and have indicated safety, to date there is an

absence of reports of efficacy.[10] The majority of human trials for the treatment of retinal disease use adeno-associated viral vectors (AAV) and dozens of such trials have now been completed, are ongoing or are currently recruiting.[10,11]

AAV is a single-stranded DNA parvovirus that belongs to the genus *Dependoparvovirus*. As indicated by its name and phylogenetic classification, AAV is a helper-dependent virus that requires the presence of another virus, including adenovirus and herpes simplex virus, to promote replication. The AAV genome is flanked by two inverted terminal repeats (ITRs), that contain *cis* elements required for replication and packaging and the packaging-competent form of the AAV genome is ~4.7 kilobases (kb).[12,13] Importantly, the AAV ITRs, which induce transgene expression and play a central role in ensuring long-term cellular transduction, contain all the necessary *cis*-functions required for genome packaging. Thus, the basis for the production of recombinant AAV (rAAV) vectors is the fact that the *rep* and *cap* genes can be deleted from the viral genome and provided in *trans*. The viral genes can be replaced by a transgene with transcriptional control elements, resulting in a vector genome of approximately 4.5 kb flanked by the viral ITRs. The complete removal of viral coding sequences permits engineering of the AAV vector for gene therapy and contributes to their low cytotoxicity and immunogenicity as a delivery platform.[14] Indeed, substituting the *rep* and *cap* genes with an expression cassette containing a promoter (for example, human rhodopsin kinase (RK) promoter), a therapeutic transgene (*RPGR*, which encodes retinitis pigmentosa GTPase regulator), and polyadenylation signal forms the essence of AAV gene therapy vectors. To date, at least 12 natural serotypes and over 100 variants of AAV have been isolated and adapted as gene delivery vehicles with different tissue-type and cell-type tropism profiles. Researchers have pursued a variety of approaches to genetically engineer AAVs to enhance their transduction and production and to overcome immunity barriers in patients, including natural discovery, rational design,

and directed evolution.[12,15-20] These efforts have played a substantial role in the advancement of these vectors for *in vivo* delivery.

With growing evidence of both safety and efficacy,[21-24] it is not surprising the first Food and Drug Administration-approved AAV gene therapy is for the treatment of an inherited retinal disease (LCA). Application of AAV gene therapy vectors in clinical trials have focused on gene supplementation strategies for autosomal recessive and X-linked conditions, although such approaches are also being applied for multifactorial diseases such as age-related macular degeneration.[25-27] The vectors share common characteristics and carry transgenes that contain the genetic elements that enable expression of a correct copy of the gene of interest in the desired cell type of the retina. Data published over the past decade from clinical trials have been critical for developing appropriate surgical techniques and establishing the safety of AAV vectors for retinal delivery.[28,29] Clinical trials using AAV-gene therapy are currently underway for choroideremia (*CHM*),[30] X-linked retinitis pigmentosa (*RPGR*),[24] autosomal recessive retinitis pigmentosa (*MERTK, PDE6A,*[31] *PDE6B,*[32,33] *RLBP1*[34]), X-linked retinoschisis (*RS1*),[35] Bietti's crystalline dystrophy (*CYP4V2*),[36,37] and achromatopsia (*CNGA3*,[38] *CNGAB3*[39]).

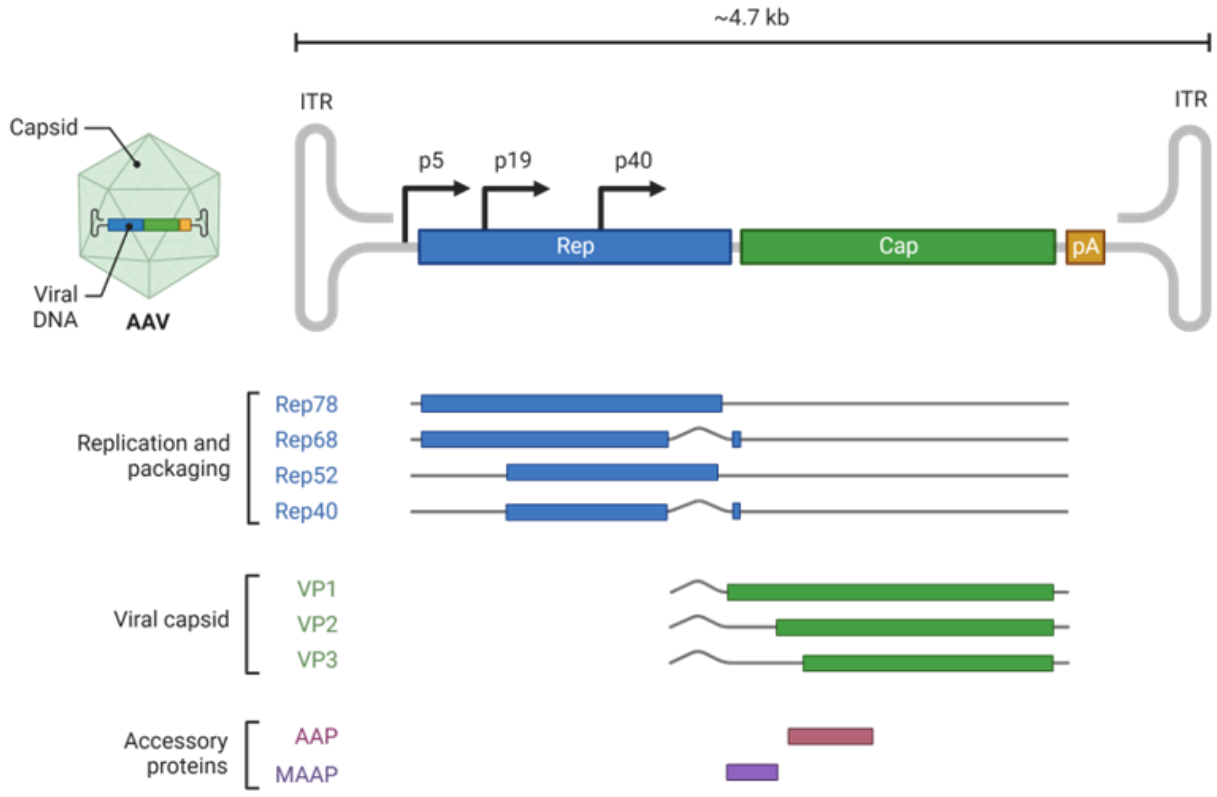


Figure 1.3 | AAV Vector biology

AAV is a single-stranded DNA parvovirus that belongs to the genus *Dependoparvovirus*. The AAV genome is flanked by two inverted terminal repeats (ITRs), that contain *cis* elements required for replication and packaging and the packaging-competent form of the AAV genome is ~4.7 kilobases (kb). AAV ITRs, which induce transgene expression and play a central role in ensuring long-term cellular transduction, contain all the necessary *cis*-functions required for genome packaging. Thus, the basis for the production of recombinant AAV (rAAV) vectors is the fact that the *rep* and *cap* genes can be deleted from the viral genome and provided in *trans*.

1.2.2 Other therapeutic strategies

The application of gene supplementation strategies is relatively limited as a large proportion of inherited retinal diseases do not benefit from such treatments. There are scenarios where gene supplementation might be a suitable strategy but cannot be implemented due to the packaging limitation of AAV vectors. For example, the most

common form of childhood-onset macular degeneration arises from mutations in *ABCA4*, but the coding sequence for this gene exceeds the packaging capacity of AAV and therefore requires less efficient dual vector [40,41] or lentiviral vector [42,43] approaches. Whilst the dual AAV vector system appears feasible, developing new strategies that specifically target and correct the genome may be beneficial for this particular disorder and indeed other forms of inherited retinal disease caused by mutations in large genes (e.g., >4.5 kb; *USH2A, EYS, ABCA4, CDH23, MYO7A*). The design of appropriate treatment strategies for given retinal diseases is largely guided by knowledge and understanding of the genetic causation (Figure 1.4).

With gene supplementation approaches limited to the treatment of loss of function mutations, new treatment options are also required for the large number of retinal diseases that result from gain of function and/or dominant negative effects, which cannot be overcome by provision of the correct form of the gene. In such a situation, the temptation might be to attempt silencing of the mutated allele, but the issue of haploinsufficiency is an important consideration, as having only one correct copy of a gene is not always sufficient to enable normal function.[44] In situations where mutations lead to dominant negative or toxic gain of function effects, for example with the *RHO* variant P23H,[45,46] gene augmentation has proved ineffective.[47] More recently, encouraging therapeutic strategies have employed a combined approach of mutation-independent RNA interference knockdown and gene supplementation.[48] Nevertheless, achieving the appropriate balance of knockdown and augmentation has proved difficult in pre-clinical testing. For such diseases, correction of the underlying genetic mutation would be the most desirable therapeutic strategy.

Despite concerns of haploinsufficiency, some forms of inherited retinal disease may benefit from an allele-specific gene silencing approach, while others will rely on the development of direct genome editing methods. Clustered regularly interspaced short

palindromic repeats (CRISPR) genome engineering therefore holds great promise in being the solution to the current absence of treatment options for many retinal diseases. Nevertheless, there are still challenges with translational feasibility of genome editing approaches. Given the large number of genes in which mutations arise and cause inherited retinal disease, as well as the allelic heterogeneity within those genes, the potential number of therapeutic vectors to be designed and optimized are vast. Currently, more than 1,200 disease-causing variants in the gene *ABCA4* alone have been identified, with patients carrying different combinations of disease-causing alleles.[49] To this end, it is important to not only consider the arsenal of genetic medicines available, but also the translational implications and practical considerations of using such molecular mechanisms to treat inherited retinal disease.

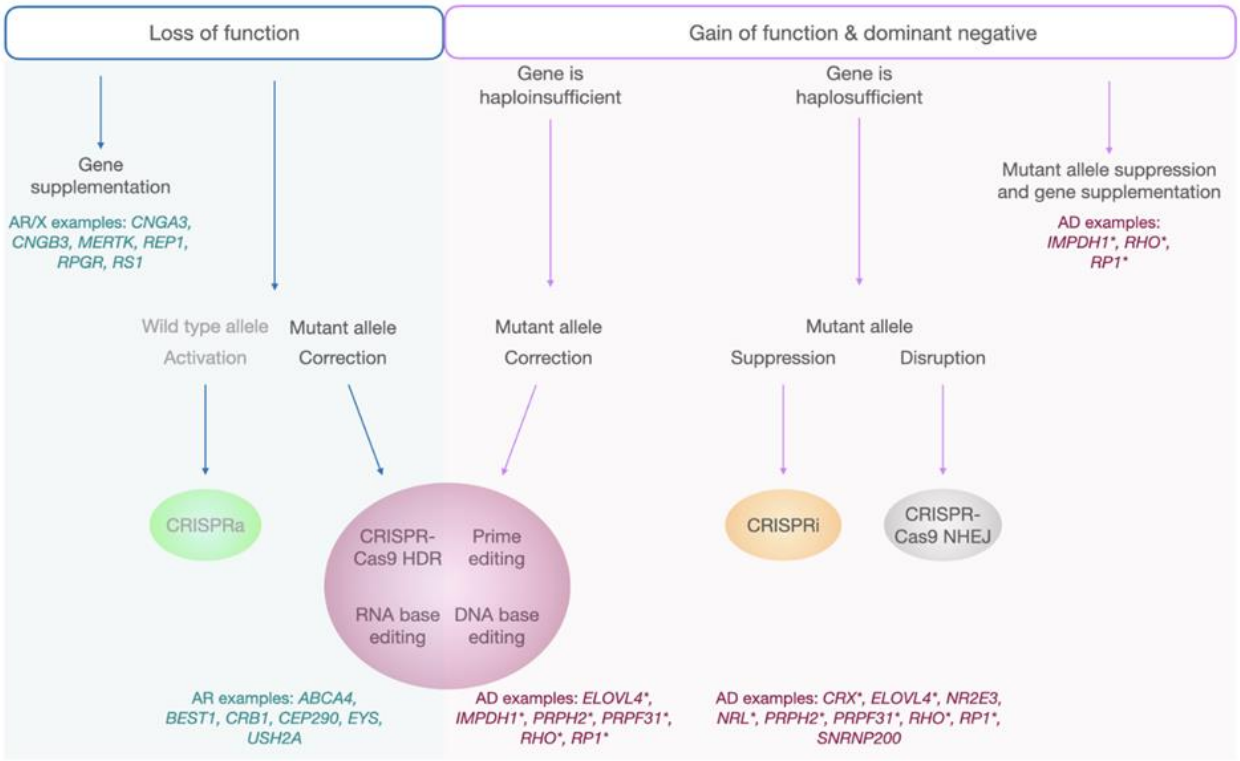


Figure 1.4 | Gene therapy approaches for retinal disease

The appropriate treatment options for particular forms of inherited disease need to be determined from their genetic origin and guided by knowledge of the molecular consequences and

subsequent pathophysiological outcomes. Gene supplementation strategies show success for autosomal recessive (AR) and X-linked disorders (X), but not all genes are deliverable by AAV vectors. Autosomal dominant (AD) mutations are good candidates for genome correction and editing, with some also suitable targets for epigenetic modification. ATP-binding cassette transporter protein family members 4 (*ABCA4*), bestrophin 1 (*BEST1*), centrosomal protein 290 (*CEP290*), crumbs cell polarity complex component 1 (*CRB1*), cyclic nucleotide gated channel subunit alpha 3 (*CNGA3*) and beta 3 (*CNGB3*), cone-rod homeobox (*CRX*), elongation of very long chain fatty acids (*ELOVL4*), eyes shut homolog (*EYS*), inosine monophosphate dehydrogenase 1 (*IMPDH1*), MER proto-oncogene tyrosine kinase (*MERTK*), nuclear receptor subfamily 2 group E member 3 (*NR2E3*), neural retina leucine zipper (*NRL*), peripherin 2 (*PRPH2*), pre-mRNA processing factor 31 (*PRPF31*), Choroideremia Rab escort protein 1 (*REP1*), retinoschisin 1 (*RS1*), rhodopsin (*RHO*), retinitis pigmentosa 1 axonemal microtubule associated protein (*RP1*), retinitis pigmentosa GTPase regulator (*RPGR*), small nuclear ribonucleoprotein U5 subunit 200 (*SNRNP200*), usherin (*USH2A*). *Mutation dependent.

1.3 Genome engineering in retinal diseases

1.3.1 Discovery of CRISPR-Cas

Genome engineering using zinc finger nucleases (ZFNs) or transcription activator-like effector nucleases (TALENs) have existed for some time, but the clinical application of these techniques has been limited by the complexity of protein engineering and low *in vivo* efficiencies.[50,51] From its humble beginnings in cheese and yogurt fermentation, the discovery of the mechanisms of the clustered regularly interspaced short palindromic repeats (CRISPR)-Cas9 system[52-56] and subsequent adaptation into a powerful gene editing tool has revolutionized the field of molecular biology and generated excitement for the potential to treat numerous human conditions.

CRISPRs were first identified in *E. coli* in 1987 by a Japanese scientist, Yoshizumi Ishino, and his team, who accidentally cloned an unusual series of repeated sequences

interspersed with spacer sequences while analyzing a gene responsible for the conversion of alkaline phosphatase.[57] The actual function of this unique sequence remained enigmatic until the mid-2000s, when Francisco Mojica and Christine Pourcel independently observed that the spacer regions between the repeat sequences are homologous to sequences of bacteriophages, prophages, and plasmids.[58,59] The function of the CRISPR-Cas system as a prokaryotic acquired immune system was finally experimentally proven in 2007, using the lactic acid bacterium *Streptococcus thermophilus*.[60] Finally, the subsequently Nobel prize-winning manuscript was published by Doudna, Charpentier, and colleagues in 2012 demonstrating that the purified Cas9-CRISPR RNA (crRNA) complex was capable of cleaving the target DNA *in vitro*.[54,61] Shortly thereafter, the CRISPR-Cas system of *Streptococcus pyogenes* was applied to perform genome editing in human nerve and mouse kidney cells.[62,63]

1.3.2 CRISPR genome editing

The CRISPR/Cas system encompasses a variety of components which differ widely in mechanisms of action and offer therapeutic potential by direct genome interaction and/or editing. Despite the complexity of the Cas family, all systems share a requirement for CRISPR RNA (crRNA) for defined target specificity whilst type II variants have an additional requirement for trans-activating RNA (tracrRNA),[64,65] which forms a scaffold structure. For gene editing applications, the two CRISPR RNAs described above are joined as one small guide RNA (sgRNA), which greatly simplifies delivery. The Cas9: sgRNA complex randomly interrogates DNA in the cell, searching first for the appropriate protospacer adjacent motif (PAM), a short motif adjacent to the target sequence. Upon recognition of the PAM sequence, the Cas9 protein unwinds the DNA, allowing the Cas9-associated sgRNA to hybridize with the exposed DNA strand (the protospacer). If the DNA sequence matches the sgRNA target sequence, the HNH

and RuvC catalytic domains of the endonuclease cleave both strands of the target DNA, generating a double stranded break (DSB).[54,66]

1.3.2.1 Repair of Cas-induced DSBs

In eukaryotic organisms, Cas9-induced DSBs are mended either by error prone non-homologous end joining (NHEJ)[67-71] or homology-directed repair (HDR).[69,72-74] Typically, CRISPR-induced DSBs are repaired by NHEJ, an efficient and prevalent mechanism in human cells that results in random insertions or deletions (indels) and gene disruption in the target region. HDR is a well-established mechanism that can be harnessed to insert a specific DNA template for precise restoration of the DNA sequence, with limited off-target activity or on-target alterations.[75] HDR-mediated insertion, however, requires the presence of the correct template and is typically characterized by lower efficiencies than NHEJ repair. In addition, the correction of a point-mutation by HDR has been shown to be highly ineffective particularly in non-dividing cells, such as those present in the retina, and the dsDNA break formation by Cas9 nuclease generates undesired indel mutations at a substantial frequency that annuls the potential benefit from corrected mutation.[76] Thus, correction of patient derived iPSCs, followed up autologous transplantation of the corrected retinal cells, has been readily employed for CRISPR-mediated HDR in the retina. Bassuk and colleagues utilized CRISPR-Cas9-triggered HDR to repair an *RPGR* mutation that causes X-linked RP in primary fibroblasts that were transduced to produce patient-specific iPSCs.[77] The authors showed 13% correction of the c.3070 G > T mutation and conversion of the wild-type allele, providing proof-of-concept for a targeted iPSC-based transplantation approach for retinal disease. Similar studies have demonstrated correction of mutations in patient-derived iPSCs in *RPGR, Pde6β, MAK, CEP290, N2RE3,* and *RHO* genes.[78-82] Recently, Cai and colleagues reported HDR-mediated correction of a mutation causing autosomal dominant retinitis pigmentosa (adRP) *in vivo*.[83] The authors developed a Cas9/*Escherichia coli* recombinase

A (RecA) protein technique, which incorporated *Streptococcus pyogenes* Cas9 (SpCas9) and sgRNA-targeted RecA, to precisely correct the naturally occurring *Pde6b* missense mutation in postnatal *rd1* mice. Similarly, Suzuki and colleagues devised a homology-independent targeted integration (HITI) strategy, which showed enhanced DNA knock-in efficiencies in non-dividing cells.[84]

The NHEJ DNA repair pathway is currently the more commonly adopted approach in developing treatments for retinal diseases, especially for mutations arising from autosomal dominant diseases. Through careful design of the guide RNA, the mutant allele can be preferentially disrupted while preserving the wild-type allele. In the absence of haploinsufficiency mechanisms, this could ameliorate disease phenotypes and has been successfully demonstrated across several genetic targets and retinal disease models. Bakondi and colleagues demonstrated the first *in vivo* functional correction of an inherited dominant mutation using CRISPR,[85] providing proof-of-concept that CRISPR/Cas9 can be utilized to treat retinal degenerations. The authors showed that a single subretinal injection of gRNA/Cas9 plasmid in combination with electroporation generated allele-specific disruption of the S334ter mutation (Rho^{S334}) in a transgenic mouse model, which prevented retinal degeneration and improved visual function. Subsequently, the Broccoli, Liu, and Li groups described a spacer-mediated allele-specific knockout approach to specifically inactivate the P23H *RHO* mutant, which represents approximately half of all *RHO*-associated adRP cases.[85-87] To broaden the breadth of targetable *Rho* mutations, Tsai and colleagues developed a two-pronged ablate-and-replace strategy that destroyed expression of endogenous genes in a mutation-independent manner and enabled expression of functional protein through exogenous cDNA.[88] The authors validated the approach in two human *RHO* mutation knock-in mouse models, Rho^{P23H} and Rho^{D190N}, leading to significant survival of functioning

photoreceptors. More recently, a similar approach was utilized to target autosomal dominant cone-rod dystrophy (CORD6) in mice and primates.[89]

Editor design	Delivery method	Model	Gene Target	Mutation	Model of inheritance	Summarized outcomes	Ref
Genome editing							
SpCas9: HDR	Nucleofection	Patient-derived iPSCs	*MAK*	c.1513ins353	Autosomal recessive RP	Restoration of expression of the wild-type allele.	[80]
SpCas9: HDR	Plasmid transfection	Patient-derived iPSCs	*NR2F3*	*c.119-2A>C; c.219G>C (p.Arg73Ser)*	Enhanced S-cone syndrome	Restoration of expression of the wild-type allele.	[78]
SpCas9: HDR	Plasmid electroporation	*rd10* mice	*Pde6b*	*c.1678C>T (p.Arg560Cys)*	Autosomal recessive RP	Correction of mutation with improved visual responses up to 3 months post-treatment.	[81]
SpCas9 /RecA: HDR	Plasmid electroporation	*rd1* mice	*Pde6b*	*c.1041C>A (p.Tyr347ter)*	Autosomal recessive RP	Correction of mutation promoted photoreceptor cell survival and improved visual responses.	[83]
SpCas9: HDR	Plasmid transfection	Patient-derived iPSCs	*RPGR*	*c.3070G>T (p.Glu1024X)*	X-linked RP	13% correction of the mutant allele by conversion to wild-type.	[77]
SpCas9: HDR	Plasmid electroporation	Patient-derived iPSCs and retinal	*RPGR*	*c.1685_1686delAT c.2234_2235delGA*	X-linked RP	Correction of mutation in iPSCs with development into retinal organoids	[79]

		organoids				revealing correction of photoreceptor defects.	
SpCas9 & SaCas9 : NHEJ & HDR	Nucleofection & electroporation	Patient-derived iPSCs	*CEP290*	*c.2991+1665A>G*	Leber congenital amaurosis	Restoration of expression of the wild-type allele.	[80]
SaCas9: NHEJ	AAV5	Retinal explants, IVS26 knock-in mice and non-human primates	*CEP290*	*c.2991+1665A>G*	Leber congenital amaurosis	16% functional editing in retinal explants, 21% in knock-in mice, 28% in non-human primates with evidence of safety and efficacy.	[90]
SaCas9: NHEJ	AAV5	GC knockout mice and macaques	*Gucy2e / GUCY2D*	*Wild-type*	Autosomal dominant CORD	Editing achieved in 44% of transduced mouse photoreceptor cells and 6-20% in macaques.	[89]
SaCas9 & SpCas9: NHEJ & HDR	Transfection & AAV5	Patient-derived iPSCs & P23H knock-in pigs	*RHO*	*c.163C>A (Pro23His)*	Autosomal dominant RP	Repression of the mutant variant.	[80]
SpCas9 : NHEJ	Plasmid electroporation	Rho^{S334} rat	*Rho*	*S334ter*	Autosomal dominant RP	Mutant allele-specific disruption with subsequent prevention in retinal degeneration	[85]

						evident by 9-fold increase in photoreceptor nuclei.	
SpCas9-VQR : NHEJ	Plasmid electroporation	P23H knock-in mice	*Rho*	*c.163C>A (Pro23 His)*	Autosomal dominant RP	Mutant allele-specific disruption with a subsequent 20% increase in wild-type mRNA with delayed retinal degeneration.	[87]
SpCas9 : NHEJ	Plasmid electroporation	P23H knock-in mice	*Rho*	*c.163C>A (Pro23 His)*	Autosomal dominant RP	Reduction in mutant protein.	[91]
SpCas9 : NHEJ & supplementation	Dual AAV8 Y733F	D190N knock-in mice P23H knock-in mice	*Rho*	*c.163C>A (Pro23 His) c.568G>A (Asp190 Asn)*	Autosomal dominant RP	Mutation-specific gene destruction with provision of wild-type gene for functional protein and improved retinal function.	[88]
SpCas9-VQR : NHEJ	Plasmid electroporation & AAV9-PHP.B	P23H knock-in mice	*Rho*	*c.163C>A (Pro23 His)*	Autosomal dominant RP	10% editing of photoreceptor cells achieved *in vivo*.	[86]
CjCas9 - NHEJ	AAV9	Wild-type mice	*Vegfa & Hif1a*	*Wild-type*	Choroidal neovascularization	Knockdown of *Vegfa* and *Hif1a* with associated reduction in the area of laser induced choroidal neovascularization.	[92]

SpCas9 - HITI	Dual AAV8 or AAV9	Royal College of surgeons rat	*Mertk*	*1.9kb mutation*	Autosomal recessive RP	Expression of Mertk with associated improved photoreceptor layer thickening and visual responses.	[84]
Base editing							
SpCas9 -CBE : TARGET-AID	Plasmid transfection	HEK293A-CFH	*CFH*	*c.1204C>T (Tyr402His)*	Age-related macular degeneration	Cytosine to thymine correction in 21% of sequencing reads with minimal off target edits.	[93]
SpCas9 -ABE	Lentivirus	*rd12* mice	*Rpe65*	*c.130C>T (p.R44X)*	Autosomal recessive RP	Mutation correction in 29% of assessed genetic material extracted from treated eyes with associated restoration of visual function.	[94]
Epigenetic editing							
SpCas9 -KRAB : CRISPRi	Dual AAV8	*Rho* knockout and *rd10* mice	*Nrl*	*Wild-type*	Autosomal recessive RP	Reprogramming of rod photoreceptors to achieve 25% increase in cone preservation with associated improved visual acuity.	[95]

Table 1.1 | Summary of *in vivo* CRISPR studies targeting inherited retinal disease

Summary of currently published studies investigating CRISPR-Cas mediated genome and epigenome engineering *in vivo* targeting retinal disease. Models refer to mice unless otherwise specified. Summary table captures studies published to October 2022.

1.3.3 HDR-independent DNA editing systems

Although HDR-mediated gene editing can be harnessed to insert a specific DNA template for precise restoration of the DNA sequence, this pathway is characterized by low efficiency and high rates of undesired indel mutations that nullify the potential benefit from repairing the mutation.[75] Recently, CRISPR-Cas-mediated single base pair editing systems (or 'base editing' systems) have been devised to bypass these limitations.[96-98] DNA base editing and the more recent prime editing technologies have remarkable potential as therapeutic tools to correct disease-causing mutations in the human genome. CRISPR-mediated HDR are confined to editing within dividing-cells, since these pathways are restricted to the S and G2 phases of the cell cycle. Conversely, base editing employs cellular mismatch repair machinery and can be applied to reverse these defects in both dividing and terminally differentiated cell types.[99] Gene therapy is a major area where DNA base editing and prime editing toolkits can be applied because they have already been adapted to characterize, model, and correct the underlying causes of human genetic conditions.

Two classes of DNA base editors have been described: cytosine base editors and adenine base editors.[100,101] DNA base editors encompass two key components: a Cas enzyme for programmable DNA binding and a single-stranded DNA modifying enzyme for targeted nucleotide alteration. Collectively, all four transition mutations (C→T, T→C, A→G, and G→A) can be installed with the available CRISPR-Cas base editor systems.[102] Recently, Kurt *et al.* described the engineering of two novel base editor architectures that

can efficiently induce targeted C-to-G base transversions.[103] In addition, recent studies report dual base editor systems for combinatorial editing in human cells.[104-106] Together, these new base editors expand the range of DNA base editors to transversion mutations and may allow for targeting of more complex compound edits than are currently achievable by a single DNA base editor.

1.3.3.1 Cytosine base editing

The first-generation base editor (CBE1) was developed by David Liu and co-workers in 2016 [96,107]. It was engineered by fusing a rat-derived cytosine deaminase Apolipoprotein B MRNA Editing Enzyme Catalytic Subunit 1 (APOBEC1) to the amino terminus of catalytically deficient, or "dead", Cas9 (dCas9). In a narrow window of the non-targeted strand, CBE1 deaminates cytosine to uracil. Uracil is then recognized by cell replication machinery as a thymine, resulting in a C-G to T-A transition. Importantly, although CBE1 mediated efficient, targeted base-editing *in vitro* (up to 37% editing with a 1.1% indel formation rate), it was not effective in human cells.[107] This decrease was largely due to cellular-mediated repair of the U-G intermediate in DNA by the base excision repair (BER) pathway. BER of U-G in DNA is initiated by uracil N-glycosylate (UNG), which recognizes the U-G mismatch and cleaves the glycosidic bond between the uracil and the deoxyribose backbone of DNA, resulting in reversion of the U-G intermediate created by the base editor back to the C-G base pair.[108,109] Keeping in view the low editing efficiency and limitations of CBE1, a series of improved base editors were developed further. To improve base editing efficiency, a second-generation cytosine base editor (CBE2) was developed by fusing an uracil DNA glycosylase inhibitor (UGI) to the C-terminus of BE1, inhibiting the activity of UDG. The inhibition of BER by BE2 resulted in a threefold increase in editing efficiency in human cells. To further improve editing efficacy, BE3 was developed by restoring histidine at position 840 (H840, HNH catalytic domain) in dCas9 to generate a base editor that uses Cas9 nickase (nCas9). The variant induces a nick in the

G-containing strand of the U-G intermediate (non-edited DNA strand) to bias cellular repair of the intermediate towards a U-A outcome, further converted to T-A during DNA replication. This modification further increased editing efficiency by sixfold in BE3 over BE2.

Further optimization of CBE was performed to reduce indel formation during base editing, improve editing efficiency, and narrow the editing window. An improved fourth-generation cytosine base editor (CBE4) was generated by fusing an additional copy of UGI to the N terminus of nCas9 with an optimized 27 bp linker.[110] YEE-BE3 was developed by screening several mutations previously reported to modulate the catalytic activity of cytosine deaminases in the APOBEC family to generate an improved rAPOBEC1 with a narrower editing window and reduced "bystander editing" compared to CBE3. Gam, a DNA-binding protein from bacteriophage Mu, can form a complex with free-ends of DBSs, thus preventing NHEJ-mediated repair and reducing indel formation.[111] These changes resulted in BE4-Gam, characterized by higher base editing efficiency, increased product purity, and decreased indel frequency.[112] Nevertheless, Gam binding has been shown to induce the death of DSB-containing cells,[113] a key limitation towards its therapeutic adaptability.

Separately, Koblan *et al.* added two Nuclear Localization Signals (NLS) to nCas9 and performed codon-optimization and ancestral sequence reconstruction on APOBEC, yielding BE4max and ancBE4max.[114] Another base-editing system, Target-AID (activation-induced cytidine deaminase), was developed which was composed of nCas9, *Petromyzon marinus* cytidine deaminase 1 (pmCDA1).[115] The use of alternative cytosine deaminase enzymes yielded base editors with alternative sequence motif preference and the ability to efficiently edit methylated cytosines. Most recently, Liu and colleagues used phase assisted continuous evolution (PACE) to evolve CBEs and generate evoAPOBEC1-

BE4max, which can efficiently edit cytosine in G/C sequences (a disfavored context for wild-type APOBEC1 deaminase).[116]

To increase the number of targetable bases, researchers have developed base editors incorporating different CRISPR-associated nuclease enzymes. A variety of engineered Cas9 variants with altered PAM sequences and improved cleavage specificity have been developed and may allow for further expansion of the targeting scope of CRISPR-base editing reagents.[117-120] These constructs enable efficient single-vector AAV delivery and may prove especially useful for therapeutic applications that are constrained by viral-vector packaging capacity.

1.3.3.2 Adenine base editing

The cytosine base editor is limited to installing a C–G to T–A mutation, greatly restricting the range of correctable disease-causing mutations. Importantly, cytosines are vulnerable to high rates of spontaneous cytosine deamination,[121] and nearly half of all pathogenic point mutations in principle can be corrected by converting an A-T base pair to a G-C base pair. As such, base-editing capabilities and study of genetic diseases were further expanded by the development of a new class of adenine base editors that could induce A to G conversions.[122] ABE-mediated DNA editing operates under a similar mechanism as CBE. The ABE-dCas9 fusion binds to a target DNA sequence in a guide RNA-programmed manner, and the deoxyadenosine deaminase domain catalyzes an adenine to inosine transition. In the context of DNA replication, inosine is interpreted as guanine, and the original A-T base pair is replaced with a G-C base pair at the target site. Unlike cytosine deaminases, ssDNA adenosine deaminase enzymes do not occur in nature. Attempts at utilizing RNA adenosine deaminases to act on DNA resulted in no detectable RNA editing.[122] David Liu and group overcame this limitation through extensive protein engineering and directed evolution of *E. coli* tRNA adenosine

deaminase, TadA (ecTadA). EcTadA converts adenine to inosine in the single-stranded anticodon loop of $tRNA^{ARG}$, and shares sequence similarity with the APOBEC family.

The first-generation adenine base editors were developed through an antibiotic resistance complementation approach in bacteria. To test TadA on a DNA target, *E. coli* cells were equipped with TadA mutants and defective antibiotic resistance genes. To grow in the presence of antibiotic, a mutant TadA-dCa9 fusion had to correct the targeted adenine in a mutant chloramphenicol resistance gene. The first-generation ABE (ABE1.2) was generated by fusing the evolved TadA variant (TadA*) to the N-terminus of nCas9 through XTEN (a 16 amino acid linked used in BE3), with the C terminal of nCas9 fused with a nuclear localization signal (TadA*-XTEN-nCas9-NLS).[122] In comparison with cytosine base editing, adenine base editing by ABE yields a much cleaner product that has virtually no indels, and there are no reports of significant off-target (A-to-non-G) edits to date. Consistent with this observation, unlike UGI-mediated inhibition of UDG in CBEs, ABE editing in cells lacking alkyl adenine DNA glycosylase (AAG), the enzyme known to recognize and remove inosine in DNA, failed to increase editing efficiency or product purity compared with cells containing wild-type AAG. Indeed, even early generations of ABE recovered ≥99.9% pure product with a negligible rate of indels (≤0.1%).[122-124]

In its native context, TadA acts as a homodimer, with one monomer catalyzing deamination and the other monomer enabling tRNA substrate binding.[125] To optimize ABEs, Gaudelli *et al.* engineered a single-chain heterodimer comprised of a wild-type non-catalytic TadA monomer and evolved ecTadA monomer (TadA-TadA*). To improve editing efficiency, further optimization of ABE was performed. Extensive PACE and protein engineering resulted in seventh generation ABEs (ABE7.10), which converted target A-T to G-C efficiently (~50%) in human cells.[122]

Only about one-quarter of pathogenic transition mutations encompass an appropriately located NGG PAM site that facilitates SpCas9-mediated base editing. Unlike CBEs, which have proven to be broadly customizable with many Cas orthologs, ABEs have shown limited compatibility with Cas9 of any origin other than SpCas9. Although some homologs such as SaCas9 and circularly permuted Cas9 (CP-Cas9) have been adapted,[123] editing efficiencies are substantially lower than those demonstrated with CBE counterparts.[126] This incompatibility is due to the low DNA-bound residence time of non-SpCas9, coupled with the slow enzymatic rate of deoxyadenosine deaminase. To address this problem, Richter *et al.* utilized phage-assisted continuous and non-continuous evolution (PACE and PANCE) methods to enhance the catalytic rate of the deoxyadenosine deaminase enzyme by 590-fold compared to that of ABE7.10.[127] This next generation of ABEs, designated ABE8e, show greatly enhanced activity and compatibility with diverse Cas9 homologs. As expected, the targeting scope of ABE8e also increased off-target RNA and DNA editing. However, the authors show that the off-target editing can be ameliorated by introduction of an additional point-mutation (V106W).[127] Together, ABE8e expands the targeting range, editing efficiency and broad functionality of ABEs.

1.3.3.3 Prime editing

Despite the profound capabilities of CBEs and ABEs to edit the DNA, a major limitation of the current base-editing technologies has been the ability to generate precise base-edits beyond the four transition mutations. Recently, a method to overcome these shortcomings, known as prime editing, was described by Anzalone and colleagues.[128] As with CRISPR-mediated base editing, prime editing does not rely on DSBs. Prime editors use an engineered reverse transcriptase fused to Cas9 nickase and a prime editing guide RNA (pegRNA). Importantly, the pegRNA differs significantly from regular sgRNAs and plays a major role in the system's function. The pegRNA contains not only (a) the sequence complimentary to the target sites that directs nCas9 to its target sequence, but

also (b) an additional sequence spelling the desired sequence changes.[128] The 5′ of the pegRNA binds to the primer binding site (PBS) region on the DNA, exposing the non-complimentary strand. The unbound DNA of the PAM-containing strand is nicked by Cas9, creating a primer for the reverse transcriptase (RT) that is linked to nCas9. The nicked PAM-strand is then extended by the RT by using the interior of the pegRNA as a template, consequently modifying the target region in a programmable manner. The result of this step is two redundant PAM DNA flaps: the edited 3′ flap that was reverse transcribed from the pegRNA and the original, unedited 5′ flap. The choice of which flap hybridizes with the non-PAM containing DNA-strand is an equilibrium process, in which the perfectly complimentary 5′ would likely be thermodynamically favored. However, the 5′ flaps are preferentially degraded by cellular endonucleases that are ubiquitous during lagging-strand DNA synthesis.[129] Thus, the 5′ flap is usually degraded, and the 3′ flap inserted and ligated. In the PE3 system, the introduction of a nick in the non-edited strand using a separate gRNA serves to direct the prime-editing complex to the unedited strand. As a result, the edited strand is thus preferentially used as a template for DNA repair, and the resulting heteroduplex containing the unedited strand and edited 3′ flap is preferentially resolved and stably integrated into the host genome via cellular replication and repair process.

The first generation of PEs (PE1) was comprised of Moloney murine leukemia virus reverse transcriptase (M-MLV RT), linked to the c-terminus of nCas9 and pegRNA, which was expressed on a second plasmid. The efficiency of PE1 reached maximum editing efficiency of 0.7–5.5%.[128] To further enhance the efficiency of the reverse transcriptase, Anzalone and colleagues tested different M-MLV RT variants that have been shown to enhance binding, enzyme processivity, and thermostability. Finally, as was previously applied to enhance editing in CBE and ABE systems, the authors directed a separate sgRNA to introduce a nick in the non-edited strand, thus directing DNA repair

to that strand using the edited strand as a template. This yielded the latest generation prime editor, designated PE3, which performed all 12 possible transition and transversion mutations (24 single-nucleotide substitutions) with average editing efficiencies of 33% (±7.9%).[128] The number of off-target effects observed with PEs was greatly reduced, likely due to the need for complementation at Cas9 binding, PBS binding, and RT product complementation for flap resolution.[128] Prime editing owns other advantages over previous CRISPR-mediated base-editing approaches, including less stringent PAM requirements due to the varied length of the RT template and no "bystander" editing. Notwithstanding, prime editing is still in its infancy, and its specificity and potential for off-target modifications remain to be studied. The latest generations of base-editors are much more closely characterized, particularly *in vivo*, and offer higher efficiency rates and lower-index formation. Thus, at this stage these tools should be used over prime editors whenever possible. In any case, the prime editing system is an enormous milestone in the development of a universal method for genome editing, and its clinical adaptation towards the correction of known pathogenic mutations may prove tremendous.

Base Editor	Architecture	Editing Efficiency	Notes	Refs
BE1	rAPOBEC1- dCas9	0.8% - 7.7% in human cells	First-generation BE	107
BE2	rAPOBEC1-dCas9-UGI	Up to 20%	Prefers TC motifs	107
HF2-BE2	rAPOBEC1-HF2 nCas9- UGI	11.6 - 50%	Prefers TC motifs	130,131
BE3	rAPOBEC1-SpnCas9-UGI	Varies widely by cell type & target genes	Prefers TC motifs	107,112, 131-144
HF-BE3	rAPOBEC1-HFnCas9-UGI	21 ± 3%	Reduced off-target editing	132

YE1-BE3	rAPOBEC1 (W90Y, R126E) SpnCas9-UGI	Comparable to BE3	Narrowed editing window	110
EE-BE3	rAPOBEC1 (R126E, R132E) SpnCas9-UGI	Comparable to BE3	Narrowed editing window	110
YEE-BE3	rAPOBEC1 (W90Y, R126E, R132E) -SpnCas9-UGI	Comparable to BE3	Narrowed editing window	110
VQR-BE3	rAPOBEC1 – VQR SpnCas9-UGI	14.5 – 52%	Expanded PAM targeting	110
EQR-BE3	rAPOBEC1 – EQR SpnCas9-UGI	7.5 – 35%	Expanded PAM targeting	110
VRER-BE3	rAPOBEC1 – VRER SpnCas9-UGI	11 – 32%	Expanded PAM targeting	110
SaKKHBE3	rAPOBEC1 – KKH SanCas9-UGI	14–62%	Expanded PAM targeting	110
FNLS-BE3	rAPOBEC1-SpnCas9-UGI	41–93%	Additional N-terminus NLS; Increased editing efficiency	144
RA-BE3	rAPOBEC1 (RA)-SpnCas9-UGI	30–58%	Increased editing efficiency	144
A3A-BE3	hAPOBEC3A-SpnCas9-UGI	22.5%	Preferential deamination of cytidines in a TCR motif	145
eA3A-HF1-BE3-2xUGI	APOBEC3A-HF1 SpnCas9-UGI-UGI	17.5%	Deaminates cytosines with preference TCR>TCY>VCN; Increased editing efficiency	145
eA3A-Hypa-BE3-2xUGI	APOBEC3A-Hypa SpnCas9-UGI-UGI	14%	Deaminates cytosines with	145

			preference TCR>TCY>VCN; Increased editing efficiency	
hA3A-BE3	hAPOBEC3A-SpnCas9-UGI	2 – 62%	Efficient editing in methylated region and in GpC context	[146]
hA3B-BE3	hAPOBEC3B-SpnCas9-UGI	2 – 62%	Intermediate editing efficiency	[146]
hA3G-BE3	hAPOBEC3G-SpnCas9-UGI	2 – 62%	Greatly decreased editing efficiency	[146]
hAID-BE3	hAPOBEC3A-SpnCas9-UGI	2–62%	Intermediate editing efficiency	[146]
SaCas9-BE3	rAPOBEC1-SanCas9-UGI	~50–75%	Expanded targeting range	[110]
xCas9-BE3	rAPOBEC1-xnCas9-UGI	37% (NGG PAM)	Expanded targeting range	[139]
ScCas9-BE3	rAPOBEC1-ScnCas9-UGI	19–41%	Affinity to minimal 5′-NNG-3′ PAM sequences	[147]
SniperCas9-BE3	rAPOBEC1-SnipernCas9-UGI	0.04–50%	Increased sgRNA scope; further reduced off-target activities	[148]
iSpyMac-BE3	rAPOBEC1-iSpyMacnCas9-UGI	50%	Elevated editing efficiencies on 5′-NAAN-3′ targets	[149]
Target-AID	SpnCas9-CDA1-UGI	17–55%	First-generation base editor	[115]
Target-AID-NG	SpnCas9 (NG)-CDA1-UGI	1–38%	Expanded targeting range	[150,151]
CRISPR-X	SpdCas9-MS2-hAID	N/A	High activity; used for random mutagenesis	[152]

TAM	SpdCas9-hAID (P182X)	N/A	High activity; used for random mutagenesis	[153]
BE-PLUS	SunTag-SpnCas9-scFv-rAPOBEC1-UGI	2 – 38%	Broadened targeting window; reduced off-target editing	[154]
BE4	rAPOBEC1-SpnCas9-UGI-UGI	Varies widely by cell type & target genes	Increased editing efficiency	[112,114,131,140]
BE4-Gam	Gam-rAPOBEC1-SpnCas9-UGI-UGI	17 – 58%	Increased editing efficiency and product purity	[112,140]
BE4-Max	rAPOBEC1-SpnCas9-UGI-UGI	69 – 77%	Codon optimized for mammalian cells	[114]
AncBE4-Max	rAPOBEC1-SpnCas9-UGI-UGI	75 – 84%	Ancestral reconstruction of the deaminase component	[114]
SaCas9-BE4	rAPOBEC1-SanCas9-UGI-UGI	25 – 60%	Expanded PAM targeting	[112]
SaCas9-BE4-Gam	Gam-rAPOBEC1-SanCas9-UGI-UGI	42 – 67%	Increased editing efficiency and product purity	[112]
evoBE4max	rAPOBEC1-SpnCas9-UGI-UGI	Up to plateau levels (~60 – 80%)	Improved efficiency in GC context	[116]
evoFERNY-BE4max	rAPOBEC1-SpnCas9-UGI-UGI	Up to plateau levels (~60 – 80%)	29% smaller than APOBEC1	[116]
Cas12a-BE	rAPOBEC1-dLbCpf1-UGI	3 – 46%	Can target T-rich PAM sequence	[155]
ABE7.8/9/10	ecTadA-ecTadA*-SpnCas9	1.7 – 20%	First generation ABE	[122]
xCas9-ABE7.10	ecTadA-ecTadA*-nxCas9	69% (NGG PAM)	Expanded PAM targeting	[139]

VQR-ABE	ecTadA-ecTadA*-Sp VQR nCas9	20%	Expanded PAM targeting	[124]
Sa(KKH)-ABE	ecTadA-ecTadA*-Sa KKH nCas9	16%	Expanded PAM targeting	[124]
ABEmax	ecTadA-ecTadA*-SpnCas9	27 – 52%	Improved editing efficiency	[114]
ABE7.10max	ecTadA-ecTadA*-SpnCas9	19.2 – 40.7%	Improved editing efficiency	[156]
ABE8e	ecTadA-ecTadA*-SpnCas9	18% – 86%	Improved editing efficiency	[127]
PE1	dSpCas9-MMLV-RT	0.7 – 5.5%	First generation PE	[128]
PE2	dSpCas9-MMLV-RT	1.6- to 5.1-fold improvement over PE1	Targets all transition / transversion mutations; small indels	[128]
PE3	nSpCas9-MMLV-RT	20 – 50%	Targets all transition / transversion mutations; small indels	[128]

Table 1.2 | Evolution of CRISPR base editing and prime editing tools

Summary table of CRISPR base editing and prime editing tools, as of August 2022. Editing efficiencies *in vitro* unless otherwise stated. *Engineered TadA domain

1.3.4 RNA editing

Site-directed RNA editing is a base editing approach that targets the transcriptome rather than the genome. Post-transcriptional mRNA modifications occur naturally to a number of native transcripts in mammalian cells by a class of endogenous Adenosine Deaminase Acting on RNA (ADAR) enzymes. These deaminases convert adenosine bases to inosine, which is structurally similar to guanosine and read as such during splicing

and translation.[157] This effectively creates an A>G edit in RNA which can be harnessed for the correction of G>A mutations. RNA editing strategies can be broadly separated into two approaches depending on what ADAR is used. Exogenous ADAR strategies deliver the full-length ADAR protein or the deaminase domain ($ADAR_{DD}$) fused to another RNA binding protein to recruit the target RNA. Endogenous approaches do not introduce ADAR into cells but rely on recruiting the endogenously expressed enzyme. A range of strategies have now been engineered to direct ADAR to edit targets of interest.[158]

1.3.5 Epigenome editing

Epigenome editing, the precise placement of epigenetic marks with programmable Cas- fusions, is a valuable method for research, biotechnology, and medicine by enabling control over gene regulation without changing DNA sequence. CRISPRi interference (CRISPRi) and CRISPR activation (CRISPRa) are techniques derived from the CRISPR-Cas9 system that are used to down- and up-regulate expression of a target gene by influencing its transcription. Transcription in eukaryotes is determined by interactions between DNA elements and regulatory proteins. Briefly, RNA polymerase II forms a complex with a range of transcription factors, which determine its ability to bind to a gene's promoter. Initiation of transcription is then determined by interactions with distal regulatory elements. Transcription factors contain specific protein domains which decrease or increase gene expression (called repressor and activator domains, respectively) through interactions with other cellular proteins.

The CRISPRi and CRISPRa systems typically consist of two components. Firstly, a gRNA which targets a regulatory region of a gene (usually the promoter but distal regulatory regions can also be targeted). Secondly, a fusion protein of catalytically inactive Cas9 and transcriptional activator or repressor domains.[54] The dCas9 protein binds to DNA via the gRNA but cannot cleave DNA as it is an inactive nuclease. Here

the repressor or activator domains act as transcription factors, influencing the transcription rate by triggering native regulatory pathways. When targeting the promoter, the optimal gRNA binding site relative to the transcriptional start site is roughly -50 to +250 bp for CRISPRi and -40 bp to +400 bp for CRISPRa.[159,160]

1.3.5.1 Transcriptional repression

Site-specific gene silencing with engineered Cas9-repressor fusions offers an alternative to traditional gene suppression methods such as RNA interference (RNAi) and nuclease-mediated gene knockout. RNAi silences target protein-coding genes by mRNA transcript degradation and translational inhibition mediated by small interfering RNAs. RNAi, however, has been limited by inefficient knockdown,[69,161] off-target effects,[162,163] and toxicity associated with oversaturation of endogenous microRNA pathways.[64,162,164] Furthermore, programmable Cas9-repressors can target anywhere in the genome, facilitating silencing of regulatory elements and non-coding genes that cannot be targeted by RNAi. Genes and regulatory elements can also be disrupted with classic site-specific nucleases,[165-168] but nuclease-mediated genome editing is a stochastic and often inefficient process that also alters DNA sequence permanently, precluding dynamic epigenetic regulation.

While dCas9 alone can be used to drive CRISPRi, fusion of a repressor domain significantly improves knock down.[169-172] One of the most commonly used repressors is the Krüppel-associated box (KRAB) repressor which alters the histone methylation state of the gene locus.[159,170,173,174] Eukaryotic DNA is wound around histone proteins that can be chemically modified, influencing how closely they associate.[175] The KRAB repressor interacts with histone modifying proteins to create a tightly wound histone state which is inaccessible to RNA polymerase II and therefore reduces gene transcription.[159,173,174,176-178] dCas9-KRAB has driven clinically significant gene repression *in vivo* in a range of disease models, including retinitis pigmentosa, familial hypercholesterolemia, and

obesity.[95,179,180] Although eukaryotic cells host a variety of potential epigenetic modifying domains, only a small fraction of which have been utilized for epigenome engineering applications thus far.

1.3.5.2 Transcriptional activation

The direct fusion of potent transcriptional effector domains to designed DNA binding domains (DBDs) can induce transcriptional activation when targeted to endogenous genes. Prior to CRISPRa, increasing expression of a target gene relied on gene augmentation. Overexpression of transgenes by gene augmentation may be associated with toxic effects to retinal cells.[181-183] The level of gene activation with CRISPRa has the potential to be tailored by varying the number of activators recruited to a particular site, ensuring the level of expression is non-toxic.[184,185]

One of the first transcriptional activator effectors linked to DBDs to activate coding and noncoding genes via targeting of promoters and regulatory elements was VP64, a tetramer of VP16 domains,[186-193] though this system drove only modest levels of gene activation. Recruitment of multiple activator effectors to a single target locus is often required to elicit a robust transcriptional response.[194-196] This is achieved through the delivery of multiple gRNAs or by creating more complex fusion proteins. A comparison of CRISPRa constructs revealed that the SunTag, VPR, and SAM systems typically drive the highest activation.[197] In the SunTag system, dCas9 is fused with a peptide chain containing 10 binding sites for the single-chain fragment variable(scFv)-GCN4 scFv intrabody, and VP64 is fused with scFv-GCN4. This allows the recruitment of multiple VP64 copies to a promoter with a single gRNA.[198] The dCas9-VPR system uses a quadruple fusion protein of dCas9 to three transcriptional activators: VP64, p65, and Rta.[197] The SAM system delivers dCas9-VP64 and a modified gRNA which contains a binding site for the fusion protein MPH. MPH includes activator domains p65 and heat

shock factor 1, allowing the recruitment of these plus VP64 to the target site.[199] Recently, p300 core fusions were shown to be particularly promising for transcriptional activation, as they do not require multiplexing and can activate distal enhancers that were unresponsive to dCas9-VP6448. Finally, dCas9 can be fused to proteins to deliver heritable changes to gene activity. These strategies can include modifying the methylation status of promoters or modifying chemical tags on histone molecules.[200,201]

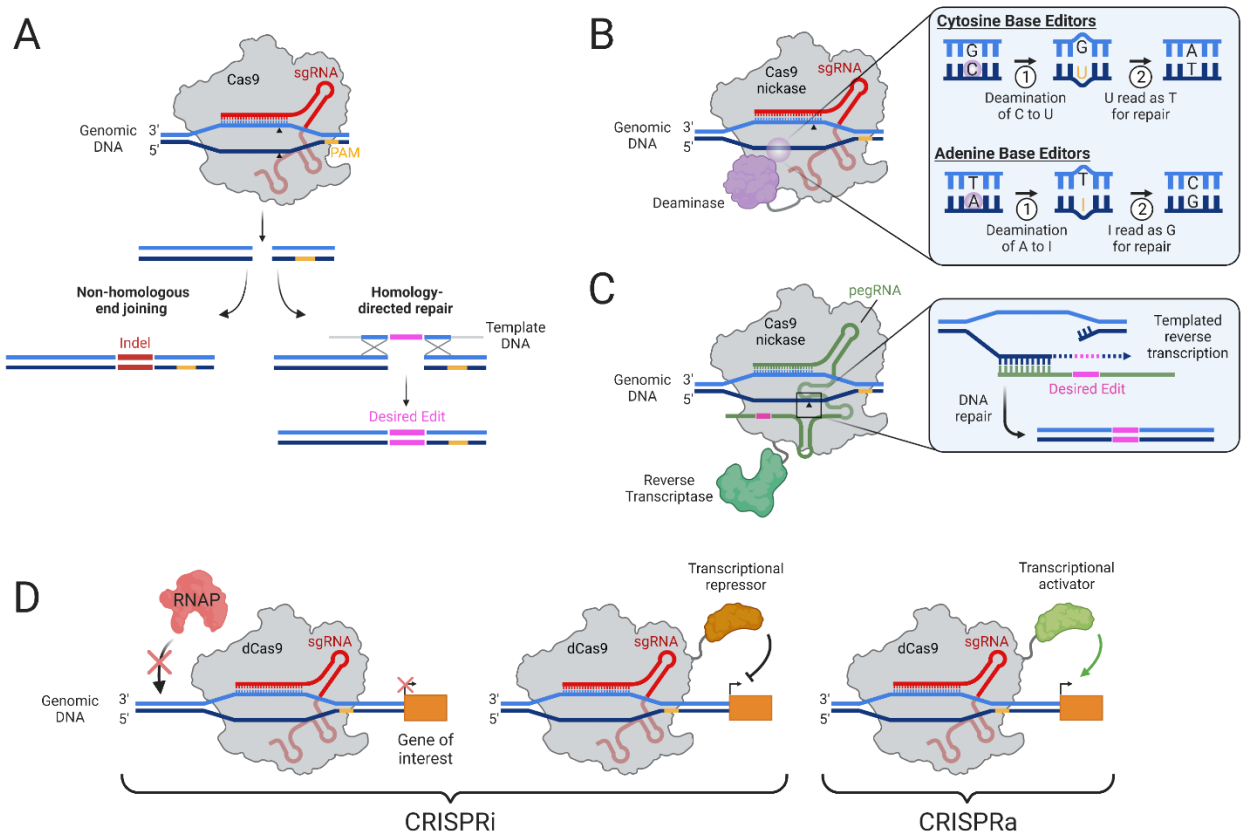


Figure 1.5 | Summary of therapeutic CRISPR-based genome-editing strategies

A. CRISPR-Cas9-induced double-strand breaks. In eukaryotic cells, breaks are repaired through either the error-prone non-homologous end-joining pathway, leading to indel mutations, or the high-fidelity homology-directed repair pathway, which may be leveraged to introduce precise edits in dividing cells. *Black triangles* indicate Cas9 cut sites. **B.** DNA editing with Base Editors.

Base editors consist of a Cas9 nickase fused to a DNA deaminase and use an sgRNA to locate a target sequence, where the deaminase either converts C to T, via U (cytosine base editors) or A to G, via I (adenine base editors). **C.** DNA editing with Prime Editors. Prime Editors use a Cas9 nickase fused to a reverse transcriptase, with a pegRNA. The nicked DNA strand base pairs with the 3′ end of the pegRNA, which templates the desired DNA edit to be introduced by reverse transcription. **D.** CRISPRi and CRISPRa. A catalytically deactivated dCas9 is guided by a sgRNA to locate a regulatory region of a gene of interest. CRISPRi involves either steric exclusion of RNAP by the dCas9 (*left*) or fusion of a transcriptional repressor (*center*) to reduce gene expression, whereas CRISPRa fuses a transcriptional activator to dCas9 to upregulate gene expression (*right*).

Figure adapted from Quinn J, Musa A, Kantor A, *et al.* Genome-Editing Strategies for Treating Human Retinal Degenerations. *Hum Gene Ther*. 2021;32(5-6):247-259. doi:10.1089/hum.2020.231

1.4 *In vivo* delivery of CRISPR agents

One of the major challenges facing clinical implementation of CRISPR-Cas gene editing technologies is the safe and efficient intraocular and intracellular delivery of gene editing system components. Gene delivery systems are typically classified as viral or non-viral systems where the latter can be further divided into physical and chemical approaches.[202] Whilst AAV is the viral vector of choice for current retinal delivery strategies, some of the safety concerns relating to immunogenic risks and undesired genome editing may be possible to mitigate by use of non-viral delivery methods.

Potential advantages of using non-viral delivery systems include their transient nature (thus relative biosafety), lower cost and ease of production.[203-208] However, non-viral carriers encapsulating gene editing tools must overcome extracellular barriers, be endocytosed by the cells of interest, unpackage the payload in the cytoplasm or nucleus to achieve their objectives. Thus far, therapeutic applications of non-viral gene delivery

systems have been hindered by problems such as low transduction efficiency of target cells, cytotoxicity, and mutagenicity of the chromosomal DNA and have been reserved for *in vitro* and *ex vivo* delivery of CRISPR-Cas genome engineering regents.[209-213] Access to the photoreceptor cell bodies from the subretinal space by transfection is likely to be particularly challenging due to the presence of stacks of outer segment discs.

Chemical and physical methods for delivering CRISPR-Cas9 components into target tissues are under investigation, including lipid/gold/polymer/exosome nanoparticles, electroporation and cell-penetrating peptides (CPPs).[214] Delivery of Cas9-sgRNA ribonucleoproteins either in suspension or via synthetic gold or lipid nanoparticles, which naturally degrade after approximately 3 days, could provide transient genome editing whilst minimizing off-target effects. Cationic lipid nanoparticles have been chemically engineered to deliver CRISPR-Cas9 ribonucleoproteins (RNPs) via intravenous administration to elicit multiplex editing of lung and liver tissues in mouse models.[215] PEGylated nanoparticles based on a cationic α-helical polypeptide have been used to deliver Cas9 plasmids and sgRNA into mouse tumor tissue.[216] Whilst CRISPR-Cas systems have yet to be reported as being successfully delivered by non-viral delivery to outer retinal cells *in vivo*, use of such methods for delivering genetic material has been tested in a range of settings.[217] Johnson and colleagues described the use of a novel peptide delivery for small and large molecules across the plasma membrane of ocular tissue.[218] The authors delivered fluorophores, siRNA, DNA and quantum dots, achieving robust silencing of transgene expression and penetration of the RPE, photoreceptors and ganglion cells[218]. Similarly, intravitreal delivery of florescently labelled peptides were found to localize to the photoreceptors and RPE.[219] Other studies have used compacted DNA nanoparticles (NPs) formulated with polyethylene glycol-substituted poly-l-ysine (CK30PEG) to subretinally deliver the *Rds* coding sequence into mice carrying a haploinsufficiency mutation in the retinal degeneration slow *($rds^{+/-}$)* gene.[220] Similar

approaches have been shown to mediate improved structural changes in the retina of several ocular disease models, including the *Abca4* knockout model of Stargardt disease and the rhodopsin knockout and P23H models of rhodopsin associated RP. [221-224]

1.5 Thesis aims and overview

Inherited retinal diseases (IRDs) are the most common cause of untreatable blindness in the working age population. The engineering of the clustered regularly interspaced short palindromic repeats (CRISPR)-CRISPR-associated (Cas) nuclease system has revolutionized the field of molecular biology and generated excitement for the potential of novel therapeutic approaches to treat retinal diseases. The overall aim of this thesis was to explore the development of CRISPR-Cas9 tools and their therapeutic adaptation towards the treatment of retinal disease. To this end, the following objectives were explored, described by chapter:

I. To develop and optimize CRISPR constructs towards *in vivo* adaptation

In Chapter 3, I developed an optimized a CRISPR backbone which formed the foundation for downstream epigenetic editing and DNA base editing experiments. A reporter assay was established for direct comparison of different Cas orthologues and regulatory elements and DNA-wrapped gold nanoparticles were assessed for non-viral delivery of genetic payloads to the retina.

II. To develop CRISPR-Cas repressors for targeted epigenome editing

In Chapter 4, I generated a novel CRISPR-dCas9 epigenome editor which can be packaged within an AAV vector for targeted transcriptional repression and validated the system *in vitro* against *NRL*. I developed an *in vitro* cell line for facile screening of dCas9-repressor constructs and evaluated repressor effectors and bipartite combinations for robust gene silencing.

III. To evaluate Cas9-repressors in patient iPSC-derived retinal organoids and conduct a pilot study in an NRL-EGFP mouse model

In Chapter 5, I evaluated a dCas9-repressor-mediated approach for targeted silencing of *hNRL* and *mNrl* genes in therapeutically relevant models, including in human iPSC derived 3D retinal organoids and in an *Nrl.EGFP* mouse model. I generated AAV vectors expressing dSaCas9-KRAB and dCas9-KRAB-MeCP2 repressor constructs described and cloned in Chapter 4. Subsequently, I characterized gene expression profiles in patient iPSC derived retinal organoids and evaluated the expression, efficacy, and specificity of AAV-directed dCas9-repressors for the repression of rod photoreceptors in 3D-organoids. Finally, I conducted a pilot *in vivo* study to evaluate the expression and efficacy of AAV-directed dCas9-repressors following subretinal administration in an *Nrl.EGFP*$^{+/-}$ mouse model.

IV. To develop and evaluate CRISPR mediated DNA base editing & prime editing technologies

In Chapter 6, I developed and optimized HDR-independent DNA base editing and prime editing technologies. I established an *in vitro* cell line for facile screening of DNA base editing and prime editing constructs. Subsequently, I designed and cloned a dual-vector delivery strategy for evaluation of Adenine base editors. Finally, I generated deletions in the Moloney Murine Leukemia Virus Reverse Transcriptase (M-MLV RT) of prime editor (PE) systems and evaluated the on-target activity induced by truncated PE variants utilizing a luciferase-based assay.

2. METHODS & MATERIALS

All experiments were conducted under controlled laboratory conditions using calibrated instruments. Plasmid schematics, nucleotide sequences, kits, and software used for the general methods are detailed in the Appendix.

2.1 Molecular biology

2.1.1 Polymerase chain reaction

Polymerase chain reaction (PCR) was used to amplify DNA from custom primers (Sigma-Aldrich; Integrated DNA Technologies (IDT)) using a SimpliAmp thermocycler (Thermo Fisher Scientific). Primers were designed *in silico* using Primer3 (ELIXIR). Where possible, primers were designed according to the following general criteria:

1. Length, 18 – 30 nucleotides
2. Melting temperature (T_m), 55-70°C with maximum T_m difference of 5°C between primers
3. GC content, 40% – 60%, with minimum of 1GC nucleotide within 2 bases of the 3′ end of the primer
4. Addition of an enzyme restriction site at the 5′ end, as well as a minimum of 4 nucleotides after the restriction site to facilitate efficient cleavage

A list of primers is provided in the Appendix and referenced throughout.

PCR reactions were performed using KOD Hot Starter Mastermix (Sigma-Aldrich) in accordance with manufacturer instructions. Typically, reactions were carried out in a total volume of 20-50 μL containing 10-25 μL KOD Mastermix, 1-20 ng of plasmid DNA, 100 ng of genomic DNA, or 1-5 μL of reverse transcription reaction (cDNA). Forward and reverse primers were added at a final concentration of 0.3-0.5 μM each, with the

remaining volume made up with molecular biology grade water. Following amplification by thermocycler, all products were run on a 0.5%-2% agarose gel to check sizes of products and note any non-specific products or contaminants. When required, a gradient PCR was performed by running a series of individual PCR reactions of the same composition at a range of temperatures to determine optimal annealing temperature for a set of primers.

PCR conditions are outlined in Table 2.1 below:

Step	Amplicon <0.5 kb	Amplicon 0.5 – 1 kb	Amplicon > 1kb
1. Polymerase activation	95 °C for 2 minutes		
2. Denature	95 °C for 20 seconds		
3. Annealing	Lowest primer T_M for 10 seconds		
4. Extension	70 °C for 10 seconds	70 °C for 15 seconds	70 °C for 20 sec/kb

Table 2.1 | Standard PCR conditions for cloning and sequencing applications

In general, a cycle number of 30-35 was used.

2.1.2 Plasmid cloning methodologies

2.1.2.1 Oligonucleotide annealing & phosphorylation

Unless otherwise specified, all oligonucleotide pairs, including gRNA forward and reverse oligonucleotides, were designed to form a double stranded fragment with 5′ and 3′ end complementarity. All oligonucleotides were reconstituted using RNAase and DNAase free water to a 100 μM stock. A 20 μL reaction was created containing equal volumes of the equimolar forward and reverse oligonucleotide (1.25 μM), 1 μL T4

polynucleotide kinase (PNK) (Thermo Fisher Scientific), reaction buffer A for T4 PNK (1×) and adenosine triphosphate (ATP, 1mM). Phosphorylation was performed at 37°C for 20 mins, and then oligonucleotides annealed by incubating at 95°C for four minutes before gradually cooling to 25°C over 45 minutes. Following annealing and phosphorylation, all oligonucleotide reactions were stored on ice.

2.1.2.2 DNA ligation

Plasmid ligations were performed using 1 μl T4 DNA ligase and 1 μl T4 ligase 10x buffer (NEB) in a total reaction volume of 10 μl at room temperature. For ligation of annealed oligonucleotides, 1 μL of a 1:25 dilution of the annealing reaction was added to the ligation mix. Depending on the ligation reaction and size of dsDNA fragment, a mass of insert was used that corresponded to a 2:1 to 7:1 molar ratio of the backbone mass. In all cases, a ligation control reaction was performed in parallel using vector DNA alone. At the end of the incubation period, T4 ligase enzyme was inactivated by heating samples to 65°C on a heat block for ten minutes. A list of all plasmids utilized, and their source(s), is detailed in the Appendix.

2.1.2.3 Multiple fragment Gibson assembly

NEBuilder Hifi DNA Assembly (NEB) was used for the assembly of three or more fragments according to the manufacturer's instructions. Unless otherwise stated, assembly reactions were 20 μL in total volume and prepared to contain 10 μL of total DNA (containing 10 – 100 ng of each DNA fragment (such that DNA ratios are equimolar) and 10 μL of 2X NEBuilder HiFi DNA Assembly Mastermix. Reactions were incubated at 50°C for 60 minutes and stored on ice prior to transformation.

2.1.3 Bacterial transformation

A range of *E. coli* cells were used across different cloning applications. 5-Alpha competent cells (NEB) were used for simple plasmids ligated with annealed oligos such as guide RNA cloning. Stable Competent cells (NEB) were used for plasmids assembled with NEBuilder HiFi assembly. XL10-Gold Ultracompetent E. Coli Cells (Agilent Technologies) pretreated with 1 μL of 1.43 M β-mercaptoethanol per 30 μL of cells were used for transformation of plasmids containing AAV inverted terminal repeats (ITRs). The tubes were incubated on ice for 10 minutes, with mixing of the cell suspension at 2-minute intervals.

A general transformation protocol was used across all kit types. Briefly, 1-5 μL of ligation product were added to 25-50 μL of cell suspension and incubated on ice for 30 minutes. The cells were heat shocked at 42°C for 30 seconds, incubated on ice for 2 minutes, and then added to 450 μL super optimal broth with catabolite repression (SOC) outgrowth medium (Thermo Fisher Scientific) or Stable Outgrowth Medium (NEB). The cells were then placed into an incubator-shaker at 37°C for 225rpm for 45 to 60 minutes. 100-200 μL of outgrowth medium was added to Luria Broth (LB)-Agar plates (prepared with 100 μg/mL ampicillin) (Sigma-Aldrich) and incubated at 37°C overnight. All experiments were conducted with a plasmid only control (to check sufficient digestion and/or vector recombination) as well as positive and negative transformation controls to ensure successful transformation and rule out potential for contamination.

2.1.4 Colony selection, plasmid isolation & amplification

Individual colonies were selected using sterile 200 μL pipette tips and cultured in 4 mL of LB with ampicillin (100 μg/mL) in an incubator-shaker at 37°C at 225 rpm overnight. The culture broth was centrifuged at 5,000 *g* (Megafuge, Thermo Fisher Scientific) to obtain bacterial cell pellets, and plasmids isolated from the lysed cells using

a plasmid miniprep kit in accordance with the manufacturer's protocol (GenElute Plasmid Miniprep Kit, Sigma-Aldrich; Zyppy Plasmid Miniprep Kit, Zymo Research; QIAprep Spin Miniprep Kit, Qiagen; NucleoSpinPlus Plasmid Miniprep Kit; Clontech, a Takara Bio Company) and eluted in 50 μL of molecular grade water or elution buffer.

Plasmid minipreps were screened for correct ligation products using a restriction digest assay, followed by commercial Sanger sequencing (Source Bioscience; Genewiz; Eurofins Genomics). After confirmation of the correct plasmid sequence by Sanger sequencing, glycerol stocks were created by mixing 500 μL of retained turbid culture media with 500 μL of autoclaved 50% glycerol solution. All glycerol stocks were stored at -80°C.

For downstream use in mammalian cell culture or for *in vivo* application, plasmids were amplified from bacterial glycerol stocks. Briefly, starter cultures were created by inoculating LB-ampicillin broth with bacteria from glycerol stocks and placed in an incubator-shaker for eight hours. Larger overnight culture for midipreps were created by adding 100 μL of starter culture to 50 to 100 mL of LB broth, or for maxipreps by adding 250 uL of starter culture to 250 to 500 mL of LB broth. Cell cultures were pelleted down in 500 mL Nalgene flasks in a Megafuge at 5,000 *g* for 20 minutes at 4 °C. Plasmids were purified from commercial endotoxin-free kits in accordance with manufacturer's instructions using PureLink HiPure Plasmid Midiprep Kit (Thermo Fisher Scientific), EndoFree Plasmid Maxi Kit (Qiagen), or NucleoBond Xtra Maxi EF Kit (Clontech, a Takara Bio Company). For applications where high plasmid DNA concentrations were required (>3 μg/μL), DNA was precipitated by adding 0.7 volumes of isopropanol and centrifugation at 5,000 *g* for 60 minutes at 4 °C.

2.1.5 Restriction digestion

Unless otherwise specified, all restriction enzymes were obtained from NEB, Roche Applied Science, Sigma Chemical Corporation, or Takara Bio Group. Reactions (volume 20-50μL) containing restriction enzyme at a ratio of 1 unit to 1 μg of substrate DNA and 1× buffer solution were incubated at 37 °C for 30-60 minutes. All new enzymes were validated prior to use with linear target DNA, and a no template control was run in parallel with every restriction digest to confirm enzyme activity. In some cases, methylation-sensitive restriction enzymes were used, and all steps and all steps were followed in accordance with the manufacturer's protocol, with no additional changes as per the above. Where required, plasmid backbones were dephosphorylated with calf intestinal alkaline phosphatase (NEB) or shrimp alkaline phosphatase (NEB). All digestions were confirmed by running the products on a 1% agarose gel.

2.1.6 Agarose gel electrophoresis

Agarose gels were created using agarose (Sigma-Aldrich) diluted at 0.5-2% in Tris/Acetate/EDTA (TAE) buffer (Thermo Fisher Scientific) and 0.5 μg/mL ethidium bromide (Thermo Fisher Scientific). 0.5% and 1% agarose gels were run using a 1kb DNA ladder (UltraRanger), while 2% agarose gels were run using a 100bp DNA ladder (PCRRanger) to visualize DNA amplicons <500 kb in length.

Gels were completely submerged in a tank containing TAE buffer across which a voltage of 100-120V was applied for a period of 1-2 hours. Following electrophoresis, gels were visualized and photographed using an ultraviolet (UV) transilluminator (U:Genious, Syngene). DNA was extracted from the excised gel bands using a QIAquick gel extraction kit (Qiagen) in accordance with manufacturer's instructions.

2.1.7 Genomic DNA extraction

For extraction from cell pellets, pellets were resuspended in PBS and proteinase K. DNA extraction was performed with a QIAamp DNA mini kit (Qiagen) in accordance with manufacturer's instructions and eluted in 30 μL of molecular grade water or elution buffer.

2.1.8 RNA extraction

Prior to RNA extraction, all surfaces and instruments were treated with decontamination solution to remove environmental RNases (RNaseZAP wipes, Invitrogen). All RNA samples were stored at - 80°C and thawed on ice prior to extraction.

RNA was extracted from cell pellets using the RNeasy Plus Mini kit (Qiagen). Cellular lysis was achieved using the supplied RLT Plus buffer supplemented with 10μL β- mercaptoethanol (2- mercaptoethanol) per mL and homogenized by vortexing. Lysates were run through supplied DNA eliminator columns. Additional DNA removal was performed by on-column DNase digestion (Qiagen) in accordance with the manufacturer's protocol. RNA was then isolated in accordance with manufacturer's instructions and yields determined by spectrophotometry.

For samples with minimal RNA (retinal organoids., $<1x10^6$ total cells), RNA extraction was performed using the Monarch Total RNA Miniprep Kit (NEB). Cell lysis was performed using 200 μl of the supplied RNA lysis buffer. Lysates were run through supplied DNA eliminator columns. Additional DNA removal by on-column DNase digestion incubation was extended to 30 minutes. 25 μl of molecular grade water was added and the column was incubated for 10 minutes to maximize recovery of RNA.

For RNA extraction from neural retina, animals were sacrificed, and retinal tissue rapidly dissected in sterile PBS. The phenol-chloroform based (TRIzol) miRNeasy Mini

kit (Qiagen) was used for RNA extraction from retinal tissue, as well as for samples where short RNA species (e.g., guide RNAs) were required to be isolated. MiRNeasy Kits enabled efficient enrichment of RNA down to approximately 18 nt in size. In this protocol, samples were thawed on ice, combined with TRIzol and homogenized and disrupted using a handheld homogenizer and pestle (Fisher Scientific). RNA was then isolated in accordance with manufacturer's instructions.

2.1.9 cDNA synthesis

RNA was reverse transcribed to complementary DNA (cDNA) using the Superscript III first strand synthesis system (Thermo Fisher Scientific). A standardized input of 500 ng of RNA (where possible) was combined with a nucleoside triphosphate solution, reverse transcription primers and water and incubated at 65°C for 5 minutes. Unless otherwise stated, Oligo(dT) primers (Thermo Fisher Scientific) that hybridize to 3' Poly(A) tails were used. Superscript III reverse transcription enzyme was added to a mixture of buffer, reducing agent (DTT), magnesium ($MgCl_2$), and RNase inhibitor, and added to the RNA solution. The reaction was incubated at 50°C for 50 minutes before the reaction was terminated. RNase H solution was added to the solution to digest remaining RNA. The cDNA was subsequently purified using the QIAquick PCR Purification Kit (Qiagen). Negative controls were run in parallel where no reverse transcriptase was added to the reaction.

For samples with minimal RNA (retinal organoids., <200 ng total RNA), the EvoScript Universal cDNA Master Kit was utilized (F. Hoffmann-La Roche AG). The full RNA volume was mixed with the EvoScript Universal cDNA Master, Reaction Buffer (random primers, anchored oligo$(dT)_{18}$, dNTP, and $Mg(OAc)_2$, 5x conc.), mixed, and incubated on ice for 10 minutes. 3 µl of EvoScript Universal cDNA Master, Enzyme Mix (Enzyme Blend for reverse transcription and Protector RNase Inhibitor, 10x conc.) was added to the RNA-

Reaction Buffer mix. The standard reverse transcription protocol and all subsequent steps were observed per the manufacturer protocol (v4).

2.1.10 Real-time quantitative reverse transcription PCR

Real time quantitative PCR (RT-qPCR) was used to determine levels of gene expression from complementary DNA (cDNA) samples using gene-specific primer pairs. All reactions were performed in triplicate using newly opened sterile filter pipette tips and opaque 96 well plates (Bio-Rad Laboratories) using a real time PCR machine (CFX Connect Optics Module, Bio-Rad Laboratories). Two different qPCR chemistries were used, SYBR Green and TaqMan.

Dye-based SYBR green (Bio-Rad Laboratories) assays were performed in a total reaction volume of 10 μL consisting of 1 μL cDNA template, 1 μL of both forward and reverse primers (each at a concentration of 10 μM), 2 μL molecular grade water, and 5 μL SYBR Green 2X PCR Mastermix. Melt curve analysis was performed after the cycling protocol, consisting of 60 - 95 °C with 0.5 °C increments (each held for five seconds) to confirm a single amplification product.

Probe-based TaqMan chemistry assays were performed using custom or predesigned TaqMan Assays (Thermo Fisher Scientific). TaqMan assays were performed in a total volume of 20 μL consisting of 2 μL cDNA template (diluted 1:10 where required), 1μL TaqMan assay mix (which includes a pair of unlabeled PCR primers and a TaqMan probe with a dye label (FAM) on the 5′ end and a mini groove binder (MGB) and non-florescent quencher (NFQ) on the 3′ end), 10 μL TaqMan Universal Mastermix and 7 μL molecular grade water. Reactions were performed using the following settings: 95°C for 20s, then 40 cycles of denaturation for 3 seconds at 95°C and annealing and extension for 30 seconds at 60°C.

All assays and primer pairs were validated prior to use in test plates using seven $\log_{10}$ dilution series of the linear target DNA. No template control samples were included on every plate to assess for contamination during reaction setup. No-reverse-transcription controls were run to assess for carryover genomic DNA contamination. Reaction efficiencies between 90-105% were considered acceptable for experimental application.

PCR conditions for SYBR Green assays consisted of an initial polymerase activation period at 95°C for three minutes. This was followed by 40x two-step cycles of denaturation at 95°C for ten seconds and annealing/extension at the previously optimized temperature (typically 55-62°C) for 30 seconds. This was followed by a melt curve analysis to determine purity of the amplified product.

TaqMan thermal cycling conditions consisted of an initial polymerase activation period at 95°C for ten minutes, followed by 40x PCR cycles of denaturation at 95°C for ten seconds and annealing/extension at 60°C for one minute.

For transgene expression assays, qPCR reactions were run for detection of both the gene of interest and of a housekeeping gene for internal normalization. No template control (NTC) samples run using molecular-grade water in place of cDNA were included in every plate as negative controls. Gene expression levels were calculated from cycle threshold (C_t) values as measured during the exponential phase of the PCR reaction. Gene expression relative to housekeeper was assessed via the Livak method ($2^{-\Delta\Delta CT}$). First, $2^{-\Delta t}$ was calculated, where ΔC_t represents the difference between the gene and housekeeper geometric mean C_t values from three technical replicates:

ΔC_t= *mean* C_t *(transgene) - mean* C_t *(housekeeper)*

Gene expression levels were calculated from cycle threshold (C_t) values as measured during the exponential phase of the PCR reaction.

$\Delta\Delta C_t = \Delta C_t$ *(experimental sample)* – *mean* ΔC_t *(control samples)*

C_t values were determined using regression mode in CFX Maestro Software (Bio-Rad Laboratories). Statistical comparisons between groups were performed on raw ΔC_t data.

2.1.11 *In silico* design

Geneious (Biomatters) and SnapGene (Insightful Science) software was used for design of all cloning experiments and interpretation of sequencing chromatograms. Cloning experiments using NEBuilder HiFi DNA Assembly (New England Biolabs (NEB)) were designed with the NEBuilder Assembly Tool. Primer3 (ELIXIR) software was used for primer design. CRISPick and pegFinder software were used for design of guide RNAs and prime editing guide RNAs, respectively. GlobPlot 2.3, PSIPRED, Clustal Omega, and ICM-Browser programs were utilized for all protein modeling applications. All software and algorithms used for *in silico* design are detailed in the Appendix.

2.1.12 TIDE analysis

TIDE software quantifies the editing efficacy and identifies the predominant types of insertions and deletions (indels) in the DNA of a targeted cell pool by comparing traces of CRISPR-edited DNA and untransfected controls. Briefly, PCR primers were designed to amplify a 700 bp region, with primers binding 200 bp upstream and 500 bp downstream of the predicted cut site, respectively. The target region was amplified by PCR (see Section 2.1.1) and the PCR product was sent for Sanger sequencing using the primer closest to the predicted cut site. Chromatogram sequencing files (file extension. ab1) were uploaded into the TIDE online software (Deskgen) along with unmodified DNA control samples. The decomposition window was adjusted to the length of the high quality read on the control sample, if required. All PCR primer combinations used are detailed in the appendix.

2.1.13 Sanger sequencing

Sanger sequencing was performed commercially (Source Bioscience; Genewiz; Eurofins Genomics) using custom sequencing primers (designed using Primer3 (ELIXIR)).

2.1.14 Protein extraction

Protein was extracted from cell pellets and neuroretina through lysis in radioimmunoprecipitation (RIPA) buffer (Sigma Aldrich) (150 mM NaCl, 1.0% IGEPAL CA-630, 0.5% sodium deoxycholate, 0.1% SDS, 50 mM Tris, pH 8.0) supplemented with Roche cOmplete, Mini Protease Inhibitor Cocktail (Roche Diagnostics). If the sample was analyzed for fluorescence, the pellet was resuspended in complete FIPA buffer (NaCl 150 mM, Tris base 50 mM, EDTA 2 mM, 1 % TritonX-100; adjusted to pH 7.4 with HCl).

Cells were disrupted with a handheld homogenizer and pestle (Fisher Scientific), left on ice for 30 minutes and then centrifuged for 10 minutes at 10,000 g at 4. The supernatant containing the protein was transferred to a new tube for downstream use and the pellet discarded.

Total protein was quantified from lysates using the Pierce bicinchoninic acid (BCA) Protein Assay Kit (Thermo Fisher Scientific) in accordance with manufacturer's instructions. Samples were diluted 1 in 10 and incubated in darkness with the assay reagents at 37°C for 30 minutes. All reactions were performed in duplicate, and colorimetric absorbance readings taken at 562nm using the iMark microplate reader (Bio-Rad Laboratories). Protein concentration was determined using a standard curve derived from diluted bovine serum albumin (BSA) standards (25-2000µg/mL). Additionally, spectrophotometric quantification was used to confirm protein concentrations (see below).

2.1.15 Spectrophotometric quantification

Nucleic acid quantification was performed to determine the average concentration and purity of DNA or RNA in a sample prior to proceeding with downstream experiments. Quantification was performed using a NanoDrop spectrophotometer (Thermo Fisher Scientific). The ratio of absorbance at 280 nm/260 nm was examined, with a ratio of 1.7 to 1.9 indicating acceptable purity for DNA and ~1.8 to 2 for RNA. The ratio of absorbance at 230 nm/260 nm assessed for sample contamination, with an acceptable ratio ranging from 2.0-2.2. The nanodrop was also used to quantify protein concentrations, with a target 260 nm/280 nm purity ratio of 0.6.

2.1.16 Western blot

Protein lysate samples were diluted in RIPA buffer / protease inhibitor and combined with 5X reducing sample buffer (National Diagnostics) at room temperature for 20 minutes. After denaturation, samples were loaded into wells of a pre-cast 10% Tris-Glycine gels (Criterion TGX, Bio-Rad Laboratories submerged in Tris-Glycine Sodium-Dodecyl-Sulfate PAGE (SDS-PAGE) running buffer (National Diagnostics). Samples were loaded to wells adjacent to 5 μL protein size ladder (BLUeye, GeneFlow). The loaded gel was subjected to electrophoresis at 100V for one hour and 45 minutes, at the end of which the gel was removed for blotting.

Low fluorescence polyvinylidene difluoride (PVDF) membranes (Bio-Rad Laboratories) were activated with methanol and prepared in transfer stacks soaked in 1× Transblot Turbo transfer buffer (Bio-Rad Laboratories). proteins were transferred using the semi-dry Trans-Blot Turbo transfer system (Bio-Rad Laboratories) set to the 'Mixed Weight' (2.5A/25V, 7 minutes) or ‘High MW’ (2.5A/25V, 10 minutes) programs.

Following protein transfer, PVDF membranes were washed in Tris-Buffered Saline (TBS) (Bio-Rad Laboratories) and then incubated in Odyssey blocking buffer (TBS, LI-

COR) or dilute (10%) skim milk in TBS solution for 45 minutes at room temperature under agitation. Membranes were then incubated in primary antibodies diluted 1:1000 in PBS with 0.1% Tween-20 (PBST) supplemented with 10% blocking buffer under agitation overnight at 4 °C. This was followed by three washes in PBST under agitation for seven minutes each. Membranes were then incubated in in secondary antibody solution containing appropriate florescent labelled antibodies (IRDye 800CW donkey anti-mouse and IRDye 680RD donkey anti-rabbit, both LI-COR) diluted 1:10,000 in PBST for 45 minutes under agitation and protected from light. The membranes were subsequently washed a further three times as above before being removed and allowed to dry at room temperature.

The processed PVDFs were imaged using the Odyssey Fc imaging system (LI-COR) with 700 nm and 800 nm detection channels and an exposure time of two or ten minutes. In cases where protein was to be quantified, expression relative to stably expressed loading control was calculated from acquired images by band densitometry using Image Studio Lite software (v5.2.5, LI-COR Biosciences).

2.1.17 Fluorescence spectroscopy

Fluorescence spectroscopy assays were performed for quantification of protein knockdown using Cas9 and epigenetic editing constructs. For both assays, HEK293 cells were seeded in 12 well plates and transfected with 1 μg of plasmid. In either case, wells were photographed 48 - 72 hours later using standardized acquisition settings, after which cells were pelleted and resuspended in 100 μL of complete Fluorescence immunoprecipitation (FIPA) buffer (NaCl 150mM, Tris base 50mM, EDTA 2mM, 1% TritonX-100; adjusted to pH7.4 with HCl) supplemented with protease inhibitor (Roche Diagnostics, one tablet per 10 mL). Samples were then processed for protein extraction and quantification as described in Section 2.1.15. For each sample, 10 μg of protein was

loaded 96 well black microplate (Greiner Bio-one) in duplicate and the volume made up to 300 μL with FIPA buffer / protease inhibitor. The outermost wells of the plate were not used. The Viktor^3 1420 Multilabel plate reader (Perkin Elmer) was used to measure the Fluorescence (in arbitrary units) with excitation at 485 nm, detection at 535 nm, and an exposure time of 1 second. To account for background fluorescence, the mean reading from untransfected cells and background-only control (containing only FIPA buffer) was subtracted from all experimental fluorescence readings.

2.2 Cell culture

2.2.1 Cell culture and maintenance

2.2.1.1 Cell culture

Cell culture was performed in a designated tissue culture laboratory within class II biological safety cabinets with positive pressure ventilation hoods and using aseptic technique. All cells were stored in liquid nitrogen.

Immortalized cell lines were stored in liquid nitrogen. Frozen cell stocks were thawed at 37°C and centrifuged at 300 g for 5 minutes. The supernatant was discarded, the cell pellet resuspended in 6 mL media, and the cells transferred to a T25 flask. Once confluent, the cells were transferred to a T75 flask.

After resuscitation, cells were passaged at least three times prior to experimental application. All cell cultures were maintained in a designated humidified tissue culture incubator at 37°C with 5% CO_2.

2.2.1.2 Cell lines and maintenance

Human embryonic kidney 293 cells expressing mutant simian virus-40 (SV40) T antigen (HEK293T) were cultured in complete Dulbecco's Modified Eagle Medium

(complete DMEM) containing phenol red, L-glutamine (4 mM) and sodium pyruvate (1 mM) and supplemented with 10% filtered fetal bovine serum (FBS), and 1% penicillin-streptomycin (100units/mL-0.1mg/mL). HEK293 cells were maintained within sterile T75 culture flasks and were passaged twice per week when 70-90% confluent. For passage, old culture media was removed, and the cell monolayer gently washed with 5 mL pre-warmed sterile phosphate buffered saline (PBS). Cells were dissociated with 2 mL of TrypLE Express dissociation reagent (Thermo Fisher Scientific) and the flask incubated at 37°C for five minutes. A further 8 mL of pre-warmed complete DMEM was then added and the cells completely resuspended by pipetting up and down. 1 to 2 mL (10-20%) of this cell suspension was then added to fresh pre-warmed DMEM in a new sterile T75 flask for ongoing culture.

Human embryonic kidney 293 cells that stably express enhanced green florescent protein (EGFP) (HEK293-EGFP cells, #SC001, GenTarget) under a CMV promoter were cultured in complete high glucose (25 mM) DMEM containing phenol red, L-glutamine (4 mM) and sodium pyruvate (1 mM) supplemented with 10% FBS, 1% penicillin-streptomycin (100units/mL-0.1mg/mL), and 1% non-essential amino acids (1×). HEK293-EGFP cells were maintained with identical conditions to HEK293T cells as described above.

Human embryonic kidney 293 cells harboring proline-glutamate-serine-threonine-rich (PEST) destabilized-GFP (dGFP) under a CMV promoter (HEK293-dGFP), as well as modified dGFP cell lines with ATG to ACG missense mutation (HEK293-CBE) and TGG to TAG nonsense mutation (HEK293-ABE) were cultured and maintained in identical conditions to the HEK293-EGFP cells.

Human retinoblastoma (Rb) cell lines Y79 and WERI-RB-1 (both obtained from American Type Culture Collection) were maintained in suspension culture. Cells were cultured using Roswell Park Memorial Institute (RPMI)-1640 medium (Thermo Fisher),

supplemented with 2 mM glutamine, 15% FBS and 1% penicillin-streptomycin (100units/mL-0.1mg/mL). For attachment cultures, plates were coated with 500 μL 1 mg/mL poly-D-lysine (Sigma) and incubated at room temperature. Subsequently, the poly-D-lysine was removed, and the wells washed in 500 μL molecular grade water. Next, plates were coated with 500 μL 1 mg/mL human fibronectin and incubated for an additional 30 minutes. The human fibronectin was removed, and the plate left to dry in positive pressure ventilation hoods for 2 hours, with the lid removed. The coated plates were then kept in the fridge for up to 1 day before use. Rb cell lines were maintained within sterile T175 culture flasks and passaged once per week when 90% confluent. For passage, cells were resuspended at a density of $5x10^5$ cells/mL in 60 mL of medium.

2.2.2 *In vitro* transfection and transduction

2.2.2.1 Cell seeding

The cell lines were dissociated when approaching confluence (as described in section 2.2.1.2), resuspended in 10 mL of DMEM and centrifuged for 5 minutes at 300 *g* at 20°C. The supernatant was discarded, and the cells resuspended in 10 mL of fresh pre-warmed DMEM ± phenol red. A 10μL sample of the diluted cell suspension was mixed with equal volume of undiluted 0.4% Trypan Blue Solution to assess for cell viability, and cells were counted with a TC20 automated cell counter (Bio-Rad Laboratories). The cell suspension was diluted to the required concentration in DMEM and seeded into Sarstedt adherent tissue culture plates at seeding densities optimized for each well plate. Seeding density of 8.0×10^5, 4.5×10^5, and 2.5×10^5 cells per well were used for seeding in the 6-well, 12-well, and 24-well sterile culture plates, respectively, and identical seeding conditions were used across all adherent cell lines. Suspension Rb cell lines were seeded at a density of 5×10^5 cells/well unless otherwise noted. For all luciferase assay applications, HEK293T cells were seeded in 96-well Corning White Polystyrene

Microplate (Sigma-Aldrich) at a seeding density of 5.5×10^4 cells per well. The seeding densities of all cell types is described in Table 2.2 below.

Cell Type	**Plate / Well Size (cm^2)**	**Seeding density (cells / well)**
HEK293T	6 well (8.87)	8.0×10^5
	12 well (3.65)	4.5×10^5
	24 well (1.82)	2.5×10^5
	96 well (0.32)	4.5×10^4
HEK293-GFP	6 well (8.87)	8.0×10^5
	12 well (3.65)	5×10^5
	24 well (1.82)	2×10^5
HEK293-dGFP	6 well (8.87)	8.0×10^5
	12 well (3.65)	4×10^5
	24 well (1.82)	2×10^5
	96 well (0.32)	4×10^4
HEK293-CBE	6 well (8.87)	8.0×10^5
	12 well (3.65)	4.5×10^5
	24 well (1.82)	2.5×10^5

	6 well (8.87)	8.0×10^5
HEK293-ABE	12 well (3.65)	4.5×10^5
	24 well (1.82)	2.5×10^5
Y79 / WERI-Rb-1	24 well (1.82)	5×10^5

Table 2.2 | Cell seeding density for plasmid transfection

Cell seeding density (cells per well) in Sarstedt adherent tissue culture plates. For luciferase assays with HEK293T cells (96-well plate), protocol was optimized for Corning White Polystyrene Microplate (Sigma-Aldrich).

2.2.2.2 Plasmid transfection and viral transduction

Adherent and suspension cell lines approaching confluence in a T75 flask were dissociated and seeded as described in Section 2.2.2.1. Cells were transfected at 24 hours following seeding when cells had reached between 60% - 90% confluence, depending on application. Transfection was conducted with TransIT-LT1 (MirusBio), FuGENE (Promega), ViaFect (Promega), or Lipofectamine 3000 (ThermoFisher) reagents. TransIT-LT1 transfection reagent (Mirus Bio) was mixed with OptiMEM reduced serum media (Thermo Fisher Scientific) and endotoxin-free plasmid. DNA complexes were allowed to form at room temperature, and the solution was added to the plates. FuGene HD transfection reagent was mixed with DNA diluted to 2 μg per 100 μL of OptiMEM, and 2–10μL of FuGENE Transfection Reagent: DNA mixture were added to each well of cells to be transfected and mixed gently. ViaFect transfection reagent was mixed with DNA diluted to 1 μg per 100 μL of OptiMEM, and 5–10 μL of ViaFect Transfection Reagent: DNA mixture were added to each well of cells to be transfected. Lipofectamine 3000 transfection reagent was mixed with plasmid DNA (concentration of 1-3 μg/μL), OptiMEM, P300 (Thermo Fisher Scientific) reagent mixture and added to the wells.

For gold nanoparticle nanotransfection experiments, DNA-wrapped gold nanoparticles were introduced in each well with seeded cells. Photothermal plasmon resonance of the DNA-gold nanoparticles was activated by white light irradiation 1 to 2 hours post-nanotransfection.

Unless otherwise stated, OptiMEM reduced serum media was used for transfection experiments, incubations of DNA and transfection reagent occurred for 20-30 minutes at room temperature, and ratio of transfection reagent to plasmid DNA was optimized by application. Plates were swirled gently following addition of transfection mixture to ensure homogenous distribution of complex to the entire well. Cells were harvested for further analysis at 48-96 hours post transfection.

For *in vitro* viral transduction experiments, HEK293T or HEK293-EGFP cells approaching confluence were diluted in DMEM and seeded into 12 or 24 well tissue culture plates (Sarstedt) at a density of 4.5×10^5 cells/well and 2.5×10^5 cells/well, respectively. Cells were transduced at 18 to 24 hours following seeding when cells had reached 70% to 90% confluence. AAV diluted to the appropriate concentration and volume in PBS and added dropwise to cells. The plate was gently rocked to mix and then returned to the incubator.

For DNA adenine base editing and prime editing experiments, HEK293T cells or HEK293T or HEK293-ABE cells approaching confluence were transfected at 24 hours following seeding when cells had reached 75-90% confluence. Transfection was conducted with TransIT-LT1 (MirusBio) or Lipofectamine 3000 (ThermoFisher) reagents, using 1.25 μg DNA per well for 24-well experiments and 6 μg DNA per well for 6-well experiments. The same amount of lipofection reagent was utilized as per the recommended manufacturer protocol (i.e., 1 μL P3000 Reagent for 24-well plate size, 5 μL for 6-well plate size), and all subsequent steps were completed as described above. At 24-hours post transfection, the media was changed. At 72-hours post transfection, cells

were split 1:2, cells were counted, and viability was assessed. To maximize editing efficiencies during CRISPR reagent optimizations and gRNA screening, the above protocol was then repeated, and cells were harvested for further analysis at 72-hours post the second transfection.

2.2.3 Microscopy imaging

Transmission and Fluorescence images of live cells were taken using the Invitrogen EVOS FL Auto 2 Cell Imaging System (ThermoFisher). The gain in each channel was adjusted to ensure the image was not saturated, and this was kept constant between channels and time points for each experiment. In different experiments, the images were taken either using brightfield or phase contrast depending on the cell type and which image provided to most useful representation of the cells. For quantitative analysis of florescent protein expression between samples, the light intensity and gain for each channel was kept constant across experiments.

2.3 AVV manufacture

All AAVs referred to in this thesis were manufactured in a designated tissue culture laboratory using aseptic technique. Recombinant AAV gene transfer vectors were produced by transient transfection of HEK293T cells with plasmids encoding the necessary elements for AAV formation:

1. Transgene plasmid (pTransgene), containing the intended AAV transgenic genome flanked by inverted terminal repeat sequences (ITRs).
2. Rep/Cap plasmid, containing sequences required for viral replication and capsid synthesis.
3. Helper plasmid, containing genes from adenovirus essential for AAV replication.

For AAV5 production, a single plasmid encoding both the *rep*/*cap* and helper genes (pDP5 (*rep2*/*cap5*), PlasmidFactory) was used together with pTransgene in a dual plasmid transfection. For tyrosine mutant AAV8 (AAV8-Y733F) production, a triple transfection method using pTransgene together with separate plasmids encoding the helper genes (pAdΔF6) and the rep2/cap8-Y733F genes (pAAV2/8-Y733F). All plasmids utilized for AAV production are detailed in the Appendix.

Large scale plasmid purification was performed in all cases using the Qiagen Endotoxin-free Plasmid Mega Kit (Qiagen) and NucleoBond Endotoxin-free Plasmid Maxi Kit (Clontech, a Takara Bio Company) in accordance with manufacturer's instructions. All plasmids were stored at -20°C after purification, fully sequenced, and digested with XmaI to confirm the presence of both ITRs. All primers for AAV sequencing are detailed in the Appendix. A summary of the AAV production methodology is outlined in Figure 2.1 below.

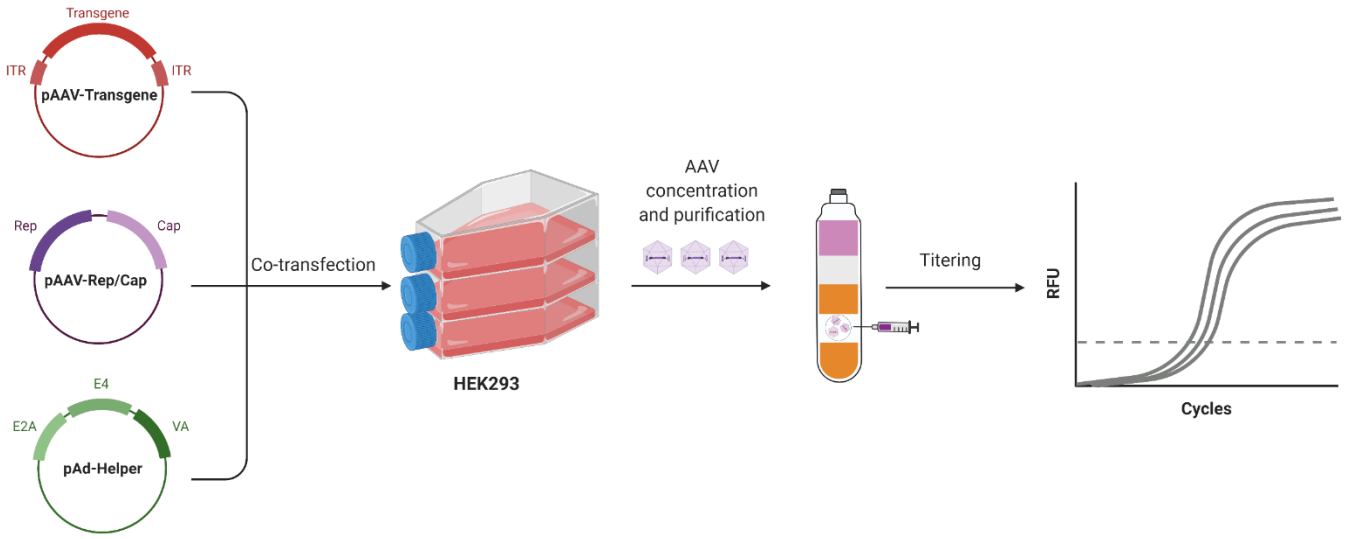


Figure 2.1 | Adeno-associated virus production, purification, tittering

Summary of recombinant AAV production methodology. AAV production in HEK293 cells via triple transfection in HEK293 cells. The transfer plasmid contains the viral transgene for packaging within ITRs. Two *trans*-plasmids produce the AAV *rep, cap* genes for AAV packaging, allowing for alternative capsid genes to be provided for AAV pseudotyping. A helper plasmid encoding the adenovirus E4, E2A and VA genes, in addition to E1 expressed in HEK293 cells, is provided to mediate AAV replication. Virus is harvested and lysed 72 hours post-transfection, and AAV is isolated by iodixanol gradient ultracentrifugation. Viral particles are tittered by real time quantitative PCR.

2.3.1 HEK293T cell culture

HEK293T cells were cultured in complete DMEM with phenol red (Gibco) supplemented with 10% filtered FBS, L-glutamine (2 nM), penicillin (100 U/mL) and streptomycin (100 μg/mL). Cells harvested from three confluent T75 flasks were seeded into two CellBIND Surface HYPERflasks (Corning) per vector to be made and hyperflasks were topped up with complete DMEM until full (~560 mL total volume per flask), and bubbles carefully removed. Seeded hyperflasks were incubated at 37 °C 5% CO_2 for 72 hours until 80% confluent.

2.3.2 Transfection

Two hyperflasks were used to produce each AAV batch. Hyperflasks were transfected using the cationic polymer polyethyleneimine (PEI) protocol. Each hyperflask was transfected with a total of 500 μg of plasmid DNA, where the mass of each plasmid transfected was calculated to adjust for plasmid size so that each construct was delivered at with identical molar ratio, as shown in the table below.

AAV5			**AAV8-Y733F**		
Plasmid	**Size (kb)**	**Mass (μg)**	**Plasmid**	**Size (kb)**	**Mass (μg)**

pTransgene	T	T X R	**pTransgene**	T	T X R
pDP5 ***(rep2/cap5)***	21.8	21.8 X R	**pAdΔF6**	15.4	15.4 X R
			pRepCap	7.3	7.3 X R
Total	K	500 μg	**Total**	K	500 μg
Ratio (R) mass/kb	500/K		**Ratio (R) mass/kb**	500/K	

Table 2.3 | Calculations to determine plasmid concentrations for rAAV production

To produce an rAAV containing a transgene of a given size (T), the mass of each plasmid to transfect was calculated so that the ratio (R) of transgene to helper and rep/cap plasmids was equimolar for a total (K) of 500 μg of plasmid DNA transfected. The ratio R is multiplied by the respective plasmid size to yield the amount of plasmid needed for one transfection.

The three plasmids were well mixed, and the solution made up to 10 mL with 150 mM NaCl in a 50 mL Falcon tube. In a separate 50 mL Falcon tube, 1.125 mL of 1 mg/mL PEI was mixed with 8.875 mL of 150 mM NaCl. The DNA was then complexed with the diluted PEI by adding the total volume of the latter to the former in a dropwise fashion. The complexed DNA was incubated for 20 minutes at room temperature to allow polyplex formation before being added in its entirety to 500 mL of pre-warmed transfection media prepared with complete high glucose (25 mM) DMEM containing phenol red, L-glutamine (4 mM) and sodium pyruvate (1 mM) supplemented with 2% HI-FBS and 1% penicillin-streptomycin. The hyperflask culture media were carefully drained and the transfection media containing complexed DNA slowly added. The hyperflasks were topped up with fresh transfection media until full, bubbles were removed and the hyperflasks again incubated at 37°C 5% CO_2 for a further 72 hours.

2.3.3 Cell harvesting & lysis

After 72 hours of incubation, 200 mL of media was drained from the hyperflask and discarded. To dissociate the cells, hyperflasks were then shaken vigorously until all cells had been loosened into suspension (as confirmed by light microscopy).

The cell suspension was poured into 500 mL autoclaved bottles cells were then pelleted by centrifugation at 1,200 g for 10 minutes at room temperature before the supernatant was aspirated. This cell suspension was transferred into a 50 mL Falcon tube and again centrifuged at 1200g, 20°C for 20 minutes to generate a more secure pellet which allowed complete removal of the remaining media.

For lysis, 15 mL of autoclaved lysis buffer containing 1M tris (hydroxymethyl) aminomethane (VWR) with 150 mM NaCl (Sigma-Aldrich) was added to each pellet and the lysate carefully pipetted up and down. A protease inhibitor solution containing 1 tablet of cOmplete mini protease inhibitor (Sigma-Aldrich) in 1 mL of lysis buffer was prepared, and 500 µL added to the cell lysate and mixed.

Each lysate was then subjected to three freeze-thaw cycles. The cell lysate was frozen at - 80°C for 45 minutes, before being incubated in a water bath at 37°C for 15 minutes and shaken forcefully halfway through this incubation. This was repeated twice more before being stored at -80°C until the AAV isolation step.

2.3.4 Isolation of AAV particles

After completion of the final freeze-thaw cycle, benzoate enzyme (Merck Millipore) was added to the thawed lysate to a final concentration of 50 U/mL. The lysates were then incubated at 37°C for 45 minutes with vigorous shaking every 15 minutes. Subsequently, the lysates were centrifuged at 3700 *g* at room temperature for 20 minutes.

AAV was isolated using iodixanol gradients (Sigma-Aldrich). Gradients were assembled using fractions of different concentrations prepared as per Table 2.4.

Fraction	Iodixanol	5M NaCl	5X PBS-MK	H_2O	Phenol Red
15%	6 mL	4.8 mL	4.8 mL	8.4 mL	-
25%	7.5 mL	-	3.6 mL	6.9 mL	30 µl
40%	10.05 mL	-	3 mL	1.95 mL	-
60%	15 mL	-	-	-	30 µl

Table 2.4 | Preparation of iodixanol gradients

Volumes of constituent parts required to prepare two iodixanol gradients. OptiPrep density gradient medium (Sigma-Aldrich); 5× PBS-MK: PBS with 5 mM MgCl2 plus 12.5 mM KCl; H2O: sterile molecular biology grade water (Sigma-Aldrich); Phenol Red: 0.5% solution (Sigma-Aldrich).

All gradients were prepared using UV treated 5 mL long-neck Pasteur pipettes. First the 15% fraction was pipetted directly into the base of a 32.4 mL OptiSeal ultracentrifuge tube (Beckman-Coulter Life Sciences). Next, the 25% fraction, 40% fraction, and finally 60% fraction were successively underlaid into the ultracentrifuge tube. The supernatant from the centrifuged lysates was then carefully pipetted on top of the iodixanol gradients. All microcentrifuge tubes were filled to the top with any remaining volume being made up with lysis buffer. Tubes were then sealed with caps and centrifuged at 59,000 rpm in a 70 Ti rotor in an Optima XE-90 ultracentrifuge (Beckman Coulter) for 90 minutes at 20 °C.

AAV particles were isolated by aspirating 1.5-2 mL of the colorless 40% fraction where AAV is concentrated following centrifugation (Figure 2.2). An 18G needle was

attached facing bevel up to a 5 mL syringe and used to pierce each OptiSeal tube at the base of the 40% phase, angling up into the 40% fraction and taking care not to aspirate the other fractions. 1.5-2 mL of this fraction was extracted from each ultracentrifuge tube, and the collected fractions were stored overnight at 4°C.

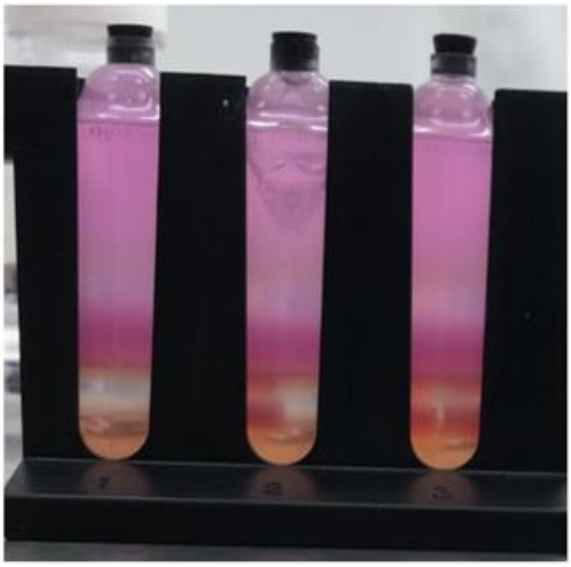


Figure 2.2 | Iodixanol gradients following ultracentrifugation

Iodixanol gradients within 32.4 mL OptiSeal ultracentrifuge tubes following ultracentrifugation. AAV particles were isolated by aspirating 1.5 — 2 mL of the colorless 40% fraction where AAV is concentrated following centrifugation.

2.3.5 Purification & concentration of AAV

15 mL of sterile PBS was added to an Amicon Ultra 100K filter tube (Millipore) which was then spun at 3000g for 15 minutes at 20°C in a tabletop centrifuge (Megafuge, Thermo Fisher Scientific). The flow-through liquid was subsequently discarded. The collected iodixanol fraction was made up to a volume of 15 mL with sterile PBS and the solution mixed well by pipetting. The total volume was then transferred into the pre-wet Amicon filter centrifuged at 3000 *g* at 20 °C to concentrate the volume to less than 500 µL (typically between 60 – 90 minutes). To this, a further 15 mL of sterile PBS was added,

and the solution mixed well by pipetting up and down. The filter was washed by adding 15 mL of PBS and centrifuging until concentrated to ~500 μL, and the washing step was repeated an additional two times. After the final wash step, total volume was concentrated to <250 μL and then divided into 10 μL aliquots for storage in -80 °C.

Finally, after collected of concentrated AAV suspension, a 'wash' suspension was created by adding 500 μL of PBS to rinse the empty filter and collect any remaining AAV particles (wash suspension was divided into 50 μL aliquots and similarly stored at -80°C).

2.3.6 Viral titration and capsid analysis

Capsid yield and purity of the AAV preparations was determined by SDS-PAGE analysis. After staining the gel for protein, three distinct bands corresponding to proteins of 87, 72 and 62 kDa in size should be visible following successful virus preparation. These correspond to the three proteins that make up the capsid of an AAV virion: VP1, VP2 & VP3.

For SDS-PAGE analysis, samples of pure AAV (10 μL) and AAV wash (24 μL) were denatured by adding 5× reducing sample buffer (National Diagnostics) and heating to 95°C for 15 minutes. Samples were loaded in pre-cast 10% Criterion Tris-Glycine extended (TGX) gels (Bio-Rad) submerged in in Tris/Glycine/SDS running buffer (National Diagnostics). Electrophoresis was performed at 100V for 1 hour and 45 minutes together with 5 μL of protein size ladder (BLUeye, GeneFlow). Following electrophoresis, gels were washed three times for five minutes in distilled water under agitation. To stain for protein, gels were submerged in EZBlue Gel Staining Reagent (Sigma-Aldrich) for 90 minutes with gentle agitation. Gels were then further washed three times, and then imaged using the Odyssey Fc imaging system.

Viral genome titer in each purified rAAV preparation was determined by RT-qPCR. First, rAAV samples were digested with DNase enzyme to eliminate any

contaminating plasmid DNA present outside of the viral capsid. A total volume of 10 μL was prepared containing 1 μL of concentrated or wash AAV sample, 1 μL of DNase I (NEB), 1 μL of DNase 10× buffer, and 7 μL of molecular biology grade water. Samples were incubated at 37 °C for 30 minutes and subsequently denatured and heat-inactivated at 95°C for 10 minutes. The latter step was performed to inactivate the DNase enzyme and at the same time denature viral capsids.

The DNase digested AAV samples were subsequently diluted 1:10 and 1:100 for PR-qPCR. Standard curves were constructed using a seven $\log_{10}$ dilution series of linearized, digested, and gel extracted plasmid containing the transgene used to generate the vector. All reactions were performed in triplicate and the geometric mean C_t used for analysis. RT-qPCR was performed as described in Section 2.1.11. Viral genome copy number was determined for AAV samples by interpolation from within the standard curve.

2.4 *In vivo* procedures

All animal procedures were conducted in accordance with the Animals (Scientific Procedures) Act 1986, UK and with the Association for Research in Vision & Ophthalmology (ARVO) statements on the care and use of animals in ophthalmic research, and with the University of Oxford policy on the use of animals in scientific research. Animal procedures were conducted under UK Home Office Personal License I41744949 (AK) and Project License PP3038118 (Expiry 18 Dec 2025). Mice were housed in individually ventilated cages at the Biomedical Sciences Division, University of Oxford with a 12-hour light/dark cycle and food and water available *ad libitum*.

2.4.1 Anesthesia & pupil dilatation

Mice were anaesthetized by intraperitoneal injection of ketamine (Narketan, Vetoquinol, final concentration 8 mg/mL) and xylazine (Rompun, Bayer, final concentration 1 mg/mL) in 0.9% normal saline at a dose of 0.1 mL/10 g bodyweight. Anesthesia was reversed at the end of procedures by intraperitoneal injection of atipamezole (Antisedan, Zoetis, 2mg/kg body weight). During recovery, mice were placed in a temperature-controlled chamber set to 35°C and Viscotears Liquid Gel was applied to prevent corneal desiccation until the blink reflex was re-established. Pupil dilatation was achieved where required using guttae tropicamide 1% and phenylephrine hydrochloride 2.5% applied in sequence (both Minims, Bausch & Lomb).

2.4.2 Subretinal injection

Mice were anesthetized and the pupils dilated as described above. Prior to injection, guttae proxymetacaine (Minims, Bausch & Lomb) was applied to provide additional topical anesthesia. The animal was positioned on a customized foam operating mat to stabilize the head and a microsurgical operating microscope (Leica Biosystems) was used for appropriate visualization. A paracentesis was performed by brief puncture of the mid-peripheral corneal with a 33G needle, inducing the efflux of a small bleb of aqueous after which the wound self-sealed. This purpose of this step was to lower intraocular pressure to minimize the risk of trans-scleral reflux during or after subsequent subretinal injection.

Carbomer gel (Viscotears Liquid Gel (0.2 mg/g polyacrylic acid) was then applied liberally to the corneal surface and a 6 mm round glass coverslip rested on top. This allowed direct visualization of the posterior pole through the operating microscope. A 35G beveled NanoFil needle was mounted on a Nanofil 10μL syringe (both World Precision Instruments) and 1.5μL of AAV suspension or PBS was drawn up in

preparation for injection. The superior rectus muscle was grasped with notched forceps to stabilize the eye, and the needle carefully introduced through the sclera adjacent to the superior rectus and into the subretinal space under direct visualization until the needle bevel was visible beneath the retina. Once the entirety of the needle's bevel was visible beneath the retina, the superior rectus muscle was released, and the syringe plunger depressed creating a bullous superior hemi-retinal detachment. The needle was then carefully withdrawn, the glass cover slip removed, and 0.5% chloramphenicol topical drops were applied. Any complications such as epiretinal, subretinal or vitreous hemorrhage, extraocular reflux of injected substance, or inadvertent retinotomy were recorded at the time of surgery and excluded from analysis.

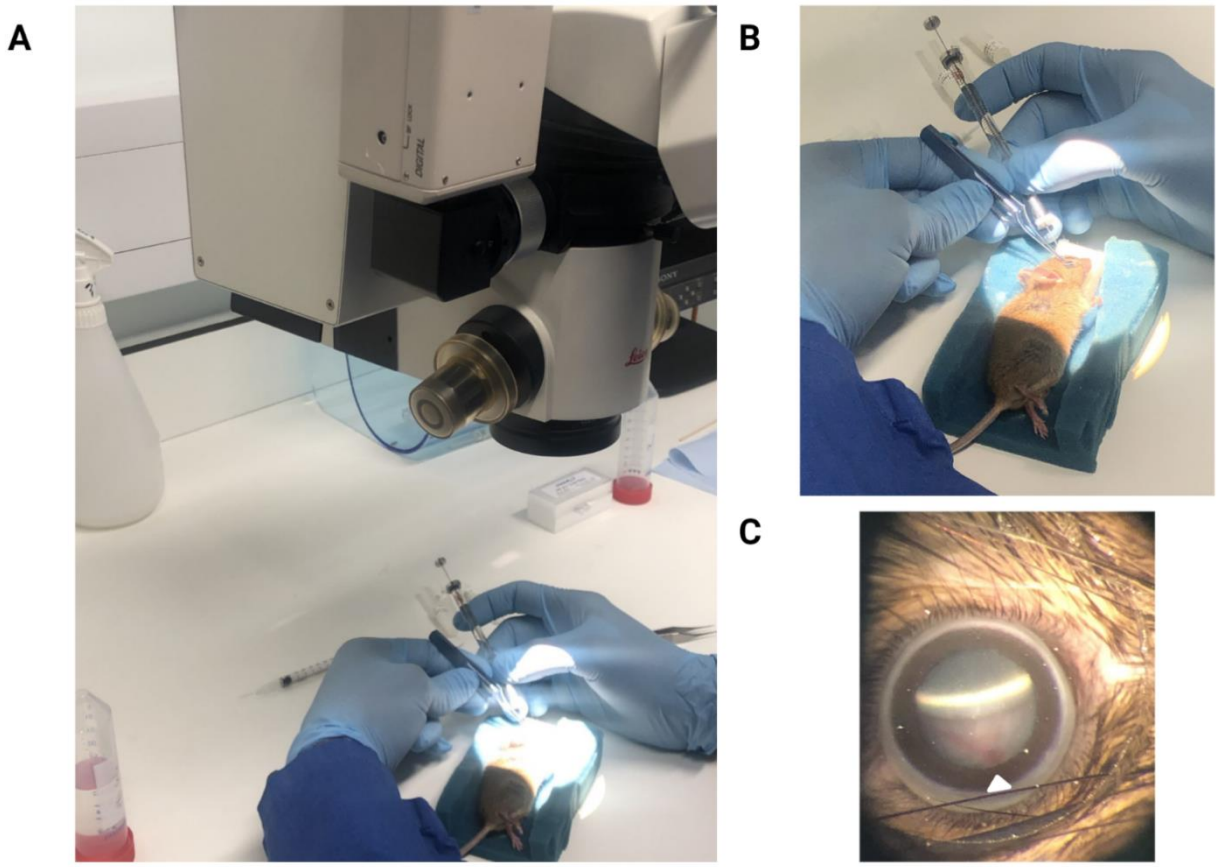


Figure 2.3 | Subretinal injection

A-B. Set up and positioning for subretinal injection. Positioning of animal and instruments for subretinal injection. Following anterior chamber paracentesis, a rounded cover slip was placed over a liberal quantity of Viscotears liquid gel covering the corneal surface. Whilst grasping the superior rectus muscle with notched forceps, the tip of a 35g NanoFil needle was passed trans-sclerally into the subretinal space under direct visualization. **C.** Surgeon's view through the operating microscope following successful subretinal injection with creation of a superior large hemi-retinal bleb that extends below the horizontal meridian without complications achieved for most injections. The optic nerve head is marked with a white arrow.

2.4.3 Retinal imaging

Retinal imaging was performed using the Spectralis ophthalmic imaging platform (Heidelberg Engineering, Germany) fitted with a 55° camera lens. *En face* images were acquired using the inbuilt confocal scanning laser ophthalmoscope (cSLO), whilst spectral domain optical coherence tomography (SD-OCT) was used for cross-sectional imaging of the retina. Mice were anesthetized and pupils dilated as described in Section 2.4.2. Coupling fluid (guttae hypromellose 0.3%; Blumont Healthcare) was applied to the cornea, and then a custom-made polymethyl methacrylate contact lens of specification 3.2 mm diameter, 1.7 mm back optic zone radius, 0.4 mm central thickness, straight sides (Cantor and Nissel) were applied to both eyes and centered over the dilated pupils. The contact lenses served to create a uniform refractive surface for imaging, as well as acting to prevent corneal dehydration, which would otherwise result in the formation of reversible cataract. Mice were placed on a platform mounted on the chin rest of the Spectralis so that its eyes were positioned at the height marking for a human patients' eye position.

2.4.3.1 Confocal scanning laser microscopy

Confocal scanning laser ophthalmoscopy (cSLO) generates high resolution *en face* retinal images using a narrow wave-length laser swept across the retina to excite florescent signal at each point scanned. All cSLO images were acquired in 'High Resolution' mode (8bits/pixel and 1536 x 1536-pixel resolution) with automatic real-time (ART) averaging set to 20 images with normalization turned off. In ART mode, multiple images are acquired and averaged to create a composite with increased resolution. The eye is actively tracked during this process based on high contrast landmarks, thus compensating for small movements of the eye such as those that occur because of respiration.

Careful image alignment was required for optimal imaging. In all cases, a reference image was first taken of the external aspect of the eye using the near infrared (NIR) reflectance mode (which utilizes an 815 nm wavelength diode laser) before the laser arm was moved forwards and the image focused on the retina with the optic nerve positioned at the center of the field of view. The dioptric focus was used to locate the plane of highest paracentral NIR reflectivity with the greatest number of saturated pixels when using a detector sensitivity with slight overexposure. As the highest bands of reflectivity on optical coherence tomography (OCT) approximate the RPE and use a similar excitation wavelength, this plane likely represents the outer retina. Uniform illumination of the posterior pole was achieved by ensuring balanced exposure in the superior, temporal, nasal, and temporal quadrants.

An NIR reflectance image was captured as an average of five or more stills taken in ART mode. Fluorescence cSLO images were subsequently acquired using the inbuilt blue autofluorescence (BAF) and indocyanine green angiography (ICGA) modules of the Spectralis platform. For acquisition of images for *in vivo* EGFP quantification, BAF mode was used with a 486 nm blue diode excitation laser coupled with a 500 nm barrier filter.

Emission was recorded between 500 nm and 700 nm. Images were collected at sensitivities in descending steps from 100% to 50%. The latter modality consisted of a diode laser of 768 nm wavelength and barrier filter at 830 nm, with detection of emission at longer wavelengths. Fluorescence fundal images were captured at the same focal plane as that used for NIR reflectance image acquisition.

2.4.3.2 Optical coherence tomography

Spectral domain optical coherence tomography (SD-OCT) images were captured with the Spectralis OCT module using a super luminescence diode laser (weighted average wavelength of 870 nm) to produce a cross-sectional B scan of the retina. For SD-OCT, the mouse remained in the same position on the viewing platform with the contact lens in situ. The positioning of the camera was adjusted to ensure a flat section oriented horizontally in the image. The imaging protocol consisted of eight equally spaced radially orientated scans centered on the optic disc. Each image was captured using a 55° lens in ART mode from an average of 25 individual B-scans. Photoreceptor layer (PRL) thickness was measured at a fixed 3000 μm distance from the optic disc defined by an overlaid Early Treatment of Diabetic Retinopathy Treatment Study (EDTRS) grid centered on the optic disc in the HEYEX software. Mean PRL thickness for a given eye was measured using software calipers, with eight measurement recordings from superior, superonasal, nasal, inferonasal, inferior, inferotemporal, temporal and superotemporal retinal loci.

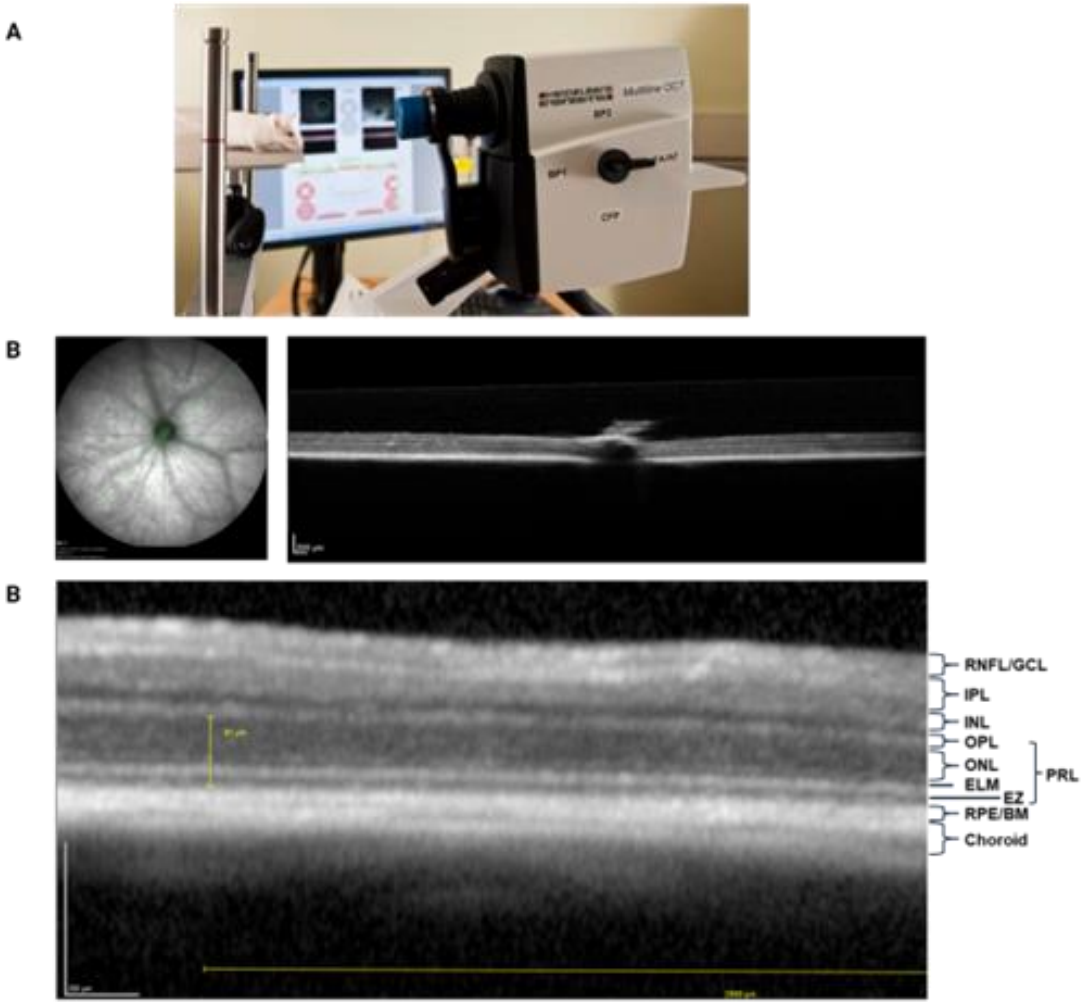


Figure 2.4 | Retinal imaging by cSLO and OCT

A. The mouse is positioned on the platform on the Heidelberg Spectralis with the head perpendicular to the camera and at the level of the notch indicating positioning eye. **B.** *En face* infrared cSLO image demonstrating the location of eight radial scans centered on the optic nerve with representative example of an OCT from a PBS-injected mouse demonstrating the cross-sectional image of the retina. **C.** OCT cross section of PBS-injected mouse retina. PRL thickness was measured at a fixed 3000 μm distance from the optic disc defined by an overlaid EDTRS.

RNFL, retinal nerve fiber layer; GCL, ganglion cell layer; IPL, inner plexiform layer; INL, inner nuclear layer. OPL, outer plexiform layer; ONL, outer nuclear layer; ELM, external limiting membrane; EZ, ellipsoid zone; PRL, photoreceptor layer; RPE, retinal pigment epithelium.

2.4.4 Electroretinography

Prior to electroretinography (ERG), mice were dark-adapted overnight (minimum 12 hours) within a purpose-built light-tight cabinet. The procedure was conducted in a designated windowless room with only dim red illumination used during setup where required. Active contact lens electrodes were created by attaching silver-coated nylon thread Dawson, Trick & Litzkow (DTL) Plus electrodes (Diagnosys) to custom contact lenses created from achromatic Aclar (Honeywell International). Mice were anesthetized and pupils dilated as described in Section 2.4.1. The animal was then transferred onto a heated platform set to 35°C inside a light-tight Faraday cage dark containing a Ganzfield stimulator dome (Colordome Electroretinography Machine, Diagnosys) and monitored via a video feed. Reference electrodes were placed subcutaneously oriented cranially in the midline, in the flank at the tail base and between the eyes respectively. Guttae hypromellose 1% (Alcon) coupling solution was instilled bilaterally and an active contact lens electrode placed centrally on each cornea. Active electrode impedance was maintained between 5-10 kΩ. Once in position, the mouse was left to acclimatize for a period of 10 minutes prior to commencing the custom ERG protocol using Espion software (Diagnosys) as referenced in Table 2.5. Electroretinogram (ERG) a- and b-wave amplitudes were measured manually using Espion software. The a-wave was defined as the first negative deflection and is mainly reflective of the physiological response of photoreceptors. The b-wave was defined as the peak of the subsequent larger positive deflection, reflecting the response of the more inner retina, predominantly bipolar and Müller cells. Flicker stimuli amplitudes were measured from the peak to the trough at approximately 200 ms post-stimuli onset. For all recordings, a 0-500 Hz bandpass filter

was used with line filtering, an amplifier gain of 8, a 4000 Hz sampling frequency and 600 ms sweep length.

Step	**Photopic Log (cd.s/m²)**	**Background (cd/m²)**	**Sweeps (n)**	**Intersweep delay (ms)**	**Description**
1	1×10^{-6}	0	16	2000	Single 0.5Hz 1×10^{-6} cd.s/m²
2	1×10^{-5}	0	16	2000	Single 0.5Hz 1×10^{-5} cd.s/m²
3	1×10^{-4}	0	9	5000	Single 0.5Hz 1×10^{-4} cd.s/m²
4	1×10^{-3}	0	9	5000	Single 0.5Hz 1×10^{-3} cd.s/m²
5	1×10^{-2}	0	9	5000	Single 0.5Hz 1×10^{-2} cd.s/m²
6	1×10^{-1}	0	4	20000	Single 0.5Hz 1×10^{-1} cd.s/m²
7	0	0	4	20000	Single 0.5Hz 1.0 cd.s/m²
8	1	0	2	40000	Single 0.5Hz 1×10 cd.s/m²
9	1.4	0	1	0	Single 0.5Hz 25 cd.s/m²

10	0.5	0	20	0	Continuous 10Hz 3.0 cd.s/m^2
11	0.5	0	20	0	Continuous 20Hz 3.0 cd.s/m^2
12	0.5	0	20	0	Continuous 30Hz 3.0 cd.s/m^2
13	0.5	30	10	1000	Single 0.5Hz 1.0 cd.s/m^2
14	0.5	30	20	0	Continuous 20Hz 3.0 cd.s/m^2
15	1	30	5	1000	Single 0.5Hz 10 cd.s/m^2

Table 2.5| ERG recording protocol

Standard ERG recording protocol used for the assessment of photopic and scotopic retinal function of mice, programmed with Espion software (Diagnosys).

2.5 Cell & tissue processing

2.5.1 Retinal tissue collection

Eyes were extracted from mice immediately after confirmation of death. In cases where radial orientation of the final section was important, the eye was removed together with its superior rectus muscle which acted as a downstream marker for the dorsal aspect of the globe. The eye was transferred into sterile PBS and other extraocular muscles and

conjunctival tags removed. The cornea was then punctured with a 23G needle and then excised with Vannas scissors peripherally just anterior to the limbus. The iris and zonules were bluntly dissected and then the lens gently extracted with forceps to avoid retinal traction.

For immunohistochemistry the resulting eye cup was fixed in cold 4% paraformaldehyde (PFA) on ice for 30 minutes and then washed briefly in PBS. The eyecup was cryoprotected using a sucrose gradient, in which it was sequentially incubated into 10%, 20% and finally 30% sucrose solutions, each for a period of at least 60 minutes (until the eyecup had sunk to the bottom of the solution). Eye cups were incubated in 30% sucrose overnight at 4°C, washed briefly in PBS, dried, and then embedded in optimal cutting temperature (OCT) compound in foil molds with the optic nerve oriented up. Specimens were then frozen in cooled isopentane on dry ice and stored at -80°C prior to cryosectioning.

For extraction of the neural retina, the optic nerve was trimmed at the base and then the sclera removed with a combination of blunt and sharp dissection to leave the intact neural retina. Retinas were snap frozen on dry ice and stored at -80 °C until further processing.

2.5.2 Immunohistochemistry

Eyes to be sectioned were removed from the -80°C freezer and transported on dry ice to a cryostat (Leica Biosystems) that had been pre-chilled to between -20 and -22°C. Frozen sections 16-18 μm thickness were cut on a cryostat (Leica Biosystems) pre-chilled to -20°C, mounted onto Superfrost Plus slides (VWR) and allowed to dry at room temperature overnight. A hydrophobic barrier pen was used to create an encircling border around the sections. Slides were stored at -20°C and thawed at room temperature for subsequent use.

For immunohistochemistry (IHC), slides were thawed at room temperature, condensation removed with a tissue and a perimeter border created with a hydrophobic barrier pen (Thermo Fisher Scientific). On each slide, a small area containing at least two tissue sections was separately demarcated with hydrophobic barrier pen Tissue sections in this region were incubated with PBS in place of primary antibody solution during the subsequent IHC protocol to act as negative control samples. The IHC protocol was as follows:

1. Sections were fixed in 100% Ethanol/IMS at 4°C for a period of twenty minutes.
2. slides were washed with a standard wash step by immersion in 0.01M PBS three times for five minutes per wash.
3. Tissue sections were permeabilized by incubation of slides in 0.3% Triton X-100 in 0.01M PBS for 20 minutes.
4. Three further PBS washes were performed as above.
5. Tissue sections were then incubated in 400 μL 0.01M PBS with 5-10% serum (Normal Goat Serum, NGS; or Normal Donkey Serum, NDS), 1% bovine serum albumin (BSA) and 0.3% Triton X for 20 minutes at room temperature.
6. Three further PBS washes were performed as above.
7. Primary antibody diluted in 250 μL 0.01M PBS with 1% serum, 1% BSA and 0.1% Triton X-100 was then added to the main section of slides. A smaller secondary-only control area of each slide was covered in diluent only. Slides were incubated overnight at 4°C.
8. Slides were washed by submersion in 0.05% Tween-20 in 0.01M PBS for five minutes. This process was repeated in fresh Tween-20/PBS solution before a final five-minute wash in 0.01M PBS was performed.

9. Secondary antibody (conjugated to a florescent dye) diluted 1:500 in 0.01M PBS with 0.1% Triton X-100 was then applied to the slides which were incubated in the dark at room temperature for two hours.
10. Slides were washed twice in 0.05% Tween-20 in 0.01M PBS as described above.
11. Tissue sections were counterstained through incubation in Hoechst 33342 (Life Technologies) diluted 1:1000 in 0.01M PBS for 30 minutes.
12. A final wash step was performed by submersion of slides in 0.01M PBS for five minutes.
13. Slides were removed from the PBS and excess liquid dried from the edges of the slide using tissues.
14. Small drops of ProLong Diamond antifade mounting medium (Thermo Fisher Scientific) were applied to the sections onto which glass cover slips were carefully placed

Details of specific antibodies used may be found in the methods sections of relevant experimental chapters. Secondary antibodies used were AlexaFluor antibodies (Thermo Fisher Scientific) raised in the appropriate species for the blocking agent (goat or donkey) against the appropriate species for the primary antibody (see Appendix). At the end of the staining protocol, slides were left to cure overnight in the dark at room temperature after which they were stored at 4°C.

2.5.3 Confocal microscopy

Confocal microscopy was performed using the LSM-710 inverted confocal microscope system using Zen software (Zeiss). Areas of interest were first identified using epiFluorescence illumination before XY confocal image capture using oil-immersion objectives (40×, 63×) with an optical section thickness of approximately 500 nm. Image exposure was optimized with adjustments to laser power, gain and offset. Z-

stack images were acquired at the optimal thickness determined by the software for the objective and laser configuration. For analysis image files were exported from the Zen software in *.lsm* file format and processed using FIJI ImageJ software (National Institutes of Health). Z-stack images were merged as maximum intensity projections.

2.6 Statistical analysis

All graphing and statistical analysis was performed using Prism software (v9.2.0, GraphPad). Quantitative measures and errors are presented as mean ± standard error of the mean (SEM) unless otherwise stated. Broadly, data was assessed for normality by frequency distributions, QQ plots and the Shapiro-Wilk test when data set size was large enough. When two matched or unmatched groups were to be compared, paired or unpaired two-tailed t-tests were used respectively, with Welch's correction applied in cases where the standard deviation between the groups could not be assumed to be equal. In circumstances where three or more groups were to be compared, or the effects of multiple factors were to be determined within two or more groups, one- or two-way analysis of variance (ANOVA) tests were performed respectively. If significant statistical interaction was confirmed between factors, appropriate post-hoc tests were applied which accounted for multiple comparisons. In all cases, p values less than 0.05 were considered statistically significant.

3. DEVELOPMENT AND OPTIMIZATION OF CRISPR CONSTRUCTS TOWARDS *IN VIVO* ADAPTATION

3.1 Introduction

3.1.1 Developing an efficient system for AAV-directed delivery of CRISPR reagents

The recent discovery of the clustered regularly interspaced short palindromic repeats (CRISPR)-Cas system has revolutionized the field of molecular biology and medicine. The CRISPR/Cas system encompasses a variety of components which differ widely in mechanisms of action and offer therapeutic potential by direct genome interaction and/or editing. The most widely adopted CRISPR-Cas genome editing platforms are the Cas9 endonucleases that create double-strand breaks in target DNA sequences complementary to a designed single-guide RNA. Among these, the most broadly used Cas9 homolog has been *Streptococcus pyogenes* Cas9 (SpCas9), which exhibits robust editing efficiencies, as well as a broad targeting range due to its short 5′-NGG-3′ PAM.

Viral vectors, especially AAV, remain the most attractive mode of delivering CRISPR-Cas systems to the retina given their proven clinical efficacy and safety. Delivery of most of these compact Cas9s within single-vector AAVs, whereby both the Cas9 and sgRNA components are packaged into the same virion, has been validated *in vivo*[92,225-230] and is the preferred approach for clinical translation. Although co-delivery of multiple AAV vectors has shown some promise in animal models,[231-233] an all-in-one strategy avoids

limitations of multi-vector approaches such as low co-transduction efficiencies and higher-potential for off-target effects. More importantly, the combined AAV dosages required for multi-vector strategies raise significant concerns about safety during clinical translation,[234,235] especially in light of tragic deaths in human trials of a high-dose AAV gene therapy.[236]

Naturally found Cas9 variants are large proteins, which adds particular limitation when it comes to packaging and delivery to target cells. Indeed, the SpCas9 protein is 1368 amino acids (aa), making therapeutic delivery challenging, especially when utilizing AAV vector systems that are severely constrained in cargo size.[230] To address these limitations, other CRISPR systems are actively being explored to identify Cas9-like effector proteins that may have differences in their sizes, PAM requirements, and targeting specificity. Some such Cas9 homologs, including Sth1Cas9 (1120 aa),[62] Nme1Cas9 (1082 aa),[237,238] SaCas9 (1053 aa),[229] CjCas9 (984 aa),[92] Nme2Cas9 (1082 aa),[226] and SauriCas9 (1061 aa)[227] are substantially smaller. Despite the positive attributes conferred by smaller Cas9 proteins, they suffer from a more limited targeting scope than what is imparted by SpCas9, due to their more complex PAM sequences that are less abundant throughout the genome. For example, SaCas9 requires a 5′-NNGRRT-3′ PAM sequence whereas CjCas9 requires a 5′-NNNNACAC-3′ PAM sequence.

In addition to Cas9 orthologues, other key elements in typical AAV expression vectors are promoter sequences to drive RNA transcription, poly(A) signals to drive cleavage and polyadenylation at the 3′ of pre-mRNAs, as well as other regulatory elements to enhance gene expression and stability. The requirement of these additional components, in addition to the pair of inverted terminal repeats (ITRs) flanking the ssDNA wildtype AAV genome, makes it difficult to deliver genes with coding sequences larger than 4 kb.

To date, published studies have utilized different genetic targets, construct designs and regulatory elements making it difficult to draw conclusions about the comparative efficiencies and specificities of Cas9 orthologues and regulatory elements. In this chapter, I sought to optimize an all-in-one system for efficient AAV-mediated delivery of CRISPR-Cas9 reagents. I developed a reporter system for direct evaluation of different components of the AAV expression cassette and genome engineering reagents on the same target and harboring identical vector backbones and regulatory elements. Using this system, I present highly efficient CRISPR-mediated gene knockdown delivered by a single vector.

3.1.2 Non-viral delivery using DNA-wrapped gold nanoparticles

One of the major challenges facing therapeutic adaptation of CRISPR-Cas-mediated technologies is the safe and efficient intraocular and intracellular delivery of gene editing system components. In addition to the limited packaging capacity of AAV vectors outlined above, these vector systems may also possess safety concerns relating to pre-existing anti-capsid immunity and vector-induced immunogenicity, as well as potential for genotoxicity and undesired genome editing. The use of non-viral delivery systems may mitigate these limitations and presents an attractive alternative for delivery of genome engineering reagents to the retina.

Despite the promise of non-viral delivery, therapeutic applications have been hindered by problems such as low transduction efficiency of target cells, cytotoxicity, and mutagenicity of the chromosomal DNA and have been reserved for *in vitro* and *ex vivo* delivery of CRISPR-Cas genome engineering regents to date. Recently, a delivery vehicle comprised of gold nanoparticles conjugated to DNA and complexed with cationic endosomal disruptive polymers, has demonstrated proof-of-concept for non-viral delivery of the RNA-guided endonucleases Cas9 and Cpf1 across different cell types and

for *in vivo* correction.[239,240] Moreover, preliminary results using DNA-wrapped gold nanoparticles have demonstrated successful delivery cultured differentiated retinal pigment epithelium (RPE) cells.[241] Here, I assessed the utility of DNA-wrapped gold nanoparticles for plasmid delivery *in vitro*. Additionally, I explored delivery of nanoparticle-delivered reporter plasmids in a pilot *in vivo* study and evaluated aspects of their safety including retina structure and function by optical coherence tomography and electroretinography.

3.2 Chapter aims

The overall goal of this chapter is to develop and optimize a CRISPR backbone which can be adapted for downstream genome and epigenetic editing experiments, and which can be packaged in a viral or non-viral vector system for *in vivo* delivery to efficiently target photoreceptors. To achieve this, the following aims will be explored:

1. Develop a reporter assay and design gRNAs for direct comparison of different construct elements.
2. Identify and screen Cas9 orthologues and small regulatory elements including promoters and PolyA sequences that permit minimalization of the construct size for packaging of CRISPR reagents within an AAV vector.
3. Assess gold nanoparticles as a non-viral delivery vehicle *in vitro* in HEK293T cells.
4. Evaluate the efficacy of gold nanoparticle-delivered reporter plasmids *in vivo* and characterize aspects of their safety including effects on retinal structure and function.

3.3 Methods & materials

3.3.1 Plasmid cloning

The general protocol for plasmid cloning is detailed in the general methods. Three plasmid constructs were generated containing Elongation factor 1-alpha 1 (EFS-1α) promoter driving the expression of SpCas9, SaCas9, and CjCas9 variants and the respective gRNA scaffold under a hU6 promoter. The pX601-AAV-CMV:NLS-SaCas9-NLS-3xHA-bGHpA;U6;BsaI-sgRNA (plasmid #61591, Addgene, USA) (a gift from Feng Zhang) was used as the backbone for all Cas9 variant designs. The optimized all-in-one SpCas9 backbone (AAV- EFS-1α-3xFLAG-2xNLS-Cas9-NLS-U6-gRNA) was utilized for direct evaluation of promoter elements and minimal polyA sequences. Plasmid identity was confirmed with Sanger sequencing. A table of cloning plasmids used, cloning detail, and plasmid origin is summarized below (Table 3.1).

Guide RNAs were subcloned with BsaI (NEB). Standard cloning protocols for annealed oligos as described in the general methods were performed. All primer and gRNA sequences are listed in the Appendix.

Cloning Elements	Detail	Source
pX601-AAV-CMV:NLS-SaCas9-NLS-3xHA-bGHpA;U6:BsaI-sgRNA	Plasmid backbone for all Cas9 orthologue comparisons and evaluations of promoter elements and minimal PolyA sequences.	Addgene Plasmid #61591
pX551-CMV-CjCas9	CjCas9 orthologue was amplified from plasmid via PCR with Phusion DNA polymerase (NEB) with 5′ extensions on the forward primers to generate	Addgene Plasmid #107035

	complementary overhangs. PCR amplification product was digested with AgeI / MfeI enzymes.	
pSpCas9(BB)-2A-Puro (PX459) V2.0	SpCas9 orthologue was amplified from plasmid via PCR with Phusion DNA polymerase (NEB) with 5′ extensions on the forward primers to generate complementary overhangs. PCR amplification product was digested with NdeI / NotI enzymes.	Addgene Plasmid #62988
Promoters: EFS-1α, CMV-IE Minimal polyA elements: bGH, SV40	A double-stranded fragments (IDT) encoding CMV and EFS promoters was cloned into the pX601 backbone digested with SpeI and HindIII enzymes. For cloning of polyA sequences, a double-stranded fragment (IDT) encoding the bGH and SV40 polyA elements was cloned into the pX601 backbone digested with SpeI and XbaI enzymes.	Integrated DNA technologies (IDT)
Kozak sequence, 3xFLAG, SV40 NLS (2x)	GBlocks encoding the Kozak consensus sequence, 3xFLAG, SV40 NLS (2x) and nucleoplasmin NLS were synthesized (IDT), and all fragments assembled with the Px601 backbone.	Integrated DNA technologies (IDT)

AAV-EFS-SpCas9-bGH-U6-gRNA	Final plasmid harboring SpCas9 orthologue in an optimized all-in-one vector backbone	Generated
AAV-EFS-SaSas9-bGH-U6-gRNA	Final plasmid harboring SaCas9 orthologue in an optimized all-in-one vector backbone	Generated
AAV-EFS-CjSas9-bGH-U6-gRNA	Final plasmid harboring CjCas9 orthologue in an optimized all-in-one vector backbone	Generated

Table 3.1|Cloning of all-in-one AAV plasmids

Cloning details for each AAV plasmid generated for Cas9 orthologue comparison and evaluation of promoter elements and PolyA sequences. All sequences of key plasmid elements and IDT gBlocks gene fragments are detailed in the Appendix.

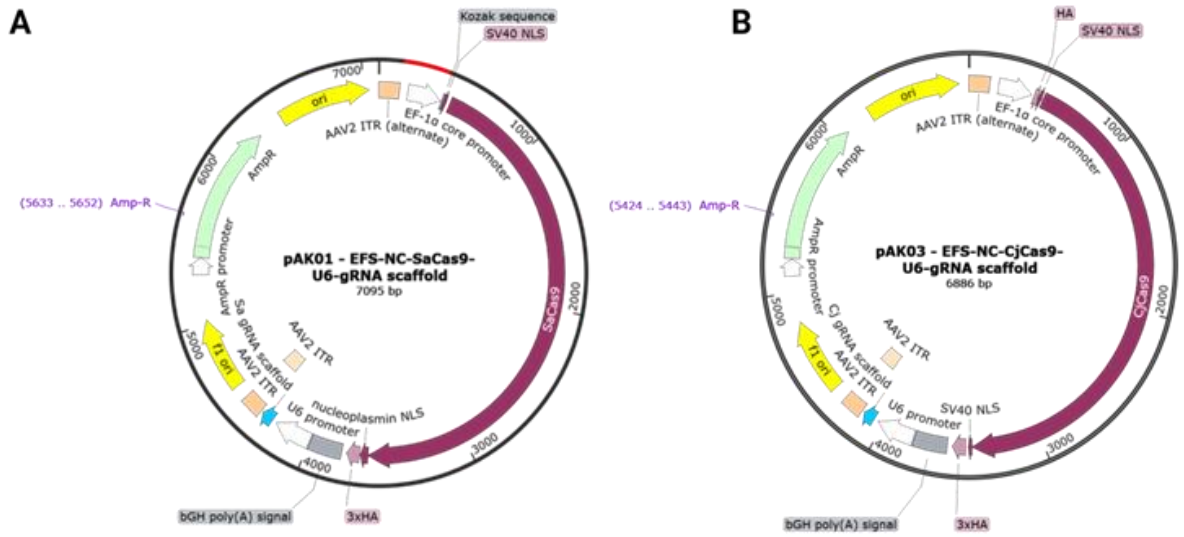


Figure 3.1 |Representative full plasmid maps of all-in-one SaCas9 and CjCas9 plasmids

A-B. Schematic showing the plasmid maps of final cloned product. All-in-one AAV plasmid constructs (AAV-EFS-1α-3xFLAG-2xNLS-Cas9-NLS-U6-gRNA) harboring SaCas9 (right) and CjCas9 (left) variants.

3.3.2 Cell culture

All transfections were performed in HEK293T and HEK293-EGFP cells maintained as described in the general methods. For experiments targeting EGFP, cells were seeded in 6-well plates and transfected with 2 μg of plasmid. Cells were harvested 72-96 hours post-transfection.

3.3.3 Protein fluorescence assays

Fluorescence spectroscopy assays were performed for quantification of protein knockdown following DNA editing. All assays were performed as described in the general methods. HEK293 cells seeded in 12 well plates were pelleted and resuspended in 100 μL of complete Fluorescence immunoprecipitation (FIPA) buffer (NaCl 150mM, Tris base 50mM, EDTA 2mM, 1% TritonX-100; adjusted to pH7.4 with HCl) supplemented with protease inhibitor (Roche Diagnostics, one tablet per 10 mL). Samples were then processed for protein extraction and quantification as described in the general methods. For each sample, 10 μg of protein was loaded 96 well black microplate (Greiner Bio-one) in duplicate and the volume made up to 300 μL with FIPA buffer / protease inhibitor.

Fluorescence emission from the protein lysate was measured in technical duplicates using a VICTOR3 plate reader (PerkinElmer, USA) with excitation at 485 nm, detection at 535 nm, and an exposure time of 1 second.

3.3.4 Analysis of editing efficiency (TIDE)

Locus PCR of the relevant target was performed with a high-fidelity polymerase (KOD Hotstart Mastermix, Merck-Millipore, USA) to generate ~700 bp amplicons from genomic DNA. The target region was amplified by PCR, the products were analyzed on an agarose gel to confirm a single band and sent for Sanger sequencing using the primer closest to the predicted cut site. DNA editing was calculated by uploading chromatograms to the Tracking of Indels by Decomposition (TIDE) online software along with unmodified DNA control samples. The decomposition window was adjusted to the length of the high quality read on the control sample, if required. All primer sequences are listed in the appendix.

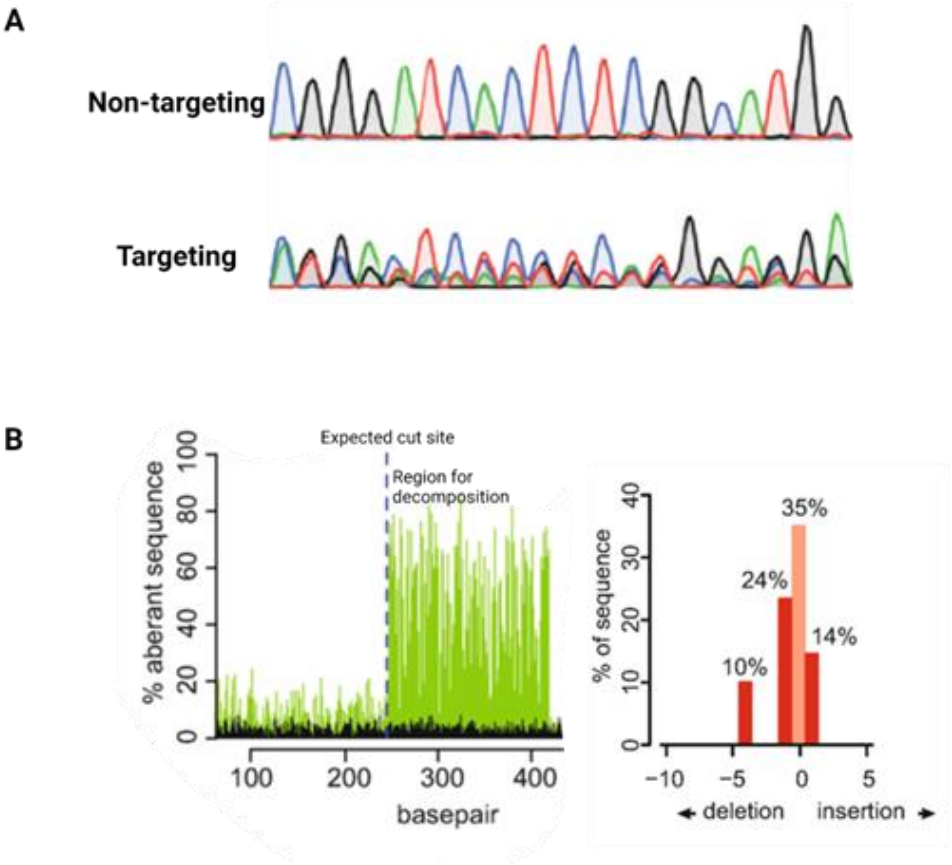


Figure 3.2 | Example output of TIDE analysis

A. TIDE is a simple and accurate assay to precisely determine the spectrum and frequency of targeted mutations generated in a pool of cells by genome editing tools such as CRISPR/Cas9. An example of a Sanger sequencing chromatogram of an amplicon from non-targeting (top) and targeting (bottom) guide RNAs. Cas9-mediated DNA double-strand breaks at the cut site were repaired by the non-homologous end joining-mediated pathway, resulting in generation of indels at the target loci. **B.** Analysis of the resulting raw sequencing files using the TIDE software. The algorithm accurately reconstructs the spectrum of indels from the sequencing traces and reports the identity of the detected indels and their frequency.

3.3.5 Gold nanoparticle production and nanotransfection

40 nm diameter, optical density (OD) 1 gold nanoparticles (NPs), stabilized suspension in citrate buffer, were purchased from Sigma-Aldrich (USA; S-741981). 100 μL of gold NPs at OD1 were spun down and resuspended in 10 μL of Milli-Q water and mixed with 1 μL (0.250 μg/μL) of EGFP and DsRed reporter plasmid DNA per well (see Appendix for plasmid construct and sequence detail). Plasmid DNA-gold hybrid structures were produced by allowing conditions in which double-stranded DNA loops wrap over the surface of the nanoparticle. DNA wrapped gold NPs were a gift from Sònia Trigueros.

DNA-wrapped gold nanoparticles were introduced in each well with seeded cells as described in the general methods. Photothermal plasmon resonance of the DNA-gold nanoparticles was activated by white light irradiation 1 to 2 hours post-nanotransfection. Cells were allowed to grow for 24 h / 48 h for EGFP/dsRed expression studies.

3.3.6 Animal procedures

C57BL/6J (Charles River, UK) were used for all animal experiments. Subretinal injections were performed as described in the general methods using a single 1 μL

injection delivered to the superior retina. Electroretinography, CSLO and OCT imaging was performed as described in general methods. Measurement and analysis were performed blind to experimental conditions applied. Dr Ahmed Salman assisted with animal procedures and blinded assessments.

3.3.7 Imaging and statistical analyses

Transmission and fluorescence images of live cells were taken using the Invitrogen EVOS FL Auto 2 Cell Imaging System (ThermoFisher). Image analyses were performed using ImageJ (FIJI) software 1.52i. For statistical analysis, three independent replicates were performed per condition. Values, ratios and statistical significance were analyzed using Prism software (v9.2.0, GraphPad).

3.4 Results

3.4.1 Design of an optimized all-in-one CRISPR vector

To develop an optimized vector for assessing CRISPR-mediated gene knockdown by a single vector, an all-in-one construct was designed. Constructs were cloned into an AAV-backbone with two 145-nucleotide-long inverted terminal repeats (ITR) at the termini. Vectors were comprised of an Elongation factor 1-alpha 1 (EFS-1α) short intron-less promoter[242] driving the expression of *Streptococcus pyogenes* Cas9 (SpCas9), followed by the SpCas9 guide RNA scaffold under the expression of an hU6 promoter. EFS-1α is a clinically validated cellular-derived enhancer/promoter with decreased cross-activation of nearby promoters, therefore hypothetically decreasing the risk of genotoxicity. All constructs were designed to contain 2 copies of the SV40 nuclear localization sequence (SV40-NLS) flanking SpCas9, as well a nucleoplasmin NLS cloned at the 5′ end.[243] The bovine growth hormone polyadenylation (bGH-PolyA) signal was employed in all constructs.[244] Finally, a 3X-FLAG peptide tag was included in all constructs for downstream detection by immunostaining assays (Figure 3.3). The cloning methodology for generation of the all-in-one vector is summarized in Section 3.3.1, and all key elements, primer sequences, and plasmid sources are detailed in the Appendix.

3.4.2 Evaluation of promoter elements and minimal PolyA sequences

An experimental approach was developed for screening of different promoter elements and minimal PolyA sequences against the same target. Minimal promoter and PolyA elements were cloned in a stepwise manner, such that all other elements of the validated construct were kept identical (Figure 3.3). The major immediate-early promoter and enhancer of the human cytomegalovirus (hCMV-MIE) promoter was cloned in place of the EFS-1α in the vector backbone. This promoter was selected as it is one of the most

potent DNA elements driving recombinant gene expression in mammalian cells.[245] Separately, the SV40 PolyA (Simian virus 40 PolyA) sequence,[246] a minimal sequence (240 bp) that possesses the activity of transcription termination and can add PolyA tail to mRNA, was cloned in place of the bGH PolyA (Figure 3.3). Prior studies have shown that SV40 could demonstrate polyadenylation of SaCas9 for transcriptional modulation at levels equivalent to the longer bGH PolyA.[247]

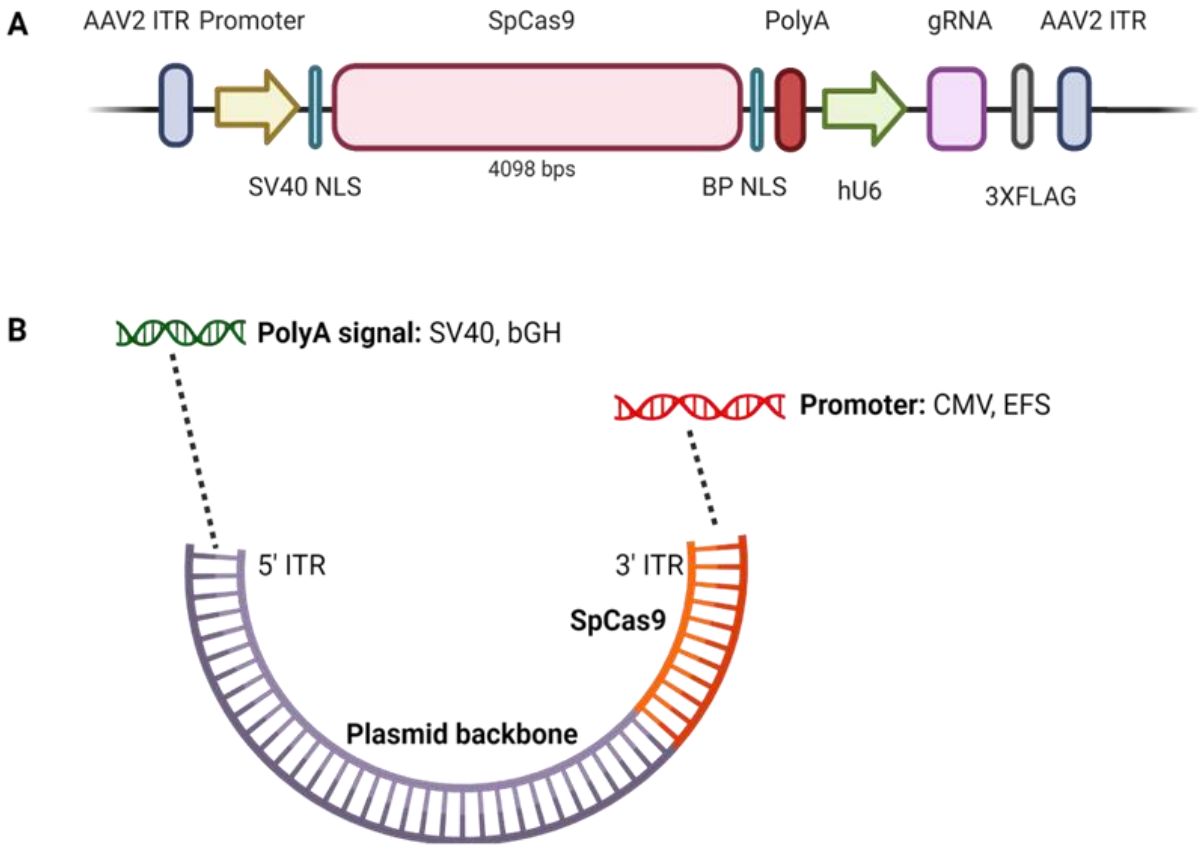


Figure 3.3 | Cloning of regulatory elements for gene suppression

A. Schematic summarizing the vector design. The same construct backbone was utilized for all comparison experiments, with promoter and PolyA elements cloned in a stepwise manner, such that all other elements were kept identical. **B.** The major immediate-early promoter and enhancer of the human cytomegalovirus (hCMV-MIE) promoter was cloned in place of the EFS-1α in the

vector backbone. The Simian virus 40 (SV40) PolyA was cloned in place of the bGH polyA. Key element sequences are detailed in the Appendix.

There were no significant difference (p=0.23) in editing rates across the two promoters evaluated, and HEK293-EGFP cell lines transfected with the SpCas9 vector harboring the hCMV-MIE promoter and gRNA-1 showed editing rates of 77.2% ± 4.2%, versus indel rates of 74.9% ± 6.3% with the EFS-1α promoter targeting the same guide (Figure 3.9). In the experiment investigating PolyA sequences, the construct comprised of the SV40 PolyA showed editing rates of 43.2% ± 6.8%, significantly lower (p<0.01) than the 73.4% ± 4.6% observed with the bGH PolyA containing construct (Figure 3.9).

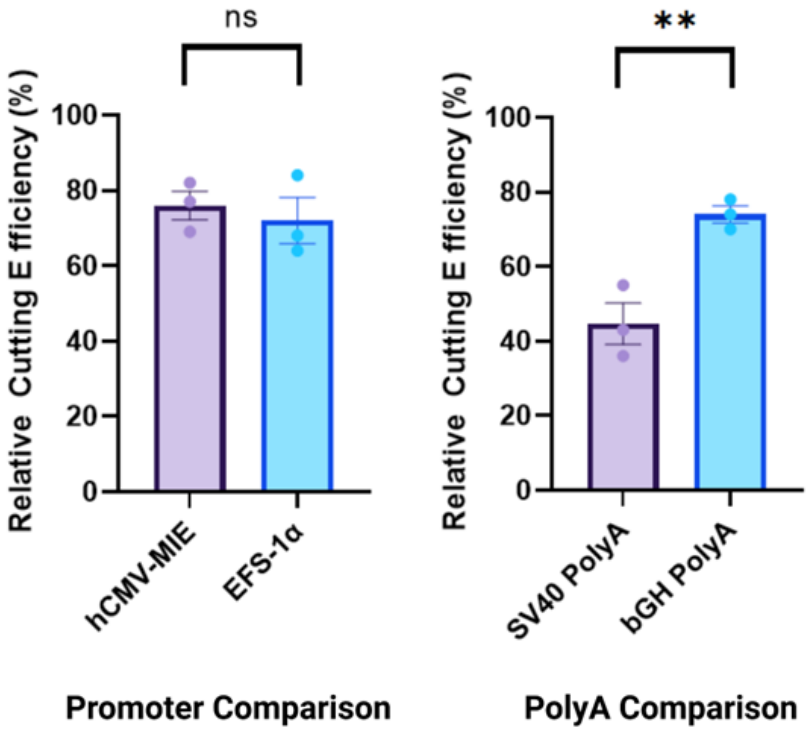


Figure 3.4 | Evaluation of minimal promoter and PolyA signals

Comparison of on-target cutting efficiency across minimal promoter (left) and PolyA signals (right), as measured by TIDE analysis. HEK293-EGFP cell lines transfected with the SpCas9 vector harboring the hCMV-MIE promoter and gRNA-1 showed editing rates of 77.2% ± 4.2%. The same construct with the EFS-1α promoter showed indel rates of 74.9% ± 6.3%. The data are presented

by mean value ± SEM with all data points from independent experiments shown. ***p<0.01, Sidak's multiple comparison test. All other comparisons were not significant.

3.4.3 Cas9 orthologue screening for gene suppression activity

Although SpCas9 is the most widely used CRISPR orthologue for genome manipulation, with a highly flexible '5-NGG-3' PAM sequence requirement, its large size (1368 aa) makes therapeutic delivery challenging. A number of different Cas nucleases have been used for genome and epigenome perturbations, each possessing differences in their size, PAM requirements, and targeting specificity. Furthermore, studies published to date have utilized different genetic targets, construct designs and regulatory elements, making it difficult to draw conclusions about the comparative efficiencies and specificities of each nuclease.

Having evaluated the differences in cutting efficiency across different promoter elements and minimal PolyA sequences, Cas9 orthologues were subsequently screened. Since the established experimental approach for regulatory element screening allows for evaluation of other components against the same target, identical gRNAs targeting the HEK293-EGFP cell line were applied for the regulatory element evaluation.

To directly investigate the efficiencies of different Cas9 variants, three constructs were cloned harboring different orthologues. All constructs used exactly the same regulatory elements and were assembled into identical vectors for delivery (Figure 3.5). *Staphylococcus aureus* (SaCas9) was selected due to its broad utility for genome engineering and compact size (1053 aa) enabling packaging in AAV vectors. Importantly, the first CRISPR-based experimental medicine in clinical trials for retinal disease, EDIT-101 (Editas Medicine Inc., Cambridge, MA, USA), uses a CRISPR-SaCas9 editing system. Moreover, despite sharing only 17% sequence identity with SpCas9, SaCas9 recognizes the PAM-distal region of the guide RNA–target DNA in a similar manner to SpCas9.

Finally, I investigated *Campylobacter jejuni* (Cj)-derived Cas9, the smallest Cas9 orthologue (984 aa) characterized at the time of this experiment. Previously, Kim and colleagues characterized the PAM sequence and optimal sgRNA length for CjCas9 and generated a high-titer all-in-one AAV vector harboring CjCas9 for efficient editing of retinal pigment epithelium cells.[92]

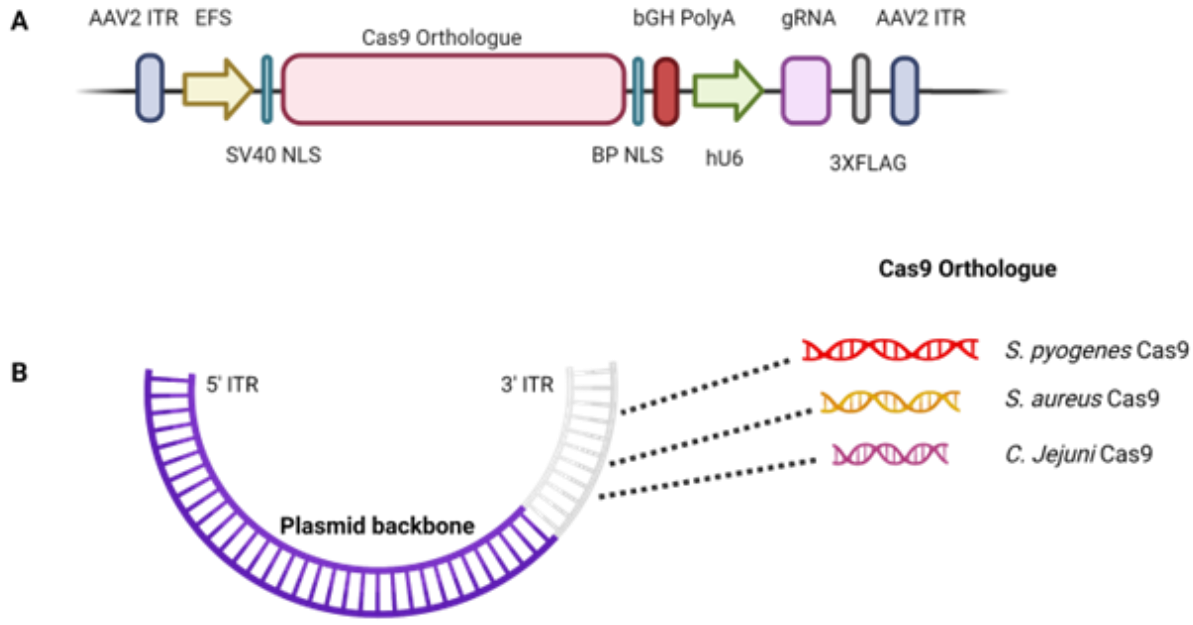


Figure 3.5 | Cloning of an all-in-one vector harboring different Cas9 orthologues

A. Schematic summarizing the vector design. The construct backbone (AAV-EFS-1α-3xFLAG-2xNLS-Cas9-NLS-U6-gRNA) was optimized with regulatory elements and nuclear localization signals to enhance editing rates. A FLAG peptide tag was included in all constructs for downstream detection by immunostaining assays. **B.** Three plasmid constructs were generated harboring SpCas9, SaCas9, and CjCas9 orthologues, respectively. All constructs used the same regulatory elements and were assembled into identical vectors for delivery. Key element and primer sequences are detailed in the Appendix.

3.4.3.1 Guide RNA design against transgenic HEK293-EGFP cell line

To assess the comparative efficiencies of each nuclease, a commercially available transgenic HEK293-EGFP cell line (constitutively expresses EGFP from a CMV promoter) was used. Two gRNAs (EGFP-13 and EGFP-15) were previously identified to have the highest on target editing efficiency in a screen of gRNAs targeting EGFP (Caroline Peddle). However, when tested, these guides edited at a relatively low efficiency of 10-12% (unpublished data). To optimize editing efficiencies and identify genomic targets amenable to editing across the different Cas9 orthologues, an additional gRNA screen was conducted, informed by *in silico* design (CRISPick, Broad Institute). 3 different genomic regions were identified within close proximity of PAM sequences for the respective Cas9 orthologues, designed to minimize any target specific binding preferences (Figure 3.6). Since SpCas9 PAM site (NGG) is flexible and SaCas9 (NNGRR(N) and CjCas9 (NNNNRYAC) PAMs are more restrictive, identical gRNAs were designed between SpCas9 and the other Cas9 counterparts. Thus, SpCas9 was used as the standardization control to directly compare relative editing efficiencies between the three different orthologues investigated (Figure 3.6). Importantly, the cut-sites across the enzymes were identical, eliminating the effect of non-homologous end joining-mediated repair on editing outcomes.

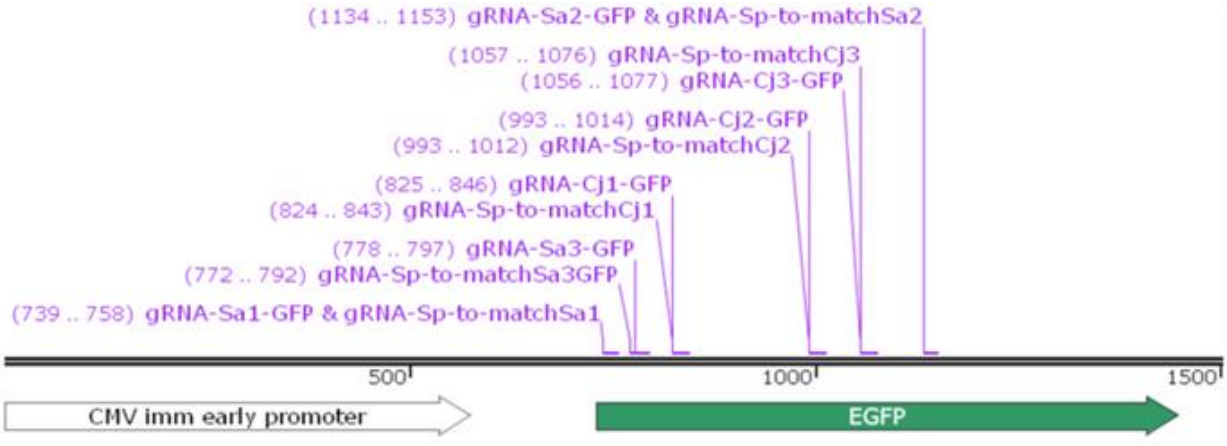


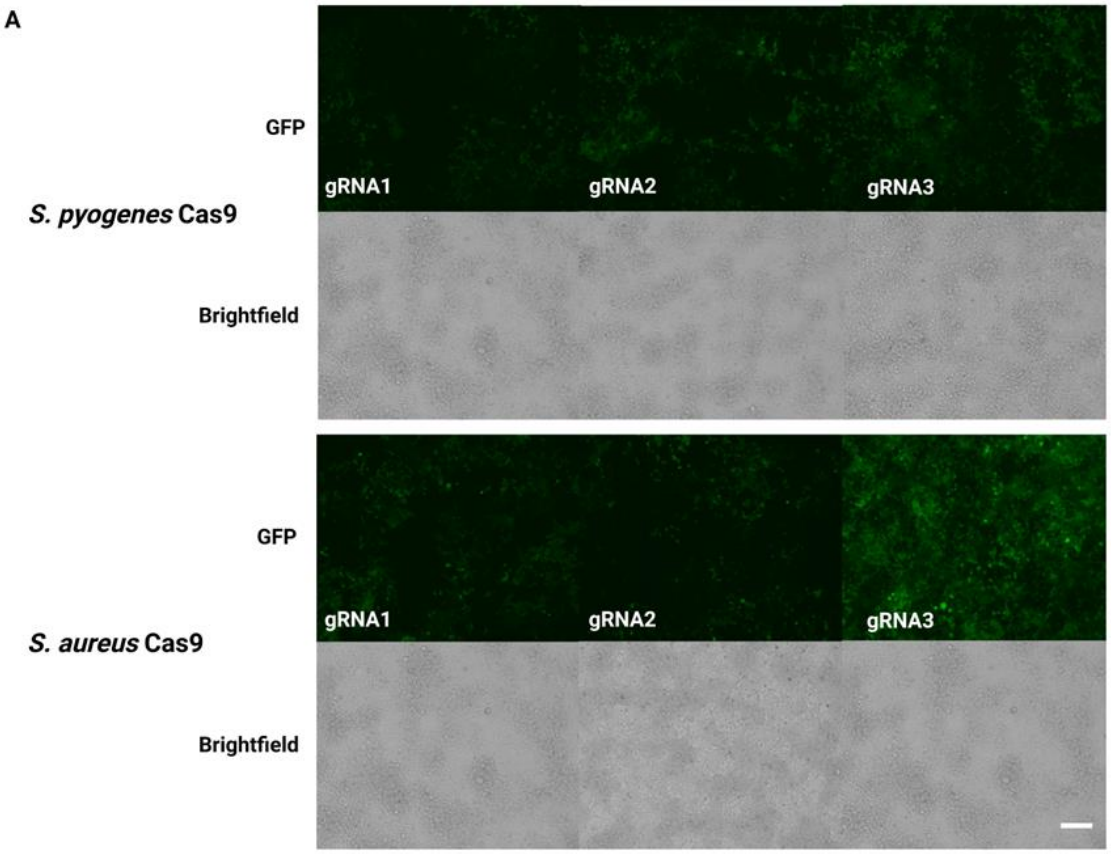
Figure 3.6 | Guide RNA design for Cas9 orthologue comparison

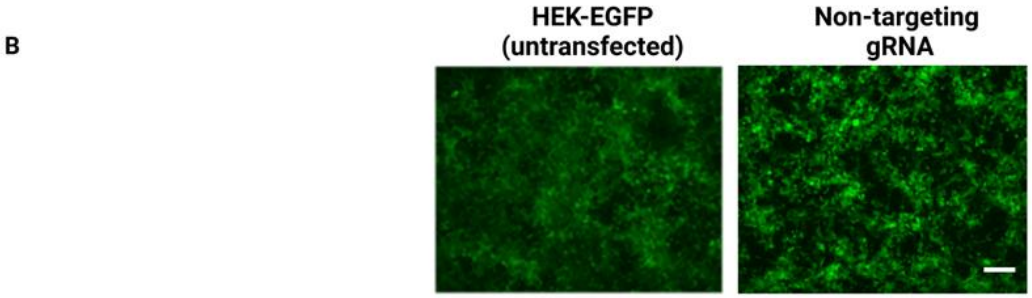
Guide RNAs were designed *in silico* (CRISPick) to target EGFP in a transgenic HEK293-EGFP cell line. 3 different genomic regions were identified within close proximity of PAM sequences and possessing identical cut-sites across the different Cas9 variants. gRNAs were cloned to SpCas9 to match SaCas9, and SpCas9 to match CjCas9, due the more promiscuous PAM targeting range of SpCas9. Guides were designed to minimize any target specific binding preferences or variability in NHEJ-mediated gene knockdown outcomes.

3.4.3.2 Effect of Cas9 orthologue on EGFP expression levels

To evaluate editing efficiencies, HEK293-EGFP cells were transiently transfected with plasmids expressing the EGFP-targeting guide and the respective Cas9 orthologue, as well as non-targeting gRNA controls. A CAG-dsRed plasmid (a gift from Michelle McClements) was used as a positive transfection control, and transfection conditions were optimized to enhance editing efficiencies and reduce inter-replicate variability by altering the plate size (6-well vs. 24-well), vector concentrations (500 ng up to 3 μg), and cell imaging and harvesting times (24 hours up to 96 hours). At the final transfection dosage of 2 μg, no dose-limiting toxicity or cell death was observed. Relative expression of Cas9 and gRNA was assessed via RT-qPCR, with no differences in the relative expression levels of the different constructs (data not shown). Notably, significant differences in EGFP knockdown were observed across all tested constructs and gRNA combinations ($p<0.01$, two-way ANOVA) as assessed via both fluorescence microscopy imaging taken 72 hours after transfection and a protein fluorescence assay (Figure 3.7). Guide RNAs varied in their EGFP knockdown efficiencies, with gRNA-1, targeting the proximal 5′ region of the EGFP, achieving greater knockdown in all three Cas9 orthologues as compared to gRNA-3, oriented towards the center of the EGFP transgene (Figure 3.6). The highest rates of gene knockdown were achieved by SpCas9, with up to 87%, 62%, and 21% EGFP knockdown with gRNAs 1-3, respectively, as assessed by

fluorescence spectroscopy. SaCas9 showed slightly lower but still robust rates of 82%, 61%, and 11% EGFP knockdown across gRNAs 1-3, respectively (Figure 3.7). Together, this study supports that SpCas9 generates the highest levels of gene knockdown, though SaCas9 editing was only significantly lower in the worst performing gRNA-3, and the SaCas9 variant is almost 400 aa smaller than its SpCas9 counterpart.


A
GFP
gRNA1
gRNA2
gRNA3
S. pyogenes Cas9
Brightfield
GFP
gRNA1
gRNA2
gRNA3
S. aureus Cas9
Brightfield


B
HEK-EGFP (untransfected)
Non-targeting gRNA

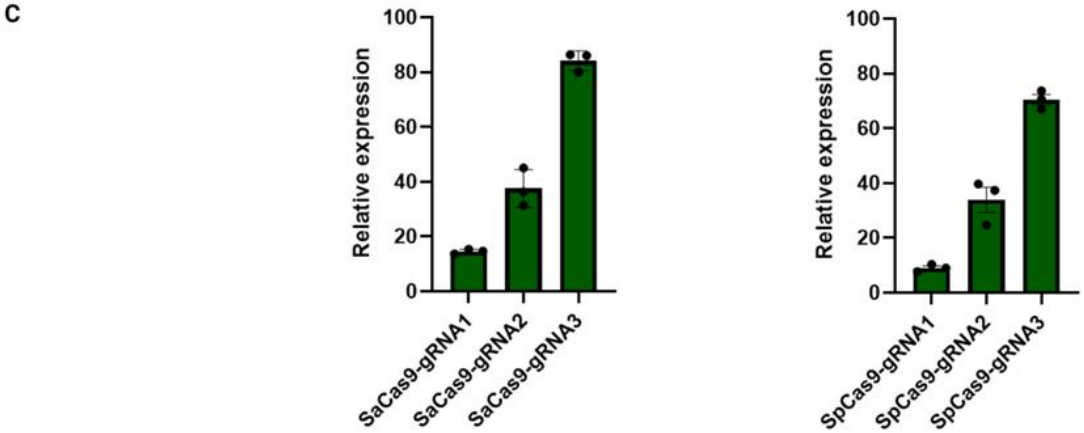

C
Relative expression
100
80
60
40
20
0
SaCas9-gRNA1
SaCas9-gRNA2
SaCas9-gRNA3
Relative expression
100
80
60
40
20
0
SpCas9-gRNA1
SpCas9-gRNA2
SpCas9-gRNA3

Figure 3.7 | Comparison of SpCas9 and SaCas9 editing efficiency

A. Representative fluorescence microscopy images taken 72 hours following transfection. Guide RNAs varied in their EGFP knockdown efficiencies, with gRNA-1, targeting the proximal 5' region of the EGFP, achieving greater knockdown, and gRNA-3 showing the lowest levels of EGFP suppression. At the transfection dose (2 μg), no dose-limiting toxicity or cell death was observed. **B. B.** No EGFP knockdown was observed with a non-transfected control or using a non-targeting gRNA. **C.** EGFP expression in protein lysates as assessed via a protein fluorescence assay. SpCas9 showed 87%, 62%, and 21% EGFP knockdown with gRNAs 1-3, whereas SaCas9 showed knockdown rates of 82%, 61%, and 11% EGFP across gRNAs 1-3, respectively. All analysis was normalized to samples transfected with a non-targeting gRNA control. The data are presented by mean value ± SEM with all data points from independent experiments shown. Scale bar, 100 μm.

Although a significant difference in EGFP expression levels was observed across all tested constructs when standardized against samples transfected with a non-targeted gRNA control, and the editing efficiencies were very similar across SpCas9 and SaCas9 variants, the minimal CjCas9 orthologue showed substantially lower editing rates (Figure 3.8). While different gRNAs were designed to compare between SpCas9 and CjCas9 (Figure 3.8), the same trend was observed for the screened guides, with gRNA-1 being the best performing guide and gRNA-3 being the worst performing gRNA across both orthologues. However, whereas robust EGFP knockdown rates of 76%, 63%, and 49% were observed with SpCas9 across gRNAs 1-3, CjCas9 editing rates were 26%, 12%, and 9%, respectively (Figure 3.8). Previously validated gRNAs were tested, demonstrating similar levels of knockdown as observed in the original manuscript by *Kim et al.* Moreover, no differences in the relative expression levels of the different constructs were observed by RT-qPCR, with (data not shown). Together, this data suggests that lower rates of editing may be caused by lower activity of CjCas9 as compared to SpCas9 and SaCas9 orthologues.

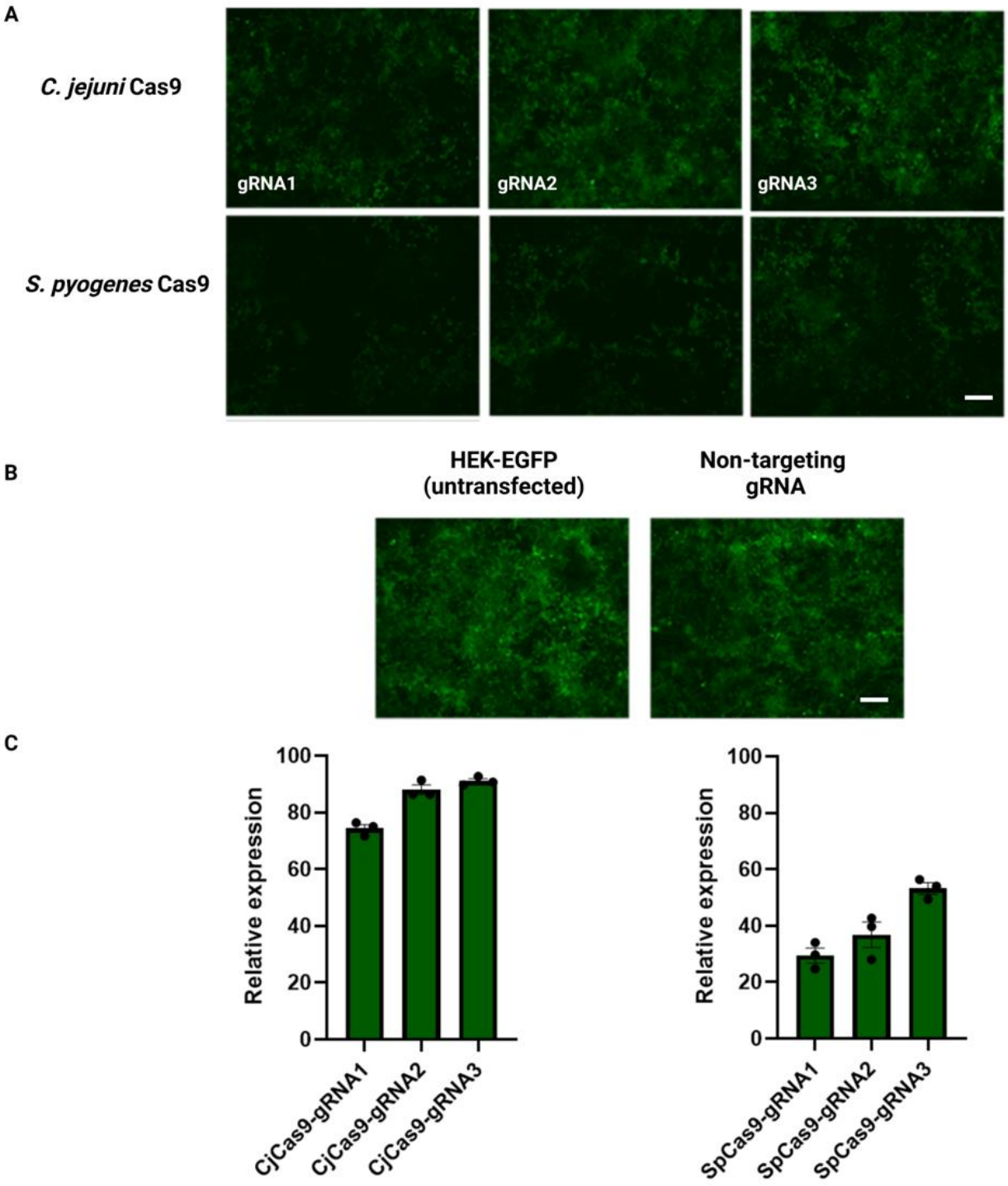

A
C. jejuni Cas9
S. pyogenes Cas9
gRNA1
gRNA2
gRNA3
B
HEK-EGFP (untransfected)
Non-targeting gRNA
C
Relative expression
100
80
60
40
20
0
CjCas9-gRNA1
CjCas9-gRNA2
CjCas9-gRNA3
SpCas9-gRNA1
SpCas9-gRNA2
SpCas9-gRNA3

Figure 3.8 | CjCas9 shows substantially lower levels of editing compared to SpCas9 and SaCas9 orthologues

A. Representative fluorescence microscopy images taken 72 hours following transfection. At the transfection dose (2 μg), no dose-limiting toxicity or cell death was observed. **B.** No EGFP knockdown was observed with a non-transfected control or using a non-targeting gRNA. **C.** EGFP expression in protein lysates as assessed via a protein fluorescence assay. EGFP knockdown rates of 76%, 63%, and 49% were observed with SpCas9 across gRNAs 1-3, whereas CjCas9 editing rates were 26%, 12%, and 9%, respectively. Scale bar, 100 μm.

3.4.3.3 Quantifying editing rates by TIDE analysis

To quantify editing rates across the different Cas9 orthologues evaluated and confirm that the detected EGFP knockdown is a result of a target-specific NHEJ-mediated mechanism, genomic regions encompassing the target sites were amplified from the genomic DNA and PCR products were analyzed by Sanger sequencing. Editing rates were quantified using Tracking of Indels by Decomposition (TIDE) software. Samples transfected with SpCas9 showed on-target editing rates of 78.2% ± 3.2%, 74.2% ± 2.6%, and 24.4% ± 6.8% across gRNAs 1-3, respectively. Samples transfected with SaCas9 showed slightly lower editing rates of 67.4% ± 4.3%, 64.1% ± 7.4%, and 9.6% ± 2.7% across the three gRNAs (Figure 3.9). In the study comparing CjCas9 and SpCas9, the SpCas9 orthologue showed similar editing rates of 79.1% ± 3.7%, 68.2% ± 2.1%, and 21.2% ± 4.9% across gRNAs 4-6, compared to 20.3% ± 3.4%, 36.2% ± 5.3%, and 4.2% ± 2.9% cutting efficiency with CjCas9 (Figure 3.9). No on-target editing was detected in samples transfected with non-targeting guides. Rates of each replicate quantified by TIDE analysis were closely correlated with the fluorescence images and protein fluorescence analyses, with CjCas9 gRNA-2 (SpCas9 gRNA-5) showing higher rates of targeted indel generation by Sanger sequencing as compared to the outputs observed in the prior study. However, there was higher inter-replicate variability between these samples and a lower editing

rate of the guides. Together, TIDE analysis supports the conclusion that the gene suppression observed in HEK293-EGFP cells transfected with targeting Cas9 constructs is due to NHEJ-mediated knockdown on EGFP, and not a spurious decrease in EGFP expression secondary to other mechanisms.

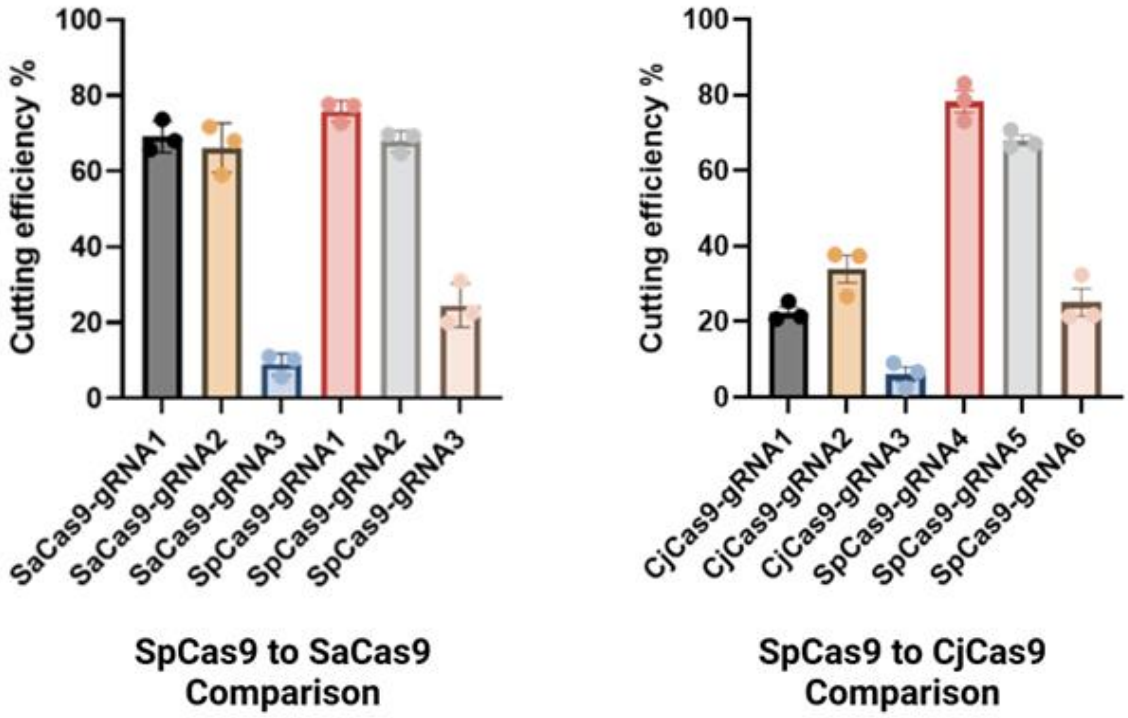


Figure 3.9 | Quantifying cutting efficiency of Cas9 orthologues by TIDE analysis

Comparison of on-target cutting efficiency across different Cas9 orthologues, as measured by TIDE analysis. Samples transfected with SpCas9 showed on-target editing rates of 78.2% ± 3.2%, 74.2% ± 2.6%, and 24.4% ± 6.8% across gRNAs 1-3. Samples transfected with SaCas9 showed editing rates of 67.4% ± 4.3%, 64.1% ± 7.4%, and 9.6% ± 2.7% across the three gRNAs. Comparing CjCas9 and SpCas9 (right), SpCas9 showed similar editing rates of 79.1% ± 3.7%, 68.2% ± 2.1%, and 21.2% ± 4.9% across gRNAs 1-3, compared to 20.3% ± 3.4%, 36.2% ± 5.3%, and 4.2% ± 2.9% cutting efficiency with CjCas9. All analysis was normalized to samples transfected with a non-targeting gRNA control. The data are presented by mean value ± SEM with all data points from independent experiments shown.

3.4.4 Nanotransfection of HEK293 cells with DNA-wrapped gold nanoparticles

Realizing the promise of therapeutic *in vivo* gene editing requires the ability to deliver gene editing reagents safely and efficiently to relevant organs and tissues *in vivo*. Non-viral delivery vehicles, including nanoparticles (NPs), offer unique advantages, especially for delivery of gene editing agents. Although *a priori* NPs might yield lower transgene expression levels compared to viral vectors, they present superior biosafety, lower cost and ease of production, and most importantly, broad DNA packaging capacity for delivery of bulky genome and epigenome editors.

Gold nanoparticles (AuNPs) has been investigated both *in vitro* and *in vivo* in the CNS[239] and muscle[248] and may be adapted for gene editing in ocular tissue. It is easy to cross-link AuNPs with sulfhydryl (-SH) substances through Au-S bonds and manipulate their surface charge and hydrophilicity. After constructing AuNP surface-modified cationic peptides, pCas9 can be adsorbed by electrostatic interactions.[249] Recently, Sònia Trigueros and colleagues assessed the novel physical properties at the nanoscale of inorganic gold nanoparticles for delivering genes to the retinal pigment epithelium (RPE).[250] They demonstrated preliminary results using DNA-wrapped gold nanoparticles for successful *in vitro* gene delivery on human retinal pigment epithelium (ARPE-19) cell cultures.[250]

To further investigate the potential of AuNPs for gene delivery, DNA-wrapped gold nanoparticles were prepared by Sònia Trigueros at the University of Barcelona. 100 μL of gold NPs at OD1 were spun down and resuspended in 10 μL of Milli-Q water and mixed with 1 μL (0.250 μg/μL) of EGFP and dsRed reporter plasmid DNA per well (see Section 3.5.5). HEK cells were seeded in 6-well plates as described in the general methods, and DNA-wrapped gold NPs, wrapped with pEGFP and pDsRed, were used to transfect

HEK293T cells. The plasmon resonance of DNA-gold NPs was activated by white light for 1-minute. After 12-, 24-, 48-, and 72-hours post-transfection, fluorescence images were obtained. Reporter fluorescence in the GFP or RFP channels was observed within 12-hours of fluorescence, with the highest signal observed at 48-hours post-transfection (Figure 3.10). Similar expression levels were observed in the GFP and RFP protein lysates as assessed via a protein fluorescence assay (data now shown). No reporter fluorescence was seen in any samples transfected with empty AuNPs or NPs wrapped with a control dsDNA cloning vector. No toxicity was observed across any of the nano-transfection conditions (Figure 3.10).

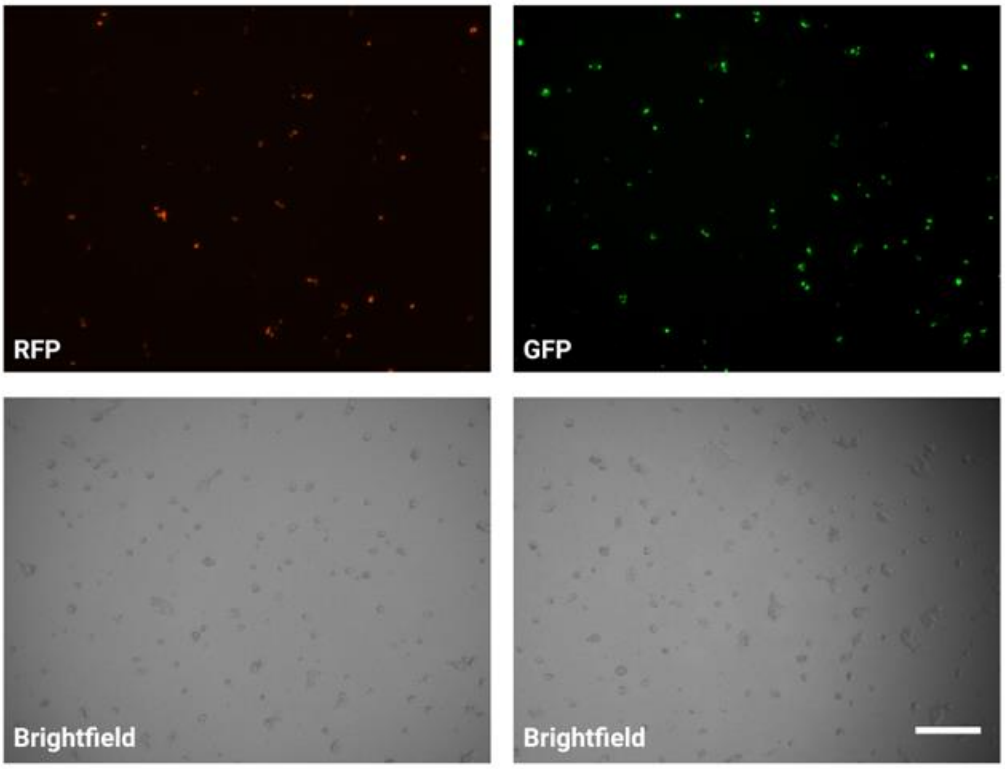


Figure 3.10 | Transfection of HEK293T cells with gold nanoparticles wrapped with EGFP and DsRed reporter plasmids

Representative light-microscope images (10X magnification) of HEK293T cells 48-hours after nano-transfection with pEGFP and pDsRed wrapped gold nanoparticles. Reporter fluorescence

in the RFP (left) or GFP (right) channels was observed within 12-hours of fluorescence, with the highest signal observed at 48-hours post-transfection. No reporter fluorescence was seen in any samples transfected with empty AuNPs or NPs wrapped with a control dsDNA cloning vector. No toxicity was observed across any of the nano-transfection conditions (brightfield channel). Scale bar, 100 μm.

3.4.5 Pilot *in vivo* experiment with gold nanoparticles

3.4.5.1 Assessment of EGFP expression with cSLO autofluorescence imaging

To explore the capacity of AuNPs for *in vivo* gene delivery to the retina, four-week-old C57BL/6 (Charles River, Harlow, UK) mice received a 1 μL subretinal injection to create a superior hemi-retinal bleb with one of two nanoparticles, a 40nm AuNP (40nm NP) that was investigated in *in vitro* study (Figure 3.10), and a 40 nm diameter, methyl terminated, PEG 2000 coated AuNP (NP-PEG). Both NPs were wrapped with pEGFP, prepared by Sònia Trigueros at the University of Barcelona, and shipped and maintained at 4°C prior to injection. The plasmon resonance of DNA-gold NPs was activated by white light for 1- and 3-minutes post injection. For all subretinal injections, the contralateral eye received a matched buffer control injection (Buffer) to control for the effect of surgical trauma or buffer-related toxicity. Additionally, un-injected C57BL/6 mice (WT) were monitored as a negative control (Figure 3.11).

EGFP expression was examined *in vivo* at 1-,2-,4-, and 8-weeks post-injection using blue autofluorescence (BAF) confocal scanning laser ophthalmoscope (cSLO) imaging (Figure 3.11). As the lateral spread of the AuNP vector is limited and transfection is mostly confined to the bleb area created in the superior hemi-retina, EGFP expression was expected to localize superior to the optic nerve. No EGFP expression was observed across any of the tested AuNPs in the retina. (Figure 3.11). Expression of EGFP mRNA was assessed by RT-qPCR from harvested retinas (superior retina, inferior retina, or

whole retina), with no expression detected across any experimental conditions (data not shown; TaqMan probe sequence in the Appendix).

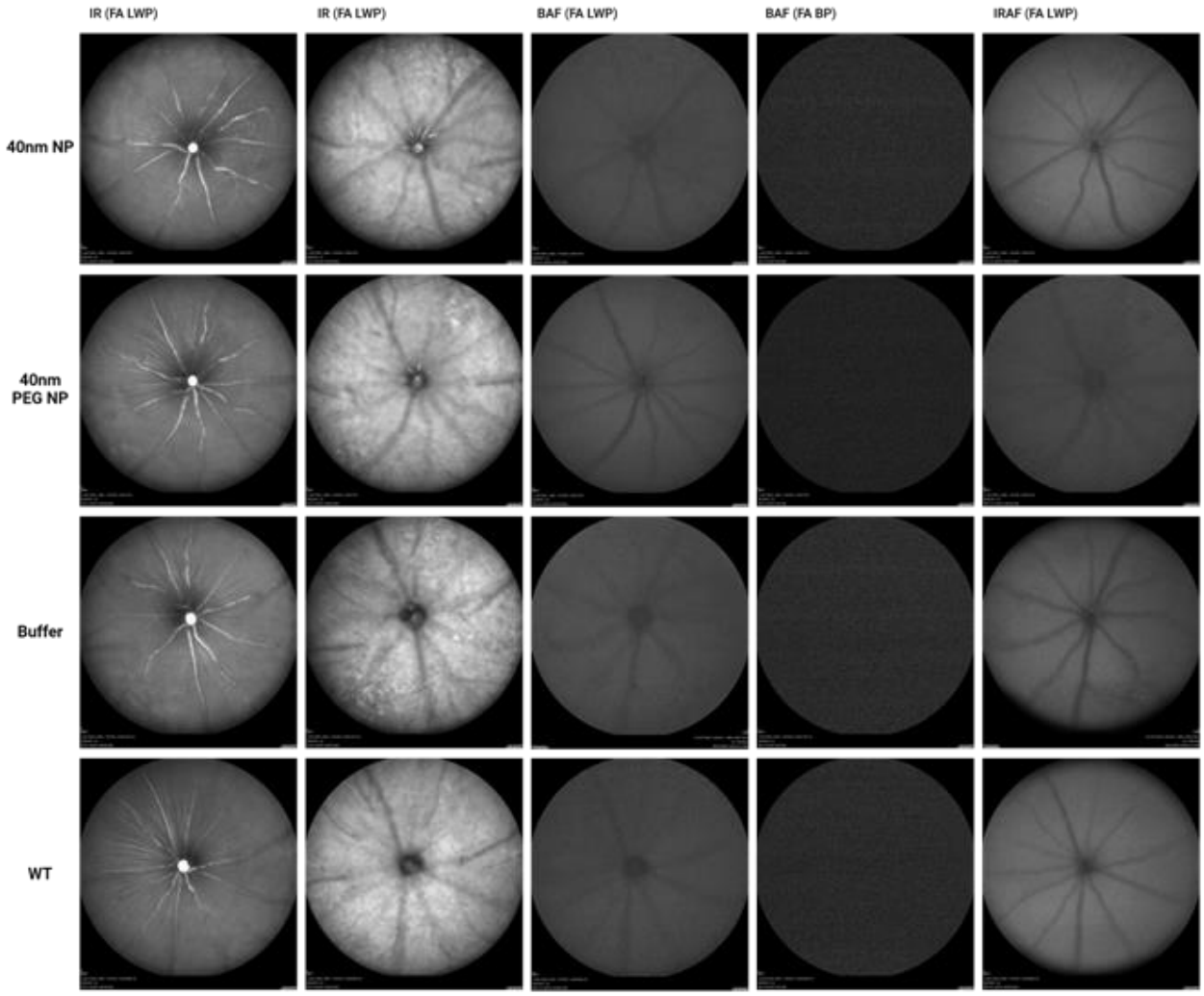


Figure 3.11 | *En face* cSLO imaging following subretinal injection

Retinal imaging of paired eyes from mice 8-weeks following subretinal injection with gold nanoparticles wrapped with pEGFP. Two NPs were investigated, a 40nm AuNP (40nm NP; top panel) that and a 40 nm diameter, methyl terminated, PEG 2000 coated AuNP (NP-PEG; second panel). Both NPs were prepared by Sònia Trigueros at the University of Barcelona. The plasmon resonance of DNA-gold NPs was activated by white light for 1- and 3-minutes post injection. For all subretinal injections, the contralateral eye received a matched buffer control injection (Buffer; third panel) to control for the effect of surgical trauma or buffer-related toxicity and un-injected

C57BL/6 mice (WT; bottom panel) were concurrently monitored. For each panel, the columns show blue autofluorescence (BAF) confocal scanning laser ophthalmoscope (cSLO) imaging using infrared reflectance (IR), a bandpass filter (BP), and infrared autofluorescence (IRAF). No EGFP expression was observed across any of the tested AuNPs in the retina, and no expression of EGFP mRNA was detected by RT-qPCR.

3.4.5.2 SD-OCT and electroretinogram assessment of retinal structure and function following treatment

Because this pilot study is the first examination of gold nanoparticles for *in vivo* gene delivery to the retina, even though no EGFP signal was detected, the effect of AuNP injection on retinal structure and function was assessed by spectral domain optical coherence tomography (SD-OCT) at all cSLO imaging timepoints and by electroretinography (ERG) at 8-weeks post injection. SD-OCT is a sensitive measure of photoreceptor degeneration related to either the effect of the subretinal injection, or toxicity related to the gold nanoparticle composition. Electroretinography is a diagnostic test that measures the electrical responses of various cell types in the retina, allowing for evaluation of the effect of AuNP injection on retinal function.

Consistent with the BAF imaging (Figure 3.11), there were no significant differences in the mean ratio of PRL thickness between superior and inferior retina across all buffer injected groups, supporting that there was minimal damage due to surgical trauma as detected by OD-OCT (Figure 3.12). Moreover, in the groups injected with AuNPs, no PRL structural changes were observed and 2-, 4-, or 8-weeks. No focal thickness loss was observed at the superior retina at any timepoint, demonstrating preservation of normal retinal structure in gold nanoparticle and sham cohorts.

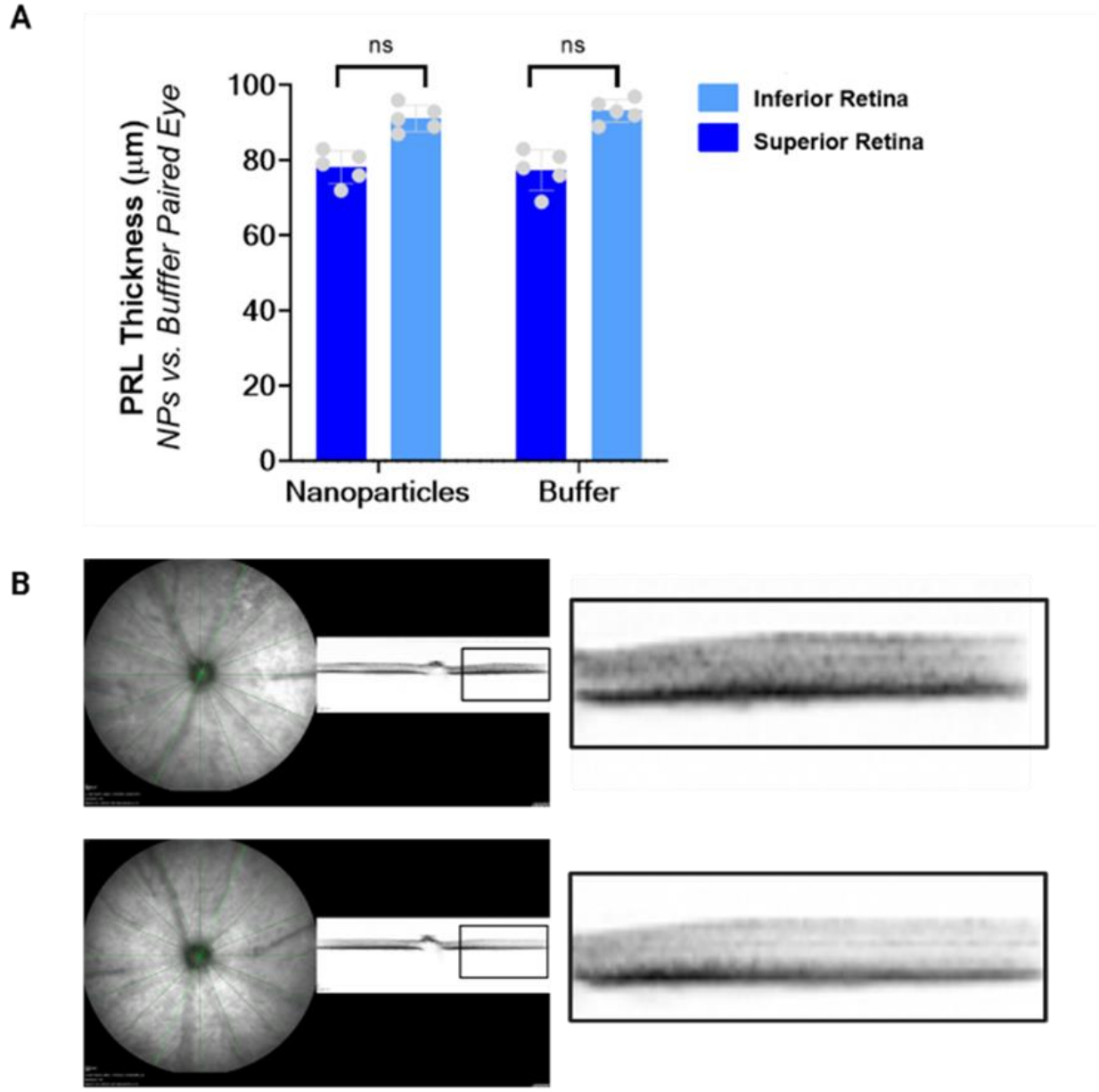


Figure 3.12 | Photoreceptor layer thickness following subretinal injection of gold nanoparticles

A. Photoreceptor layer thickness was measured by SD-OCT for gold-nanoparticle and sham-injected cohorts (n=7) 4-weeks post-subretinal injection in the superior retina (injection site) and inferior retina (non-injection site). Values for each eye represent the mean PRL thickness as

measured at eight points distributed around the mid-peripheral retinal as described in Section 2.4.3.2. Repeated measures two-way ANOVA tests were used throughout. **B.** Representative OCT b-scans from superior (right) and inferior (left) sections, centered on the optic nerve. OCT images from the superior retina (right) demonstrate preservation of normal retinal structure in gold-nanoparticle and sham cohorts following subretinal injection.

Finally, at week 8 post-injection, ERG was performed to assess retinal function. Full-field dark-adapted ERG demonstrated no difference in a-wave (p=.32, two-way ANOVA for effect of treatment) or b-wave (p=0.37, two-way ANOVA) responses across either 40nm AuNPs or PEG coated nanoparticles when compared to paired buffer injected eyes (Figure 3.13). Additionally, no difference was observed in dark- and light-adapted flicker assessment used to isolate cone function (=0.46, two-way ANOVA) (Figure 3.13).

Together, these studies support that DNA-wrapped gold nanoparticles are safe for *in vivo* delivery to the retina, with no effect on retinal structure or function, though further work is needed to understand the mechanism of cell-NP interaction, investigate the reasons why no EGFP was detected, and explore the biodistribution (if any) of gold nanoparticles in ocular tissue.

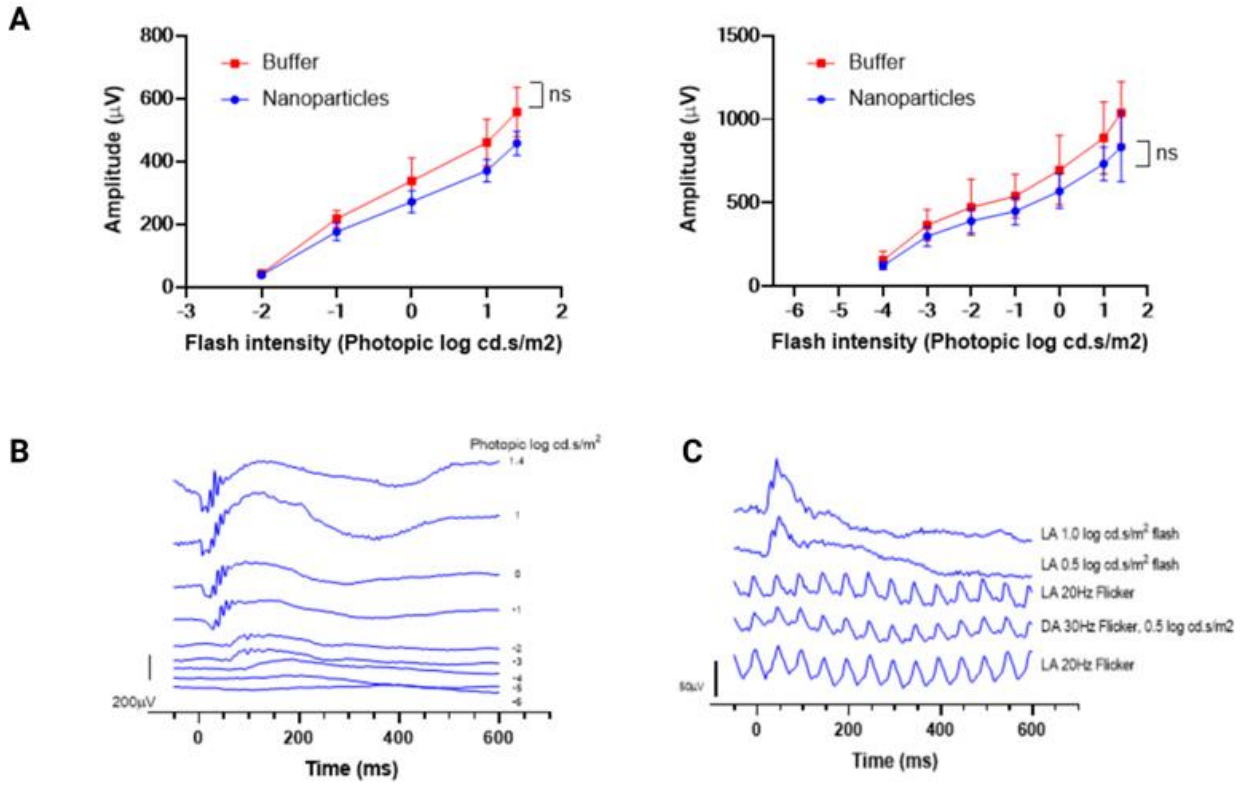


Figure 3.13 | Assessment of retinal function by electroretinography

Full-field dark- and light-adapted ERG irradiance-response curves for gold nanoparticle and sham-injected cohorts at 12-weeks post injection. **A.** Dark-adapted ERG irradiance-response curves from nanoparticle and sham injected cohorts (n=6). Full-field dark-adapted ERG demonstrated no difference in a-wave (p=.32, two-way ANOVA for effect of treatment) or b-wave (p=0.37, two-way ANOVA) responses across either 40nm AuNPs or PEG coated nanoparticles when compared to paired buffer injected eyes. **B.** Representative traces of a-wave and b-wave amplitudes from nanoparticle injected cohort. **C.** Representative traces of cone function with light-adapted ERGs from nanoparticle injected cohort. All data represents mean signal ± SEM. All comparisons were not significant, repeated measures two-way ANOVA for effect of injection.

3.5 Discussion

3.5.1 Development of an all-in-one CRISPR construct for genome modification

The direct evaluation of different CRISPR components and regulatory elements is complicated by the lack of a standardized system to draw conclusions about the comparative efficiencies and specificities of respective vector elements. The HEK293-EGFP reporter system used in this chapter was employed to overcome this limitation to evaluate the gene suppression activities of Cas9 orthologues, promoter elements, and PolyA sequences. The use of TIDE editing analysis assays further confirmed that the gene suppression observed HEK293-EGFP cells transfected with targeting Cas9 constructs was due to NHEJ-mediated knockdown on EGFP rather than an extraneous mechanism.

In addition to their relative efficacies, the vector elements in this study were further screened for their packaging versatility within a single AAV vector. From a clinical perspective, an all-in-one AAV vector containing the entire genetic therapy system is the ideal strategy. Single vector approaches consistently demonstrate increased efficiency compared to a variety of dual vector systems. This might be due to the various limiting steps required for efficient transduction of dual or triple AAV vectors including proper DNA concatemer formation and stability of the heterogeneous mRNA and splicing efficiency across the junctions of the vectors. A single vector approach also reduces the likelihood of the creation of unwanted truncated protein by-products potentially generated by approaches that use techniques such as AAV genome recombination or inteins to reconstitute protein fragments into a full-length product.[251,252] The single vector construct and vector optimizations developed in this chapter served as

the backbone for the epigenetic editing and prime editing tools developed in subsequent chapters.

3.5.1.1 Comparison of Cas9 orthologues

A number of different Cas nucleases have been used for genome and epigenome perturbations. Nevertheless, their delivery via adeno-associated vector (AAV) is limited due to the small packaging capacity of the delivery platform. In this chapter, three different Cas9 variants were evaluated: SpCas9, the most widely used CRISPR orthologue for genome manipulation, SaCas9, the orthologue used in the first CRISPR-based experimental medicine in clinical trials for retinal disease, and CjCas9, the smallest Cas9 orthologue (984 aa) characterized at the time of this study. In direct comparison of these orthologues in the reporter assay, SpCas9 generated the highest levels of gene knockdown, though SaCas9 editing was only significantly lower in the worst performing gRNA-3. Moreover, SaCas9 is almost 400 aa smaller than its SpCas9 counterpart, enabling broader genome editing applications that are not feasible due to the large size of SpCas9. For subsequent studies fusing different repressor effector domains for epigenetic editing, or adenine deaminases for single base-pair DNA editing, SaCas9 was the orthologue of choice to enable single-vector AAV delivery.

Whereas robust EGFP knockdown rates were observed with SpCas9, CjCas9 editing rates were substantially lower across the same genomic targets. Investigation of previously published gRNAs was tested, demonstrating similar levels of knockdown as observed in the original manuscript. Moreover, no differences in the relative expression levels of the different constructs were observed by RT-qPCR. Further studies will further characterize the mechanism behind the lower editing rates with CjCas9, as factors including varying PAM requirements, anticipated activity windows, sgRNA target sequence compositions, target sequence contexts, and locus-dependent differences in

DNA-binding proteins may influence editing outcomes. Nevertheless, the direct comparison using the reporter assay suggested that lower editing rates observed are due to lower activity of CjCas9 compared to SpCas9 and SaCas9 orthologues.

At the time this study was initiated, CjCas9 was the smallest Cas9 orthologue characterized. Recently, Pausch and colleagues describe a CRISPR-CasΦ system that uses a single active site for both CRISPR RNA (crRNA) processing and crRNA-guided DNA cutting to target foreign nucleic acids.[253] This hypercompact system has a molecular weight half that of Cas9 genome-editing systems and demonstrated activity *in vitro* in human and plant cells with expanded target recognition capabilities relative to other CRISPR-Cas proteins. Interestingly, in evaluating CRISPR-CasΦ in the reporter system, editing rates were significantly lower than those achieved with CjCas9, with detectable on-target editing observed only with one of three gRNAs tested (data not shown). These findings suggest that hypercompact Cas9 systems, while offering advantages for cellular delivery, show diminished editing activity when compared to SpCas9 and SaCas9 variants.

The reporter assay developed in this study is broadly applicable to evaluate a range of different genetic elements and CRISPR components, and I demonstrate proof-of-concept of its utility across both Cas orthologue screening and evaluation of regulatory elements. Nevertheless, a limited range of components were evaluated, and further studies are needed to develop an optimal CRISPR system in high-throughput. Though at inception of this study there were limited Cas orthologues for evaluation, a number of different groups are now exploring other CRISPR systems to identify Cas-like effector proteins that may have differences in their sizes, PAM requirements, and targeting specificity. Recent advances in metagenomics, the sequencing of DNA extracted directly from natural microbial communities, provides access to the genetic material of a huge array of uncultivated organisms.[254-256] Interrogation of environmental microbial

communities, combined with validation of *in vivo* RNA-guided DNA interference activity, allows for access to an unprecedented diversity of genomes, the context of which expands the repertoire of Cas orthologues. As demonstrated with the CasΦ experiments, the established reporter system would be broadly translatable to evaluate these novel Cas orthologues.

Although screening of elements towards maximizing gene suppression was prioritized, safety is of upmost priority in developing genetic medicines. It is known that Cas9 activity and editing outcome vary depending on both the protein and the guide RNA, and thus empirically determining optimal enzyme-guide combinations may be helpful, particularly for clinical applications. Importantly, the reporter system developed in this study is compatible with a number of techniques that assess off-target cleavage, and future studies will investigate the genome wide specificity of my all-in-one vector systems.

3.5.1.2 Evaluation of minimal regulatory elements

Following evaluation of Cas9 orthologues, two ubiquitous promoters, the hCMV-MIE and EFS-1α, and two different PolyA elements, SV40 and bGH PolyA, were evaluated in the reporter system. As the EFS-1α produced similar editing rates to the reference plasmid with the hCMV-MIE promoter, with a construct size that is ~300bps smaller, the EFS-1α promoter was selected for subsequent experiments. Although prior studies have shown that SV40 could demonstrate polyadenylation of SaCas9 for transcriptional modulation at levels equivalent to the longer bGH, significantly lower levels of editing were observed with this PolyA sequence.

Although only two promoter and PolyA elements were evaluated in this pilot study, it remains encouraging that robust editing levels can still be achieved *in vitro* when using minimal promoter and polyadenylation elements for all-in-one delivery.

Moreover, it is notable that substantial differences in editing rates were observed across the polyadenylation sequences. These findings suggest that extensive screening of different CRISPR elements and regulatory sequences is needed towards their preclinical translation.

While only ubiquitous promoters were evaluated in this study, ideally, tissue-specific promoters driving robust photoreceptor expression would be used for therapeutic interventions targeting retinal diseases. Investigation of retinoblastoma derived cell lines such as WERI, and Y79 or the immortalized cone photoreceptor line 661W have all demonstrated that these cells do not transfect reliably (Section 4.4.3.1), complicating generation of stably-transduced photoreceptor reporter assays. Future studies might apply a similar reporter strategy to rapidly evaluate CRISPR reagents in retinal organoids, which represent tissue structures with physiological relevance to the *in vivo* human retina. In place of this, direct testing *in vivo* with subretinal injection of AAV vectors is an alternative. Development of a secreted reporter system *in vivo* would further enable evaluation of dynamic changes in editing activities.

3.5.2 Assessment of gold nanoparticles for non-viral delivery

Therapeutic methods for delivering gene editing agents *in vivo* must efficiently target desired cells and deliver sufficient quantities of editing agents into those cells. Gene editing agents can be delivered into cells either as DNA or mRNA encoding their expression, or directly as proteins or ribonucleoproteins (RNPs). In all cases, successful *in vivo* delivery of gene editing agents requires overcoming several biological and molecular barriers to the intracellular delivery of macromolecules. Over multiple decades, researchers have identified and engineered several classes of delivery vehicles that can overcome these complex molecular obstacles to intracellular delivery.

Viruses naturally evolved to overcome barriers to *in vivo* delivery and can natively deliver nucleic acid cargos to many cell types. AAV vectors remain the favored delivery vehicle for retinal gene therapy, due to strong photoreceptor and RPE transduction and established clinical safety profile. They are a leading option for the delivery of CRISPR-Cas transgenes for therapeutic gene editing for inherited retinal disease, and accordingly, AAV vectors been used in the majority of *in vivo* pre-clinical studies, as well as the only clinical trial of retinal gene editing to date. Nevertheless, AAV vectors possess limitations, including limited packaging size for delivery of bulky payloads and risk of immunogenicity and cytotoxicity driven by sustained expression of genetic cargos.

The unique physical properties of the gold nanoparticles enable them to form an endocytic or "fusion-like" structure with the plasma membrane lipid bilayer,[257] which aids the direct biomolecular entry to the cytoplasm without disturbing the phospholipid structure. Nanoparticle mediated delivery offers several advantages over AAV systems, especially when delivering gene editing agents. AuNP delivery results in transient expression of gene editing agents, which is known to minimize the potential for off-target editing relative to prolonged expression from episomal or integrated viral genomes.[119,258] Prolonged expression of gene editing agents could also result in immune recognition of edited cells, which might impact the long-term persistence of edited cells.[258,259] Additionally, since nanoparticles are synthetic, the immunogenicity of AuNPs may be lower than that of viruses and can support repeat dosing in some cases. Importantly manufacturing for large-scale production of non-viral vectors is simpler and more cost-effective than viral vector systems,[260] opening up avenues for additional clinical programs that use gold nanoparticle delivery for *in vivo* gene editing.

3.5.2.1 Insights from pilot gold nanoparticle study

The plasmonic properties of the AuNPs make them, in theory, a very promising non-viral delivery platform for CRISPR/Cas cargo: they allow flexibility in cargo packaging and can be manipulated to be tissue- and cell-type specific. Given their light absorbance properties, AuNPs allow temporal activation upon need, which can be very advantageous for reducing off-target effects.

Previous research on the potential of the non-viral delivery of nanomaterials to the retina has achieved variable degrees of success. Kim and colleagues showed successful targeting and editing of the RPE cells *in vivo* by subretinal injection of Cas9 RNPs targeting the *VEGFA* gene.[261] Huu and colleagues investigated the use of a non-invasive nanoparticle depot to release drugs for the treatment of wet AMD using a light-sensitive triggering system for cargo release from the nanoparticles.[262] Separately, Asteriti and colleagues investigated the possibility of delivering recombinant proteins encapsulated into lipid nanoparticles to the photoreceptors by intravitreal injections.[263]

Nevertheless, despite the promise of these early studies, non-viral studies to date have shown limited activity *in vivo*, and particularly in targeting photoreceptor cells. In my study, while modest rates of nanotransfection were achieved *in vitro* in HEK293 cells, no visible expression was detected in the *in vivo* pilot study. Nevertheless, it is encouraging that AuNPs were well tolerated by subretinal injection, with no effects on retinal structure or function. In evaluating the lack of *in vivo* activity, key areas for troubleshooting and further investigation are discussed in detail below, and some follow-on studies are already underway. Indeed, the pilot *in vivo* study outlined in this chapter contributes to the emerging literature around state-of-the-art non-viral delivery approaches in the eye.

3.5.2.2 Hurdles for nanoparticle delivery to the retina

The results of this gold nanoparticle pilot study raise several key questions and areas for further investigation. There are substantial hurdles for non-viral delivery of genetic payloads to the retina, including (i) difficulty in reaching target cell types of interest, especially photoreceptors; (ii) rapid degradation of the therapeutic transgene or agent; and (iii) potential for immunogenicity or genotoxicity stemming from the delivery agent. Although these challenges exist when targeting any tissue or cell type, the retina has a unique anatomical structure that comes with its own respective challenges in delivery of genetic cargos.

Physical Barriers (The Retinal Pigment Epithelium/Bruch Membrane and the Choroid)

The retinal pigment epithelium (RPE) is a monolayer of pigmented cells that provide support to the adjacent photoreceptors. The RPE is part of the outer blood–retina barrier (BRB) along with the Bruch membrane (BM), a highly-organized layer of basement membrane situated between the RPE and the choroid. The RPE supports photoreceptors through multiple mechanisms including clearance of the photoreceptor membrane, transport of nutrients, and removal of waste products generated during daily photoreceptors renewal.[264] One of the hallmarks of RPE maturation, essential to its function, is the formation of tight junctions between the RPE cells. Although the formation of tight junctions establishes the BRB and regulates the epithelial transport carried out by the RPE, it also anatomically and physiologically protects the eye from toxins, complicating nucleic acid delivery to the eye.

Importantly, DNA-wrapped gold nanoparticles were injected subretinally, enabling delivery of the payload in the subretinal space, between the RPE and photoreceptor outer segment. Indeed, in some OCT images, deposition of particles was visually observed in the subretinal space (data not shown), which may support that the

nanoparticles penetrated the RPE. Labeling of the gold nanoparticles and evaluation by histology will be explored in future studies to confirm successful delivery

Photoreceptor outer segment

Due to the highly specialized structural arrangement of its plasma membrane, the photoreceptor outer segment is particularly difficult to penetrate for targeted delivery of payloads to photoreceptor cells. Photoreceptor outer segments contain many flattened membranous structures called discs that contain rhodopsin and the proteins important for phototransduction. The discs are composed of a hydrophobic, hydrophilic phospholipid bilayer that enables the selectivity of the plasma membrane. The presence of cholesterol, an essential membrane constituent, reduces the permeability of the plasma through interaction with the phospholipids and results in the thickening of the bilayer.[265]

Further complicating delivery, the outer segment is in a constant state of degradation and renewal as part of the visual signal transduction cascade. The membrane discs are continuously displaced to the apical tip of the outer segment as new discs are formed and the old discs are shed and degraded by the RPE.[266] This continuous renewal/degradation process may lead to degradation of phagocytosis of genetic payloads out of the outer segment prior to reaching the photoreceptor nucleus. Together, these hurdles make it difficult to penetrate the photoreceptor outer segment and may explain the lack of expression observed in the pilot nanoparticle study. Future studies are needed to explore successful penetration of the photoreceptor outer segment, applying similar labeling experiments as outlined above.

3.5.2.3 Nuclear localization of DNA-wrapped gold nanoparticles

Eukaryotic cells have developed sophisticated subcellular structures to ensure compartmental functions and genetic diversity, and to protect cells from invasion of disadvantageous non-self-nucleic acids. DNA translocation from the cytoplasm to the

nucleus is a well-known limiting step for non-viral gene transfer, especially in terminal non-dividing cells such as retinal photoreceptors. Productive transfection and gene transfer require extracellular DNA to cross the plasma membrane, traffic through the cytoplasm, enter the nucleus, be transcribed, and have the resulting mRNA be exported into the cytoplasm for translation, and the ultimate modification and localization of the expressed protein.

The nucleus is isolated from the cytoplasm by a double membrane known as the nuclear envelope (NE). The NE is punctuated by nuclear pore complexes (NPCs), through which exclusive passage into and out of the nucleus proceeds.[267] The precise mechanism by which the carrier–cargo complex is translocated through the NPCs remains controversial. However, it is generally accepted that cargos with classic nuclear localization signals (NLSs) are recognized by members of the importin superfamily of cellular nuclear transport proteins and are then translocated into the nucleus.[268,269] A number of different approaches have been used to improve the nuclear import of plasmids, including attaching NLS peptides, NLS proteins, and other importin interacting peptides to the DNA.[270]

In this pilot study, I utilized a single reporter comprised of the cytomegalovirus-immediate early (CMV-IE) promoter driving expression of a GFP transgene. Future studies should matrix additional DNA structures compatible with gold-nanoparticle mediated delivery, such as linear or circular dsDNA. Mini-circle DNA, a recent improvement to the production of pDNA free of prokaryotic *cis*-acting elements, uses an inducible recombinase to specifically delete the prokaryotic moiety from the bacterial mini-circle shuttle plasmid.[271,272] Mini-circle DNAs have been used *in vivo* for long-term gene expression in mice, and for generating induced pluripotent stem cells (iPSC) *in vitro*.[273] Li and colleagues describe an alternative method for the high-yield production of eukaryote-derived, prokaryotic-sequence-free DNA for gene transfer, comprised of an

expression cassette flanked by adeno-associated virus inverted terminal repeats. The authors demonstrate that systemic delivery of these closed-ended, linear duplex molecules (which they term "CELiD" DNA) resulted in long-term, stable transgene expression *in vivo*.[274] The genetic organization of CELiD-vector DNA resembles rAAV vector DNA, but differs in conformation, and as such, unlike encapsidated AAV vector genomes, has no packaging constraints imposed by the limiting space within the viral capsid. Exploration of different DNA structures and nuclear import elements would be of interest not only for enhanced gold NP delivery to photoreceptors, but to enhance gene expression utilizing non-viral delivery vehicles more broadly. Finally, future experiments evaluating the nucleocytoplasmic diffusion of genetic cargos, for example using living HeLa cells, would confirm successful perforation of the photoreceptor nucleus.

3.5.3 Conclusions

The results of this chapter highlight three key points. Firstly, a reporter assay was developed for direct evaluation of different components of the AAV expression cassette and genome engineering reagents on the same target and harboring identical vector backbones and regulatory elements. I demonstrate proof-of-concept of the utility of the reporter assay across both Cas orthologue screening and evaluation of regulatory elements, and the established assay is broadly applicable to evaluate a range of different genetic elements and CRISPR components in future studies. Secondly, I present the adaptation of the assay towards the development of an all-in-one vector for efficient CRISPR-mediated gene knockdown. The single vector construct and vector optimizations developed in this chapter serve as the backbone for the epigenetic editing and prime editing tools developed in subsequent chapters. Thirdly, I investigated the utility of DNA-wrapped gold nanoparticles for plasmid delivery *in vitro* and *in vivo*. I demonstrated the ability of gold nanoparticles to efficiently deliver genes *in vitro* and assessed aspects of their safety including effects on retinal structure and function.

Although I was not able to detect gene expression *in vivo*, these studies advance the understanding of nanoparticle-mediated delivery to the retina. Finally, I propose potential areas of investigation to support the future development of the non-viral delivery arsenal.

4. EVALUATION OF CRISPR-CAS9 REPRESSORS FOR TARGETED EPIGENOME EDITING

4.1 Introduction

The discovery and optimization of CRISPR/Cas systems has enabled facile, programmable genome editing in human cells and prompted a deluge of research focused on the translation of genome engineering reagents to the clinic. In addition to gene editing, CRISPR-Cas can also be utilized for transcriptional regulation, where nuclease-null deactivated (or dead) Cas9 (dCas9) has been repurposed as a synthetic DNA binding platform. These systems have been used to reorganize chromatin architecture and to recruit transcriptional activator or repressor domains that alter the epigenome and gene expression at specific loci. Due to the relatively simple targeting of genomic DNA by altering the protospacer sequence within gRNAs, dCas-based effectors have revolutionized our ability to edit the epigenome and have greatly increased our understanding of epigenetic regulation.

Site-specific gene silencing with engineered dCas9-repressor fusions offers an attractive alternative to RNAi, which has been limited by inefficient knockdown, off-target effects and toxicity associated with oversaturation of endogenous microRNA pathways.[162,164] Programmable epigenome repressors can also target any portion of the genome, facilitating silencing of regulatory elements and noncoding genes that cannot be targeted by RNAi. While genes are regulatory elements can be targeted with conventional genome editing, nuclease-mediated editing is a stochastic process in contrast to generally

more uniform gene repression techniques. Moreover, genome editing alters DNA sequence permanently, precluding dynamic epigenetic regulation and leading to the risk of cellular toxicity due to the formation of DNA double-strand breaks.

Localization of dCas9 alone without a repressor effector domain can drive gene silencing by steric interference of transcription factor binding and RNA polymerase elongation, although gene repression by steric hindrance alone is often not sufficient for robust gene silencing.[168] Further improvement in transcriptional inhibition can be achieved by addition of effectors that recruit endogenous epigenetic modifiers of histone marks and DNA methylation. Krüppel-associated box (KRAB), a naturally occurring motif in mammalian zinc-finger transcription factors, is the silencing domain most commonly used with DNA-binding proteins, and dCas9-KRAB fusion protein is the current gold standard for dCas9-based repression studies.[159,170,275,276]

While widely adopted, the dCas9-KRAB system still suffers from inefficient knockdown and poor performance when compared to Cas9 nuclease-based methods. Previous work has shown that fusing several transcriptional regulators to dCas9 in tandem can lead to a synergistic increase in activity, with initial efforts focused on building more potent transcriptional activators.[189,198,277,278] Although specific editing effectors and combinations robustly function at some loci, there is broad variation in gene silencing outcomes mediated by gRNA positioning effects as well as cell-type specific variations and local chromatin effects.[279-281] Moreover, RNA-guided gene regulators have an additional payload of the epigenetic effector molecule, limiting AAV-based packaging of single-effector and bipartite-effector strategies for *in vivo* delivery.

Here, I describe the development and cloning of potent repressor domains to engineer a highly effective dCas9-transcriptional repressor and demonstrate robust gene silencing across multiple targets.

4.2 Chapter aims

The overall goal of this chapter is to develop a novel CRISPR-dCas9 epigenome editor which can be packaged within an AAV vector for targeted transcriptional repression and validate the system *in vitro* against therapeutically relevant targets. To achieve this, the following aims will be explored:

1. Develop an *in vitro* cell line for facile screening of dCas9-repressor constructs.
2. Design, clone, and screen repressor effectors and bipartite combinations for robust gene silencing.
3. Screen efficient gRNAs targeting the human *NRL* (*hNRL*) and mouse *NRL* (*mNrl*) genes *in vitro* utilizing a luciferase-based assay.
4. Characterize the expression profile of cell lines expressing photoreceptor transcripts and explore their utility for evaluation of dCas9-repressor constructs targeting *hNRL*.

4.3 Methods & materials

4.3.1 Cloning of all-in-one repressor constructs

The general protocol for plasmid cloning is detailed in the general methods. An all-in-one AAV plasmid construct was utilized to as the backbone for molecular cloning. Site-directed mutagenesis was utilized to introduce the H559A and D8A deactivating mutations in the RuvC-like and HNH domains (see Appendix for primer sequences). dSaCas9 effector was amplified from plasmid via PCR with Phusion DNA polymerase (NEB) with primers to remove the stop-codon downstream of the dSaCas9. The all-in-one dSaCas9 vector (AAV-EFS-1α-3xFLAG-2xNLS-Cas9-NLS-U6-gRNA) was used as a backbone for generating all epigenetic repressor constructs. The cloning methodology for generating the repressor effectors is detailed in Table 4.1.

Guide RNAs were designed *in silico* using CRISPick and RNAfold and subcloned using BsaI (NEB). Standard cloning protocols for annealed oligos as described in the general methods were performed. All primer and gRNA sequences are listed in the Appendix.

Repressor effector	Detail	Source
DNMT3A	DNMT3A effector was amplified from plasmid via PCR with Phusion DNA polymerase (NEB) with 5′ extensions on the forward primers to generate complementary overhangs.	pcDNA3/Myc-DNMT3A (Addgene Plasmid #35521; a gift from Arthur Riggs
HDT1	HDT1 effector was amplified from plasmid via PCR with Phusion DNA polymerase (NEB) with 5′ extensions on the forward primers to generate complementary overhangs.	pHDT1:GUS (Addgene Plasmid #108441; a gift from Ton Bisseling)

HDAC8	HDAC8 effector was amplified from plasmid via PCR with Phusion DNA polymerase (NEB) with 5′ extensions on the forward primers to generate complementary overhangs.	HDAC8 Flag (Addgene Plasmid #13825; a gift from Eric Verdin)
KRAB	A GBlock encoding the KRAB sequence was synthesized (IDT), and the fragment assembled with the dSaCas9 all-in-one backbone.	Integrated DNA technologies (IDT)
MeCP2	MeCP2 was amplified from plasmid via PCR with Phusion DNA polymerase (NEB) with 5′ extensions on the forward primers to generate complementary overhangs.	dCas9-KRAB-MeCP2 (Addgene Plasmid #110821; a gift from George Church)
MeCP2 TRD	A GBlock encoding the MeCP2 TRD sequence was synthesized (IDT), and the fragment assembled with the dSaCas9 all-in-one backbone.	Integrated DNA technologies (IDT)
KRAB-MeCP2	KRAB-MeCP2 fusion was amplified from plasmid via PCR with Phusion DNA polymerase (NEB) with 5′ extensions on the forward primers to generate complementary overhangs.	dCas9-KRAB-MeCP2 (Addgene Plasmid #110821; a gift from George Church)
KRAB-MeCP2 TRD	GBlocks encoding the KRAB-MeCP2 TRD, connected by a glycine-serine-rich linker, were synthesized (IDT), and all fragments assembled with the dSaCas9 all-in-one backbone.	Integrated DNA technologies (IDT)

Table 4.1 | Cloning of epigenetic repressors

Cloning details for each repressor effector generated for epigenetic repression. All sequences of key plasmid elements and IDT gBlocks gene fragments are detailed in the Appendix.

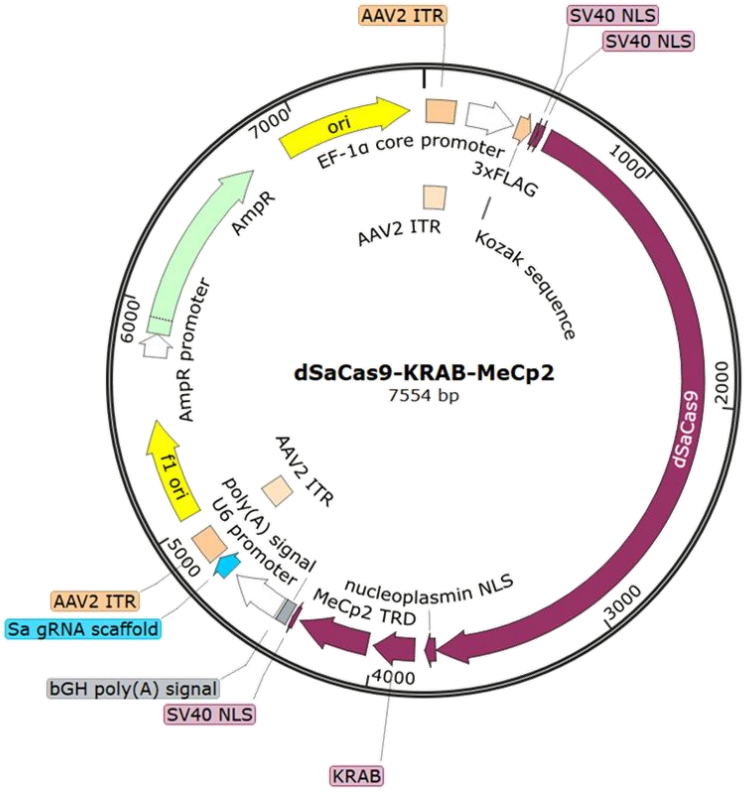


Figure 4.1| Representative full plasmid map of all-in-one dCas9-repressor

Schematic showing the plasmid map of final cloned product. All-in-one dCas9-repressor plasmid constructs were generated, comprised of identical vector backbones as optimized in Chapter 3. The vector configuration for the KRAB-MeCP2 TRD dCas9 vector is as follows: AAV-EFS-1α-3xFLAG-2xNLS-dSaCas9-KRAB-MeCP2 TRD-NLS-U6-gRNA.

4.3.2 Dual luciferase assay design and cloning

Dual luciferase constructs for epigenetic editing reporting were cloned using the psiCHECK-2 vector (a gift from Michelle McClements, Addgene plasmid #35672). A simian virus 40 (SV40) promoter drives expression of the Renilla luciferase open reading frame, which is used as the primary reporter gene. 100bp *mNrl* and *hNRL* target

sequences, complementary to the gRNA for the repressor effector and gRNA combination of interest, were cloned into the NheI site located downstream of the Renilla luciferase translational stop codon. The Vector contains a second reporter gene, firefly luciferase, is designed for endpoint lytic assays and allows for normalization of Renilla luciferase expression, achieving robust and reproducible results.

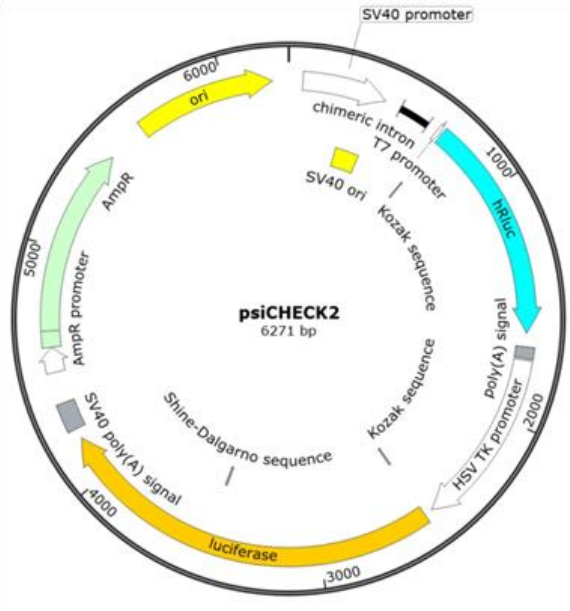


Figure 4.2 | PsiCHECK-2 dual luciferase assay for Cas9 orthologue comparison

Map of the dual luciferase reporter assay plasmid. The human and mouse *Nrl* sequences with complementarity to the gRNA of interest were cloned into the NheI site located downstream of the Renilla luciferase translational stop codon. A second reporter gene, firefly luciferase, allowed for normalization of Renilla luciferase expression.

4.3.3 Cell line generation for reporting transcriptional repression

pCMV-GFP (Addgene plasmid #11153), modified for generation of cell lines for reporting transcriptional repression, was a gift from Connie Cepko. The GFP sequence was modified by addition of a fragment encoding for mouse ornithine decarboxylase (ODC) proline-glutamate-serine-threonine-rich (PEST) sequence in order to target the

protein to the proteasomes and achieved an unprecedentedly fast GFP turnover in permanently transfected human cells. The PEST GFP sequence (dGFP) was amplified from pAMS366-4xCDRE-GFP-PEST (Addgene plasmid #pAMS366-4xCDRE-GFP-PEST, a gift from Sabrina Büttner) via PCR with Phusion DNA polymerase (NEB) with 5' extensions on the forward primers to generate complementary overhangs. The GFP gene within the pCMV-GFP vector was digested with NotI / SpeI enzymes and the dGFP sequence was ligated into the construct. The dGFP construct was validated by Sanger sequencing. The Duke Viral Vector Core provided lentivirus for generation of the dGFP cell line. Transgene localization confirmed single GFP copy number across all reporter lines, consistent with the low doses of lentiviral vector used and selection with puromycin for the generation of the cell lines. All primers and plasmid sequences and detailed in the Appendix.

4.3.4 Cell culture and transfections

All transfections were performed in HEK293T, HEK293-GFP and HEK293-dGFP cells maintained as described in the general methods. For EGFP suppression experiments, cells were seeded in 6-well plates and transfected with 2 μg of plasmid. Cells were harvested 72-96 hours post-transfection. For luciferase assays, 100uL of HEK293T cells at a density of 5.5×10^4 cells/well were seeded in Corning white-walled 96 well adherent plates (Sigma-Aldrich) in phenol-red-free Dulbecco's Modified Eagle Medium (DMEM) (Thermo Fisher Scientific), supplemented with L-glutamine (2 mM) (Sigma-Aldrich), sodium pyruvate (1 mM) (Thermo Fisher Scientific), 10% heat-inactivated fetal bovine serum (HI-FBS) (Thermo Fisher Scientific) and 1% penicillin-streptomycin (Sigma-Aldrich). Cells were transfected with Transit-LT1 (Mirus Bio) at 24 hours post-seeding with 100 ng of dual luciferase reporter, and 250 ng of the repressor construct unless otherwise stated. Positive and negative control wells were included on all plates, transfected with identical quantities of luciferase plasmid, repressor effector and non-

targeting (scrambled) gRNA plasmids as in the experimental plates. All transfected plasmid preparations were made with endotoxin-free mini- (Zymo Research) or midi-prep kits (Clontech, a Takara Bio Company).

4.3.5 Imaging and statistical analyses

Transmission and fluorescence images of live cells were taken using the Invitrogen EVOS FL Auto 2 Cell Imaging System (ThermoFisher). Image analyses were performed using ImageJ (FIJI) software 1.52i. For statistical analysis, three independent replicates were performed per condition. Values, ratios and statistical significance were analyzed using Prism software (v9.2.0, GraphPad).

4.4 Results

4.4.1 Designing and cloning all-in-one dCas9 repressor fusions

Endogenous gene repression can be achieved with engineered repressor fusions through a variety of mechanisms. Localizing a DBD without an effector domain to promoter regions or downstream of the transcription start site can silence gene expression. In these strategies, repression is caused by steric interference of transcription factor binding and RNA polymerase elongation. However, gene repression by steric hindrance alone is often not sufficient for meaningful silencing.[168]

Each type of epigenetic repressor provides unique advantages conferred by its mechanism of action. The silencing domain most commonly used with DBDs is the Krüppel associated box (KRAB), a naturally occurring motif in mammalian zinc finger transcription factors. The KRAB domain acts as a recruiter, and the complex of heterochromatin-modifying enzymes localized to target DNA by KRAB likely contributes to its versatility and potency for silencing protein-coding genes, non-coding RNA, and regulatory elements.[159,173,174,176-178] Nevertheless, the dCas9-KRAB repressor system still suffers from inefficient knockout and poor performance when compared to Cas9 nuclease-based methods.

Eukaryotic cells host a variety of potential epigenetic modifying domains, only a small fraction of which have been utilized for epigenome engineering applications thus far. Recently, a comprehensive assessment of effector domains known to play a role in transcriptional regulation and gene silencing were fused to the c-terminus of dCas9 and top-performing domains were screened in pairwise repeating and non-repeating combinations.[282] The authors identified that the dCas9 repressor consisting of Krüppel-associated box (KRAB) and methyl-CpG binding protein 2 (MECP2) was the most potent across all tested targets. RNA-guided gene regulators have an additional payload of the

epigenetic effector molecule, limiting AAV-based delivery strategies of repressor systems. The tested KRAB-MeCP2 fusion protein is ~1200bp, precluding packaging into AAV vectors even if a compact SaCas9 orthologue is utilized.

To address this limitation and to begin to design a more potent Cas9 repressor, I cloned novel dCas9 fusion proteins (Table 4.2) as described in Section 4.3.1.

Repressor Effector	Construct detail
DNMT3A	EFS-dSaCas9-DNMT3A-U6-sagRNA
HDT1	EFS-dSaCas9-HDT1-U6-sagRNA
HDAC8	EFS-dSaCas9-HDAC8-U6-sagRNA
KRAB	EFS-dSaCas9-KRAB-U6-sagRNA
MeCP2	EFS-dSaCas9-MeCP2-U6-sagRNA
MeCP2 TRD	EFS-dSaCas9-MeCP2 TRD-U6-sagRNA
KRAB-MeCP2 TRD	EFS-dSaCas9-KRAB-MeCP2 TRD-U6-sagRNA

Table 4.2 | Design and cloning of individual and bipartite dCas9-repressor fusions

Repressor architecture and vector detail for all generated repressor constructs. All plasmid sources and key sequences are detailed in the Appendix.

One of the repressor effector proteins generated *de novo* was a 104-aa MeCP2 repressor effector comprised of the MeCP2 transcriptional repression domain. Protein modeling software was applied to generate the MeCP2 TRD sequence: GlobPlot 2.3 was used to identify regions of globularity and disorder within MeCP2; PSIPRED was used to investigate protein secondary structure; Clustal Omega was utilized to make multiple protein sequence alignments; finally, ICM-Browser was applied to visualize three-dimensional molecular structures (Figure 4.3). In addition to initial results suggesting the

role of MeCP2 as a potent repressor, numerous studies on MeCP2 have yielded surprising results in terms of the diversity of its functions for epigenetic regulation. Recent studies have suggested that MeCP2 is a methyl-binding protein that operates in association with corepressor complexes such as mSin3A and HDAC.[283,284]

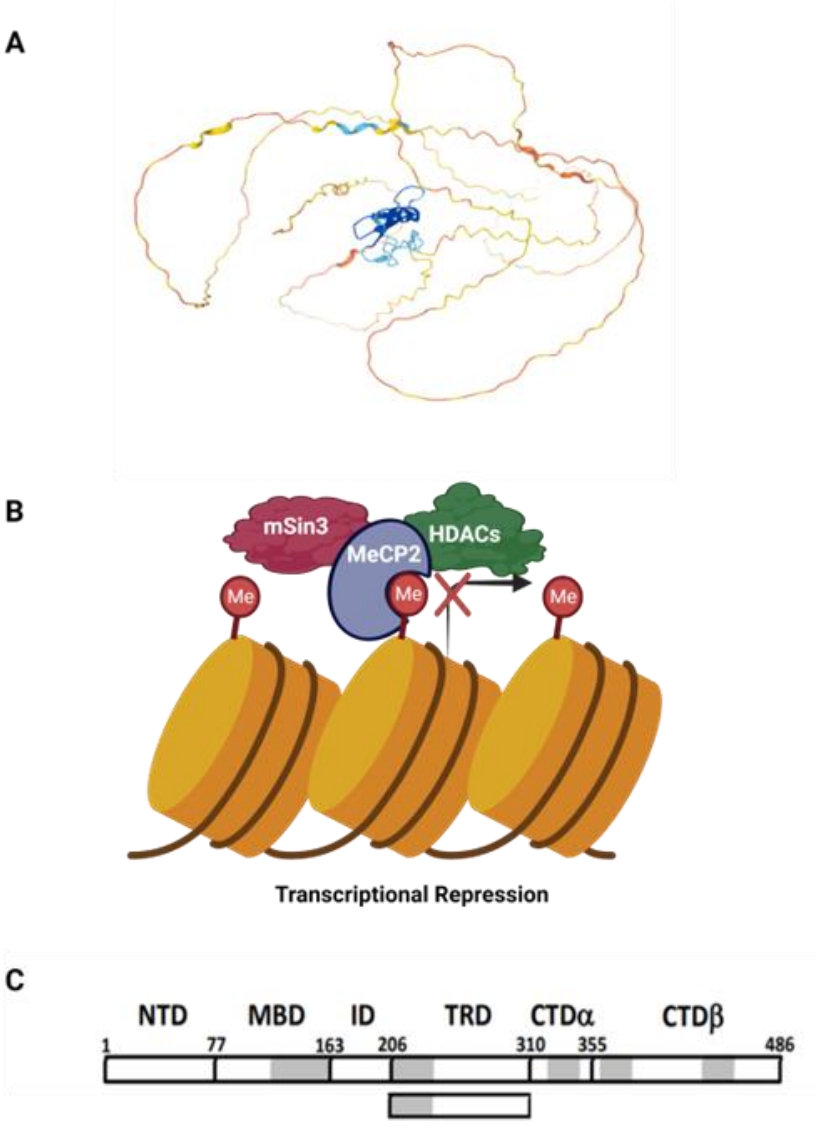


Figure 4.3 | Generation of a dCas9 bipartite repressor comprised of the Methyl-CpG Binding Protein 2 (MeCP2) transcriptional repression domain

A. Ribbon rendering of the crystal structure of MeCP2. MeCP2 is an intrinsically disordered protein (IDP) organized into six domains: N-terminal domain (NTD), methyl binding domain (MBD), intervening domain (ID), transcriptional repression domain (TRD), C-terminal domain α (CTDα), and C-terminal domain β (CTDβ). **B.** The diverse functions of MeCP2 in gene regulation and chromatin organization. Studies on MeCP2 have yielded surprising results in terms of the diversity of its functions with enormous potential for epigenetic regulation of target gene expression. MeCP2 was initially discovered as a methyl-binding protein. Further investigations on MeCP2 function led to the discovery of its role as a transcriptional repressor that operates in association with corepressor complexes such as mSin3A and HDAC. **C.** Schematic depiction of the domain organization in MeCP2. Structured regions are shown in grey. Numbers indicate the initial residue for each domain. Below the full-length MeCP2, the construct employed in this work is shown, harboring the transcriptional repression domain.

4.4.2 Pilot evaluation of dCas9-repressor effectors

After design and cloning, the resulting dCas9 fusion proteins were then transfected into a commercially available transgenic HEK293-EGFP cell line. The majority of dCas9 fusions were able to generate significant levels of *GFP* repression ($p<0.01$), with only the dCas9-HDT1 and dCas9-HDAC8 fusion not generating significant levels of GFP knockdown. No gene suppression was observed with the dCas9 only construct. Gene repression ranged from 9-16%. However, levels of repression were modest, and it was impossible to discern differences in repressive potential between different dCas9 protein fusions (Figure 4.4).

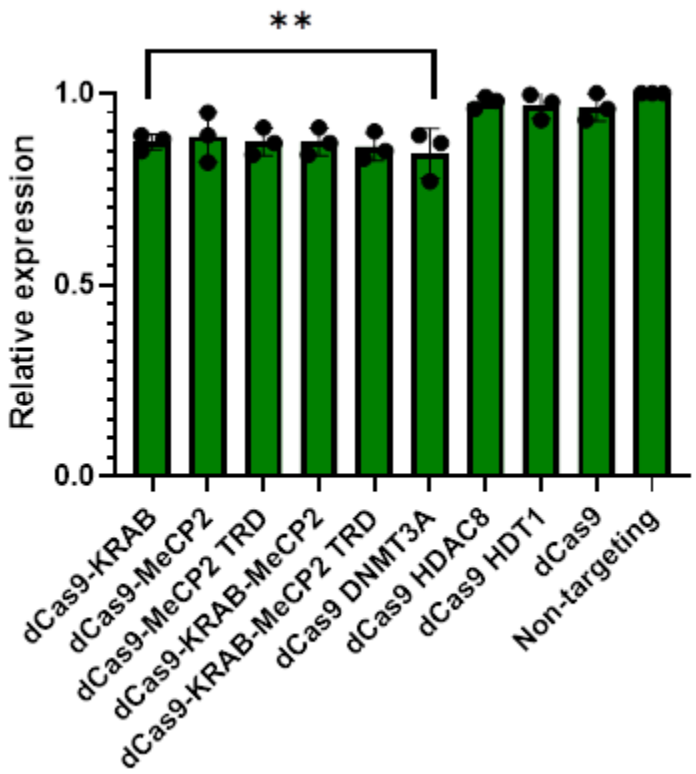


Figure 4.4 | Evaluation of dCas9-repressor effectors using HEK293-EGFP transgenic cell line

EGFP expression in protein lysates was assessed via a protein fluorescence assay. All dCas9 fusions other than dCas9-HDT1 and dCas9-HDAC8 demonstrated significant levels of repression. Gene repression ranged from 9-16%, though it was impossible to discern differences in repressive potential between different dCas9 protein fusions. No gene suppression was observed with the dCas9 only construct. The data are presented by mean value ± SEM with all data points from independent experiments shown. All analysis was normalized to samples transfected with a non-targeting gRNA control. ***$p<0.01$, Sidak's multiple comparison test. All other comparisons were not significant.

4.4.3 Development of HEK293-dGFP cell line for repressor screening

GFP is a stable protein; this property allows its accumulation and easy detection in cells. However, this stability also limits its application in studies that require rapid reporter turnover. To better assess the repression of CRISPR-repressor constructs, a novel HEK293 reporter cell line harboring a proline-glutamate-serine-threonine-rich (PEST) destabilized-GFP (dGFP) sequence (HEK293-dGFP) was generated. The HEK293-dGFP cell-line shortens the half-life of GFP by almost 4-fold, enabling more sensitive detection of GFP knockdown.[285,286] In initial evaluation of gRNAs designed with homology to the transgenic HEK293-EGFP and dGFP cell line, higher rates of GFP suppression were achieved with technical and biological consistency and reproducibility (Figure 4.5). The dCas9 fusion proteins transfected into the HEK293-dGFP cell line were able to generate significant levels of *GFP* repression ($p<0.01$), with the more sensitive reporter protein enabling screening of dCas9 fusion constructs (Figure 4.5). The dSaCas9-KRAB-MeCP2 TRD bipartite repressor generated the highest rates of gene suppression in the HEK293-dGFP reporter, showing up to a 40% decrease in GFP expression (Figure 4.5). No significant levels of gene suppression were observed with the dCas9 only construct. No improvement in gene silencing was obtained by fusing DNMT3A to the MeCP2 TRD or by dual fusion of identical KRAB or MeCP2 TRD domains, likely due to the domains recruiting identical secondary effectors that have already been recruited. Additionally, protein modeling suggested that protein folding was impaired with fusion of bulkier repressor effectors (data not shown), though linkers for effector proteins were not optimized.

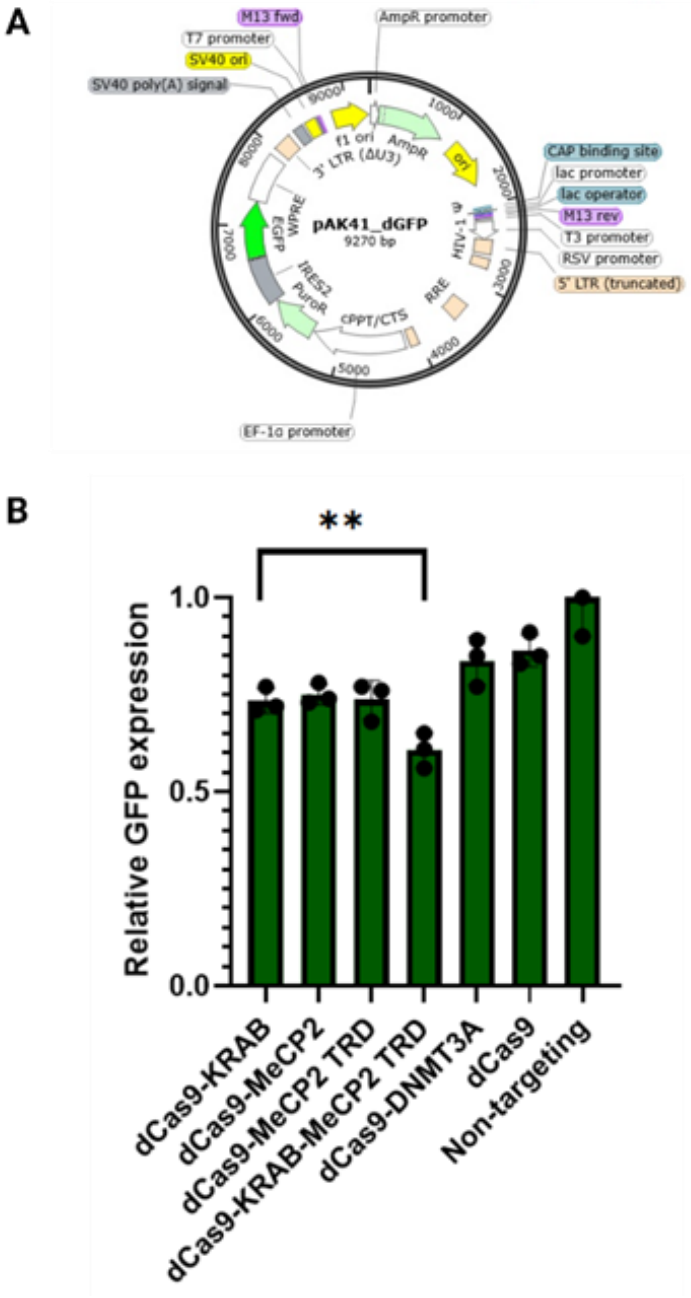


Figure 4.5 | Screening of dCas9-repressor fusions using the HEK293-dGFP cell line

A. Map of the proline-glutamate-serine-threonine-rich (PEST) destabilized-GFP (dGFP) plasmid. HEK293 cells were stably transduced with lentivirus to generate the HEK293-dGFP cell line. The HEK293-dGFP cell-line shortens the half-life of GFP by almost 4-fold, enabling more sensitive detection of GFP knockdown. **B.** EGFP expression in protein lysates was assessed via a protein

fluorescence assay. All tested dCas9 fusions other than dCas9-DMNT3A demonstrated significant levels of repression. The dSaCas9-KRAB-MeCP2 TRD bipartite repressor generated the highest rates of gene suppression in the HEK293-dGFP reporter, showing up to a 40% decrease in GFP expression. No significant levels of gene suppression were observed with the dCas9 only construct. The data are presented by mean value ± SEM with all data points from independent experiments shown. All analysis was normalized to samples transfected with a non-targeting gRNA control. ***$p<0.01$, Sidak's multiple comparison test. All other comparisons were not significant.

4.4.4 Investigation of retinoblastoma-derived cell lines for screening of CRISPR agents

Having established that the dCas9-KRAB-MeCP2 bipartite repressor generated the highest rates of gene silencing, guide RNAs were next screened against the *Nrl* promoter sequence. Since target transcripts are not expressed in commonly cultured cell lines, screening of dCas9 fusion constructs targeting the *Nrl* sequence is challenging. Thus, the utility of the Y79 human retinoblastoma cell line towards screening of dCas9 repressors targeting photoreceptor-specific genes was evaluated. Expression of rod (*NRL*, *NR2E3*) and cone (*ARR3*, *OPN1SW*) genes was detected by PCRs and RT-qPCR from RNA extracted from Y79 cells (see Appendix for primer sequences). To investigate the utility of Y79 cells for screening epigenome editing constructs and gRNA sequences, cells were transfected with an EFS-1α-mCherry reporter plasmid. Multiple different transfection conditions were applied, including plasmid DNA concentrations (500 ng to 5 μg), harvesting periods (24 hours to 96 hours), lipofection reagents (TransIT-LT1 (MirusBio), FuGENE (Promega), ViaFect (Promega), and Lipofectamine 3000 (ThermoFisher)), and transfection conditions (forward and reverse transfections). Optimal transfection conditions were achieved with 2 μg pDNA reverse transfected using Lipofectamine 3000, although transfection rates were still modest, peaking at ~40%

(Figure 4.6). Moreover, no gene suppression was observed with Cas9 or dCas9 vectors in a pilot study (data not shown).

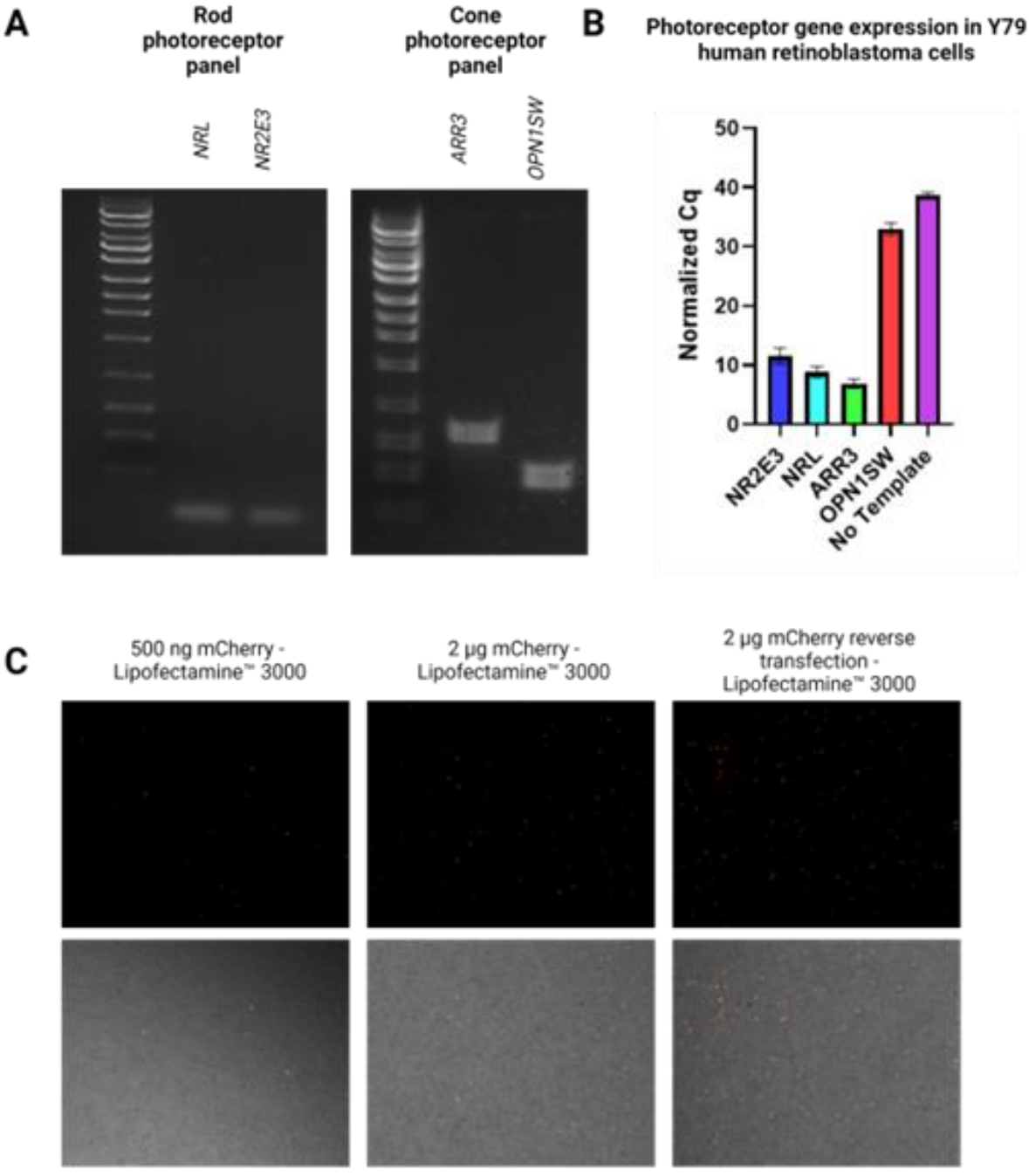


Figure 4.6 | Characterization and evaluation of Y79 human retinoblastoma cell line for screening of dCas9-repressor fusions

A. Gel electrophoresis of PCR products from DNA extracted from Y79 cell lines. Rod photoreceptor genes *NRL* and *NR2E3* (left) and cone photoreceptor genes *ARR3* and *OPN1SW* (right) were detected. **B.** Normalized C_q values showing relative expression of rod and cone photoreceptor genes assessed via RT-qPCR from RNA extracted from Y79 human retinoblastoma cells. **C.** Representative light microscopy images of Y79 cells transfected with an mCherry reporter plasmid, taken 72 hours following transfection. Multiple different transfection conditions were applied, including plasmid DNA concentrations (500 ng to 5 μg), harvesting periods (24 hours to 96 hours), lipofection reagents (TransIT-LT1 (MirusBio), FuGENE (Promega), ViaFect (Promega), and Lipofectamine 3000 (ThermoFisher), and transfection conditions (forward and reverse transfections). Optimal transfection conditions were achieved with 2 μg pDNA reverse transfected using Lipofectamine 3000 (right), though no gene suppression was observed with Cas9 or dCas9 vectors in a pilot study (data not shown).

4.4.5 Testing of dCas9-KRAB-MeCP2 TRD epigenetic repressor construct targeting *NRL*

Since Y79 human retinoblastoma cells were not suitable for evaluation of dCas9 vectors or guide sequences, a dual-luciferase assay was developed to screen gRNAs against *NRL*. The dual luciferase reporter assay system provides an effective means of performing two reporter assays, with activities of firefly and Renilla luciferases measured sequentially from a single sample. The human and mouse NRL sequences with complementarity to the gRNA of interest were cloned into the NheI site located downstream of the Renilla luciferase translational stop codon. The second reporter gene, firefly luciferase, allowed for normalization of Renilla luciferase expression (Section 4.3.2). To screen guide RNAs against *NRL* and evaluate the repressive capacity of the dSaCas9-KRAB-MeCP2 TRD construct, a gRNA screen was conducted, informed by *in*

silico design (CRISPick). 23 guide RNA sequences were designed to target NRL sequences (Figure 4.7). Initial screening of gRNA sequences revealed that top-performing gRNAs spanned the C-terminal end of the *Nrl* promoter (data not shown).

In order to develop gRNAs that could be investigated against human iPSC-derived retinal organoids and a mouse model of *Nrl-EGFP*, guide RNAs were designed with homology across both mouse and human NRL sequences. The top-performing gRNA sequences spanning the C-terminal end of the *Nrl* promoter were evaluated using NCBI Basic Local Alignment Search Tool (BLAST) to identify regions of similarity between mouse and human NRL sequences (Table 4.3)

Description	Total Score	Percent Identity	E-Value	Accession	Acc. Len
gRNA designed:	5′- caccgCAGGTTTAAACATCTCCT grna-1R				
Homo sapiens neural retina leucine zipper (NRL) RefSeqGene on chromosome 14; nuclear gene for mitochondrial product	36.2	100.00%	17	NG_011697.2	43329
Mus musculus neural retina leucine zipper (Nrl) gene, promoter region and 5' UTR	36.2	100.00%	9.2	AY526079.1	2420
gRNA designed:	5′- caccgCAGGTTTAAACATCTCCT grna-1R				
Homo sapiens neural retina leucine zipper (NRL), RefSeqGene on chromosome 14; nuclear gene for mitochondrial product	36.2	100.00%	36	NG_011697.2	43329

Mus musculus neural retina leucine zipper (Nrl) gene, promoter region and 5' UTR	42.1	100.00%	0.15	AY526079.1	2420

Table 4.3 | Guide RNA design targeting *NRL*

Guide RNAs cloned into the dSaCas9-KRAB-MeCP2 vector were designed with homology across both mouse and human *NRL* sequences. Sequences were evaluated using NCBI Basic Local Alignment Search Tool (BLAST) to identify regions of similarity between *NRL* sequences. The program compared nucleotide and protein sequences to sequence databases to calculate the statistical significance. The blast expect (E) value is a parameter that describes the number of hits that can be expected to occur by chance when searching a database of a particular size.

Having designed gRNAs based off top-performing sequences, and with homology across both mouse and human *NRL* genes, I next evaluated the dCas9 bipartite repressor in the dual luciferase assay. The RNA structures of *NRL* targets cloned into the luciferase assay was designed using RNA fold predictions (Vienna RNAfold) to optimize assay conditions and best recapitulate target binding within the *NRL* promoter (Figure 4.7). HEK293 cells were co-transfected with the psiCHECK-2 vector and dCas9-KRAB-MeCP2 TRD constructs harboring a gRNA targeting NRL complementary to the dual luciferase assay. All 4 top-performing gRNAs targeting the C-terminal end of the *Nrl* promoter indicated significant rates of *Nrl* silencing. Guide RNA-3, targeting around position 1500 of the *Nrl* promoter, demonstrated up to 55% silencing of luciferase expression (Figure 4.7). Collectively, these results support that the dSaCas9-KRAB-MeCP2 TRD bipartite repressor fusion can be utilized to mediate high levels of gene repression against both human and mouse *NRL* genes.

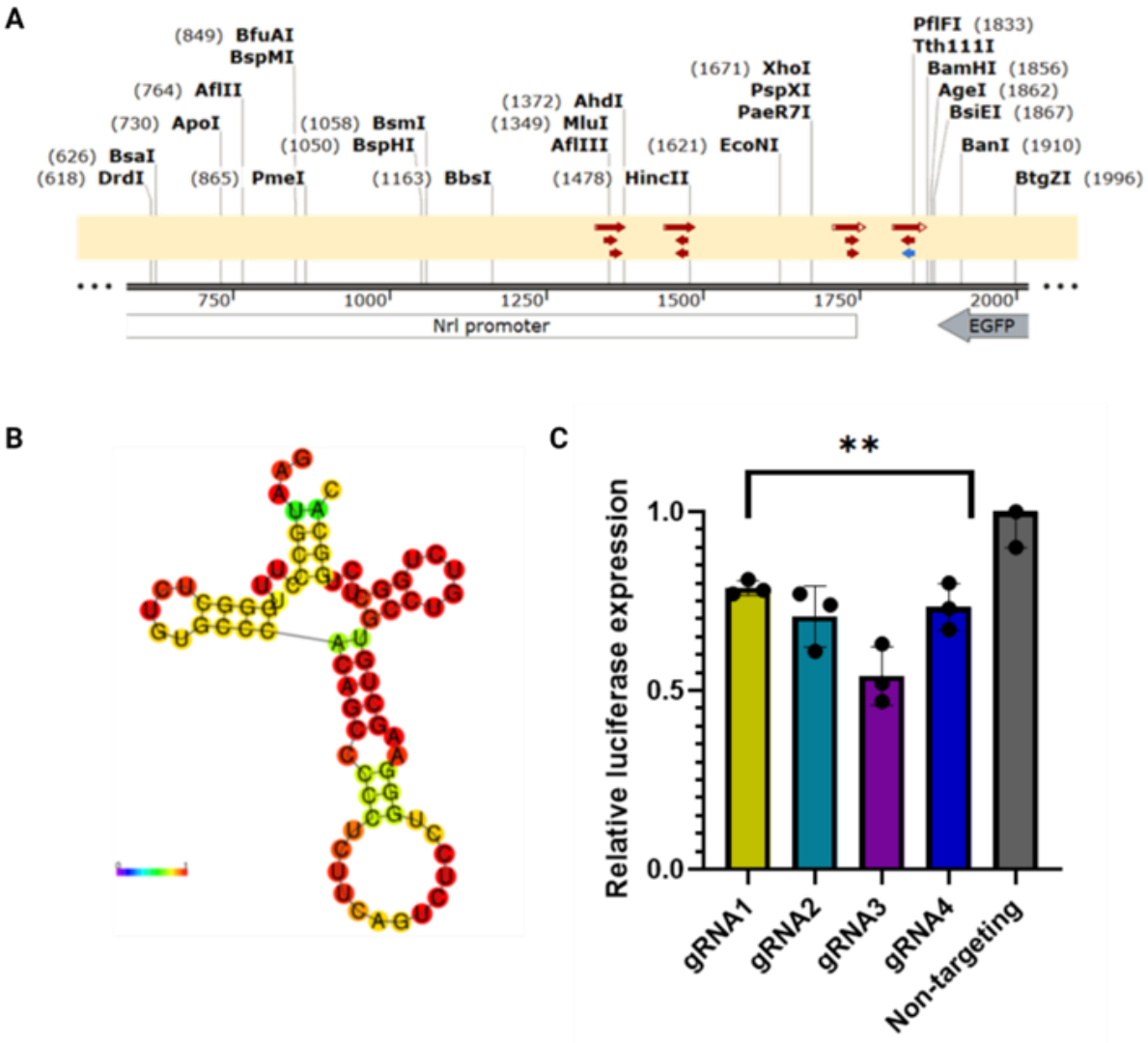


Figure 4.7 | Top-performing gRNAs against *NRL* cloned into the dCas9-KRAB-MeCP2 TRD vector and screened using a dual luciferase assay

A. Guide RNA design screening against the *NRL* sequence. 23 guide RNA sequences were designed *in silico* (CRISPick) to target *NRL* sequences. The top performing gRNAs spanning the C-terminal end of the *Nrl* promoter are highlighted. **B.** RNA structure of *NRL* targets from luciferase assay. RNA fold predictions of the 50 nt *hNRL* and *mNrl* targets from the dual-luciferase assay used to screen gRNAs. Sequence and partition function was generated with Vienna RNAfold. **C.** Relative luciferase expression from HEK293 cells co-transfected with the psiCHECK-2 vector and dCas9-KRAB-MeCP2 TRD constructs harboring a gRNA targeting *NRL*

complementary to the dual luciferase assay. 4 top-performing gRNAs targeting the C-terminal end of the *Nrl* promoter were designed with homology across both human and mouse *Nrl* sequences using NCBI Basic Local Alignment Search Tool (BLAST). All 4 gRNAs demonstrated significant levels of *Nrl* knockdown. Guide RNA-3, targeting around position 1500 of the *Nrl* promoter, demonstrated up to 55% silencing of luciferase expression. Luminescence was recorded using a FLUOstar Omega microplate reader. No significant levels of gene suppression were observed with the dCas9 only construct. The data are presented by mean value ± SEM with all data points from independent experiments shown. All analysis was normalized to samples transfected with a non-targeting gRNA control. ***$p<0.01$, Sidak's multiple comparison test. All other comparisons were not significant.

4.5 Discussion

4.5.1 Development of potent bipartite transcriptional repressor

Whereas localization of dCas9 without a repressor effector can mediate transcriptional repression by steric hindrance when targeted downstream of the transcriptional start site, or by competitively interfering with transcription factor binding when directed to promoter regions or regulatory elements, dCas9 alone is often not sufficient for achieving high levels of gene silencing.[168] Indeed, in my initial optimization of targeted gene expression, dCas9-mediated gene repression was capped at ~10% in *in vitro* experiments.

Each type of epigenetic repressor provides unique advantages conferred by its mechanism of action. To determine whether I could further improve the repression system, a number of different repressor effectors were evaluated, both on a standalone basis and combinatorically. My data show that the novel bipartite repressor outperforms different repressor effectors evaluated on a standalone basis, including KRAB, MeCP2 TRD, DNMT3A, HDAC8, and HDT1. The lack of improved repression with the other repressor combinations could be due to the domains recruiting identical secondary effectors that have already been recruited. It is also possible that the extent to which the domains fold and function properly decreases as multiple bulky effectors are fused together.

The improved performance of dCas9-KRAB-MeCP2 TRD repressor is likely due to the distinct mechanisms by which each of the fused effector's function. The KRAB domain represses transcription via interaction with KAP1, which functions as a scaffold to recruit co-repressors including heterochromatin protein 1 (HP1), histone deacetylases, and SETDB1.[159,173,174,176-178] Indeed, its function as a recruiter of heterochromatic-modifying enzymes localized to target DNA likely contributes to its versatility and potency for

silencing in different genomic contexts, including protein-coding genes, non-coding RNA, and regulatory elements. Conversely, the transcription repression domain of MeCP2 binds to a different set of transcriptional regulators (Table 4.4). The 104-amino-acid transcription repression domain (TRD) encoded within exon 4[287] interacts with histone deacetylases (HDACs) and transcriptional co-repressors Sin3A,[283,284] c-Ski and N-CoR.[288] HDAC1 and HDAC2 are histone deacetylases that combine with transcriptional repressors such as mSin3A to form a co-repressor complex. The TRD also directly interferes with assembly of the pre-initiation complex through interactions with transcription factor IIB (TFIIB), a component of the basal transcriptional machinery.[289] The maintenance DNA methyltransferase, Dnmt1, also associates directly with MeCP2 at the TRD, and immunoprecipitated MeCP2-Dnmt1 complexes show DNA methyltransferase activity to hemimethylated DNA,[290] implicating MeCP2 in the maintenance of methylation patterns during DNA replication.

MeCP2 interacting partner	Function
Brahma	Transcriptional repression
c-Ski	Transcriptional repression
H3-Lys9 histone metyltransferase	Transcriptional repression
HDACs	Transcriptional repression
HP1s	Transcriptional repression
MBD2	Heterochromatin organization
NCoR	Transcriptional repression
Sin3A	Transcriptional repression
SMRT	Transcriptional repression
SUV39H1	Transcriptional repression

Table 4.4 | MeCP2 interaction with molecular partners

Summary of MeCP2 interaction with transcriptional repressors.

4.5.2 Investigation of *in vitro* models for screening of dCas9 repressor fusions and gRNAs

4.5.2.1 Destabilized GFP cell line for screening of dCas9 repressor fusions

GFP is a highly stable protein, limiting its application in studies that require rapid reporter turnover. Moreover, the commercially available transgenic HEK293-EGFP cell line which was used for initial experiments possess multiple copies of GFP per cell (Caroline Peddle, personal communication), further limiting the sensitivity of this system for detecting gene silencing. Previous efforts by other lab members were not able to show high levels of GFP knockdown, and in a pilot study, gene suppression was modest even with highly potent transcriptional repressors.

To better assess the repression of CRISPR-repressor constructs, I developed a novel HEK293 reporter cell line harboring a proline-glutamate-serine-threonine-rich (PEST) destabilized-GFP (dGFP) sequence (HEK293-dGFP). The HEK293-dGFP cell-line shortens the half-life of GFP by almost 4-fold, and puromycin selection was applied following LV-mediated transduction to ensure only 1-2 dGFP copies per cell. This reporter cell line enables more sensitive detection of gene silencing and provides an excellent tool for future evaluation of gene knockdown technologies.

4.5.2.2 Dual luciferase assay for high throughput gRNA screening

Screening of guide RNAs targeting the disease-relevant locus requires extensive *in silico* and *in vitro* screening, as a number of factors can widely affect editing outcomes, including varying PAM requirements, anticipated activity windows, sgRNA target sequence compositions, target sequence contexts, and locus-dependent differences in DNA-binding proteins and transcriptional state. Moreover, development of an epigenetic

editing approach targeting *NRL* was challenging, as the target gene is not expressed in commonly cultured cell lines.

In this chapter, the utility of the Y79 human retinoblastoma cell line towards screening of dCas9 repressors targeting photoreceptor-specific genes was evaluated. Expression of rod (*NRL*, *NR2E3*) and cone (*ARR3*, *OPN1SW*) genes was detected by PCRs and RT-qPCR from RNA extracted from Y79 cells. However, despite extensive effort to optimize cell culturing and transfection conditions, transfection efficiencies were still modest, and no gene suppression was observed with Cas9 or dCas9 vectors in a pilot study.

Since Y79 human retinoblastoma cells were not suitable for evaluation of dCas9 vectors or guide sequences, a dual-luciferase assay was developed to screen gRNAs against *NRL*. The dual luciferase reporter assay system provided an effective means of performing two reporter assays, with activities of firefly and Renilla luciferases measured sequentially from a single sample. In comparison with other fusion approaches (such as GFP), the luciferase approach offers more convenient and rapid quantitation with higher sensitivity. Importantly, gRNA screening using the luciferase assay provided a highly reproducible approach to screen gRNAs in high-throughput format (96-wells). Further adaptations of this system could include generation of stably transduced cell-lines containing the dual luciferase transgene, as well as introduction of secreted luciferase proteins (secNluc), which would reduce the number of plasmids needed for transfection and allow for the dynamic monitoring of epigenome editing kinetics.

4.5.3 Insights from guide RNA screening

Extensive screening of gRNA sequences revealed that top-performing gRNAs all spanned the C-terminal end of the *Nrl* promoter. CRISPR-dCas9 repressor fusions targeting the C-terminus of *Nrl* may enable higher rates of gene repression by a synergistic knockdown effect mediated by both steric-hinderance of the promoter region

and target-specific repression by the bipartite dCas9 repressor. For the majority of loci tested, dCas9-KRAB-MeCP2 achieved greater degrees of gene repression than dCas9-KRAB. Yet, there were a few loci for which I observed only modest repression from either tool. Potential causes for variations in gene silencing include poorly functional guides, insufficient time between targeting and measurement of gene expression, local chromatin effects, competition for binding between Cas9 and endogenous transcriptional regulators, and interference from already present epigenetic marks preventing further modification. By and large, these site-specific inefficiencies in repression may be overcome by high throughput screening of sgRNAs targeting the same genomic target.

4.5.4 Conclusion

Collectively, this chapter investigated and engineered CRISPR-dCas9 epigenetic repressors that can be packaged within a single AAV vector for targeted gene silencing. I developed a novel cell line for facile screening of dCas9-repressor constructs, designed, cloned, and screened repressor effectors and bipartite combinations for robust gene silencing. Finally, I demonstrate that a dCas9 bipartite repressor comprised of KRAB-MeCP2 TRD can be utilized to mediate a high level of transcriptional repression against multiple targets, including both human and mouse *NRL* genes. The next chapter applies these findings to evaluate these systems in patient iPSC derived retinal organoids and *in vivo*.

5. EPIGENETIC REPRESSION IN IPSC-DERIVED RETINAL ORGANOIDS AND A PILOT STUDY IN AN *NRL.EGFP* MOUSE MODEL

5.1 Introduction

Gene therapy treatments for inherited retinal diseases have been developing rapidly in the past decade, with over 50 ocular gene therapy clinical trials ongoing in at least 17 different indications.[291] Despite substantial progress in the development of therapies for inherited retinal diseases, there is still tremendous unmet medical need, and together, IRDs are the most common cause of blindness in the working-age population.

As described in the previous chapter, site-specific gene silencing with engineered dCas9-repressor fusions has risen as a promising alternative to other gene therapy approaches as well as cleavage-dependent gene editing, providing a novel approach for targeted control of gene expression with reduced off-target effects. From a clinical perspective, targeted regulation of disease-causing genes provides novel therapeutic avenues towards many genetic diseases. Indeed, in addition to being restricted to the treatment of loss-of-function mutations, gene supplementation approaches are limited in the eye due to the extensive heterogeneity in the genetic defects underlying inherited retinal disorders. For example, in retinitis pigmentosa, the leading cause of inherited blindness, afflicted patients bear mutations in over 200 causative genes.[292] Correspondingly, as proof-of-concept of dCas9-repressor fusions, I utilized a therapeutic

in situ cellular reprogramming strategy to overcome the limitations of gene-specific approaches. In particular, *Nrl* was targeted, a master regulator of rod versus cone photoreceptor determination, which activates *Nr2e3*, a transcription factor that represses transcription of multiple cone-specific genes.[293] I conduct a pilot *in vivo* study in *Nrl.EGFP* mice, which specifically express EGFP in rods.

One of the major hurdles for translating gene therapies from laboratory settings to the clinic is the lack of adequate preclinical models. Although mouse models have provided insight into basic pathobiology underlying retinal diseases, due to species differences, these models may not faithfully recapitulate disease processes in patients.[294] Organoids derived from induced pluripotent stem cells (iPSCs), or embryonic stem cells (ESCs), have been used by researchers to create *in vitro* tissues that mimic their natural counterparts. The now-established development of retinal organoids (ROs), derived from either from embryonic stem cells,[295] or more commonly from human induced-pluripotent stem cells (iPSCs)[296,297] have been utilized as 3D models of human retinal development and diseases. Due to their easy accessibility, high stability, and proximity to native retinas, ROs have emerged as a mainstay in the preclinical evaluation of gene therapies for treatment of inherited retinal diseases.

This chapter describes all-in-one AAV-directed site-specific gene silencing with engineered dCas9-repressor fusions. I apply this system to target the master regulator, *Nrl* , in an *Nrl.EGFP* mouse model as well as in patient iPSC-derived 3D retinal organoids.

5.2 Chapter aims

The goal of this chapter is to evaluate the dCas9-repressor-mediated approach for targeted silencing of *hNRL* and *mNrl* genes in therapeutically relevant models, including in human iPSC derived 3D retinal organoids and *in vivo* in an *Nrl-EGFP* mouse model. To achieve this, the following aims will be explored:

1. Generate AAV vectors expressing dSaCas9-KRAB and dCas9-KRAB-MeCP2 repressor constructs described and cloned in Chapter 4.
2. Characterize gene expression profiles in patient iPSC derived retinal organoids
3. Evaluate the expression, efficacy, and specificity of AAV-directed dCas9-repressors for the repression of rod photoreceptors in 3D-organoids.
4. Conduct a pilot *in vivo* study to evaluate the expression of AAV-directed dCas9-repressors following subretinal administration in an *Nrl-EGFP* mouse model.

5.3 Methods & materials

5.3.1 Cell culture and transfections

All transfections were performed in HEK293T, Y79, and WERI-Rb1 cells maintained as described in the general methods. To evaluate Y79 and WERI-Rb-1 human retinoblastoma cells, multiple transfection conditions were evaluated. For forward transfections, cells were transfected 24 hours after seeding in poly-D-lysine and human fibronectin-coated plates. For reverse transfections, the transfection reaction was added to the coated plate and the cells added on top of the reagent, as described in the general methods. Transfections were conducted with TransIT-LT1 (MirusBio), FuGENE (Promega), Viafect (Promega), or Lipofectamine 3000 (ThermoFisher). In all cases, Opti-MEM was used as transfection media.

5.3.2 Differentiation of retinal organoids from human iPSCs

Retinal organoids (RO) were differentiated from iPSCs of healthy donors by Newcells Biotech (Newcastle upon Tyne, UK) and RO maintenance was completed by Michelle McClements. Briefly, the iPSC line WT3 (SB-AD4) was cultured in mTeSR1 medium (Stemcell Technologies, Vancouver, Canada) supplemented with 1% penicillin/streptomycin (Thermo Fisher Scientific, MA) on plates coated with Matrigel (Corning Inc., NY). Cell culture medium was replaced daily, and cells were allowed to grow for 4 to 5 days prior to passaging at a ratio of 1:6 with Versene ethylenediaminetetraacetic acid (EDTA; Lonza, Basel, Switzerland). The iPSCs were differentiated to retinal organoids based on a previously described method.[298] Each individual retinal organoid was maintained in a single well of a U-bottom 96-well plate.

5.3.3 AAV production

The general protocol used for AAV production is described in the general methods. Briefly, a standard polyethylenimine triple transfection method of HEK293T cells in Corning HYPERFlasks provided transgene plasmid, pAdDeltaF6 and the pRep2Cap8 Y733F (a gift from Michelle McClements). For AAV5 production, a single plasmid encoding both the rep/cap and helper genes (pDP5; PlasmidFactory GmbH, Bielefeld, Germany (*rep2*/*cap5*)) was used. Cells were harvested 72 hours post-transfection, and lysates were purified using iodixanol gradients with subsequent buffer exchange performed using Amicon Ultra-15 100K filter units (Merck, Kenilworth, NJ). AAV preparations were eluted in no Mg^{2+}, no Ca^{2+} phosphate buffered saline (PBS). For subretinal injection, AAV was diluted in PBS with 0.002% Pluoronic F68 non-ionic surfactant to reduce adherence and loss of AAV capsid within the injection syringe. DNase-treated samples were used for quantitative polymerase chain reaction (qPCR) titer with iTaq reagent (Bio-Rad Laboratories, Hercules, CA) or dye-based SYBR green (Bio-Rad Laboratories) assays. Multiple primers targeting unique sequences in the constructs were used; all primer sequences are listed in the Appendix. AAV vector titers of constructs employed in this chapter are summarized below (Table 5.1).

Construct	Titer (gc/mL)
AAV5-GRK1-dCas9-KRAB-MeCP2 TRD- gRNA3	1.82×10^{12}
AAV5-GRK1-dCas9-KRAB-MeCP2 TRD-scrambled	1.97×10^{12}
AAV5-GRK1-dCas9-gRNA3	7.82×10^{12}
AAV5-GRK1-GFP	1.04×10^{13}

Table 5.1 | AAV titers of dCas9-repressor vectors

Vector titers of each AAV (n = 2-3 replicates).

5.3.4 AAV treatment of retinal organoids

Following 150 days of differentiation, retinal organoids were treated with 1E+10 genome copies (unless otherwise stated) of AAV in a 50-μL volume. The 50:50 media changes (with no further provision of AAV) were performed every 3 to 4 days by Michelle McClements. Retinal organoids were harvested for cryosectioning and qPCR analysis at 30 days post-transduction unless otherwise stated.

5.3.5 Animal models and procedures

Heterozygous *Nrl.EGFP* mice (*Nrl.EGFP*$^{+/-}$) were generated by crossing (B6.Cg-Tg(*Nrl-EGFP*)1Asw/J) homozygotes (a gift from Anand Swaroop, National Eye Institute, Bethesda, MD, USA) with C57BL/6J (Charles River, Harlow, UK). Each allele of the *Nrl.EGFP* transgenic strain contains three copies of a transgene containing the mouse neural leucine zipper (*Nrl*) promoter driving the expression of *EGFP* specifically in rod photoreceptors. Subretinal injections were performed as described in the general methods on five-week-old animals. A single 1.5 μL of either AAV or buffer solution was delivered to the superior retina, with successful injections observed by the creation of a superior hemi-retinal bleb without complications of bleeding or retinotomy. AAV doses of 3E+9 genome copies/eye were used, with animals receiving bilateral injections of AAV and buffer. In cases where complications were observed in the bilateral eye, mice receiving unilateral uncomplicated injections were included for analysis. Electroretinography, CSLO and OCT imaging was performed as described in general methods. CSLO and OCT imaging was performed using a Spectralis device (Heidelberg Engineering) fitted with a 55° lens as described in general methods. For BAF image analysis, a detector sensitivity of 75% was used to maximize the signal dynamic range without signal saturation. Images were exported in .tiff format and using FIJI (National

Institutes of Health, USA). Measurement and analysis were performed blind to experimental conditions applied. Dr Ahmed Salman assisted with electroretinography and blinded assessments.

5.3.6 Immunohistochemistry

5.3.6.1 Retinal organoids

Organoids were harvested 30 days post-transduction by Michelle McClements. Briefly, 16 retinal organoids were selected under a light microscope and collected into a 1.5-ml microcentrifuge tube using a Pasteur pipet. Once the organoids settled to the bottom of the tube by gravity, they were washed three times with 0.01 M PBS. Organoids were fixed with 1 ml of 4% paraformaldehyde in PBS for 20 min, followed by three washes with 0.01 M PBS. Post-fixation, organoids were incubated overnight in 30% sucrose and transferred to a mold that was filled with OCT Embedding Matrix. Organoids to be sectioned were removed from the -20°C freezer and transported on dry ice to a cryostat (Leica Biosystems) that had been pre-chilled to -20°C. Frozen sections of 10 μm thickness were cut on a cryostat, mounted onto Superfrost Plus slides (VWR) and allowed to dry at room temperature overnight. Slides were stored at -20°C and thawed at room temperature for subsequent use. Immunohistochemistry was performed as described in the general methods. Briefly, sections were blocked in 1% BSA, 5-10% NGS/NDS, 0.3% Triton X-100, and a primary (overnight at 4°C, Table 7.1) and an appropriate secondary (90 – 120 minutes, room temperature) antibody staining was performed in blocking solution.



Figure 5.1 | Cryosectioning of retinal organoids

Retinal organoids were embedded in OCT compound. Frozen sections of 10 μm thickness were cut on a cryostat and mounted onto Superfrost Plus slides. Organoids are marked with the red box in the top-right.

5.3.6.2 Retinal Sections

Eyes were extracted from mice immediately after confirmation of death, and retinal tissue was collected as described in the general methods. For immunohistochemistry the resulting eye cup was fixed in cold 4% PFA on ice for 30 minutes and then washed briefly in PBS. The eyecup was cryoprotected using a sucrose gradient, washed briefly in PBS, dried, and then embedded in OCT compound in foil molds with the optic nerve oriented up. Frozen sections 16-18 μm thickness were cut on a cryostat, mounted onto Superfrost Plus slides and allowed to dry at room temperature overnight. A hydrophobic barrier pen was used to create an encircling border around the sections. Sections were blocked in 1% BSA, 5-10% NGS/NDS, 0.3% Triton X-100, and a

primary (overnight at 4°C, Table 5.1) and an appropriate secondary (90 – 120 minutes, room temperature) antibody staining was performed in blocking solution.

5.3.7 Western blot

Animals were sacrificed and eyes were freshly enucleated, dissected in ice-cold PBS to isolate the neural retina, and snap-frozen in dry ice. Western blot was performed as described in the general methods. Briefly, protein was extracted from neuroretina through lysis in radioimmunoprecipitation (RIPA) buffer (Sigma Aldrich) (150 mM NaCl, 1.0% IGEPAL CA-630, 0.5% sodium deoxycholate, 0.1% SDS, 50 mM Tris, pH 8.0) supplemented with Roche cOmplete, Mini Protease Inhibitor Cocktail (Roche Diagnostics). 20-40 μg of denatured protein lysate in RIPA buffer was loaded into 10% Tris-Glycine gels (Criterion TGX, Bio-Rad Laboratories) and run in Tris-Glycine SDS-PAGE running buffer (National Diagnostics, USA). Following protein transfer, PVDF membranes were washed in Tris-Buffered Saline (TBS) (Bio-Rad Laboratories) and then incubated in dilute (10%) skim milk in TBS solution for 45 minutes at room temperature. Membranes were then incubated in a solution containing 10% blocking buffer with primary antibodies (Table 5.2) overnight at 4 °C.

Antibody	Host	Dilution	Application	Source
β-Actin (human)	Mouse	1:10000	WB	Thermo Fisher (AM4302)
β-Actin (mouse)	Rabbit	1:5000	WB	Abcam (ab8227)
Nrl (human)	Rabbit	1:1000	WB, IHC	Abcam (ab137193)
SaCas9 (aa 100-200)	Rabbit	1:20000	WB, IHC	Abcam (ab203933)
SaCas9 (N-terminal)	Rabbit	1:1000	WB, IHC	Diagenode (C15310260)
SaCas9	Rabbit	1:1000	WB, IHC	Diagenode (C15310259)

(C-terminal)				
GFP (N-terminal)	Rabbit	1:1000	IHC	Sigma Aldrich (G1544)
FLAG M2	Mouse	1:1000	WB, IHC	Sigma-Aldrich (F1804)

Table 5.2 | Primary antibodies used for immunohistochemistry and western blot

Table of primary antibodies used for immunohistochemistry and western blot. Donkey Anti-Mouse IgG (Abcam, ab98799) and Donkey Anti-Rabbit IgG (Abcam, ab97064) secondary antibodies were used.

5.3.8 Gene expression analysis

RNA extraction, reverse transcription and qPCR were performed as described in the general methods. For retinal organoids, containing minimal mRNA (<$1x10^6$ cells/organoid), RNA extraction was performed using the Monarch Total RNA Miniprep Kit (NEB). Additional DNA removal by on-column DNase digestion incubation was extended to 30 minutes. 25 µl of molecular grade water was added and the column was incubated for 10 minutes to maximize recovery of RNA. For retinal organoid samples, the EvoScript Universal cDNA Master Kit (F. Hoffmann-La Roche) was utilized to reverse transcribe RNA to cDNA. Real time quantitative PCR (RT-qPCR) was used to determine levels of gene expression from complementary DNA (cDNA) samples using gene-specific primer pairs normalized to ACTB or GAPDH. Probe-based TaqMan chemistry assays were performed using custom or predesigned TaqMan Assays (Thermo Fisher Scientific, Table 5.3). All assays and primer pairs were validated prior to use in test plates using seven log_{10} dilution series of the linear target DNA.

Gene name	Species	Chromosome location	Assay ID (ThermoFisher)
ACTB	Human	Chr.7: 5527148 - 5530601	Hs01064292_g1
NRL	Human	Chr.14: 24078693 - 24114924	Hs01007657_m1
NR2E3	Human	Chr.15: 71810548 - 71818259	Hs00183915_m1
PDE6B	Human	Chr.4: 587593 - 670892	Hs01557860_m1
ARR3	Human	Chr.X: 70268335 - 70281840	Hs01020134_m1
OPN1SW	Human	Chr.7: 128772489 - 128775790	Hs00181790_m1
CRX	Human	Chr.19: 47821842 - 47843330	Hs00230899_m1
GAPDH	Mouse	Chr.6: 125161338 - 125166511	Mm99999915_g1
ARR3	Mouse	Chr.X: 100605480 - 100618953	Mm00504628_m1
NR2E3	Mouse	Chr.9: 59942771 - 59960834	Mm00443299_m1
NRL	Mouse	Chr.14: 55518978 - 55524981	Mm00476550_m1
sgRNA.Scaffold	Mouse & Human	AAACAAGGCAAAATGC	Custom TaqMan assay
SaCas9.Probe (FAM-labelled)	Mouse & Human	ATCGAGAAGATCAAGC TGC	Custom TaqMan assay

Table 5.3 | TaqMan probe panel used for pRT-PCR analysis of rod- and cone-specific genes in retinal organoids transduced with AAV-dCas9-KRAB-MeCP2

Table of TaqMan probes used for quantitative real-time PCR analysis of gene expression of rod- and cone-specific genes in treated human iPSC-derived retinal organoids and *Nrl.EGFP*$^{+/-}$ mice.

5.3.9 Imaging and statistical analyses

Transmission and fluorescence images of live cells were taken using the Invitrogen EVOS FL Auto 2 Cell Imaging System (ThermoFisher). Image analyses were performed using ImageJ (FIJI) software 1.52i. For statistical analysis, three independent replicates were performed per condition. Confocal images of sections were acquired using the 40× objective of a Zeiss LSM 710 confocal microscope (Carl Zeiss Microscopy, Jena, Germany). Z-stacks spanning a 10-µm depth were obtained and combined using the Max Intensity Z-Project function in Fiji/ImageJ (version 2.3.0/1.53f). Values, ratios and statistical significance were analyzed using Prism software (v9.3.1, GraphPad).

5.4 Results

5.4.1 AAV vector production

Having established a robust gene repression system *in vitro*, I next focused on applying the same in more representative preclinical models. As an initial pilot study, AAV vectors were generated using the all-in-one dCas9-KRAB-MeCP2 TRD vector cloned in the previous chapter, with the gRNA targeting mouse and human *NRL* sequences and a non-targeting guide. AAV8-Y733F capsids were initially used for vector production, as these vectors have been previously described to retain the photoreceptor tropism of AAV8 capsids, improving transduction strength by superior evasion of proteosome-mediated degradation. However, minimal vector yields were achieved with AAV8-Y773F-dCas9-KRAB-MeCP2 TRD virus, and initial HEK293 cell transduction indicated minimal expression (data not shown). Thus, AAV5, a clinically validated capsid that has demonstrated robust tropism for retinal tissue, was selected for virus production. Moreover, due to minimal editing and FLAG immunostaining observed in retinae transduced with the ubiquitous elongation factor 1-alpha 1 short intron-less promoter (Lewis Fry, personal communication), EFS-1α was replaced with a photoreceptor-specific human rhodopsin kinase (hGRK1) promoter. Previous studies have demonstrated that AAV5-hGRK1 is a safe and effective AAV serotype/promoter combination for targeting therapeutic transgene expression protein to rods and cones in a clinical setting.

Eight recombinant AAV vectors were produced to express different combinations of dCas9 repressor fusions and gRNAs. Of these, four were selected for downstream analysis, AAV5-dCas9-KRAB-MeCP2 TRD bipartite repressors with targeting and non-targeting guides, as well as a targeting dCas9-only vector and a positive control expressing GFP from the GRK1 promoter (Figure 5.2). All AAV vectors were screened with restriction enzyme digests, including XmaI to confirm the presence of ITRs, and

transgene identity was confirmed with Sanger sequencing prior to AAV virus generation. All plasmids were purified from commercial endotoxin-free kits. Denatured concentrated AAV samples were analyzed by Sodium dodecyl sulphate polyacrylamide gel electrophoresis (SDS-PAGE). The gel was subject to total protein staining to detect capsid proteins VP1 (87kDa), VP2 (72kDa), and VP3 (62kDa) at the predicted ratio of VP1:VP2:VP3 of 1:1:10 (Figure 5.2).

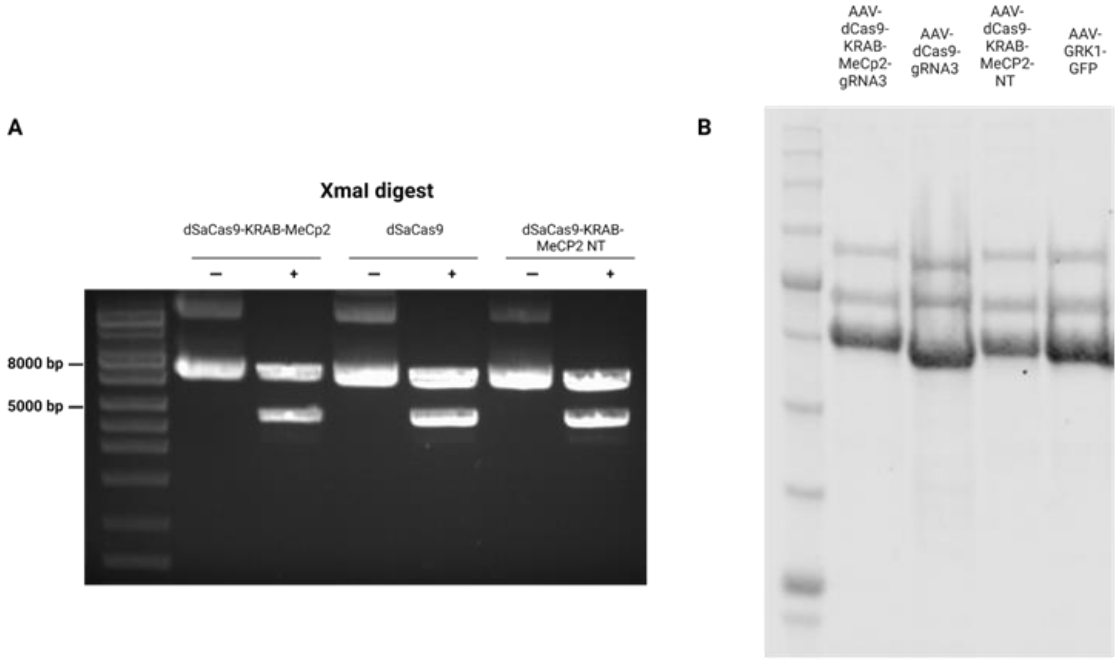


Figure 5.2 | Production of dCas9 repressor AAV vectors

A. dCas9-repressor vectors were screened with restriction enzyme digests, including XmaI to confirm the presence of ITRs, and transgene identity was confirmed with Sanger sequencing prior to AAV virus generation. **B.** Sodium dodecyl sulphate polyacrylamide gel electrophoresis (SDS-PAGE) of AAV vectors comprised of dCas9 and dCas9-KRAB-MeCP2 effectors and containing targeting (gRNA-3) and non-targeting (scrambled) gRNAs. The gel was subject to total protein staining to detect capsid proteins VP1 (87kDa), VP2 (72kDa), and VP3 (62kDa) at the predicted ratio of VP1:VP2:VP3 of 1:1:10.

5.4.2 Evaluation of AAV-directed bipartite repressors in patient iPSC derived retinal organoids

To evaluate the AAV-directed bipartite repressors in a representative preclinical model, I utilized patient iPSC derived retinal organoid 3D cultures. Retinal organoids represent tissue structures with greater physiological relevance to the *in vivo* human retina and may serve as the future of preclinical testing for the next generation of gene therapies in the eye. This is due to the well-defined laminar structure of retinal organoids, which superbly mimics both the architecture and the transcriptome profile of the mammalian retina. It is generally accepted that the outer layer of cells of retinal organoids represent photoreceptor-like cells, which have been shown to express photoreceptor-specific gene markers such as neural leucine zipper protein, recoverin, arrestin, rhodopsin, and cone opsin.[296,297,299,300]

To investigate whether the retinal organoids recapitulate key features of photoreceptor cells and can be transduced by the established transgene and capsid variants, organoid cultures were transduced with $5x10^{10}$ vgs of AAV5-dCas9-KRAB-MeCP2 TRD bipartite repressors with targeting and non-targeting guides, as well as a targeting dCas9-only vector and a positive control expressing GFP from the GRK1 promoter. Encouragingly, the AAV5 capsid demonstrated efficient and reliable transduction on organoid cultures, and the GRK1 promoter enabled reliable transgene expression in photoreceptor-like cells of retinal organoids (Figure 5.3).

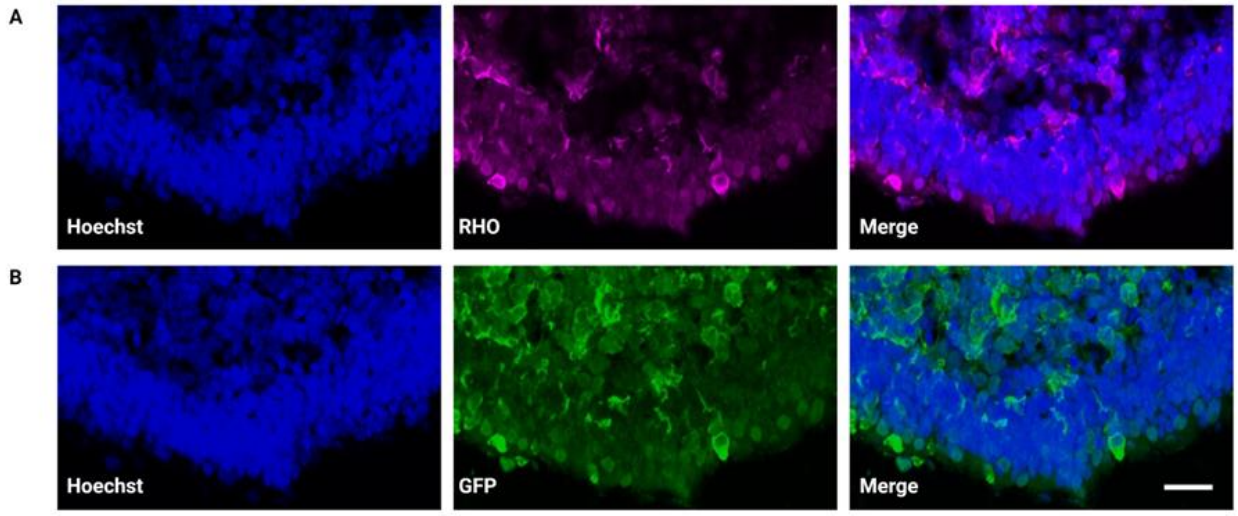


Figure 5.3 | Outer layer of patient iPSC derived retinal organoid 3D cultures represents photoreceptor-like cells

Immunohistochemistry of retinal organoid sections from wild-type cultures **(A)** or cultures transduced with AAV-GRK1-GFP (positive control) **(B)**. Treated retinal organoids were transduced with $5x10^{10}$ genome copies. GRK1 transgenes provide a more restricted expression profile locating to the outer layer of photoreceptor-like cells of retinal organoids. Scale bar, 25 μm.

5.4.3 AAV-dCas9-KRAB-MeCP2 TRD mediates high levels of gene repression in patient iPSC derived retinal organoids

Having demonstrated that AAV5-directed dCas9 and reporter constructs can efficiently transduce retinal organoid cultures, I sought to evaluate the repressive potential of the engineered bipartite repressor. Following transduction, retinal organoids were harvested for cryosectioning and qPCR analysis at 30 days post-transduction, as described in Section 5.3.4. Western blot and RT-qPCR analysis from RNA extracted from transduced retinal organoids demonstrated strong dCas9 expression (Figure 5.4).

To evaluate any repression mediated by the targeting dCas9 repressor fusion, a panel of TaqMan probes targeting rod- and cone-photoreceptor genes was assembled.

RT-qPCRs were performed from RNA extracted from retinal organoids transduced with the dCas9-bipartite repressor fusion targeting *hNRL* and a non-targeting gRNA, and all analyses were normalized to the non-targeting gRNA control. Gene knockdown of 67%, 72%, and 43% was seen in rod-specific genes *NRL*, *NR2E3*, and *PDE6B*, respectively. Gene upregulation of 33% was achieved with cone-specific gene *ARR3* (Figure 5.4). It was highly encouraging that the engineered dCas9-fusion system can be utilized to achieve a high level of transcriptional repression in patient iPSC derived retinal organoids. Moreover, the *in vitro* activity and robust gene silencing was recapitulated in retinal organoids. This is promising for the future development of the epigenome editing tools and supports the use of the dual-luciferase reporter assay system as a sensitive and reproducible methodology to evaluate CRISPR genome and epigenome engineering reagents as well as to screen disease-targeting gRNAs.

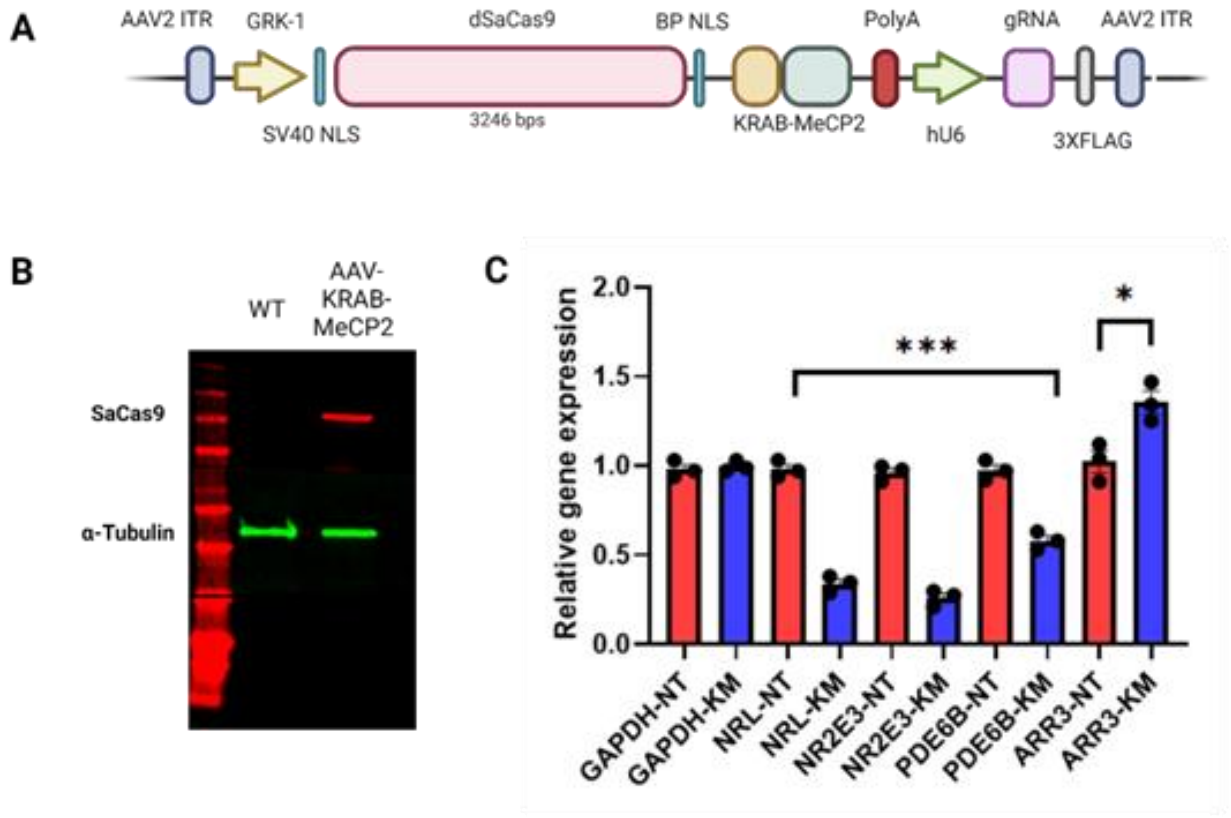


Figure 5.4 | AAV-directed dCas9-repressor fusions mediate robust gene silencing in human iPSC 3D retinal organoids

A. Schematic summarizing the vector design for the final AAV-directed dCas9 bipartite repressor. The construct is an all-in-one vector comprised of a photoreceptor-specific rhodopsin-kinase (GRK1) promoter driving the expression dSaCas9 fused to the KRAB-MeCP2 TRD bipartite repressor, with a hU6 promoter driving expression of the screened guide RNA (gRNA3) targeting the mouse and human *NRL* sequence. **B.** Western blot to detect Cas9 expression with α-tubulin as a loading control. High levels of SaCas9 expression were detected from retinal organoids transduced with dCas9-KRAB-MeCP2 TRD. dCas9-KRAB-MeCP2 TRD expression was further detected by RT-qPCR from RNA extracted from transduced retinal organoids. **C.** Normalized expression values showing relative expression of rod- and cone-photoreceptor genes assessed via RT-qPCR from RNA extracted from retinal organoids transduced with the dCas9-bipartite repressor fusion targeting *hNRL* (blue) and a non-targeting gRNA (red). Gene knockdown of 67%, 72%, and 43% was seen in rod-specific genes *NRL*, *NR2E3*, and *PDE6B*, respectively. Gene upregulation of 33% was achieved with cone-specific gene *ARR3*. The data are presented by mean value ± SEM with all data points from independent experiments shown. All analysis was normalized to samples transfected with a non-targeting gRNA control. *p<0.05; ***p<0.001; Sidak's multiple comparison test. All other comparisons were not significant.

5.4.4 Pilot study of dCas9 repressor fusions in *Nrl-EGFP* mouse model

5.4.4.1 Evaluation of AAV-GRK1-dCas9 bipartite repressor *in vivo*

Lastly, dCas9 repressor fusions were investigated in the *Nrl-EGFP* mouse model. In this pilot study, 3.0 x 10^9 vg (1.5uL) of AAV-dCas9-KRAB-MeCP2 TRD cloned with a guide targeting the *mNrl* promoter (gRNA3) or a non-targeting guide (NT) were injected subretinally into 5–6-week-old mice. 4- and 8-weeks after administration, cSLO imaging was performed to assess knockdown and any immunotoxicity. At the 16-week time point,

the final set of cSLO imaging was performed and mouse retinae were harvested for downstream analyses by WB, IHC, and RT-qPCR (Figure 5.5).

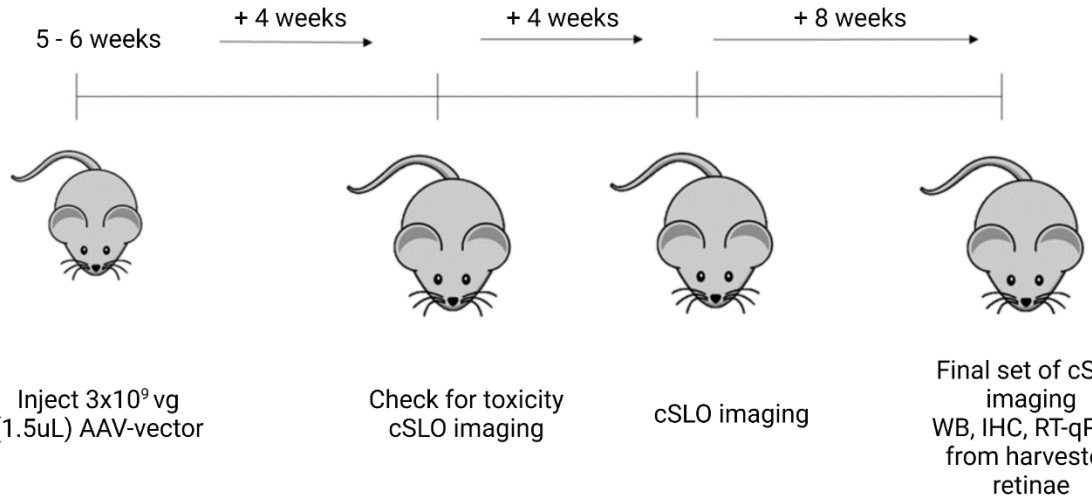


Figure 5.5 | Pilot study in the *Nrl-EGFP* mouse model

Schematic summarizing the pilot *in vivo* study in the *Nrl-EGFP* mouse model. 3.0 x 10^9 vg (1.5uL) of AAV-dCas9-KRAB-MeCP2 TRD cloned with a guide targeting the *mNrl* promoter (gRNA3) or a non-targeting guide (NT) were injected subretinally into 5–6-week-old mice. 4- and 8-weeks after administration, cSLO imaging was performed to assess knockdown and any immunotoxicity. At the 16-week time point, the final set of cSLO imaging was performed and mouse retinae were harvested for downstream analyses.

GFP repression, as well as any vector-induced toxicity, was examined *in vivo* at 4, 8-, and 16-weeks post-injection using blue autofluorescence (BAF) confocal scanning laser ophthalmoscope (cSLO) imaging. As the lateral spread of the AAV5 vector is limited and transfection is mostly confined to the bleb area created in the superior hemi-retina, EGFP expression was expected to localize superior to the optic nerve. No reduction in GFP expression was observed with the dCas9-only targeting (data not shown) or the dCas9-KRAB-MeCP2 TRD non-targeting vector at any imaging timepoints. For eyes injected with the AAV5-dSaCas9-KRAB-MeCP2 TRD *mNrl* targeting vector, GFP knockdown was observed in the superior retina (at the injection site), which increased temporally at 4-, 8,

and 16-week imaging timepoints. However, GFP knockdown was concomitant with significant superior retinal thinning (at the injection site), to a greater level than was seen solely due to surgical trauma, buffer-related toxicity in the matched buffer control, or dCas9-only and non-targeting vector controls (data not shown). Furthermore, ERG assessment showed limited difference in a-wave or b-wave responses when comparing the non-targeting repressor to paired buffer-injected eyes (data now shown), suggesting that the retinal thinning observed in the pilot *in vivo* study is targeting-vector specific, rather than dCas9-repressor fusion mediated toxicity. It is also possible that excessive ablation of *Nrl* expression mediated by robust repression led to deleterious exogenous consequences. Future studies will explore the bipartite repression in an alternative *Opn1sw.EGFP* mouse model to further characterize the safety and specificity profile of the dSaCas9-KRAB-MECP2 TRD targeting construct.

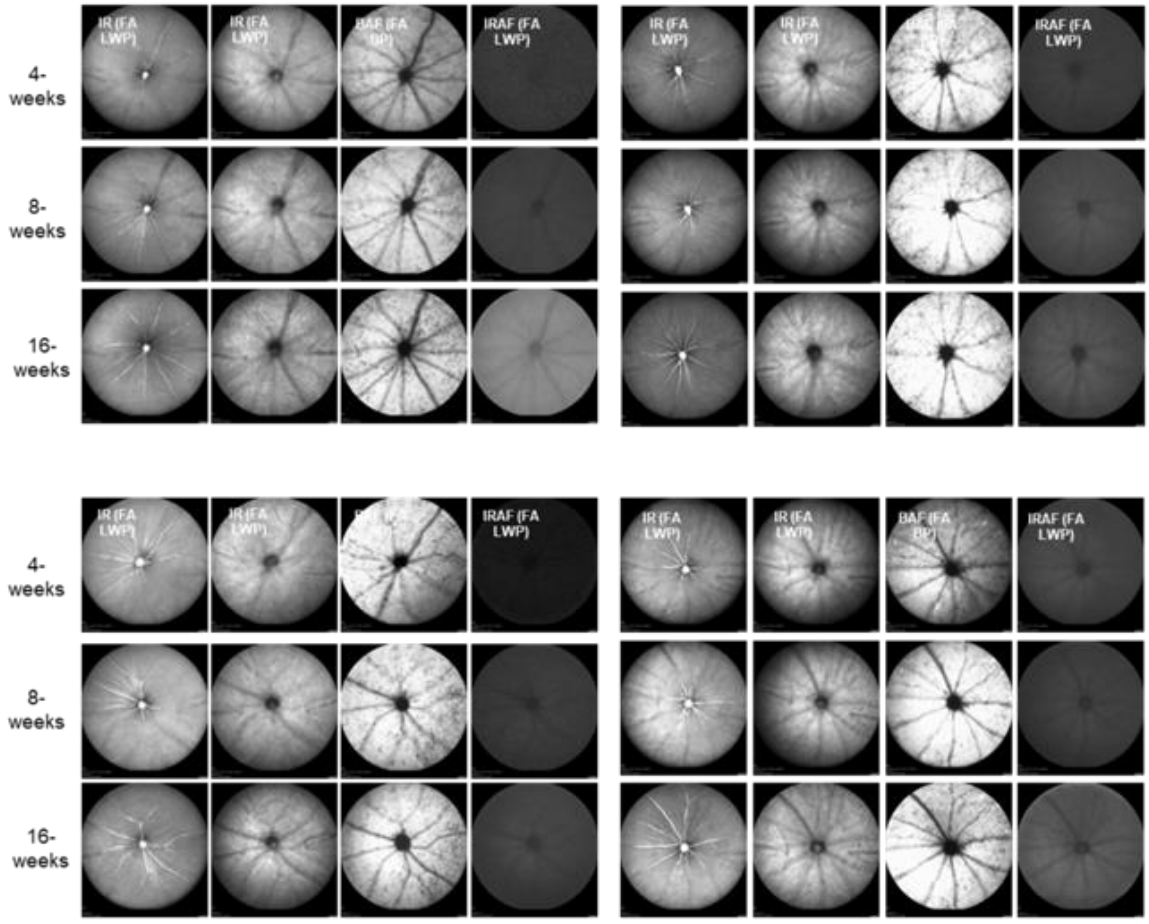


Figure 5.6 | *En face* cSLO imaging following subretinal injection with dCas9-KRAB-MeCP2 TRD non-targeting vector

Retinal imaging of paired eyes from heterozygous *Nrl.EGFP* mice (*Nrl.EGFP*$^{+/-}$) 4-, 8-, and 16-weeks following subretinal injection with AAV5-dSaCas9-KRAB-MeCP2 TRD non-targeting vector. For all subretinal injections, the contralateral eye received a matched buffer control injection to control for the effect of surgical trauma or buffer-related toxicity and un-injected C57BL/6 mice were concurrently monitored. For each panel, the columns show blue autofluorescence (BAF) confocal scanning laser ophthalmoscope (cSLO) imaging using infrared reflectance (IR), blue autofluorescence (BAF), and infrared autofluorescence (IRAF). Minor superior retinal thinning (at the injection site) was observed when compared to the inferior retina (away from the injection site), but thinning was to the same level as was seen with the matched buffer control. No other obvious differences were observed.

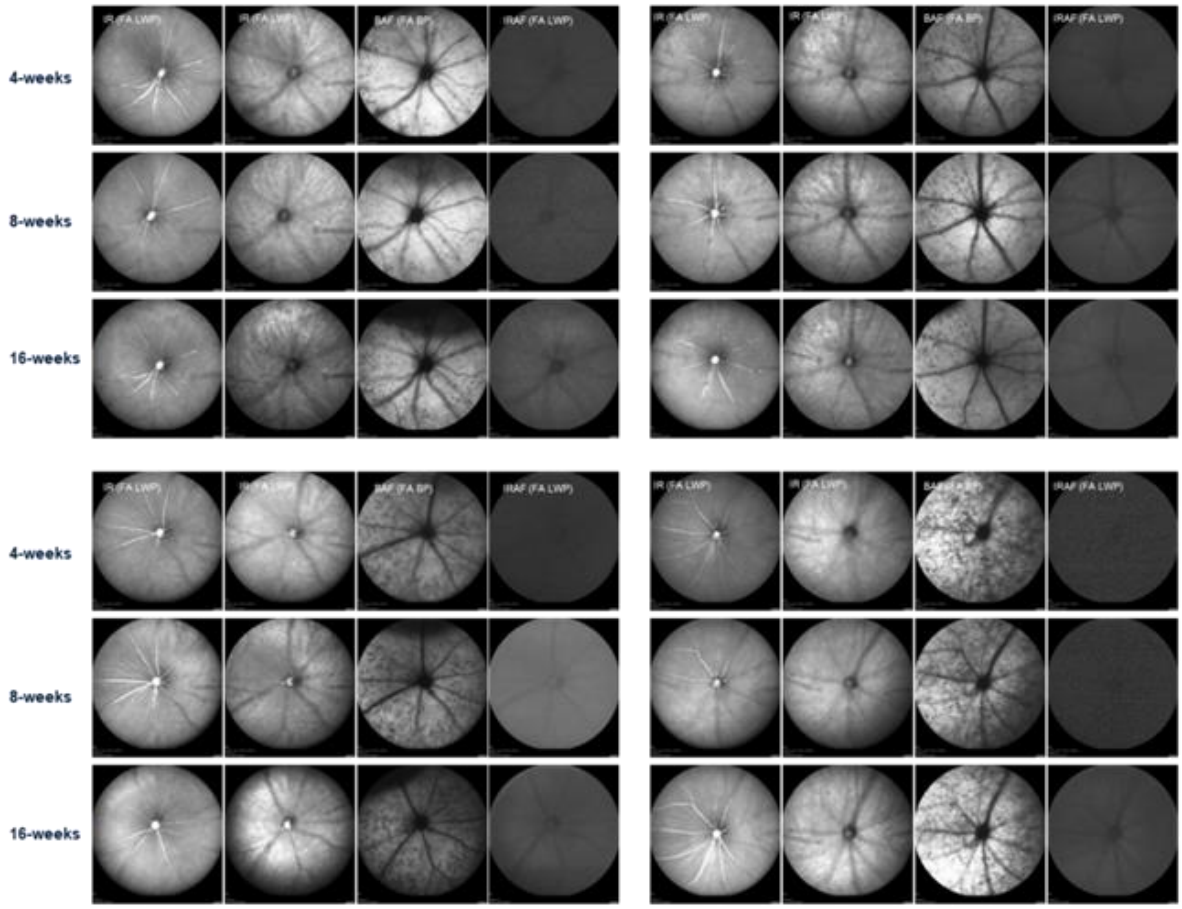


Figure 5.7 | *En face* cSLO and OCT imaging following subretinal injection with dCas9-KRAB-MeCP2 TRD targeting vector

Retinal imaging of paired eyes from heterozygous *Nrl.EGFP* mice (*Nrl.EGFP*$^{+/-}$) 4-, 8-, and 16-weeks following subretinal injection with AAV5-dSaCas9-KRAB-MeCP2 TRD *mNrl* targeting vector. For all subretinal injections, the contralateral eye received a matched buffer control injection to control for the effect of surgical trauma or buffer-related toxicity and un-injected C57BL/6 mice were concurrently monitored. For each panel, the columns show blue autofluorescence (BAF) confocal scanning laser ophthalmoscope (cSLO) imaging using infrared reflectance (IR), blue autofluorescence (BAF), and infrared autofluorescence (IRAF). EGFP knockdown was observed in the superior retina (at the injection site), which increased temporally at 4-, 8-, and 16-week imaging timepoints. However, GFP knockdown was concomitant with significant superior retinal thinning.

5.4.4.2 Evaluation of AAV-GRK1-dCas9 bipartite repressor expression

Finally, to evaluate expression as well as any repression mediated by the targeting dCas9 repressor, mouse retinae were harvested at 16-weeks post-transduction for downstream analyses by WB, IHC, and RT-qPCR (Figure 5.5). Since identical AAV-directed repressors were used for *vivo* experiments as in the retinal organoid cultures, as expected, robust AAV-directed dSaCas9 transduction was detected by immunohistochemistry and WB (Figure 5.8). Gene expression of *mNrl* was assessed by RT-qPCR, with m*GAPDH* used as a negative control, and with expression values standardized to a non-targeting gRNA. Promisingly, *Nrl* silencing of 41% was observed with the dCas9 repressor targeting construct. Gene expression of cone-specific markers was not detected by RT-qPCR in the pilot study (data not shown). Moreover, *GAPDH* knockdown of 20% was also observed with the targeting construct (Figure 5.8). This suggests potential toxicity or non-specific repression mediated by the *NRL* targeting vector leading to cell death.

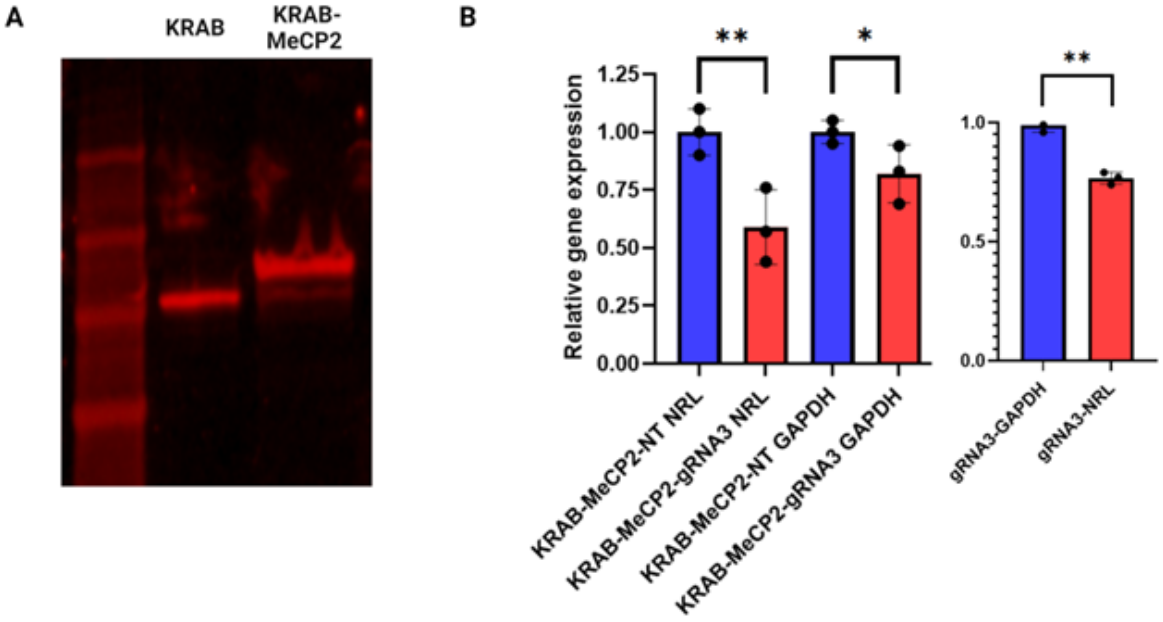


Figure 5.8 | Pilot evaluation of AAV-directed dCas9-repressor fusions in Nrl-EGFP mouse model

A. Western blot to detect Cas9 expression. SaCas9 expression were detected from retinal sections transduced with AAV5-GRK1-dSaCas9-KRAB (left) and AAV5-GRK1-dSaCas9-KRAB-MeCP2 TRD (right). **B.** Normalized expression values showing relative expression of *mNrl* and *mGapdh* (left) assessed via RT-qPCR from RNA extracted from retinae transduced with the dCas9-bipartite repressor fusion targeting *mNrl* and a non-targeting gRNA. *NRL* silencing of 41% was observed with the dCas9 repressor targeting construct. *GAPDH* knockdown of 20% was observed with the targeting construct, suggesting possible toxicity of the dCas9 targeting vector. *GADPH* normalized expression values ($\Delta\Delta C_t$) showed *Nrl* suppression of 23% (right). The data are presented by mean value ± SEM with all data points from independent experiments shown. All analysis was normalized to samples transfected with a non-targeting gRNA control. *p<0.05; **p<0.01; Sidak's multiple comparison test.

5.5 Discussion

The recent advent of dCas9-repressor fusions has emerged as a promising alternative to cleavage-dependent gene editing with broad utility and basic science and translational applications. dCas9-KRAB has driven clinically significant gene repression *in vivo* in a range of disease models, including retinitis pigmentosa, familial hypercholesterolemia, and obesity. Chapter 5 details the evaluation of engineered dCas9-based repressors in human iPSC derived 3D retinal organoids and in an *Nrl.EGFP* mouse model. This study adds to the emerging collection of literature demonstrating the potential of dCas9-repressor fusion-mediated gene repression.

5.5.1 *Nrl* as a genetic target for epigenome editing

The *Nrl* gene encodes the neural retina leucine zipper protein, a basic motif-leucine zipper transcription factor of the Maf subfamily that in mouse is initially expressed in nascent rod photoreceptor precursor cells after the terminal progenitor division and persists in rod photoreceptors thereafter. Genetic studies have shown that *Nrl* is required for the acquisition of rod identity, differentiation and homeostasis, acting as a 'molecular switch' during rod-cell development by directly modulating rod-specific genes while simultaneously inhibiting S-cone pathways through the upregulation of downstream rod target genes. Indeed, previous studies have demonstrated that *Nrl* binds to sequence elements in the *Nr2e3* promoter, a transcription factor that represses transcription of multiple cone-specific genes. Moreover, *Nrl* acts synergistically with the cone rod homeobox transcription factor, *Crx* to regulate Rhodopsin gene, *Rho,* transcription while ectopic expression of *Nrl* under the control of the *Crx* promoter leads to a rod-only retina.[301-306] In the retinae of *Nrl* $^{-/-}$ mice, loss of NRL results in enhanced S-cone like phenotype and, after transient degeneration, several layers of S-cone like cells survive and are functional throughout life.[303,307] Expression of a number of key markers are altered

in *Nrl* $^{-/-}$ retinae, supporting the proposed model that progenitors generate S-cones by a default pathway, and that *Nrl* acts like a master regulator of photoreceptor specification in mice.

In humans, heterozygous missense mutations in the *NRL* gene are associated with dominant retinitis pigmentosa (RP) phenotypes;[308-312] gain-of-function mutations (at codons 49, 50, 51, 56 in the NRL transactivation domain) lead to reduced NRL phosphorylation and enhanced activation of the rhodopsin promoter.[313] Such patients are characterized by progressive loss of vision, initially manifesting as night blindness, with subsequent loss of the peripheral visual fields, and later frequently involving deterioration of central vision.[314] Autosomal dominant RP (ad RP) accounts for 20% to 25% of all cases of RP. Conversely, homozygous and compound heterozygous loss-of-function *NRL* mutations cause recessive enhanced S-cone syndrome (ESCS). ESCS (sometimes called Goldman-Favre syndrome), is characterized by increased sensitivity to blue light, coincident with night blindness from an early age and pigmentary retinopathy. The recessive *NRL* mutations reported in ESCS patients are often nonsense or frameshift mutations.[315-317] Unaffected relatives carrying such mutations indicate that heterozygous *NRL* loss-of-function is not pathogenic.[315-317] Perhaps unsurprisingly, ESCS has also been frequently associated with *NR2E3* mutation.

While there are currently no approved treatments for *NRL*-related retinal diseases, various therapeutic strategies are being explored in the clinic. To date, viral vector mediated gene supplementation strategies have been the favored approach to correct the underlying molecular defect in inherited retinal degenerations. For adRP, inactivation of the mutant allele has been evaluated in disease models using multiple strategies including ribozymes and RNA interference.[318-321] Although encouraging, these gene-specific approaches are less practical due to the excessive heterogeneity of mutations underlying RP and other for *NRL*-related retinal degenerations. One alternative approach

consists of reprogramming adult photoreceptors by downregulating *NRL* expression, leading to loss of rod features and acquisition of cone characteristics that support longer-term preservation of cone function and viability. Consistent with this, recent studies have demonstrated that *in situ* genome editing of *NRL* results in reprogramming of rods into cone-like cells less susceptible to RP-specific mutations.[95,322]

An important question underlying this approach is whether the loss of NRL function can be exploited for treatment of reginal degenerative diseases are initiated in rods. Indeed, since diverse gain- and loss-of-function mutations in *NRL* are responsible for diverse human retinopathies, it is natural to contemplate whether loss of NRL in human rods could lead to deleterious consequences and ultimately cell death. Addressing this question requires investigation of both the timing of photoreceptor development at which gene expression is suppressed as well as the broader genome engineering strategy underlying *NRL* targeting. While NRL may possess a unilateral role in determining cell date during retinal development, its role in maintaining rod function and homeostasis is accomplished synergistically with other rod-expressed transcription factors (as described in detail above). Thus, loss of NRL in adult photoreceptors is not expected to change cell fate, but rather, the downregulation of rod genes will likely lead to de-repression of cone genes mediated by decreased *NR2E3* expression. For this reason, my study design centered on *in vivo* evaluation of CRISPR reagents in mature photoreceptors (AAV-directed dCas9-repressor delivered subretinally at 5-6 weeks) rather than during early retinal development.

As a therapeutic strategy, an advantage of using CRISPRi is that repressor-based systems provide a potentially reversible approach for gene therapy, with limited risk of mutagenesis associated with cleavage-dependent systems. Importantly, since recessive mutations in *NRL* can cause retinal degeneration, an *in vivo* gene repression strategy of

NRL to rescue cone generation is especially advantageous versus a gene editing approach given the deleterious long-term effects of *NRL* ablation.

5.5.2 Off-target effects and toxicity

Despite encouraging levels of gene knockdown observed in the an *Nrl.EGFP* mouse model, there was also substantial retinal thinning observed by cSLO and loss of retinal function by ERG. Interestingly, even greater levels of toxicity were observed by injection with AAV-dCas9-KRAB alone (data not shown), suggesting that the effect is not specific to the novel MeCP2 transcriptional repressor domain. There are possible causes for the observed toxicity of the repressor constructs, which are explored in detail below.

From an evolutionary perspective, the emergence of mammalian rods is thought to have occurred by their developmental recruitment from the S-cone lineage.[323] It is postulated that this process was predicated on the origins of novel regulatory sequences of *Nrl* that restrict its expression to rod photoreceptors in mammals.[323] Indeed, the *NRL* gene is conserved in chimpanzee, Rhesus monkey, dog, cow, mouse, rat, zebrafish, and frog, and 207 organisms have orthologs with human gene NRL (NCBI analysis; Gene ID 4901). A nucleotide sequence search using the NCBI Basic Local Alignment Search Tool (BLAST) identified 114 matches across 28 different organisms with identical sequence identity to the gRNA sequence used in the retinal organoid model and *in vivo*. A table of human and mouse targets with identical sequence identity to the selected gRNA sequence is detailed below (Table 5.4).

Description	Percent identity	Accession
Homo sapiens neural retina leucine zipper (NRL), RefSeqGene on	100%	NG_011697.2

chromosome 14; nuclear gene for mitochondrial product		
Human chromosome 14 DNA sequence BAC R-468E2 of library RPCI-11 from chromosome 14 of Homo sapiens (Human), complete sequence	100%	AL136295.3
Homo sapiens isolate CHM13 chromosome 15	100%	CP068263.2
PREDICTED: Homo sapiens uncharacterized LOC107983974 (LOC107983974), transcript variant X3, ncRNA	100%	XR_007085359.1
PREDICTED: Homo sapiens uncharacterized LOC107983974 (LOC107983974), transcript variant X2, ncRNA	100%	XR_007085358.1
PREDICTED: Homo sapiens uncharacterized LOC107983974 (LOC107983974), transcript variant X1, ncRNA	100%	XR_007085357.1
Mus musculus BAC clone RP23-203D7 from chromosome 14, complete sequence	100%	AC159002.2
Mus musculus neural retina leucine zipper (*Nrl*) gene, promoter region and 5' UTR	100%	AY526079.1
Mus musculus BAC clone RP23-11O22 from chromosome 14, complete sequence	100%	AC174678.2
Mus musculus targeted KO-first, conditional ready, lacZ-tagged mutant allele Cpne6:tm1a(KOMP)Ucd; transgenic	100%	JN953279.1
Mus musculus targeted non-conditional, lacZ-tagged mutant allele Cpne6:tm1e(KOMP)Ucd; transgenic	100%	JN945394.1

Table 5.4 | Guide RNA sequence Nucleotide BLAST

Summary of homo sapiens and mus musculus sequences with 100% homology to the screened gRNA sequence for *in vitro* and *in vivo* studies.

While a guide sequence with homology to mouse and human sequences was screened to facilitate experiments in human-derived retinal organoids and the an *Nrl.EGFP* mouse, the conserved nature of this sequence may have contributed to the retinal toxicity observed in the *in vivo* pilot study. Future studies will evaluate unique gRNA sequences without cross-taxology homology.

In addition to robust rates of *Nrl* repression achieved in retinal organoids, a panel of other rod specific genes were knocked-down, including *Nr2e3* and *Pde6b*, transcription factors modulated by *Nrl* to repress transcription of multiple cone-specific genes. Moreover, upregulation of the *Arr3* was observed, a cone-specific non-visual arrestin, providing further mechanistic support that the observed repression is repressor-specific, rather than mediated by a spurious secondary mechanism or non-specific repression. Nevertheless, future studies utilizing RNA-seq or other related transcriptomics technologies are needed to fully characterize the specificity of AAV directed dCas9-repressors.

Moreover, it is possible that the function(s) of *NRL* in mouse and human retina is different, leading to the retinal thinning that was observed in the mice. Though both species have rod-dominant retinas, the photoreceptor topology is distinct, and humans have three different cone types.[324] Therefore, in humans, *NRL* may have alternative functions and the loss of *NRL* would result in a more complex phenotype. Continued analysis of *NRL* mutations in both animal models and human patients will therefore be necessary to gain further insight into the specific roles of this retinal transcription factor.

Finally, despite the potential advantages of epi-editing as compared to Cas9 genome editing, future assessment is needed to evaluate potential off-targets on the transcriptome and methylome. To evaluate the effect of targeting *NRL* with dCas9 effector fusions on global gene expression, single-cell RNA sequencing analyses can be performed. To investigate on- and off-target effects of dCas9 bipartite repressors on the DNA methylome, large-scale DNA methylation profiling technologies could be applied to interrogate DNA methylation at CpG sites genome-wide. Lastly, it is possible that there are different kinds of responders to the epigenetic edits and future studies will need to address this mechanistic question. Most likely this biological inquiry will need to be answered at a single cell level in future studies.

5.5.3 Immunogenic response

A proportion of the toxicity also likely stems from immune response to intraocular injection and persistent expression of Cas9-associated machinery. Although the eye is considered an immune-privileged organ, intraocular inflammation remains a major cause of vision loss.[325] Toral *et al.* analyzed the presence of Cas9-reactive antibodies in serum and vitreous fluid biopsies from 13 adult human subjects and mice.[326] There was a high prevalence of preexisting Cas9-reactive antibodies in serum but not in the eye, reflecting a lower risk of immune reaction in human eyes. However, a subset of mice developed *S. pyogenes* Cas9-reactive antibodies in the vitreous fluid after intramuscular infection with *S. pyogenes*. These findings warrant further research to determine whether intraocular Cas9 exposure from epigenome editing increases the risk of inflammation or impedes therapy. Moreover, the AAV vectors themselves have been reported to elicit immune responses, as AAVs could enter the vitreous fluid and subsequently cause inflammation in the eye.[327,328] All vector preps were free from endotoxin.

Taken together, further research is needed to determine the relative contributions of each component to the observed toxicity. Indeed, as with all genome engineering tools, substantial efforts are needed to evaluate all possible immune-related risks of epigenome editing and to identify potential ways to mitigate such risks. Future experiments, including exploration of the epigenome editing approach in an alternative *OPN1SW-EGFP* mouse model, will shed additional light into the safety and specificity profile of the dCas9-epigenome editing tools.

5.5.4 Translational considerations and challenges: Safety, efficiency, and precision

Advances in precision epigenome editing technologies have opened up unprecedented opportunities for novel therapies modulating gene expression. However, applying these technologies in the clinic requires overcoming several hurdles, including safety and efficiency.

Epigenetic regulatory mechanisms play a pivotal role in controlling human gene expression and genomic activity. CRISPR/Cas-based epigenome editing has emerged as a powerful and versatile strategy to repurpose these mechanisms to control gene expression, engineer cellular phenotypes, and model and treat human diseases. In an analysis of 150,000 human genomes in the UK Biobank by Kári Stefánsson, the authors found that the vast majority (89%) of disease-causing variants occur in non-coding regulatory elements of the genome.[329] The growing toolbox of epigenome editing effectors and control systems to modulate epigenetic and transcriptional regulation have catalyzed a slew of translational applications. CRISPR-mediated epigenome editing has been used for differentiation and reprogramming of cells both *in vivo* and *ex vivo*. Epigenome editing utilizing activators such as quadruple repeats of VP16 (VP64) and other human transactivation domains, such as p65, Rta, and HSF1, have been utilized to differentiate

iPSCs into neurons,[330] muscle cells,[331] and extraembryonic lineages.[332] While these studies targeted a single reprogramming factor, multiplexed delivery of dCas9-based transcriptional activators has also been applied to reprogram differentiated somatic cells to a target cell type.[333]

Epigenetic editing has also been utilized as a powerful tool in discovering novel genetic components involved in cellular differentiation, as well as in disease modeling. Recently, Gemberling *et al.* describe the generation and characterization of two conditional transgenic mouse lines for epigenome editing, Rosa26:LSL-dCas9-p300 for gene activation and Rosa26:LSL-dCas9-KRAB for gene repression. By targeting the guide RNAs to transcriptional start sites or distal enhancer elements, the authors demonstrate regulation of target genes and corresponding changes to epigenetic states and downstream phenotypes in the brain and liver *in vivo*.[334]

Although epigenome editing systems are still earlier in their development than more established CRISPR-based genome editing tools, rapid advances have in characterizing safety and efficacy of these systems indicate that CRISPR-based clinical epigenome editing is not far off. To this end, the clinical development of zinc finger-based transcriptional activators and other genome-engineering systems may serve as an important roadmap.[335] The commercial maturity of epigenome editing tools is supported by the launch of at least three companies over the past four years aimed at altering epigenetic marks using dCas9 as their DNA-targeting machinery: Chroma Medicine (Cambridge, MA, USA), Tune Therapeutics (Durham, NC, USA), and Epic Bio (San Francisco, CA, USA). All are exploring both *ex vivo* and *in vivo* therapeutic approaches, though only two have disclosed target disease areas, at least one of them, Tune Therapeutics, is also exploring zinc finger and TALE proteins. Indeed, I anticipate that CRISPR based epigenome editing systems will have broad utility in basic science and therapeutic translation in the coming years, though systems will likely need to strike a

balance between effector type, delivery method, and precision control system for particular indications before their routine use at the bedside.

5.5.5 Conclusions

Collectively, AAV-directed dCas9-based repressor effectors provide a facile and robust method to modulate the expression of endogenous genes. The CRISPRi system developed in this chapter has several distinct therapeutic advantages, including in its reversibility and limited risk of mutagenesis due to the inactivation of the Cas9 nuclease activity. This work is the first demonstration of all-in-one packaging of a bipartite repressor system, which due to the limited cargo capacity of AAVs is an optimal approach to enable desired genome engineering applications. I show that the dCas9-repressor fusions can be utilized to mediate a high level of transcriptional repression. Furthermore, I demonstrate for the first time the utility of dCas9-repressor-mediated *in situ* gene repression in the context of patient iPSC derived 3D retinal organoids. I highlight several key areas of future investigation, including in exploration of more suitable preclinical models, better understanding off-target effects, and AAV and dCas9-repressor fusion mediated toxicity. Taken together, this CRISPR-dCas9-mediated epigenetic editing strategy presents a novel strategy for targeted modulation of gene expression in a gene and mutation independent context and may provide a novel therapeutic approach for the treatment of inherited retinal diseases.

6. DEVELOPMENT OF HDR-INDEPENDENT BASE EDITING AND PRIME EDITING TECHNOLOGIES

6.1 Introduction

Having assessed the dCas-bipartite repressors in multiple models both *in vitro* and *in vivo*, I next selected a precision-editing approach for targeted mutation correction. While there are multiple approaches for repairing deleterious mutations, due to their favorable safety profile and broad potential to treat IRDs, after extensive consideration with my supervisors, HDR-independent base editing and prime editing strategies were selected for further development.

HDR-mediated gene editing is characterized by low efficiency and high rates of undesired indel mutations that nullify the potential benefit from repairing the mutation. Recently, CRISPR-Cas-mediated single base pair editing systems (or "base editing" systems) have been devised to bypass these limitations. Two classes of DNA base editors have been described: cytosine base editors and adenine base editors. Base editors encompass two key components: a Cas9 nickase (nCas9) with one inactive nuclease domain to provide programmable DNA target binding and induce a single-stranded DNA nick, and a single-stranded DNA-modifying enzyme (either cytosine or adenine deaminase) for targeted nucleotide alteration.[336] Collectively, all four transition mutations can be introduced with the available CRISPR-Cas base editors.

Prime editors (PEs) are the latest addition to the CRISPR genome-engineering toolkit and represent a novel approach to expand the scope of donor-free precise DNA

editing to not only all transition and transversion mutations but also small indels.[128] Prime editors use an engineered reverse transcriptase fused to Cas9 nickase and a prime editing guide RNA (pegRNA). Importantly, the pegRNA differs significantly from regular sgRNAs and plays a major role in the system's function. The pegRNA contains not only (i) the sequence complementary to the target sequence that directs nCas9 to its target site but also (ii) an additional sequence spelling the desired sequence changes.

DNA base-editing and prime-editing may prove to be particularly well adapted for correction of large genes (> 4 kb). For many retinal diseases, vector-mediated gene delivery is not feasible due to the cargo limit of viral vectors as well as the expression of multiple heterogeneous variants of the target gene. The ability to target nucleotides on either the plus or complementary minus DNA strand opens up the therapeutic applications of base editors considerably. More than 25% of human pathogenic single nucleotide polymorphisms (SNPs) can be corrected by targeting the four transition mutations, and in principle prime editing could correct up to 89% of pathogenic human genetic variants in ClinVar.[107,128] Importantly, these systems employ cellular mismatch repair machinery and can be applied to reverse these defects in both dividing and terminally differentiated cells.

Despite their versatile genome editing capacity, significant challenges remain with the delivery of therapeutic base editing and prime editing systems into retinal cells. A cytosine or adenine base editor plus a guide RNA totals ~6 kb, whereas prime editors are >7 kb, both well beyond the packaging constraints of a single AAV vector.

In this chapter, I develop a reporter cell line harboring a nonsense mutation in EGFP, such that targeted adenine base editing or prime editing can revert the mutation and restore EGFP expression. I apply this cell line to screen different adenine base editors

and demonstrate high rates of on-target activity utilizing a compact *Staphylococcus aureus*-derived Cas9 orthologue.

To optimize the prime editing system, I hypothesized that it would be possible to engineer a compact prime editor by truncating the ribonuclease H (RNase H) domain of the reverse transcriptase. I selected Moloney Murine Leukemia Virus Reverse Transcriptase (M-MLV RT), a modular enzyme carrying polymerase and RNase H activities in separable domain. I used a luciferase-based *in vitro* assay harboring the mouse *Ush2a* c. 11840G>A (W3947X) mutation (a gift from L. Fry) to investigate the utility of an engineered PE tool for treatment of inherited retinal disease. The homologous human mutation is c.11864G>A (W3955X), the third most common *USH2A* pathogenic mutation reported in the LOVD dataset and comprising 23% of patients in a large European *USH2A* cohort. Together, my studies demonstrate that an engineered minimal PE variant enhances rates of prime editing *in vitro* against a therapeutically relevant target.

The results of this chapter support *in vivo* translation of DNA base editing and prime editing technologies towards the treatment of Usher Syndrome and other inherited retinal diseases.

6.2 Chapter aims

The overall goal of this chapter is to develop and optimize HDR-independent DNA base editing and prime editing technologies. To achieve this, the following aims will be explored:

1. Develop an *in vitro* cell line for facile screening of DNA base editing and prime editing constructs.
2. Design and clone a dual-vector delivery strategy for evaluation of adenine base editors.
3. Compare the on-target activity of different adenine base editors.
4. Design and clone truncations in the Moloney Murine Leukemia Virus Reverse Transcriptase (M-MLV RT) of prime editor (PE) systems.
5. Evaluate the on-target activity induced by truncated PE variants utilizing a luciferase-based assay.

6.3 Methods & materials

6.3.1 Plasmid construction

The general protocol for plasmid cloning is detailed in the general methods. The pRZ-CAS9-mCherry construct (Addgene plasmid #80974) modified for DNA base editing was a gift from Veit Hornung. The pCMV_ABEmax (Addgene plasmid #112095), ABE8e (Addgene plasmid #138489), NG-ABE8e (Addgene plasmid #138491), SaKKH-ABE8e (Addgene plasmid #138502) for adenine base editing were gifts from David Liu. The nSaCas9 S740 miniABEMax V82G construct (Addgene plasmid #135388) was a gift from Alex Hewitt. The plasmids pCMV-PE2 (Addgene plasmid #132775) expressing prime editor 2 and pU6-pegRNA-GG-acceptor (Addgene plasmid #132777) expressing pegRNA were gifts from David Liu. All sequences for key plasmid elements, primers, and guide RNAs are detailed in the Appendix.

6.3.2 Cell line generation for reporting DNA base editing

pCMV-GFP (Addgene plasmid #11153), modified for generation of cell lines for reporting DNA base editing, was a gift from Connie Cepko. Site-directed mutagenesis was utilized to introduce a TAG nonsense mutation in EGFP. All primers and plasmid sequences and detailed in the Appendix.

The Duke Viral Vector Core provided lentivirus for generation of the cell lines. Both multicolor fluorescence *in situ* hybridization (MFISH) and karyotyping analysis were conducted on the HEK-dGFP, HEK-ABE, and HEK-CBE cell lines by the Wellcome Centre for Human Genetics. Metaphase spreads from each of the cell lines were hybridized to the 24xCyte probe set (Metasystem, Germany).

6.3.3 Cloning for guide RNA screening

For bulk screening of guide RNAs, 10 – 50 gRNA constructs were cloned in parallel. The protocol for oligonucleotide annealing was performed as described in the general protocol. Unless otherwise specified, all oligonucleotide pairs, including gRNA forward and reverse oligonucleotides, were designed to form a double stranded fragment with 5' and 3' end complementarity. 1 μL of diluted (1 in 25) duplexed gRNA solution was added strip tubes using multichannel pipettes. To this, 9 μL of prepared master mix of ligation mix was added, consisting of 6 μL of MG-H_2O. 1 μL of T4 DNA ligase, 1 μL of T4 DNA ligase buffer and 1 μL of 25 – 50 ng/μL digested and PCR purified plasmid backbone. 2 μL of the ligation mix was transformed into 25 μL of XL10-Gold ultracompetent cells (Agilent) as described in the general methods. The cell mixture was then added to 450 μL super optimal broth with catabolite repression (SOC) outgrowth medium (Thermo Fisher Scientific) or Stable Outgrowth Medium (NEB). The cells were then placed into an incubator-shaker at 37°C for 225rpm for 45 to 60 minutes. Two colonies were cultured for plasmid DNA isolation (ZymoPURE plasmid miniprep kit), and all sequences were confirmed with Sanger sequencing using a universal sequencing primer upstream of the U6 type III RNA polymerase III promoter used for driving gRNA expression. All primers and nucleotides encoding ngRNA and pegRNA spacers and 3' extension sequences are listed in the Appendix. CRISPick and pegFinder software was used for design of guide RNAs and prime editing guide RNAs, respectively.

6.3.4 Protein modeling

GlobPlot 2.3, PSIPRED, Clustal Omega, and ICM-Browser programs were utilized for all protein modeling applications. GlobPlot 2.3 was used to identify regions of globularity and disorder within reverse transcriptase (RT) sequences. PSIPRED was used to investigate RT protein secondary structure. Clustal Omega was utilized to make

multiple protein sequence alignments. Finally, ICM-Browser was applied to visualize three-dimensional molecular structures and predict RT-truncations of interest. All software and algorithms used for *in silico* design of prime editor RT-truncations are detailed in the Appendix.

6.3.5 Cell culture and transfections

Cell seeding and *in vitro* transfections were performed as described in the general methods. For luciferase assays evaluating DNA base editing and prime editing experiments, 100uL of HEK293T cells at a density of 5.5×10^4 cells/well were seeded in Corning white-walled 96 well adherent plates (Sigma-Aldrich) in phenol-red-free Dulbecco's Modified Eagle Medium (DMEM) (Thermo Fisher Scientific), supplemented with L-glutamine (2 mM) (Sigma-Aldrich), sodium pyruvate (1 mM) (Thermo Fisher Scientific), 10% heat-inactivated fetal bovine serum (HI-FBS) (Thermo Fisher Scientific) and 1% penicillin-streptomycin (Sigma-Aldrich). Cells were transfected with Transit-LT1 (Mirus Bio) at 24 hours post-seeding with 50 ng of dual luciferase reporter, 100 ng of DNA editing effector and 200 ng of gRNA construct unless otherwise stated. Positive and negative control wells were included on all plates, transfected with identical quantities of luciferase plasmid, DNA editing effector and non-targeting (scrambled) gRNA plasmids as in the experimental plates. All transfected plasmid preparations were made with endotoxin-free mini- (Zymo Research) or midi-prep kits (Clontech, a Takara Bio Company).

6.3.6 Dual-Glo luciferase assay

Dual luciferase constructs harboring the *hUSH2A*-W3955X and *mUsh2a*-W3947X mutations for DNA editing reporting were gifts from Lewis Fry. Briefly, target cassettes containing the G>A mutation of interest and the 200 bp region surrounding the target

mutations were synthesized as double stranded DNA fragments and cloned into the pSGDlucV3.0 plasmid (Addgene plasmid #119760).

The Dual-Glo luciferase assay kit (Promega, USA) was used to detect luciferase expression according to the manufacturer's instructions. For cell lysis and detection of firefly activity, 60 μL of Dual-Glo luciferase reagent containing firefly luciferase substrate was added to each well and left to incubate at room temperature for 15 minutes. Luminescence was recorded using a FLUOstar Omega microplate reader (BMG Labtech, Germany). For Renilla detection, 60 μL of Stop & Glo reagent was added to quench firefly activity and provide Renilla luciferase substrate, left to incubate for 15 minutes and luminescence recorded.

6.3.7 Analysis of DNA editing with Dual-Glo luciferase assay

Mean background firefly and Renilla luminescence was calculated from transfection-reagent-only wells and subtracted from all raw values. The editing efficiency was calculated from a ratio of Renilla to firefly luciferase activity, determined for each well. Editing efficiencies were calculated using the ratios of Renilla:firefly ratios (R:F), where the experimental control represents the base editing or prime editing construct utilized, the negative control represents 0% editing, and the positive control represents 100% editing (WT sequence). The calculation for quantifying DNA editing using the dual-luciferase assay is summarized below:

$$DNA\ editing\ efficiency\ (\%) = \frac{(R{:}F\ for\ experimental\ sample) - (R{:}F\ for\ negative\ control)}{(R{:}F\ for\ positive\ control) - (R{:}F\ for\ negative\ control)}$$

6.3.8 Analysis of on-target DNA editing

To evaluate DNA editing efficiency, HEK293-ABE cells were seeded into 24-well plates 1 day prior to transfection, as described in the general methods. Cells were transfected with Transit-LT1 (Mirus Bio) at 24 hours post-seeding with 1.5 μg of the base-editor expression plasmids and 1 μg of the corresponding sgRNA plasmids. 72-hours after transfection, cells were counted, and viability was assessed. To improve efficiency, the cells were split 1:2 and re-transfected using the same conditions as described above. 72-hours post the second transfection, the cells were harvested for genomic DNA extraction using the QIAamp DNA mini kit (Qiagen) or QuickExtract DNA Extraction Solution (Lucigen) in accordance with manufacturer's instructions. The genomic regions encompassing the target sites were amplified from the genomic DNA with high fidelity KOD Hotstart Mastermix (Merck, UK) according to the manufacturer's protocols. All primers used are listed in the Appendix. The PCR products were analyzed by Sanger sequencing, with chromatograms inspected for quality prior to analysis and manually trimmed as required. DNA editing rates were quantified using EditR (Edit deconvolution by inference of traces in R), a web tool which only requires a single Sanger sequencing file of a base-edited sample and the sequence of the gRNA protospacer to disentangle the outcomes of base editing. Non-significant editing sites were set to zero.

6.4 Results

6.4.1 Development of cell lines to report adenine and cytosine DNA base editing

Novel cell lines were developed for facile detection of DNA base editing with nCas9 cytosine and adenine base editing tools. HEK-dGFP plasmids developed in Chapter 3 were modified using site-directed mutagenesis (SDM). For the cell-line amenable to cytosine base editing, SDM was utilized to introduce an ACG missense mutation, which was complemented with an out-of-frame ATG 20bps downstream of the target site. For the HEK-ABE cell line, STD was used to introduce a TAG nonsense mutation in the dGFP. All cloning constructs were validated by sanger sequencing. Lentivirus was produced by the Duke Viral Vector Core for generation of stably transduced cell-lines harboring the ABE or CBE cassettes (Figure 6.1, 6.2).

To evaluate the reporter constructs, cells were maintained as outlined in the general methods and imaged daily for 3-weeks. While the wild-type HEK-dGFP cell line showed robust green fluorescence expression at all time-points imaged, there was no fluorescence at any time-point with either the HEK-CBE or ABE cell-lines (Figure 6.1, 6.2).

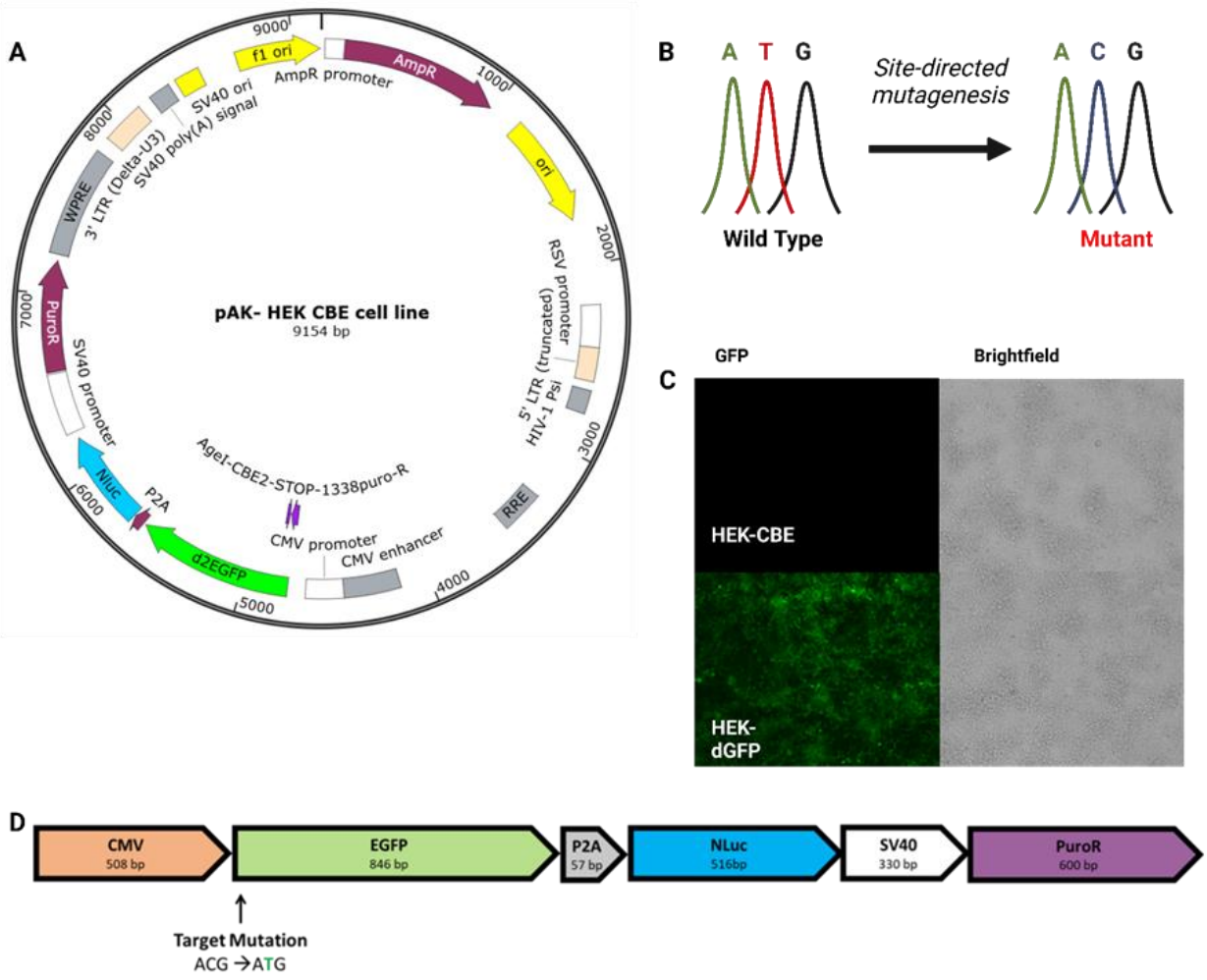


Figure 6.1 | Construction of cell line to report cytosine base editing

A. Plasmid map of the cytosine base editor reporter cell-line, comprised of a human cytomegalovirus (CMV) immediate-early enhancer and promoter driving the expression of a PEST-sequence destabilized enhanced florescent green protein (dGFP) followed by a self-cleaving P2A peptide sequence, and then NanoLuc (NLuc), a novel bioluminescence platform and a simian virus 40 (SV40) promoter controlling the expression of puromycin resistance gene (PuroR). **B.** Site-directed mutagenesis was used to introduce an ATG to ACG missense mutation in dGFP. Additionally, an out-of-frame ATG 20bp downstream of the target site was introduced. **C.** Representative light-microscope images (10X magnification) of HEK cells demonstrating robust GFP expression in the wild-type HEK-dGFP cell line, whereas CBE cell line showed no detectable

GFP expression. **D.** Transfection with Cas9-CBE restores the open reading frame and reverts the missense mutation back to ATG, thus reporting successful cytosine base editing outcomes.

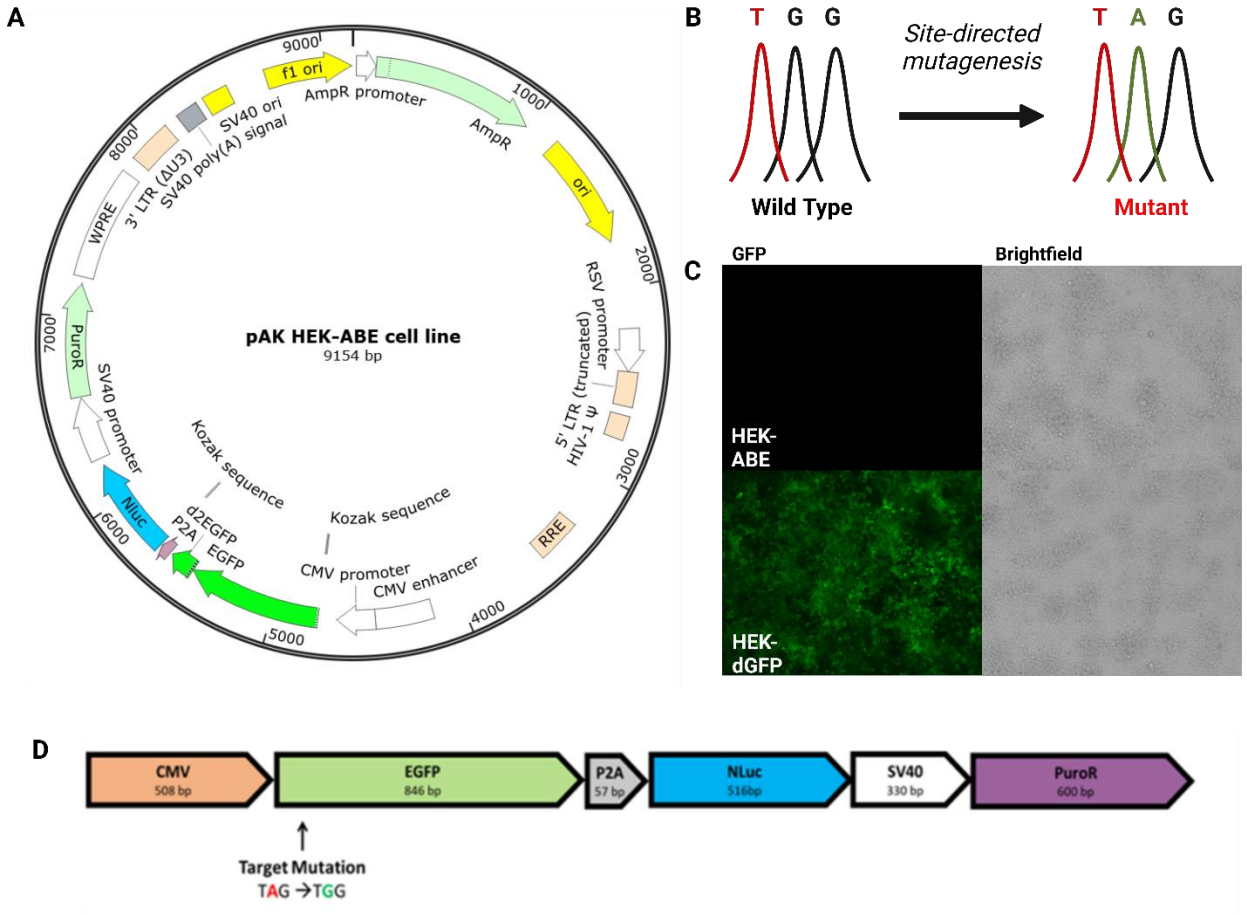


Figure 6.2 | Construction of cell line to report adenine base editing

A. Plasmid map of the adenine base editor reporter cell-line, comprised of a human CMV promoter driving the expression of dGFP followed by a self-cleaving P2A peptide sequence, and then NLuc and SV40 promoter controlling the expression of PuroR. Plasmid backbone is identical to the CBE cell line, with the exception of the modification to dGFP **B.** Site-directed mutagenesis was used to introduce an TGG to TAG nonsense mutation in dGFP. **C.** Representative light-microscope images (10X magnification) of HEK cells demonstrating robust GFP expression in the wild-type HEK-dGFP cell line, whereas ABE cell line showed no detectable GFP expression. **D.** Transfection with Cas9-ABE restores the open reading frame and reverts the nonsense mutation

back to TGG, which will switch on green fluorescence in successfully transduced cells, thus reporting successful adenine base editing outcomes.

Cell viability and division rates in the reporter cell lines was identical to the wild-type HEK-dGFP line. To further validate the reporter cell lines, both multicolor fluorescence *in situ* hybridization (MFISH) and karyotyping analysis were conducted by the Wellcome Centre for Human Genetics. Metaphase spreads from each of the cell lines were hybridized to the 24xCyte probe set (Metasystem, Germany). A minimum of 25 metaphases were acquired per cell line, and 10 karyotypes were fully reconstructed (Figure 6.3). The cell lines are near triploid, but with a different modal number of chromosomes per cell (HEK dGFP, 64; HEK-ABE, 67; HEK-CBE, 68. In brief, the generated ABE and CBE cell lines appear very similar to each other, as well the wild-type dGFP cell line from which they were derived. Finally, transgene localization confirmed single GFP copy number across all reporter lines, consistent with the low doses of lentiviral vector used and selection with puromycin for the generation of the cell lines (data not shown).

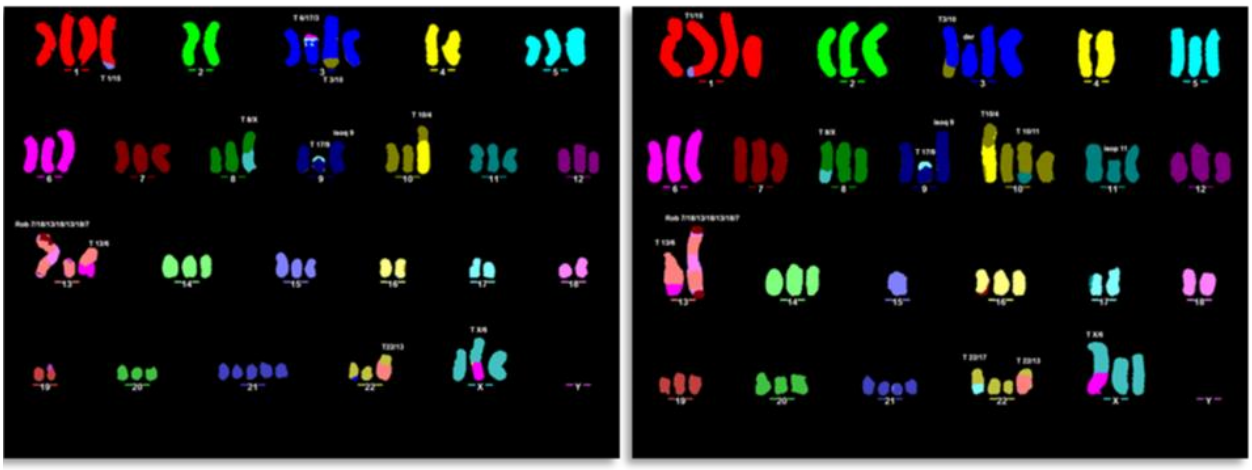


Figure 6.3 | Representative karyotypes from HEK-CBE and HEK-ABE cell lines

Representative karyotypes from HEK-CBE (left) and HEK-ABE (right) cell lines. The reporter cell lines appear very similar to the wild-type dGFP cell line.

6.4.2 Development and evaluation of DNA base editing constructs

6.4.2.1 Development of dual vector strategy for adenine base editing

Having established novel reporter cell lines for efficient and sensitive evaluation of DNA base editing constructs, different DNA editors were subsequently screened and optimized. Due to the broader range of adenine base editing-mediated corrections for the targeting of inherited retinal diseases, including for correction of the *mUsh2a*-W3947X mutation, ABE editors were selected for initial evaluation.

To rapidly screen and evaluate different ABE tools, a dual vector system was developed, with one vector harboring the nCas-ABE of interest, and the second vector comprising a U6 promoter driving the expression of the respective guide RNA scaffold (Figure 6.4). For facile interchange of different construct elements, single cutter SpeI and HindIII sites were introduced via PCR with Phusion DNA polymerase (NEB), with 5' extensions on the forward primers to generate the restriction sites. Subsequently, double-stranded fragments (IDT) encoding the U6 promoter and guide RNA scaffold cloned into the digested vector backbone. All primer and DNA fragment sequences used for the guide RNA vector generation are summarized in the Appendix. Finally, a CMV promoter expressing a mCherry transgene was introduced as a florescent reporter to ensure successful transfection for *in vitro* screening. Plasmid identity was confirmed by Sanger sequencing prior to proceeding with ABE screening experiments.

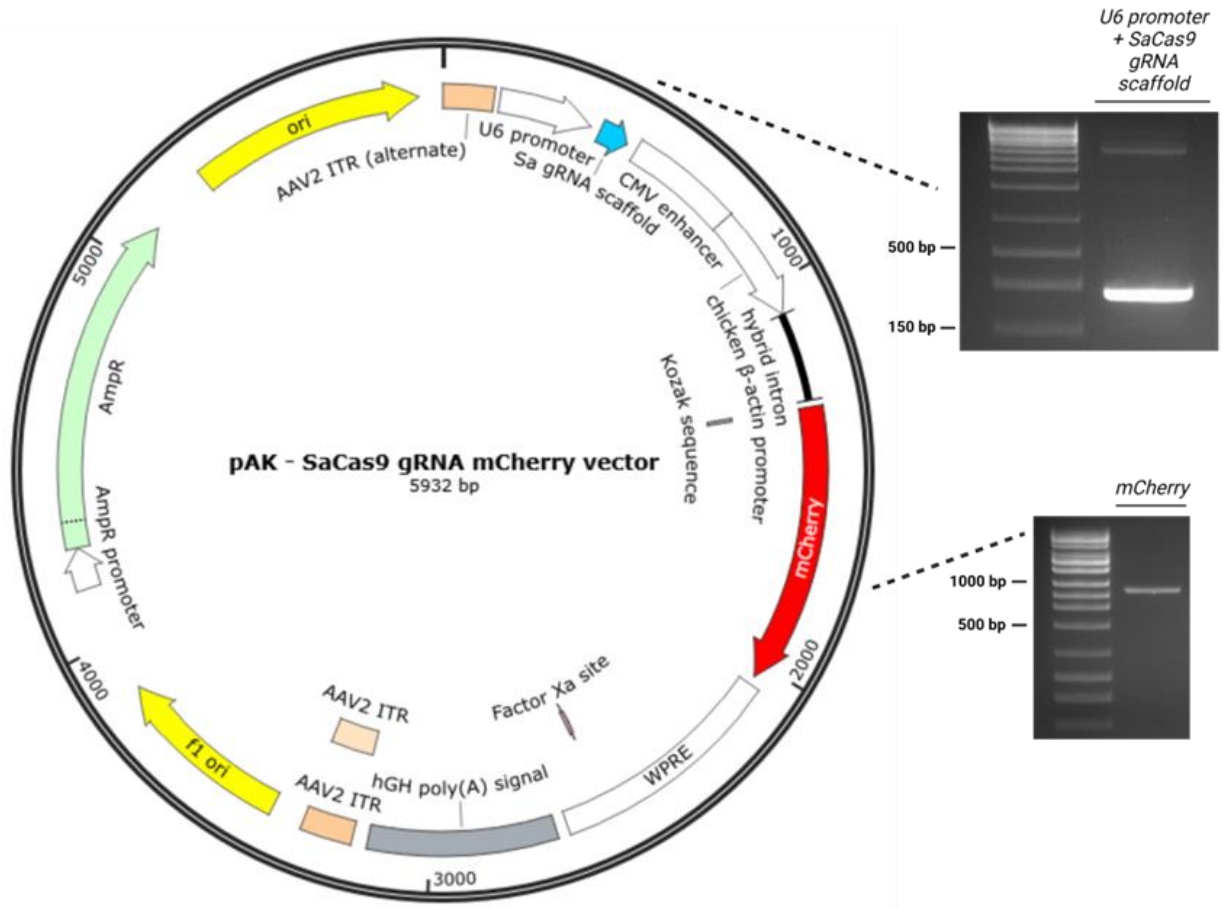


Figure 6.4 | Development of a dual vector strategy

Plasmid map of vector harboring the U6 promoter expressing a guide RNA scaffold, with an mcherry florescent marker driven by a CMV promoter. The construct was designed for facile interchange of different guide RNA scaffolds to rapidly evaluate different editors in the HEK-ABE cell line. Representative electrophoresis of PCR products following SpeI and HindIII digests (top right) and PCR amplification of the mCherry reporter (bottom right) are shown. Both show formation of appropriately sized linear fragments prior to transformation. Plasmid identity was confirmed by Sanger sequencing.

6.4.2.2 Pilot adenine base editing study

The first-generation ABE (ABE1.2) was generated by fusing the evolved TadA variant (TadA*) to the N-terminus of nCas9 through XTEN (a 16 amino acid linked used

in BE3), with the C terminal of nCas9 fused with a nuclear localization signal (TadA*-XTEN-nCas9-NLS). In its native context, TadA acts as a homodimer, with one monomer catalyzing deamination and the other monomer enabling tRNA substrate binding. To optimize ABEs, Gaudelli *et al.* engineered a single-chain heterodimer comprised of a wild-type non-catalytic TadA monomer and evolved ecTadA monomer (TadA-TadA*). To improve editing efficiency, further optimization of ABE was performed.[122] Extensive PACE and protein engineering resulted in seventh generation ABEs (ABE7.10), which converted target A-T to G-C efficiently (~50%) in human cells. The ABE7.10 editor was initially utilized to characterize and optimize the HEK-ABE cell line in the context of adenine base editing and evaluate the dual vector system.

In the pilot experiment, the HEK-ABE cells were transfected with and without ABE7.10, together with a targeting or non-targeting (scrambled) gRNA. Guide RNAs were cloned as detailed in the general methods and the gRNA sequences are detailed in the Appendix. This test demonstrated signals of GFP fluorescence within 24 hours of transfection, with expression in the RFP channel confirming efficient transfection of the gRNA vector (Figure 6.5). While encouraging, the efficiency of editing was very low, with few cells visibly florescent per imaging frame.

Importantly, no GFP fluorescence was observed in any samples transfected with a targeting guide alone (without the ABE7.10 vector), nor with the co-transfection of the ABE7.10 and a non-targeting guide. No toxicity was observed across any of the construct combinations. Together, this pilot study supports the findings from the initial cell line validation and confirms that the restoration of GFP fluorescence in the samples co-transfected with the targeting ABE constructs is due to targeted correction of the TAG termination codon, rather than unspecific fluorescence unrelated to the editing mechanism.

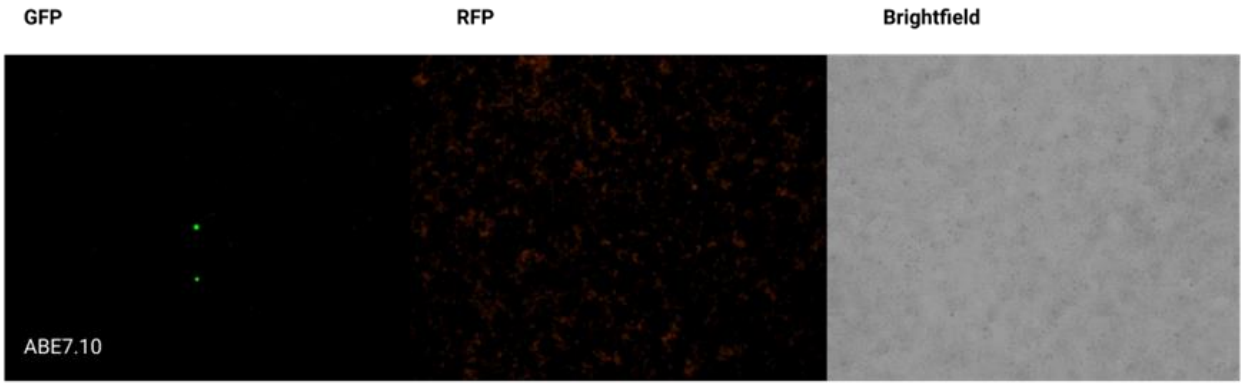


Figure 6.5 | Initial evaluation of adenine base editing in HEK-ABE reporter cell-line

The HEK-ABE reporter cell line was transfected with and without ABE7.10, together with a targeting or non-targeting gRNA. All gRNA sequences are detailed in the Appendix. GFP fluorescence was evident within 24 hours of transfection (left), with expression in the RFP channel (middle) confirming successful transfection using the gRNA-expressing vector. No toxicity was observed across any of the construct combinations, as visible in the brightfield view (right).

6.4.2.3 Guide RNA and dose optimizations

Having established that ABE7.10 could generate targeted edits in the HEK-ABE reporter line, next, various optimizations were explored.

Since broad differences in editing activity were observed using the same guide in the Cas9 orthologue screen, different ABE7.10 and gRNA vector doses and ratios were assessed. The ratio of base editing and gRNA was varied from 1:5 to 5:1 across the similar doses, and vector doses from 250 ng, 1 μg, 2 μg, and 4 μg in 24-well plates. Similar rates of editing were observed with 1 μg, 2 μg, and 4 μg of the ABE7.10 vector, while the level of GFP fluorescence increased substantially as the dose of the gRNA vector was increased. However, at the 4-μg dose level, substantial toxicity was observed, including cell viability decreasing to 50% and clear cell death visible by microscopy. Finally, cells were imaged at multiple timepoints. Maximum fluorescence was observed at 72-hours

post transfection, with signals for cell death for cells maintained >96 hours. Investigation of double-transfection experiments, in which the cells were split and re-transfected, yielded higher levels of fluorescence, with no toxicity or non-specific fluorescence detected (data not shown). Thus, 1 μg of the ABE7.10 vector and 2 μg of the gRNA vector were selected for all subsequent DNA base editing experiments, and HEK-ABE cells re-transfected and imaged at 72-hours following the second transfection (Figure 6.6B).

6.4.2.4 Screening of adenine base editors

Having validated the reporter cell line, identified active gRNAs, and optimized transfection doses and ABE vector to gRNA ratios in HEK-ABE cells, different base editors were selected for screening. Four different adenine base editor configurations were selected, all utilizing the same nSaCas9 variant: the ABE7.10 reporter construct,[122] ABE3,[101] ABE8e,[337] and microABE I744.[338]

The ABE3 construct is a first-generation adenine base editor, with limited activity anticipated in comparison to the more evolved base editors. ABE8e, the state-of-the-art adenine base editor, was selected for multiple reasons. Importantly, unlike CBEs, which have proven to be broadly customizable with many Cas orthologs, ABEs have shown limited compatibility with Cas9. This incompatibility is due to the low DNA-bound residence time of non-SpCas9, coupled with the slow enzymatic rate of deoxyadenosine deaminase. To address this problem, Richter *et al.* utilized phage-assisted continuous and non-continuous evolution (PACE and PANCE) methods to enhance the catalytic rate of the deoxyadenosine deaminase enzyme by 590-fold compared to that of ABE7.10.[337] This next generation of ABEs, ABE8e, shows greatly enhanced activity and compatibility with diverse Cas9 homologs. While the targeting scope of ABE8e also increased off-target RNA and DNA editing, off-target editing was ameliorated by introduction of an additional point-mutation (V106W). Finally, Tran *et al.* used structure-guided design to

engineer an SaCas9 ABE variant (microABE I744),[338] optimized for robust on-target activity and RNA-fidelity based upon its stereochemistry, and representing one of the smallest AAV-deliverable Cas9-ABEs available.

Adenine base editor	Detail
SaCas9-ABE8e	ecTadA(8e)-nSaCas9
SaCas9-microABE	Expression of nSaCas9 intradomain insertion of single evolved TadA monomer (V82G) at the specified position
SaCas9-ABE7.10	TadA-TadA*7.10-nCas9-NLS-HA
SaCas9-ABE3	TadA*-XTEN-nCas9-NLS

Table 6.1 | Screening of adenine base editors

Detail on base editor architecture and source for all evaluated ABEs. All plasmid sources and key sequences are detailed in the Appendix.

Applying the same targeting guide RNA used in the pilot study and optimized vector doses and ratios, GFP fluorescence was detected with all constructs except for SaABE3, for which no fluorescence was observed across any conditions (Figure 6.6). Substantially higher levels of GFP were detected in the ABE7.10 reporter construct following the transfection optimizations, as compared to the pilot study. There was no GFP fluorescence was observed in any samples transfected with a targeting guide alone or with the co-transfection of the ABE vector and a non-targeting guide. There was no toxicity across any of the construct combinations. SaABE8e demonstrated the highest rates of fluorescence restoration in all tested conditions, superior to the levels detected with the ABE7.10 construct. Interestingly, the microABE I744, one of the smallest Cas9-ABEs generated to date, was considerably less efficient than the ABE7.10 and ABE8e base editors.

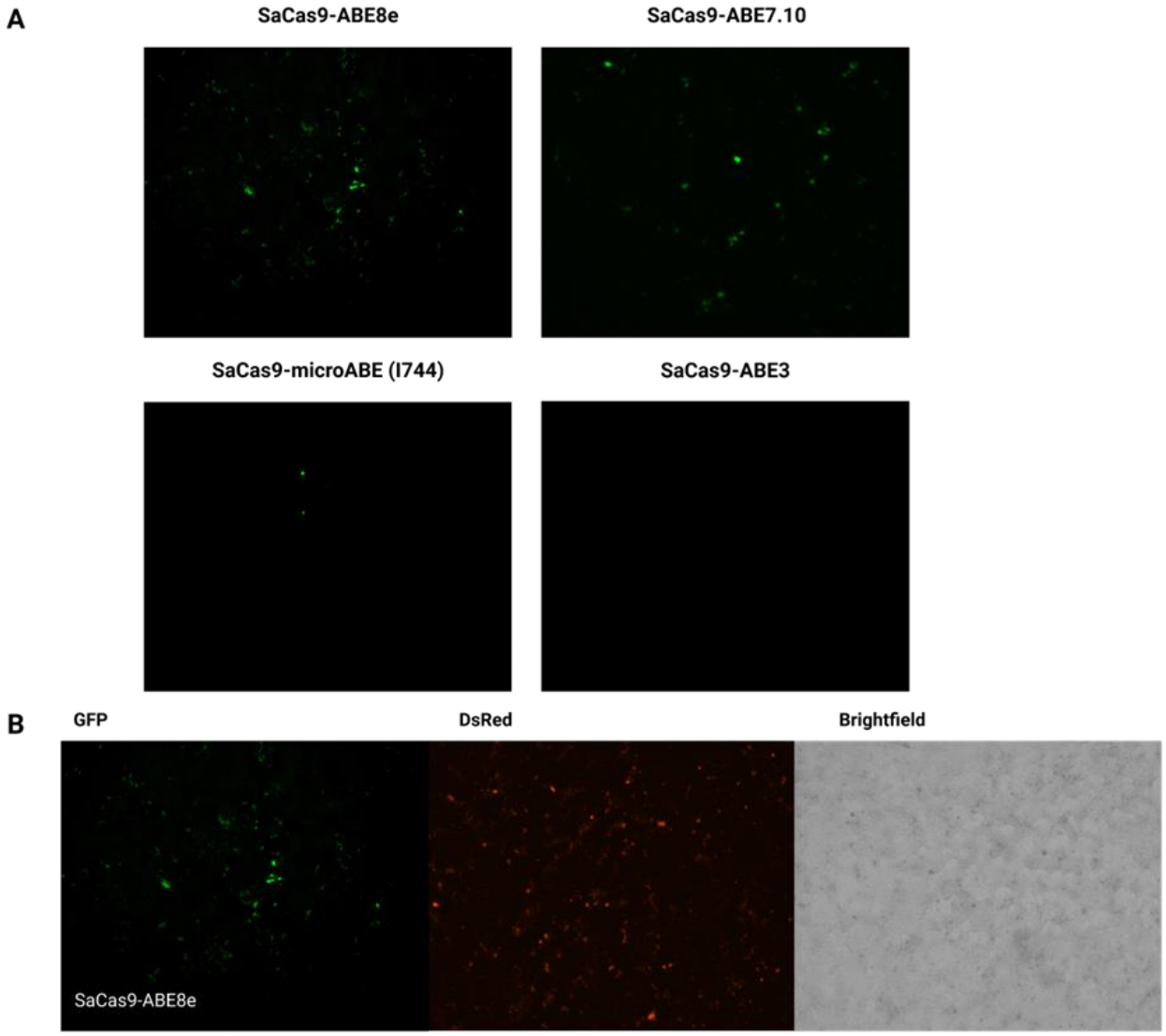


Figure 6.6 | Screening of base editor architectures

A. Representative light-microscope images (10X magnification) of HEK-ABE cells after co-transfection with an ABE vector and gRNA-expressing vector. Four different adenine base editor configurations were evaluated: SaCas9-ABE8e, SaCas9-ABE7.10, SaCas9-microABE I744, SaCas9-ABE3, with an identical targeting gRNA utilized across all ABEs. SaCas9-ABE8e demonstrated the highest rates of fluorescence restoration, while SaCas9-microABE I744 showed limited signal and no detectable fluorescence was observed with SaCas9-ABE3. **B.** Full imaging panel following co-transfection with SaCas9-ABE8e and the gRNA-mCherry vector. Robust GFP fluorescence was

observed at 72-hours following the second transfection (left), with expression in the RFP channel (middle) confirming successful transfection using the gRNA-expressing vector. As evident in the brightfield view (right), there was no evident toxicity or changes in cell viability.

6.4.2.5 Quantifying adenine base editing by Sanger sequencing

To quantify the DNA base editing rates across the different ABE configurations evaluated, and to unequivocally confirm that the detected GFP fluorescence restoration is a result of targeted DNA editing of the TAG nonsense mutation, genomic regions encompassing the target sites were amplified from the genomic DNA and the PCR products were analyzed by Sanger sequencing. DNA editing rates were quantified using EditR. Samples co-transfected with the ABE8e construct showed on-target editing rates of 16.2% ± 4.2%. The ABE7.10 construct edited at a lower on-target rate of 14.6% ± 2.8%. Finally, <2% on-target editing was detected with microABE, and <0.5% on-target editing was detected with ABE3 (Figure 6.7). No on-target editing was detected in samples transfected with non-targeting guides, or in samples transfected with a targeting guide but no editing construct. Editing rates of each replicate quantified by Sanger sequencing were closely correlated with the fluorescence observed from the HEK-ABE reporter cell line.

6.4.2.6 Evaluating SaCas9-ABEs with altered PAM recognition

Only about one-quarter of pathogenic transition mutations encompass an appropriately located NGG PAM site that facilitates SpCas9-mediated base-editing. Unlike CBEs, which have proven to be broadly customizable with many Cas orthologs, ABEs have shown limited compatibility with Cas9 of any origin other than SpCas9. Although some homologs such have been adapted, including SaCas9, the PAM targeting range is still limited. Indeed, in the pilot base editing study, while similar activity was

observed between SpCas9-ABE7.10 and SaCas9-ABE7.10, there was a significant reduction in the expression with other Cas9 orthologues evaluated (data not shown).

Rather than using a different Cas9 orthologue, one potential strategy to relieve this restriction is to relax the PAM recognition specificity of Cas9. Kleinstiver *et al.* used molecular evolution to modify the NNGRRT PAM of SaCas9.[339] One variant that was identified, referred to as KKH SaCas9, showed robust genome editing activities at endogenous human target sites with NNNRRT PAMs, thereby increasing SaCas9 targeting range by two- to fourfold.[339,340] Moreover, using GUIDE-seq, the authors showed that wild-type and KKH SaCas9 induce comparable numbers of off-target effects in human cells. Thus, based on the enhanced activity of ABE8e and compatibility with diverse Cas9 homologs, SaCas9-ABE8e was compared to the KKH-SaCas9 variant.

Since the editing rates quantified by Sanger sequencing correlated closely with GFP fluorescence restoration, and to have a more sensitive method to compare SaCas9 to the KKH variant, samples were by Sanger sequencing. Surprisingly, DNA editing rates for the SaCas9-ABE8e construct were consistent with previous experiments, with editing 15.8% ± 3.9%, slightly higher editing rates were detected with the SaCas9-KKH-ABE8e variant, totaling at 17.3% ± 4.7% (Figure 6.7). While not statistically significant ($p=0.067$), it is notable that similar, if not slightly higher, editing rates were observed with the KKH SaCas9 ABE8e construct.

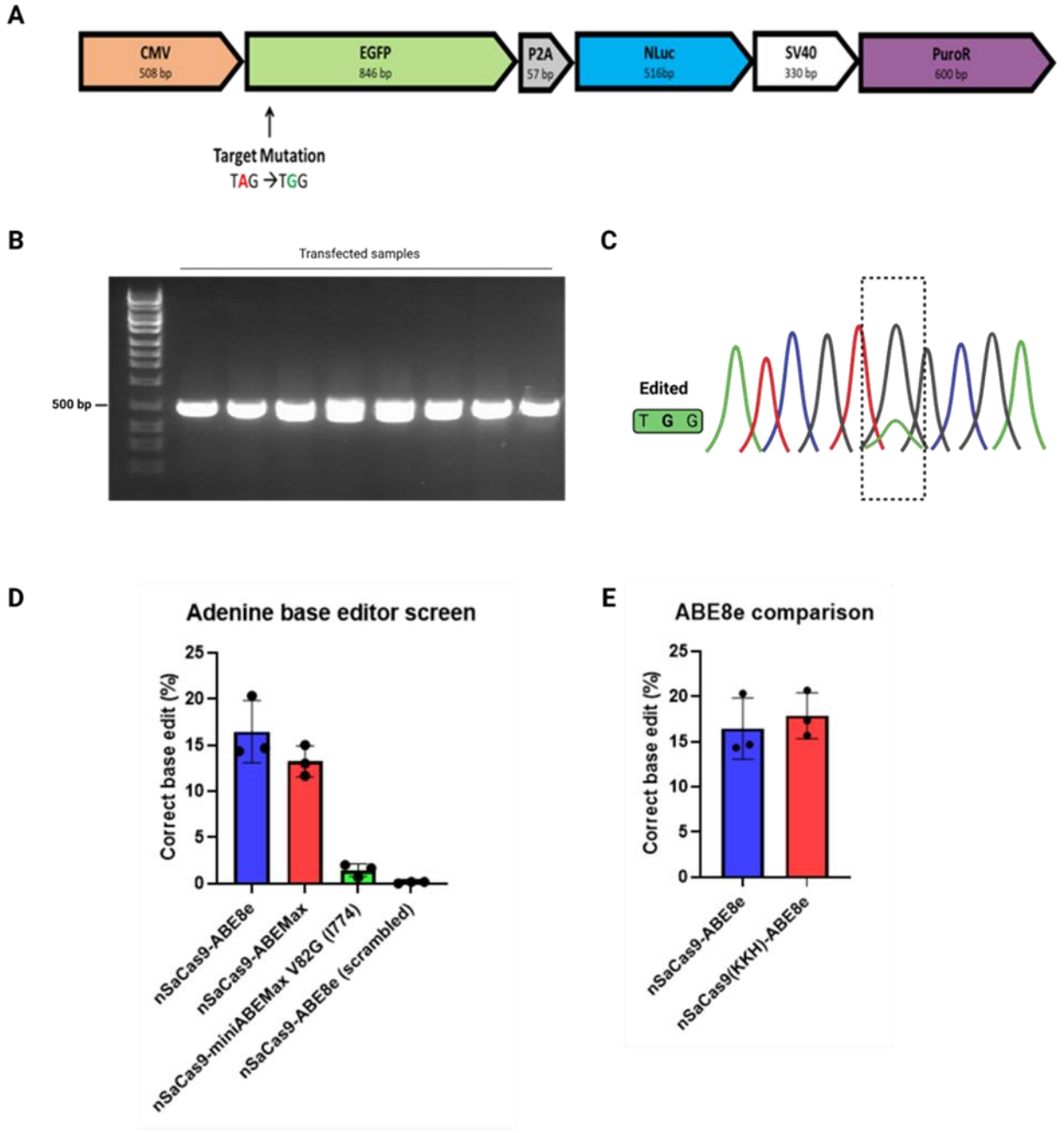


Figure 6.7 | Quantifying adenine base editing by Sanger sequencing and evaluating ABEs with altered PAM recognition

A. Schematic showing the target mutation for correction of the nonsense mutation. Base editing of TAG reverts the nonsense mutation to TGG, thus switching on green fluorescence in successfully edited cells. **B.** Electrophoresis of PCR amplification of target sites. Genomic regions

encompassing the target sites were amplified from the genomic DNA and the PCR products were analyzed by Sanger sequencing. **C.** Chromatogram showing targeted editing of the TAG to TGG. **D.** Comparison of on-target DNA base editing across different ABE configurations, as measured by Sanger sequencing. Samples co-transfected with the ABE8e construct showed on-target editing rates of 16.2% ± 4.2%. The ABE7.10 construct edited at a lower on-target rate of 14.6% ± 2.8%. <2% on-target editing was detected with microABE, and <0.5% on-target editing was detected with ABE3, respectively. No on-target editing was detected in samples transfected with non-targeting guides, or in samples transfected with a targeting guide but no editing construct. **E.** Comparison of wild-type SaCas9 variant and modified KKH SaCas9, both fused to ABE8e. DNA editing rates for the SaCas9-ABE8e construct were consistent with previous experiments, with editing 15.8% ± 3.9%. Slightly higher, though not statistically significant (p=0.067) editing rates were detected with the SaCas9-KKH-ABE8e variant, totaling at 17.3% ± 4.7%.

6.4.3 Development of an enhanced prime editing system

Despite the profound capabilities of base editing approaches to edit the DNA, a major limitation of the current base-editing technologies has been the ability to generate precise base-edits beyond the four transition mutations. The "search-and-replace" PE approach, takes gene editing a step further, not only possessing the ability to swap single DNA bases, but also correcting genomic deletions, insertions, and combinations of insertions, deletions, and/or point mutations.

Despite its broad gene editing potential, prime editing is challenged by the large PE gene (~6.4 kb), which makes delivery of the prime editing system (PE, pegRNA, and ngRNA) challenging. For instance, it is impossible to package the prime editing system into a single adeno-associated virus (AAV) vector, which is limited to ~5 kb with the inclusion of the inverted terminal repeats (ITRs). Although recent studies have reported that the PE gene can be divided in two and delivered by dual AAV vectors relying on trans-splicing intein, the large size of PE severely restricts the position of the split site, which leads to suboptimal prime editing efficiency and leaves limited space for additional functional elements. In this study, I validate the novel PE toolkit and explore optimizations to enable *in vivo* applications for the treatment of inherited retinal diseases.

6.4.3.1 Generation of minimal prime editors

To develop a compact PE packable within the constraints of AAV, I hypothesized that it would be possible to delete non-essential elements within the reverse transcriptase. The polymerase domain uses single strand RNA as template to synthesize single strand DNA, and the RNase H domain selectively degrades the RNA template of RNA/DNA hybrids. Considering that the RNase H domain is only for RNA template degradation, I thought that this domain might be dispensable for prime editing applications. I selected the murine leukemia virus reverse transcriptase (MMLV-RT) for further analysis, as in

addition to initial validation by Anzalone and colleagues, the RT is modular and may enable targeted deletions of separate domains.

M-MLV RT is a monomeric polypeptide containing fingers/palm, thumb, connection, and RNase H domains (residues 1–275, 276–361, 362–496, and 497–671, respectively), and has two active sites (DNA polymerase and RNase H) that reside in separate, distinct structural domains (Figure 6.8).[341-343] Mutating the RNase H domain, which is responsible for degrading RNA in the RNA/DNA hybrid during DNA synthesis, improves efficiency of cDNA synthesis from the protected RNA. To explore the possibility of generating shorter RT without altering the protein folding, I analyzed secondary and tertiary structures of MMLV-RT. Notably, protein modeling suggested that the Ribonuclease H (RNase H) domain of the RT is separate from the DNA polymerase domain, necessary for extension of the pegRNA in the prime editing system (Figure 6.8). Moreover, Kotewicz and colleagues previously demonstrated purification of reverse transcriptase that lacks RNase H but retains DNA Polymerase activity,[344] suggesting that the two domains reside within separate structural domains. Finally, using GlobPlot 2.3 and PSIPRED software, I analyzed key regions of globularity and disorder within the RT sequence to inform the truncation strategy (Figure 6.8).

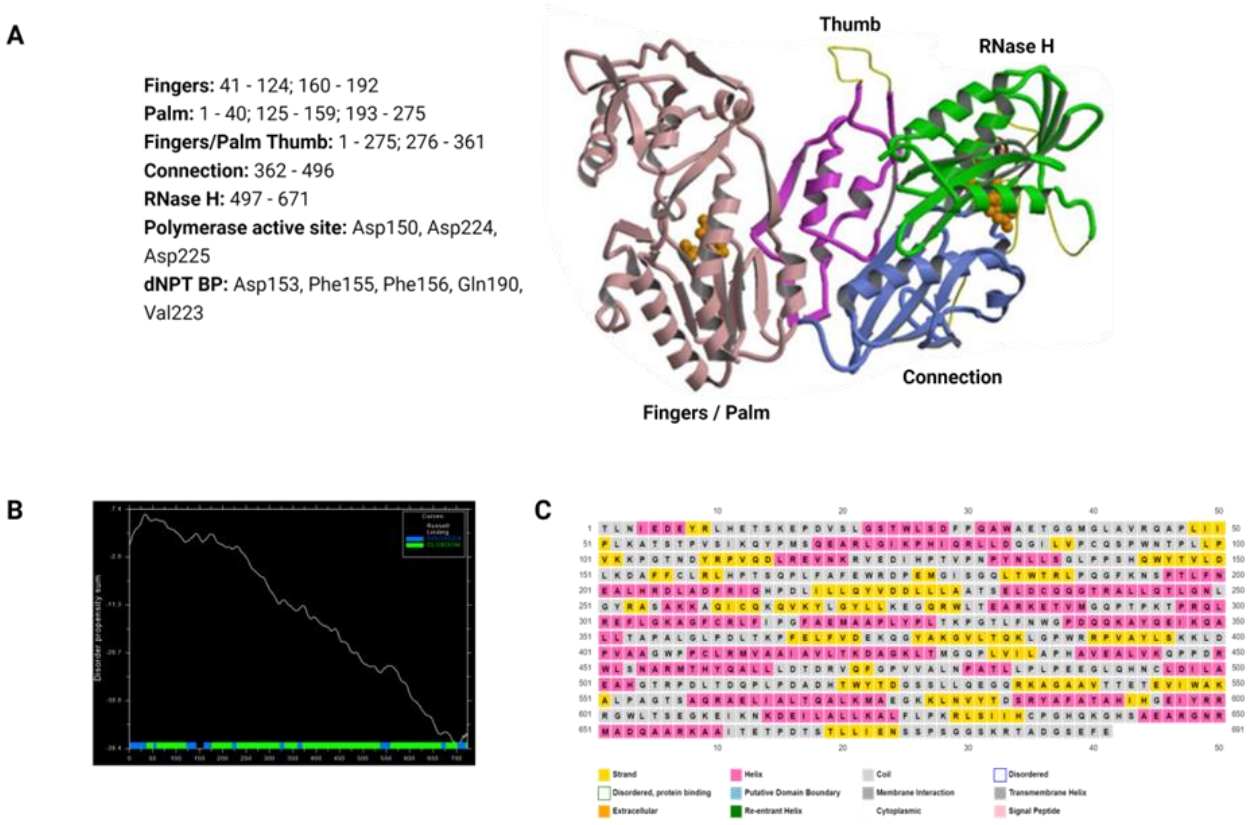


Figure 6.8 | Protein modeling of the M-MLV Reverse Transcriptase

A. Ribbon rendering of the crystal structure of M-MLV RT with fingers / palm domain in brown, thumb in yellow, connection in blue, and the RNase H in green. RT consists of an RNA-dependent polymerase domain and an RNase H domain. The polymerase domain uses single-strand RNA as template to synthesize single-strand DNA, and the RNase H domain degrades the RNA template of RNA/DNA hybrids. M-MLV RT is a monomeric polypeptide containing fingers/palm, thumb, connection, and RNase H domains (residues 1–275, 276–361, 362–496, and 497–671, respectively), and has two active sites (DNA polymerase and RNase H) that reside in separate, distinct structural domains **B.** Output from GlobPlot 2.3, highlighting regions of globularity and disorder within the RT sequence for truncation. **C.** Secondary structure of M-MLV RT output from PSIPRED showing key structural elements, including strand and helix residues and disordered sites.

Informed by the protein modeling, 4 different deletions within the RT were constructed, with progressive truncation of the RNase H and connection domains, ranging from 150aa up to 400aa (Figure 6.8). Additionally, a negative control was designed, with a deletion removing the first 220aa of the RT which contain the DNA Polymerase domain.

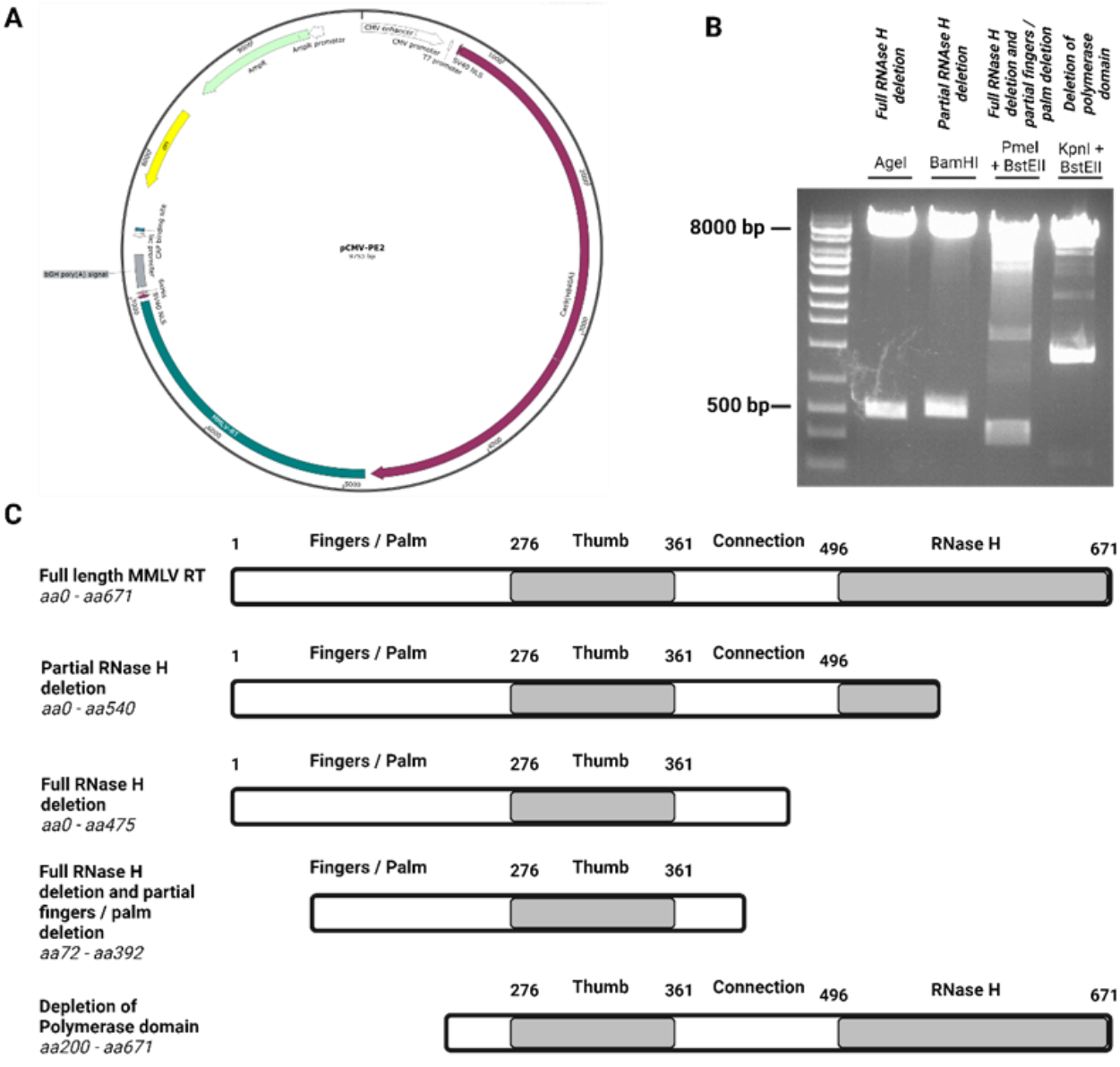


Figure 6.9 | Generation of a minimal prime editor by truncation of M-MLV reverse transcriptase

A. Plasmid map of wild-type pCMV-PE2 construct (a gift from David Liu). **B.** Electrophoresis of digested M-MLV RT constructs. AgeI digest fully removed the RNase H domain. BamHI digest was applied to generate the partial RNase H deletion. PmeI and BstEII digests were applied to fully remove the RNase H domain and partially truncate the fingers / palms region. Finally, a KpnI, BstEII double digest depleted the RNA polymerase domain. **C.** Schematic representation RT variants with C-terminal truncations. The RT is comprised of a polymerase and an RNase H domain. Wild-type M-MLV RT as published in pCMV-PE2 was used as a control (schematic 1). Serial truncations at both ends were tested with the aim of generating a minimal prime editor (schematics 2-4). Depletion of the polymerase domain (aa0-200) was used as a negative control (deletion 4).

6.4.3.2 NgRNA and pegRNA screening

Having constructed the compact PE variants, I next sought to compare their editing efficiencies. Screening gRNAs targeting the disease-relevant locus requires extensive *in silico* and *in vitro* screening, as a number of factors can widely affect editing outcomes. Prime editors are comprised of two components: 1) a catalytically impaired Cas9 nickase fused to a reverse transcriptase (PE2), and 2) a multifunctional prime editing guide RNA (pegRNA) that specifies the target site and further acts as a template for reverse transcription (RT). PegRNAs are similar to standard single-guide RNAs (sgRNAs), but additionally have a customizable extension on the 3′ end which encodes the RT template for the desired edit and the primer binding site (PBS) that anneals to the target genomic site to prime the RT reaction. These additional components considerably increase the complexity of pegRNA design compared to standard sgRNAs. PegFinder[345] was utilized for rapid *in silico* design of candidate pegRNAs.

ngRNA /pegRNA description	Sequence
sgRNA-R	caccgAGGTCTGTATTGTGGACTACgttttaga
sgRNA-L	tagctctaaaacGTAGTCCACAATACAGACCTc
Scaff-R	GCTAGAAATAGCAAGTTAAAATAAGGCTAGTC CGTTATCAACTTGAAAAAGTGGCACCGAGTCG
Scaff-L	GCACCGACTCGGTGCCACTTTTTCAAGTTGATA ACGGACTAGCCTTATTTTAACTTGCTATTTC
Extens-R	gtgcTGGACAGCCCGTGGTCCACAATACAGAC
Extens-L	aaaaGTCTGTATTGTGGACCACGGGCTGTCCA
PE3_nicksgRNA-R	caccgCTTTTACACTGTATGAGTAC
PE3_nicksgRNA-L	aaacGTACTCATACAGTGTAAAAGc
PE3b_nicksgRNA-R	caccgAGGGTGCAGTGGACAGCCCG
PE3b_nicksgRNA-L	aaacCGGGCTGTCCACTGCACCCTc
sgRNAantisenseCut113	AGGTCTGTATTGTGGACTAC
sgRNAantisenseCut114	CAGGTCTGTATTGTGGACTA
sgRNAantisenseCut121	GGGCTTCCAGGTCTGTATTG
SecondnicksgRNACut109	AGGGTGCAGTGGACAGCCCG
SecondnicksgRNACut67	CTTTTACACTGTATGAGTAC
SecondnicksgRNACut68	TTTTACACTGTATGAGTACC

Table 6.2 | Prime editing ngRNA / pegRNA cloning

Spacer and 3' extension sequences of pegRNAs and spacer sequences of ngRNAs.

6.4.3.3 Evaluation of minimal prime editors using a dual luciferase assay

To evaluate the editing efficiency of compact prime editor variants in cells, a dual luciferase assay expressing the *mUsh2a*-W3947X (a gift from Lewis Fry) was used (Figure 6.10). The *mUsh2a*-W3947X dual luciferase assay is an excellent *in vitro* test to screen minimalized PE constructs. The homologous human mutation, c.11864G>A (W3955X), results in a premature termination codon encoded in exon 61 and is the third most

common *USH2A* pathogenic mutation. Thus, in addition to allowing for comparison of different editors, the screening was conducted against a therapeutically relevant target.

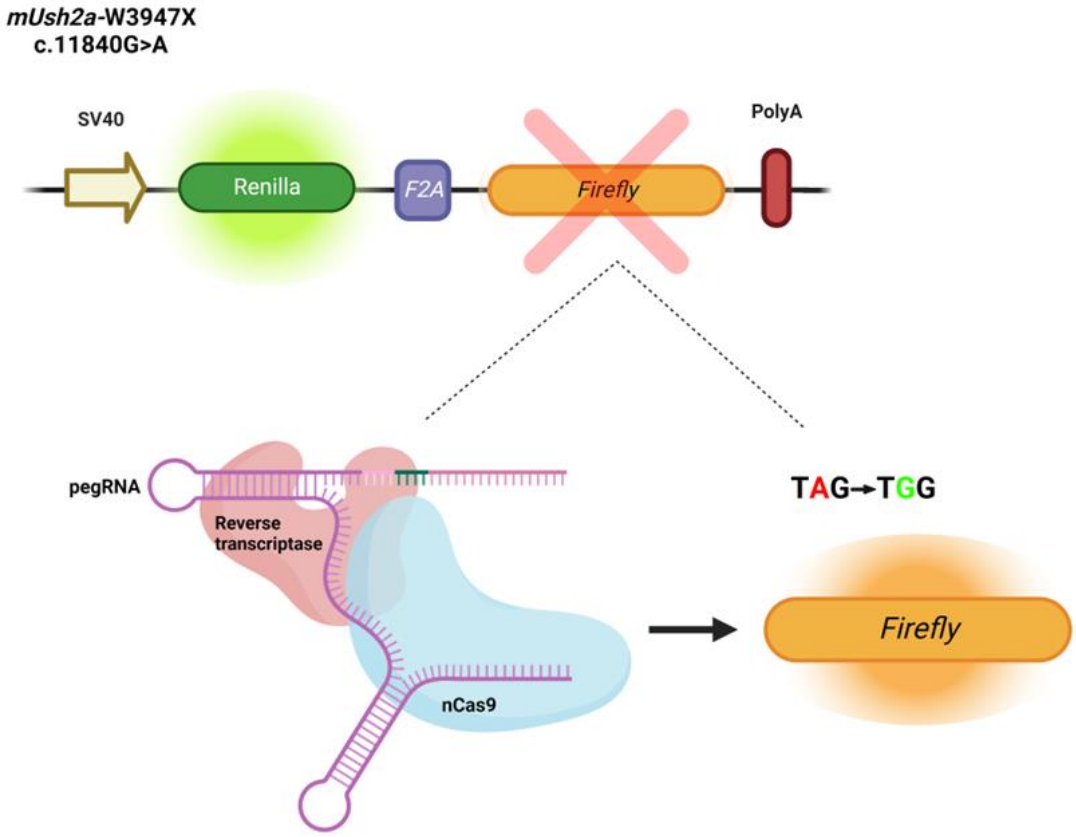


Table 6.3 | *mUsh2a*-W3947X dual luciferase reporter assay for prime editing reporting

Schematic describing the experimental dual luciferase construct (a gift from Lewis Fry). Renilla is constitutively expressed as a normalization control. When a stop codon precedes the firefly, firefly is not expressed. Successful prime editing of TAG to TGG repairs the stop codon and turns of firefly expression, enabling evaluation of editing efficiencies across constructs.

Guided by the *in silico* designs from pegFinder, an initial screen was performed to test guides against the *mUsh2a*-W3947X target. 12 pegRNAs were screened in total, with 4 pegRNAs generating detectable on-target editing (Figure 6.11). Interestingly, top hits from the pegFinder screen correlated with the best performing ngRNA, pegRNA configurations. PegRNA-1 showed editing rates of 9.9% ± 4.8%, pegRNA-2 showed

editing rates of 6.4% ± 1.9%, pegRNA-3 showed editing rates of 12.6% ± 3.7%, and pegRNA-4 showed editing rates of 2.7% ± 0.7%. Based on the highest editing efficiency, pegRNA-3 was selected for all downstream experiments. All constructs were re-transfected and harvested at 72-hours after the second transfection, as described in the optimized protocol in Section 6.2.4.3. The ngRNA was kept consistent across all pegRNAs screened, as the limited targeting range of the SpCas9 NGG PAM site limited the optionality for gRNA design. All ngRNA and pegRNA sequences are detailed in table 6.2 and in the Appendix.

Next, having established a well performing ngRNA/pegRNA targeting the *mUsh2a*-W3947X dual luciferase assay, the on-target prime editing efficiency was compared across the truncated PE variants. Non-truncated PE (positive control) and polymerase depleted PE (negative control) were included for comparison. Samples co-transfected with full length M-MLV RT indicated on-target editing rates of 13.3% ± 3.2%. The first construct, harboring a partial RNase H truncation, showed enhanced editing rates compared to the full-length prime editor, with editing rates of 20.8% ± 4.2% ($p<0.01$). However, the full RNase H deletion showed considerably lower editing efficiencies of 3.6% ± 1.2%. Finally, the largest truncation variant, which lacks not only the RNase H domain but also parts of the connection domain, as well as the polymerase depleted PE negative control, showed no detectable rates of on-target editing (Figure 6.11).

Collectively, these results demonstrate efficient prime editing against the *mUsh2a*-W3947X target, guided by *in silico* prediction and screening. Moreover, I show that the RT RNase H domain is dispensable for prime editing, and partial truncations of the domain yield enhanced rates of on target editing.

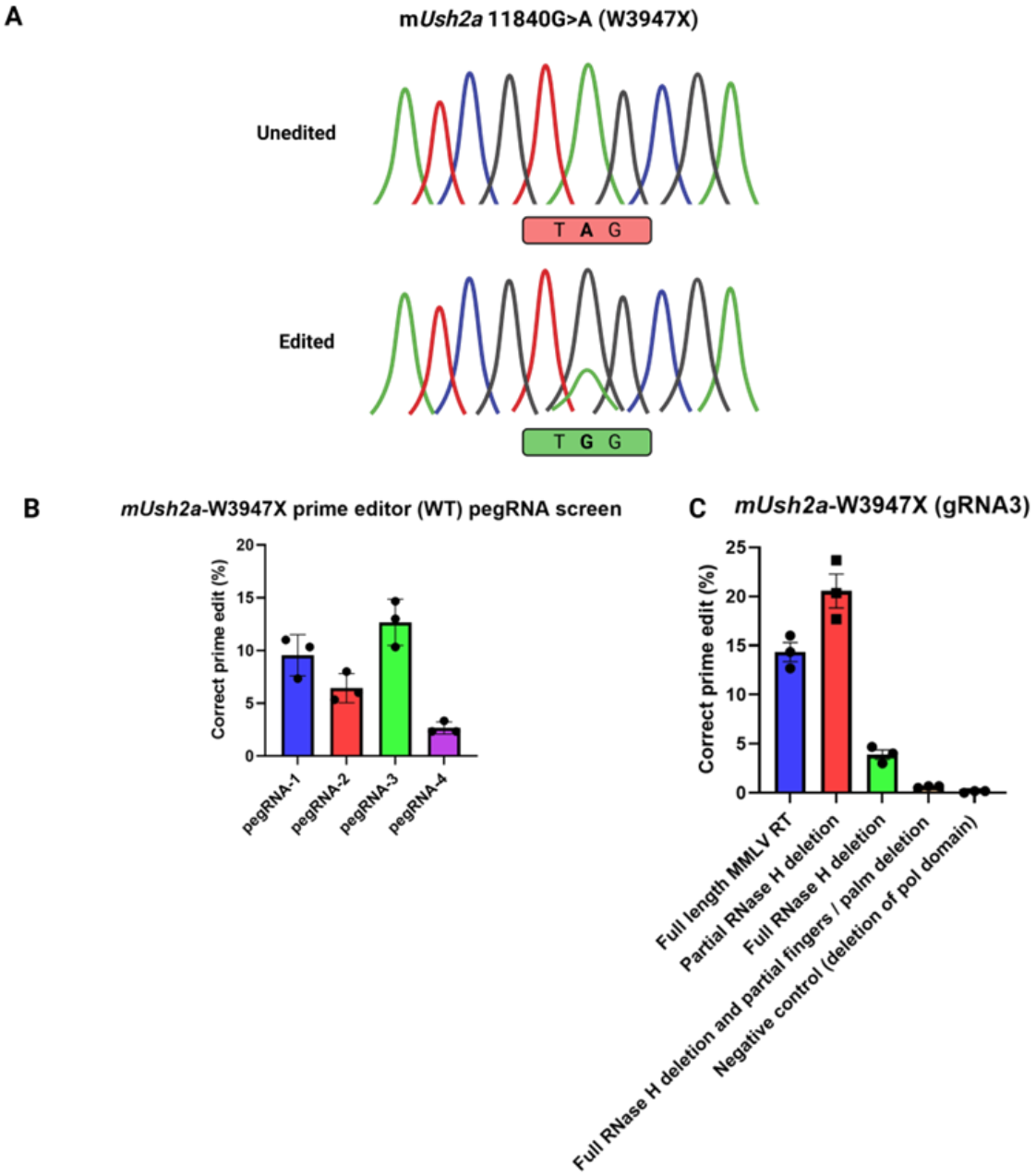


Figure 6.10 | The engineered minimal PE variant showed enhanced rates of prime editing *in vitro*

A. Chromatogram showing targeted editing of the c.11840G>A mutation. Prime editing of TAG to TGG restores the wild-type tryptophan codon. **B.** Screening of pegRNAs designed *in silico* with pegFinder software. 16 pegRNAs were screened in total (not shown), with 4 pegRNAs generating

detectable on-target editing. PegRNA-1 showed editing rates of 9.9% ± 4.8%, pegRNA-2 showed editing rates of 6.4% ± 1.9%, pegRNA-3 showed editing rates of 12.6% ± 3.7%, and pegRNA-4 showed editing rates of 2.7% ± 0.7%. Based on the highest editing efficiency, pegRNA-3 was selected for all downstream experiments. All constructs were re-transfected and harvested at 72-hours after the second transfection, as described in the optimized protocol in Section 6.2.4.3. The ngRNA was kept consistent across all pegRNAs screened; ngRNA and pegRNA sequences are detailed in table 6.2 and in the Appendix. **C.** Comparison of on-target editing efficiency induced by truncated PE variants, as measured by Sanger sequencing. Non-truncated PE (positive control) and polymerase depleted PE (negative control) were included for comparison. Samples co-transfected with full length M-MLV RT indicated on-target editing rates of 13.3% ± 3.2%. The partial RNase H construct showed editing rates of 20.8% ± 4.2% ($p<0.01$). The full RNase H deletion yielded editing rates of 3.6% ± 1.2%, No on-target editing was detected from the largest truncation variant, not the polymerase depleted PE negative control. No on-target editing was detected in samples transfected with non-targeting guides, or in samples transfected with a targeting guide but no editing construct. The data are presented by mean value ± SEM with all data points from independent experiments shown.

6.5 Discussion

6.5.1 Development of reporter cell lines

Development of a DNA base editing approach was challenged by the lack of a reliable, reproducible *in vitro* screening methodology. Screening of ngRNAs and pegRNAs targeting the disease-relevant locus requires extensive *in silico* and *in vitro* screening, as a number of factors can widely affect editing outcomes, including varying PAM requirements, anticipated activity windows, sgRNA target sequence compositions, target sequence contexts, and locus-dependent differences in DNA-binding proteins and transcriptional state. To address these limitations and enable rapid screening of editor and gRNA configurations, I developed reporter HEK293-CBE and ABE cell lines. I broadly characterized the reporter lines using both multicolor fluorescence *in situ* hybridization (MFISH) and karyotyping analysis (conducted by the Wellcome Centre for Human Genetics). Low vector doses of lentiviral vector were used in stably transducing the HEK293 cells, and transgene localization confirmed single GFP copy number, critical for enabling a sensitive system for detection of on-target edits. Finally, the pilot experiment using the HEK-ABE cell lines validated that the effect was highly target specific, with no GFP fluorescence observed in any samples transfected with a targeting guide alone (without the base editing vector), nor with the co-transfection of the ABE and a non-targeting guide.

In the context of target specific screening, as I demonstrated with PE constructs, the dual luciferase assay (a gift from Lewis Fry) provided a robust assay for high-throughput evaluation of editor and guide combinations. This reporter assay system enables an effective means of performing two reporter assays, with activities of firefly and Renilla luciferases measured sequentially from a single sample. Moreover, in the context of inherited retinal diseases, including my pilot study targeting a mutation in

USH2A, many target transcripts are not expressed in commonly cultured cell lines, further supporting the utility of this approach.

The use of reporter assays is essential for rapidly screening, characterizing, and optimizing genome engineering tools, and there are a number of further developments that could be explored. Further optimizations include the generation of a knock-in line containing a target dual luciferase transgene, as the need for multiple plasmids for co-transfection complicated the screening methodology. Use of retinal organoids, as applied in the previous chapter, would allow for evaluation of editing reagents in their endogenous chromatinized context, a key consideration for evaluating pathogenic targets. Ideally, gRNAs would be identified in a system that endogenously expresses the full-length transcript of interest, such that the biological context could be recapitulated. Finally, the development of an *in vivo* reporter model harboring a secreted reporter protein would allow for dynamic changes in editing activities to be monitored in an *in vivo* setting.[346,347]

6.5.2 Screening of adenine base editors

Sanger sequencing of adenine base editing was closely correlated with the fluorescence observed from the HEK293-ABE reporter cell line. There were substantial differences in editing rates across the different adenine deaminase configurations. As anticipated, the first-generation ABE3 construct showed limited activity in comparison to the more evolved base editor systems, speaking to the value of phase-assisted evolution and rational design approaches for engineering enhanced ABEs. Additionally, the ABE8e construct, the latest available ABE, demonstrated the highest levels of adenine base editing, with on-target editing rates of up to 16.2% with the best-performing gRNAs. Intriguingly, the recently published microABE I744, one of the smallest Cas9-ABEs generated to date, was significantly less efficient than its ABE7.10 and ABE8e

counterparts, with editing rates peaking at 1.7%. This outcome is consistent with observations from Chapter 3, where a substantial decrease in editing was seen with the minimal CjCas9 orthologues. Future studies could explore additional changes to editors, such as different nucleic acid formats and chemical modifications to the base editor and guide RNAs to enhance editing rates.

While Cas engineering has increased the scope of ABEs, not all gene editing reagents are created equal, and additional efforts are necessary to broaden the range of targetable PAM sites and modulate editing windows. Intriguingly, in my pilot comparison of the native NNGRRT SaCas9 PAM and an evolved KKH-SaCas9 variant with expanded targeting range (NNNRRT), editing rates were largely similar, with slightly higher editing rates detected with SaCas9-KKH ABE8e (17.3% ± 4.7%). Further evolution of Cas9 proteins and discovery of new nucleases expanded PAM flexibility would broaden the scope of genome targeting while maintaining editing efficiency and specificity.

Finally, although initial investigation of targeted editing in EditR showed highly targeted editing, future experiments are needed to further characterize the safety of editing systems. The off-target effects of Cas9-BEs and PEs may differ, and a separate evaluation method is needed to better assess off target editing in a genome-wide manner. Future studies should investigate both NGS sequencing of the target region, as well as whole-genome sequencing to better characterize off-target and bystander editing of DNA base editing and prime editing systems. In a recent study, sequencing of human iPSCs stably expressing an evolved CBE demonstrated C-to-T and C-to-G mutations outside the in silico predicted off-target sites. Importantly, the majority of the off-target mutations were C:G to T:A transitions or C:G to G:C transversions enriched for the APOBEC mutagenesis signature.[348]

6.5.3 Engineering of minimal prime editors

In this study, I screened ngRNA/pegRNA sequences targeting the *mUsh2a*-W3947X dual luciferase assay and evaluated different deletions within the prime editor reverse transcriptase domain. Truncations within the modular M-MLV RT were designed using protein modeling software, allowing for visualization of secondary and tertiary structure, including key regions of globularity and disorder within the RT sequence amenable to truncation.

The best performing engineered prime editing variant demonstrated up editing rates up to 20% following *in silico* and *in vitro* ngRNA/pegRNA screening and optimizations to the transfection conditions, vector doses, and guide: vector ratios. The high, reproducible rates of on-target prime editing observed speak to the extensive screening and vector / methods optimizations required to enable meaningful editing rates. In preliminary experiments, <2% of prime editing was achieved across identical ngRNA/pegRNA combinations (data not shown). Editing efficiencies in the range of 10% - 20% may be clinically meaningful for treatment of IRDs, as only small levels of protein expression may be required to improve or slow down retinal degeneration.

Shortening of the prime editing through modification of the RT helps alleviate the packaging limitations that severely restrict the *in vivo* utility of prime editors. Intriguingly, the partial RNase H truncation showed enhanced editing rates compared to the full-length prime editor. These results support that the RNase H domain is not only dispensable to PE, but, in fact, there may be a negative effect from an active RNase H domain. While further studies are required to characterize the mechanism by which the RNase H depleted RT outperforms the full-length construct, one could speculate that this domain might degrade the pegRNA region as it anneals to the reverse-transcriptase primer binding site of the respective DNA target.

Finally, a truncated PE variant may further improve the safety of prime editing systems. Indeed, a potential risk of expressing a reverse transcriptase *in vivo* is the prospect of off-target mutations by extension of the pegRNA scaffold beyond its primer sequence. Furthermore, others have shown that the RNase H domain interacts with termination factors such as peptidyl release factor 1 and 3 (eRF1 and eRF3),[349-351] essential for inducing termination of protein translation. While overexpression of PE in cells has shown minimal perturbations of the transcriptome to date, the direct effect of PE on protein translation has yet to be investigated, and it is possible that PE-mediated RNase H overexpression could promote stop codon readthrough.

6.5.4 Therapeutic possibilities with base and prime editing systems

DNA base editing and prime editing has remarkable potential as a therapeutic tool to correct disease-causing mutations in the human genome. The ability to target nucleotides on either the plus or complementary minus DNA strand opens up the therapeutic applications of base-editors considerably. Over 25% of human pathogenic SNPs can be corrected by targeting the four transition mutations, and in principle prime-editing could correct up to 89% of the 75,122 pathogenic human genetic variants in ClinVar.[107,128] CRISPR-mediated HDR are confined to editing within dividing-cells, since these pathways are restricted to the S and G2 phases of the cell cycle. Conversely, base editing employs cellular mismatch repair machinery and can be applied to reverse these defects in both dividing and terminally differentiated cell types.[143] Gene therapy is a major area where DNA base editing and prime editing toolkits can be applied because they have already been adapted to characterize, model, and correct the underlying causes of human genetic conditions. In the first generation of base-editors, Komor *et al.* converted *APOE4*, the most common genetic risk-factor in Alzheimer's disease, into the lower-risk *APOE3r* variant in immortalized mouse astrocytes.[107] Additional studies have followed this initial example and demonstrated correction of pathogenic mutations in

animal models,[131,136,352-354] human cell lines,[96,107,132,355] and even in human tripronuclear zygotes.[356] Indeed, there are multiple target types best suited to the unique properties of DNA base editing and prime editing technologies.

6.5.4.1 Editing large genes

DNA base editing and prime editing may prove to be particularly well adapted for correction of large genes (>4 kb). For many diseases, vector-mediated gene delivery is not feasible due to the cargo limit of viral vectors as well as the expression of multiple heterogeneous variants of the target gene.[357,358] The ABCA4 (coding sequence ~6.8 kb) and *USH2A* (coding sequence ~15.6kb) genes together account for almost 25% of all inherited retinal diseases.[359] Although some of the inherent limitations of viral vectors (and particularly AAVs) have been bypassed by elegant manipulation of the vector constructs,[360-363] the utility of these systems is inherently limited by reduced transduction efficiency. Furthermore, even for genes that fit within the payload constrains of AAVs, regulating transgene expression can be challenging, and constitutive overexpression from strong or leaky promoters can result in undesirable outcomes such as cellular toxicity and off-target effects.[364]

6.5.4.2 Targeting autosomal dominant diseases

In autosomal recessive mutations, the loss of gene function can be compensated by introduction of a replacement allele into the cell. In contract, dominant negative mutations display not only impaired function, but also a novel phenotype that is pathogenic to the cell.[365] Thus, gene augmentation is not a suitable approach due to the requirement for silencing or ablating the defective gene in autosomal dominant diseases. Moreover, alternative RNA-based suppression and replacement using ribozymes, short hairpin RNAs, RNAi, and RNA editors-based approaches to silence or degrade both mutated and normal RNA transcripts are transient in nature and the limited durability

of the therapy, regulation of gene expression levels, and target specificity have posed significant challenges for broad adaptation.[366-368]

DNA base editing and prime editing presents an alternative approach to treat dominant diseases by addressing these challenges. For example, 25%-30% of the cases of retinitis pigmentosa (RP), the most common inherited retinal degeneration, are autosomal dominant.[369] Mutations in at least 23 genes have been reported to cause adRP to date, including over 180 mutations in the RHO gene, which accounts for over 25% of adRP cases. Approximately half of the RHO-associated adRP cases are caused by the P23H mutation.[370] Targeted adenine or cytosine-mediated based editing would convert P23H into P23R (CAC →CGC) or P23T (CAC →TAT/C), amino-acid substitutions that have not been reported to cause adRP.

6.5.4.3 Editing premature stop codons

A large number of diseases including cystic fibrosis, Duchenne muscular dystrophy, β-thalassemia, and Usher syndrome are caused by premature stop mutations.[371] The disease phenotypes caused by premature stop mutations are frequently more severe than those that result from missense mutations, since premature stop mutations often result in a complete loss of protein function. Premature termination events are exacerbated by the spontaneous methylation of cytosine residues in context of CG (CpG), which create "hot spots" of C→T transitions that can generate the stop codon TAG upon epigenetic-mediated mutation of CGA.[372] Indeed, 12% of all mutations reported are single-point mutations that result in a premature termination codon (PTC).[373]

The therapeutic potential of base editors for correction of nonsense mutations has been demonstrated *in vivo*. Ryu and colleagues utilized an AAV targeted ABE to correct a premature stop codon (Q871X) in the *Dmd* gene.[352] Targeted base editing restored dystrophin expression in 17% of myofibers, a level which is sufficient to improve muscle

function. Lee *et al.* developed CRISPR-pass, a targeted tool for bypassing premature termination codons using CRISPR-mediated adenine base editors that showed systematic rescue of all possible cases of PTCs.[374] This approach is applicable to 95.5% of clinically significant nonsense mutations in the ClinVar database. On the other hand, CRISPR-BEs can also be used to generate stop codons for gene KO studies or towards disruption of pathogenic genes.[135] Rossidis *et al.* injected AAV vectors encoding BE3 into embryonic mouse fetuses to disrupt the wild-type *Pcsk9* or *Hpd* gene through creation of a premature stop codon.[141] The authors were able to reduce plasma *Pcsk9* levels, a key regulatory protein controlling cholesterol levels and demonstrated rescue of the lethal hereditary tyrosinemia type 1 (HT1) phenotype.

6.5.4.4 Editing splice-site variants

Alternative splicing is one of the most important post-transcriptional mechanisms, and it has been estimated that 15% of disease-causing point mutations affect pre-mRNA splicing.[375] X-linked retinitis pigmentosa is a subtype of RP that is clinically characterized by peripheral visual field constriction and night blindness; 60–80% of cases are linked to mutations in the RPGR gene.[369] The RPGR pre-mRNA undergoes alternative splicing to produce five major transcripts. Importantly, 55% of mutations affect the glutamic-rich domain within the RPGR-open reading frame-15 (ORF) region, highlighting the significance of ORF15 in the occurrence of diseases.[376]

Synthetic regulation of alternative splicing provides allows for selectively skipping mutation-containing exons while keeping normally functioning variants intact and presents a robust approach for targeting XL-RP and other inherited diseases. CRISPR-mediated CBEs and ABEs can disrupt donor/acceptor sites at AT/AA and GC/GG, respectively. Gapinske *et al.* demonstrated a novel method (CRISPR-SKIP) that utilizes cytidine deaminase single-base editors to program exon skipping by mutating target

DNA bases within splice acceptor sites.[142] The authors estimate that this approach could target ~63% (118,089 out of 187,636) of inner exons in protein coding transcripts. CRISPR-mediated modulation of RNA splicing was utilized to restore the frame of a mutant DMD gene and rescued its function in induced pluripotent stem cells (iPSCs) derived from a patient with Duchenne muscular dystrophy [377]. Recently, RNA-encoded ABE was delivered into the liver of Tyrosinemia I mice, correcting the splice-variant mutation and rescuing the phenotype.[353]

6.5.5 Conclusion

DNA base editing and prime editing systems, with their simplicity and precision, hold great promise for the correction of point mutations in human genetic diseases. In this chapter, I explored these technologies in depth and demonstrated proof-of-concept in a novel HEK293-ABE reporter cell line and against the *mUsh2a* c.11840 (W3947X) mutation. Moreover, I evaluated the on-target activity induced by truncated PE variants and demonstrated that a compact prime editor harboring a truncated RNase H domain could induce enhanced levels of prime editing *in vitro*. Collectively, these results advance the DNA base editing and prime editing technologies, with an eye towards their therapeutic translation for the treatment of inherited retinal diseases.

7. GENERAL DISCUSSION

The overall aim of this thesis was to explore the development of CRISPR-Cas9 tools and their therapeutic adaptation towards the treatment of retinal disease. This chapter describes the 4 aims that were successfully addressed in this thesis and provides insight into future translation of gene editing agents to the clinic.

7.1 Summary of thesis aims and outcomes

V. To develop and optimize CRISPR constructs towards *in vivo* adaptation

This chapter investigated three key aspects of vector and delivery development. Firstly, a reporter assay was developed for direct evaluation of different components of the AAV expression cassette and genome engineering reagents on the same target and harboring identical vector backbones and regulatory elements. I demonstrated proof-of-concept of the utility of the reporter assay across both Cas orthologue screening and evaluation of regulatory elements, and the established assay is broadly applicable to evaluate a range of different genetic elements and CRISPR components in future studies. Secondly, I presented the adaptation of the assay towards the development of an all-in-one vector for efficient CRISPR-mediated gene knockdown. The single vector construct and vector optimizations developed in this chapter served as the backbone for the epigenetic editing and prime editing tools developed in subsequent chapters. Thirdly, I demonstrated the ability of gold nanoparticles to efficiently deliver genes *in vitro* and assessed aspects of their safety including effects on retinal structure and function.

VI. To develop CRISPR-Cas repressors for targeted epigenome editing

I designed, cloned, and optimized a CRISPR-dCas9 epigenome editor which can be packaged within an AAV vector for targeted transcriptional repression and validated

the system *in vitro* against *NRL*. I developed an *in vitro* cell line for facile screening of dCas9-repressor constructs and screened repressor effectors and bipartite combinations for robust gene silencing. Finally, I demonstrated that the dCas9-repressor fusions can be utilized to mediate a high level of transcriptional repression against multiple targets, including both human and mouse *NRL* genes.

VII. To evaluate Cas9-repressors in patient iPSC-derived retinal organoids and conduct a pilot study in an NRL-EGFP mouse model

In this chapter, I evaluated a dCas9-repressor-mediated approach for targeted silencing of *hNRL* and *mNrl* genes in therapeutically relevant models, including in human iPSC derived 3D retinal organoids and *in vivo* in an *Nrl.EGFP*$^{+/-}$ mouse model. I demonstrated that AAV-directed dCas9-based repressor effectors provide a facile and robust method to modulate the expression of endogenous genes. This work was the first demonstration of all-in-one packaging of a bipartite repressor system, which due to the limited cargo capacity of AAVs is an optimal approach to enable desired genome engineering applications. Finally, I demonstrated for the first time the utility of dCas9-repressor-mediated *in situ* gene repression in the context of patient iPSC derived 3D retinal organoids.

VIII. To develop and evaluate CRISPR mediated DNA base editing & prime editing technologies

In this chapter, HDR-independent DNA base editing and prime editing technologies were evaluated and optimized. I demonstrated proof-of-concept in a novel HEK293-ABE reporter cell line and against the *mUsh2a* c.11840 (W3947X) mutation. Moreover, I evaluated the on-target activity induced by truncated PE variants and demonstrated that a compact prime editor harboring a truncated RNase H domain could induce enhanced levels of prime editing *in vitro*. Collectively, these results advance the

DNA base editing and prime editing technologies, with an eye towards their therapeutic translation for the treatment of inherited retinal diseases.

7.2 Translational considerations

With an FDA-approved gene therapy treatment for biallelic RPE65-associated inherited retinal diseases, future approvals for gene augmentation therapies targeting additional inherited retinal diseases such as choroideremia and RPGR-related retinitis pigmentosa are fast approaching. However, these AAV vector-based gene augmentation therapies are generally limited by the size of the transgene and to the treatment of autosomal recessive and X-linked diseases. Thus, genome editing systems such as CRISPR-Cas technology, capable of directly correcting disease-causing mutations in the human genome and of targeted knock-down of disease alleles, show great potential as a complementary tool for the treatment of these inherited blinding conditions.

In addition, introduction of DNA base editing, prime editing and mRNA editing methodologies are expected to make gene editing safer and adaptable for a broader range of genetic pathologies, including applications in both dividing and terminally differentiated cell types. In principle, over 25% of pathogenic SNPs may be editable by targeting the four transition mutations, with prime editing poised to correct up to 89% of known genetic variants associated with human disease. For retinal degenerative disease, gene editing techniques could be particularly well suited for the correction of large genes and treatment of the dominant diseases requiring silencing or ablation of the defective gene in addition to AAV gene augmentation therapy.

The expanding range of gene editing systems, their versatility and adaptability make them attractive for clinical development pathways, especially given the heterogeneous nature of inherited retinal diseases. With relatively small changes to the guide RNA sequence, while maintaining other components of the genetic medicine constant, a large

number of pathogenic mutations may be treated. Nevertheless, the sequence-specific nature of guide RNAs will require extensive safety and efficacy pre-clinical evaluations in human tissue (e.g., *ex-vivo* human retinal organoids or retinal explants) and likely *in vivo* in non-human primate (NHP) models.

Nonetheless, nuclease-mediated editing has made huge strides in its therapeutic translation. This approach was used to correct a splicing defect in the *CEP290* gene, which is caused by the most common mutation associated with Leber congenital amaurosis (LCA) type 10 (LCA10).[90] Mutations in *CEP290* are one of the most common causes of LCA10, accounting for up to 20% of all LCA cases. Although the function of CEP290 is not clearly understood, it is thought to play a structural role in the cilia of photoreceptor cells. [378,379] The mutation, IVS26 c.2991 + 1655 A > G in intron 26 of the *CEP290* gene, generates a novel splice donor, resulting in aberrant protein splicing and the inclusion of an additional 128-bp cryptic exon in the coding sequence of the transcript. Researchers employed *Staphylococcus aureus* (*S. aureus*) Cas9 and two sgRNAs to induce DSBs at both ends of the region of DNA to excise the intronic mutation and restore normal splicing between exons 26 and 27 in mice. Delivery of these components into mice using a single-AAV approach led to increased expression of WT CEP290 and concomitant decrease in expression of the defective CEP290. Furthermore, experiments in human retinal explants did not detect any off-target editing at over 100 candidate sites.[90]

This successful preclinical study led to clinical trials for treating LCA10 patients. EDIT-101 (Editas Medicine Inc., Cambridge, MA, USA), uses an AAV-delivered Cas9 and two sgRNAs to remove an intronic point mutation in the *CEP290* gene (the so-called IVS26 mutation), which leads to incorrect splicing of the *CEP290* transcript and causes LCA10. Similar to the preclinical study, EDIT-101 employs a single AAV containing two human U6 polymerase III promoter-driven sgRNAs and human G protein–coupled receptor kinase 1 promoter-driven *S. aureus* Cas9.[90] The promising results from

preclinical assessment of EDIT-101 supported a subsequent phase 1/2 clinical trial, BRILLIANCE, which included 11 adult patients (NCT#03872479). Although the posttreatment assessment of the patients is still ongoing, preliminary clinical results, presented at the 2021 European Society of Gene and Cell Therapy Annual Congress, reported a favorable safety profile and encouraging early signs of efficacy in the patients. A comprehensive update on safety and efficacy of the treatment is anticipated by the second half of 2022, after 12 months of follow-up evaluations.

These encouraging results are likely to pave the way for other gene editing systems to enter human trials and the results of the EDIT-101 trial are eagerly awaited. However, despite the encouraging pre-clinical data, there are still concerns and risks associated with introducing CRISPR-Cas systems into humans. The ongoing EDIT-101 trial will enlighten some of these concerns, while others will continue to require pre-clinical investigation. Of particular relevance are the risks of immune responses to the expressed Cas proteins, the rates of on-target efficacy and the consequences of undesired editing in the retina.

7.2.1 Undesired genome editing

The development of CRISPR-Cas9 genome editing tools has simultaneously created great excitement and raised technical and ethical issues, many of which have yet to be resolved. For some concerns, the consequences of use in humans remain unknown and will be informed by current trials, while others can be better anticipated, and steps have already been implemented to create safer editing tools. These modifications include the systems discussed throughout this thesis that do not directly alter the genome as well as strategies to control Cas9 activity and mitigate the risks of off-target editing. RNA editing rather than DNA editing may circumvent some risks associated with genome editing as off-target events would not result in permanent mutations. Base and prime

editing approaches also provide potentially lower risks than Cas9 genome editing. Compared with base editing, prime editing appears to be associated with lower off-target mutagenesis in human cell lines, although additional concerns may emerge as the system is studied further. Indeed, due to the infancy of CRISPR reagents, additional research is needed to further characterize and improve base and prime editing in a broad range of cell types and organisms before the full potential of these platforms can be realized for clinical use.

Whilst there is concern about the lack of control of on-target editing with CRISPR-Cas systems, particularly those that employ NHEJ mechanisms, the control of off-target editing is a central consideration. Off-target mutations have the potential to alter expression of other genes, disrupt tumor suppressor genes, cause chromosomal translocations or integration of the viral vector genome.[216,380] Prior to human trials, the potential off-target activities of gene-editing therapies must be assessed in a variety of primate-specific model systems, ranging from *in silico* predictions, to human cell lines, iPSC-derived retinal organoids, *ex vivo* tissue and *in vivo* testing in non-human primates. Computer algorithms may be used to predict off-target sites based on the sgRNA, PAM preference, chromatin accessibility, and machine learning from previous experimental data,[381-384] though their accuracies remain limited.

In vitro assays for unbiased detection of off-targets include GUIDE-seq (genome-wide unbiased identification of DSBs enabled by sequencing),[385] Digenome-Seq,[386] and CIRCLE-Seq (circularization for *in vitro* reporting of cleavage effects by sequencing).[387] Assessment of off-target mutations *in vivo* is more challenging and relies on DISCOVER-Seq (discovery of *in situ* Cas off-targets and verification by sequencing). This approach utilized chromatin immunoprecipitation sequencing (ChIP-Seq) to identify the positions of Cas9-cut DNA ends bound by MRE11, a DNA repair factor.[388] Importantly, DISCOVER-Seq can only detects DSBs at the time of the experiment and is not suitable

for assessing off-targets in base editing or prime editing therapies. For instance, cytidine or adenine deaminases within DNA and RNA base editing systems could potentially cause off-target deamination of bystander C or A within the edit window or elsewhere. The reverse transcriptase within prime editing systems may create off-target mutations by extending a short way into the pegRNA scaffold beyond its primer sequence. In order to directly assess the accumulated mutations following genome editing therapies, targeted, exome or whole genome sequencing need to be performed on treated versus untreated tissues. In this respect, pre-clinical assessments of CRISPR genome engineering systems in the eye are fortunate to have the paired eye available as an untreated control.

7.2.2 Immunogenicity concerns

Being of bacterial origin, expression of CRISPR-Cas components in the eye raises the possibility of intraocular immune responses, which could lead to cell immune cell infiltration, structural damage and reduced clinical efficacy. Pre-existing antibodies to the current most commonly used SaCas9 and SpCas9 have been detected in 78% and 58% of humans,[389,390] respectively, as well as NHPs.[90] Despite this, no significant inflammatory response was observed in NHPs following subretinal delivery of AAV5 vectors carrying a CRISPR-SaCas9 transgene for editing of *GUCY2D*, mutations in which cause cone-rod dystrophy.[89] It was observed that levels of AAV neutralizing antibodies and Cas9-induced T-cell responses correlated with the number of subretinal blebs performed yet no significant intraocular inflammation was observed in treated animals. Interestingly, the NHP with the greatest pre-existing T-cell response to SaCas9 provided the highest achieved rate of *GUCY2D* editing. A similar finding was observed in the pre-clinical NHP study performed using the EDIT-101 AAV5 vector.[90]

The absence of significant signs of inflammation despite a pre-existing response to Cas9 is encouraging but should nevertheless be taken cautiously due to the timeframes

of the studies. Testing in humans will continue for more extended periods and negative consequences may not be evident in a short term follow up. It will be important for any clinical trial to assess each patient for pre-existing antibodies to the CRISPR-Cas system being administered in order to best anticipate and interpret subsequent events.

7.2.3 Improving safety of CRISPR-Cas systems

While genotoxicity may be reduced by the use of high-fidelity Cas variants, even a very low level of off-target activity may become significant if the Cas expression is sustained *in vivo*. Several studies have described Cas9 variants evolved to increase the targeting specificity.[139,148,391,392] In addition to engineering approaches of the Cas9 protein, Kocak *et al.* demonstrated that engineering a hairpin secondary structure onto the sgRNA guiding sequence can enhance the targeting specificity by several orders of magnitude[393]. Finally, increasing or decreasing the length of the sgRNA guiding sequence by a few base pairs can enhance the targeting specificity.[394,395] Appropriate and thorough optimization of construct design should therefore be employed throughout pre-clinical testing phases of a given CRISPR-Cas system.

Temporal and spatial control of Cas9 endonuclease expression *in vivo* may be achieved via a number of strategies. Viral vectors, especially AAV, remain the most attractive mode of delivering CRISPR-Cas systems to the retina due to their proven clinical efficacy and safety. Most retinal gene augmentation therapies use ubiquitous or tissue-specific promoters to drive transgene expression within target retinal cell groups. However, with the shift in clinical need from long-term transgene expression to transient Cas9/sgRNA expression, the choice of promoters in viral vector constructs may need to be reconsidered.

Temporal control of Cas9 expression may be achieved using drug-inducible promoters. For instance, the steroid-inducible *GRE5* promoter may be used to drive Cas9

expression as corticosteroid drugs are readily available for ocular use.[396] However, basal levels of corticosteroids in the body may cause leaky expression and thus low level off-target activity, and it is possible that the increased ocular pressure caused by these steroids would limit use in patients with retinitis. The doxycycline (or tetracycline)-inducible Tet-ON expression system may afford tighter control of Cas9 expression.[397-399] Alternatively, temporal control may be achieved through protein perturbation techniques. Insertion of a 4-hydroxytamoxifen (4-HT)-responsive intein domain within Cas9 has been shown to enable internal protein splicing to generate active Cas9 in the presence of tamoxifen.[400] Fusion of the estrogen receptor-α (hERα) ligand binding domain or the destabilization domain of *E. coli* dihydrofolate reductase (DHFR-DD) to Cas9 could enable inducible Cas9 stabilization by tamoxifen or trimethoprim, respectively.[401,402] Of the exogenous regulation systems covered, tetracycline-regulated systems have been refined sufficiently such that they are on the cusp of being applied clinically. While low basal transgene expression is of concern, in a clinical setting these levels may not be sufficient to elicit a phenotypic response.

An additional approach to temporal control with minimal increase in construct size is a self-destructing CRISPR system, which contains a self-targeting sgRNA.[403,404] The Self-Limiting Cas9 circuit for Enhanced Safety and specificity (SLiCES) system consists of an expression SpCas9, a self-targeting sgRNA and a second sgRNA targeting a chosen genomic locus. Upon delivery into target cells using lentivirus, the system exploits the efficiency of viral-based delivery while simultaneously limiting its expression post transduction through SpCas9 inactivation.[405] It remains to be seen whether such a self-limiting system could provide complete inactivation of Cas9 activity *in vivo* and how it matches against transcriptional or post-translational regulatory systems. Separately, non-viral delivery of CRISPR-Cas elements could provide transient editing activity, avoid accumulation of off-target effects, and deliver bulky constructs.

7.2.4 Improving targeting scope of CRISPR-Cas systems

One constraint of Cas9 is its dependency on the PAM sequence to bind DNA. Because of the simple 50 -NGG-30 PAM sequence requirements, S. pyogenes' Cas9 (SpCas9) is used in many different applications. However, scientists are actively exploring other CRISPR systems to identify Cas9-like effector proteins that may have differences in their sizes, PAM requirements, and targeting specificity.[406-410] Naturally found Cas9 variants are large proteins, which adds particular limitation when it comes to packaging and delivery to target cells. For example, the SpCas9 protein is 4098 base-pairs (bp), making therapeutic delivery challenging due to the limited packaging capacity of adeno-associated vector (reviewed below). To this end, the discovery of smaller variants such as 3246 bp Cas9 from Staphylococcus aureus (SaCas9) and 2952 bp Cas9 from Campylobacter jejuni (CjCas9) provides great therapeutic potential. However, these smaller Cas9 proteins require more complex PAM sequences, limiting targeting scope compared to SpCas9 despite the size reduction. The SaCas9 requires a 50 -NNGRRT-30 PAM sequence whereas CjCas9 requires a 50 -NNNNACAC-30 PAM sequence.

While exploration of natural Cas diversity provides one avenue for expanding and improving PAM coverage, the efficiency of Cas varies, and to date, no variants have surpassed SpCas9 efficacy. Thus, complimentary evolution-based and structure-guided engineering approaches have been employed to modify and improve Cas9 effector scope.[339,411,412] For example, Kleinstiver *et al.* used a series of positive selection screens in bacteria to identify specific point mutations that significantly increase the coverage of SpCas9. They evolved three variants (VQR, EQR and VRER) which recognize the novel PAM sequences NGAN/NGNG, NGAG and NGCG, respectively.[339] Similarly, Cas9 of *Francisella novicida* was engineered to recognize non-canonical 5'YG-3' PAM.[355] Most recently, Walton *et al.* reported the evolution of a two novel SpCas9 variants: SpG, capable of targeting an expanded set of NGN PAMs, and a nearly-PAMless variant called SpRY.[413]

Importantly, SpRY allowed for correction of a wide range of pathogenic mutations located in previously "un-targetable" regions of the genome.

In addition to expanding the targeting scope of CRISPR tools, researchers are actively developing novel ways to increase the targeting specificity and minimize the off-target effects of the CRISPR-Cas9 system. Several studies have described Cas9 variants evolved to increase the targeting specificity of Cas9. In addition to engineering approaches at the Cas9 protein, the sgRNA scaffold can also be modified to increase the targeting specificity [414]. For example, the secondary structure of the gRNA spacer region can be modified to increase the thermodynamic barrier to gRNA binding at off-target sites [415]. Furthermore, increasing or decreasing the length of the sgRNA guiding sequence by a few base pairs can enhance the targeting specificity [416,417]. Finally, modifying the delivery platform of the CRISPR-Cas9 construct can further enhance targeting. For example, delivery of the Cas9-sgRNA complex as a ribonucleotide protein (RNP) complex results in more transient activity of Cas9 and lower rates of off-target cleavage [210,418].

7.2.5 Forthcoming development of dCas-based epigenome editing

Since CRISPR/Cas-based repressor systems generally rely upon the same backbone as cleavage-dependent CRISPR systems that are used for conventional genome editing applications, improvements in the CRISPR/Cas toolkit are often directly portable to epigenetic editing applications. Future areas for improvement include increasing the targeting specificity and minimizing off-target effects, expanding targeting ranges, reducing protein sizes for more efficient delivery, and enhancing spaciotemporal control of Cas and gRNA expression.

Although the most well-studied Cas9 protein is derived from *Streptococcus pyogenes*, exploration of natural Cas diversity has led to the identification of different orthologues requiring different protospacer adjacent motifs and displaying different off-target

profiles. As such, these orthologs augment the arsenal of options available for genome and epigenome editing. In addition to the *Staphylococcus aureus* Cas9 nuclease that was utilized in my study, smaller Cas proteins, including the recently discovered CRISPR-Casϕ,[253] are particularly advantageous for epigenome editing applications because they can be more easily packaged within current viral platforms for gene delivery. Systematic metagenomic mining and screening for DNA cleavage activity have proven to be promising in identifying novel Cas families and these approaches will play a critical role in further improvement to both genome and epigenome engineering efforts.[254]

Similar to genome editing systems, most *in vivo* delivery approaches of dCas9-repressor fusions utilize AAV-based systems. Since the limiting packaging size of AAV vectors preclude delivery of bulky Cas proteins and epigenome editing effector domains, alternative approaches have been devised to enable delivery. For example, one approach leveraged a dual AAV system to deliver CRISPRa and a dead gRNA to treat murine models of diabetes, muscular dystrophy, and acute kidney disease *in vivo*.[419] However, clinical translation of such strategies is limited by low co-transduction efficiencies and higher potential for off-target effects with multi-vector approaches. Indeed, utilizing a split-Cas9 system requires that both components, C-terminal Cas9 and N-terminal Cas9, be co-delivered to target cells to reconstitute Cas9 activity.

Non-viral delivery methods have emerged as a viable alternative that can address the size limitations of viral vectors, as well as challenges with immunogenicity and complexity with scale-up of virus production, but they require substantial improvements to reach the efficacy of their viral counterparts. Finally, the sustainability of epigenetic modifications may inform delivery strategy, as multiple treatments may be necessary with dCas9 systems. Further improvements in techniques for localized tissue-specific delivery and redosing of CRISPR-reagents may be needed to enable translation of epigenome editors to the clinic.

The development of CRISPR-dCas9-based inducible transcription systems may provide a pivotal extension for regulating transcriptional activities with high precision and spaciotemporal specificity. Similar to the need for genetic safety "switches" to titrate the activity of CAR-T cells toward tumor cells and therefore strictly control toxicities after administration of CAR-T therapies,[420] control modules may be needed to control the duration and potency of dCas9-repressor systems and mitigate any off-target effects. Tissue-specific and conditional promoters can be used to control the expression of CRISPR systems in human cells.

Other strategies for controlling gene expression mainly rely on dynamic engineering of dCas9 protein and gRNA. For controlling gRNA function, a general approach is to develop switchable gRNA structures that can restore active conformations in the presence of small-molecule ligands, light, synthetic and endogenous nucleic acids.[421] For controlling the function of dCas9 protein, the recruitment of transcriptional effectors and the complementation of split protein fragments can also be triggered by light, small-molecule ligands and endogenous nucleic acids.[397] A variety of transcriptional reporters have been exploited as the signal outputs, including florescent proteins, luciferase, and endogenous genes.[422,423] Due to the mechanistic similarities among orthologous CRISPR/Cas systems, many of these control systems are likely to be transferrable across Cas proteins and across cleavage-dependent and dCas9-repression-fusion based editing systems.

The potential to multiplex gene repression is a key advantage of dCas9-repressor fusion-based systems and could extend the epigenetic toolkit to enable targeting of complex diseases involving multiple genetic loci. CRISPR tools are constrained in this respect due to the limited number of promoters available for gRNA expression, the most common of which is the U6 type III RNA polymerase promoter. CRISPR-dCas12a (dCpf1) has shorter crRNAs and the ability to process multiple crRNAs from a single transcript,

circumventing the need for multiple promoters. This feature has been exploited to modulate the expression of up to 25 different human genes simultaneously.[424,425] Various other methods for multiplexing CRISPR have also been explored using ribozymes, tRNA, and ribonucleases to process gRNA arrays with varying degrees of success. In the same vein, since multiple epigenetic marks can coexist at the same genomic locus, repressor systems capable of effector multiplexing will be critical to fully unlocking the therapeutic utility of epigenome editors. Indeed, my study adds to the expanding scope of work demonstrating the enhanced gene modulatory effects of multipartite effector fusions in comparison to their single effector counterparts. Finally, since persistent modifications may require changes in multiple epigenetic marks, a robust repressor system capable of recruiting multiple effectors to a target locus may be critical for maintaining a sustained effect.

7.3 Future clinical application of precision editing in inherited retinal diseases

Precision medicine for IRDs has a promising outlook, as basic science has consistently led to the development of therapeutic tools to target the underlying cause of genetic diseases.

Although precision editing is an attractive treatment approach in principle, its wide-ranging clinical integration is hampered by the immense amount of cost and resources associated with designing precision therapies based on the unique genetic profile of each patient. From a practical standpoint, it not viable nor achievable to screen hundreds of CRISPR reagents and guide RNA combinations using cells derived from each patient, thoroughly characterize the safety profile, and obtain FDA approval to develop the strategy into a broadly applicable therapy within a reasonable price tag. To address this practical barrier, there needs to be an economical algorithm that can devise

a treatment tailored to address the underlying disease pathology, for example, utilizing artificial intelligence or deep machine learning models to generate the optimal editing strategy.[426,427] The *in silico*–designed editing strategy could be further validated in differentiated patient-derived fibroblasts or subsequently iPSC-derived organoids.

Induced pluripotent stem cell (iPSC) derived 3D organoids, which comprehensively recapitulate the structure and functionalities of their counterpart organs, hold great promise for facilitating the development of therapeutic treatment of inherited diseases and personalized medicine.[428-430] Unlike two-dimensional cell cultures, organoids provide insight into the intercellular interactions and the overall effect of treatment on cells in the context of their microenvironment. Moreover, organoids recapitulate many epigenomic features, which allow more accurate prediction of *in vivo* editing outcome.[431] I and others have established that patient iPSC derived retinal organoids superbly mimic the architecture of the mammalian retina and can therefore be used as a physiologically relevant *in vitro* model. Indeed, RO models represent the future of pre-clinical testing for advanced therapeutics and the next generation of genome and epigenome engineering technologies.

After thoroughly characterizing the safety profile and off-target effects, the selected editing agent can be delivered in the optimal nucleic acid format (i.e., DNA, mRNA, RNP, or mixed payload) by choosing from various vehicles, including AAV, lentivirus, eVLP, lipid nanoparticles, gold nanoparticles, and others. The custom-designed treatment would then be administered to the selected patients.

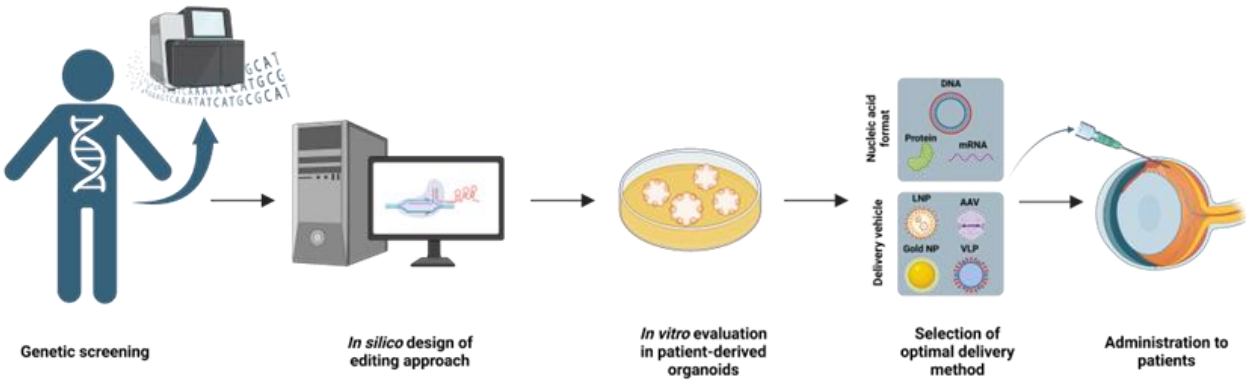


Figure 7.1 | Future clinical application of precision editing in IRDs

7.4 Final perspectives

Since the foundational and subsequently Nobel-prize winning report of the first programmable genome editing CRISPR-Cas system was published in 2012, many areas of research have been revolutionized by the potential of the molecular system. With a retinal disease having the first approved gene therapy treatment and a growing body of data confirming safety and efficacy from multiple clinical trials, it was perhaps inevitable that one of the first direct uses of a CRISPR-Cas genome engineering system would be for the treatment of an inherited retinal disease. The success of retinal gene therapy clinical trials over the past decade was always likely to be curbed by the diversity of inherited retinal diseases, which are genetically highly heterogenous. Gene augmentation strategies are, by their nature, largely limited to treating autosomal recessive and X-linked, single gene disorders. The advent of CRISPR has dramatically altered future treatment options for numerous forms of inherited retinal disease not treatable by other means.

In this chapter, I have discussed the current scope of CRISPR systems available and their varying applications for the treatment of inherited retinal. This is a rapidly

developing field and, importantly, there are still many challenges to consider, not least the impact of expressing these bacterial molecular systems in the human retina and the potential consequences of undesired genome editing activity. Progress towards these challenges appears to be occurring at an unprecedented rate and with a CRISPR clinical trial for an inherited retinal disease already ongoing, our understanding of the impact of such administration will soon be further advanced. There is no doubt that CRISPR genome engineering in the retina will be at the forefront of future developments and use in humans. Researchers now have the molecular tools to potentially treat patients destined to go blind, which provides an exciting future for scientists, clinicians and, most importantly, patients.

As this technology matures, it is our responsibility to ensure that the implementation of precision genome editing is conducted responsibly and with social license. From an economic perspective, great thought should be put into developing policies to make genome editing available to all patients with IRDs. Luxturna, which is the same formulation for all patients with the biallelic RPE65 mutations, was introduced in the United States with a heavy price tag at $425,000 per eye. This potential cost barrier raises questions about the pricing and affordability of the anticipated wave of personalized gene editing therapies. To make precision genome editing feasible as a clinically effective approach, development of novel policies and economic models for commercializing therapies for rare disease should take place simultaneously with the clinical trials.

7.5 Concluding remarks

Collectively, the data presented in this thesis explored novel editing strategies using epigenome editors *in vitro* and *in vivo*, photoreceptor delivery using DNA-wrapped gold nanoparticles, and development of novel DNA editing technologies. Meaningful

insights into the successes and shortcomings of each approach were thoroughly investigated and have generated promising pilot data from which to base further research. The development of the dCas9-epigenome editor represents the first use of an AAV-mediated all-in-one bipartite dCas9-repressor system to induce gene knockdown of photoreceptor genes. Research from this work has formed the basis for the contribution to original peer reviewed manuscripts and multiple major reviews and book chapters. Further manuscripts and patent filings around DNA and epigenome editing tools developed hitherto are in preparation.

This thesis was undertaken in a tremendous era of innovation in the field of genome engineering, with the rapid advancement of CRISPR/Cas9 and base editing technologies to the clinic. It has given me a deep appreciation for remarkable speed at which therapies can be translated from the bench to the bedside, and the transformational potential of genome editing to improve patient care. The lessons learned from my time in the MacLaren group and the life-altering potential of biomedical advances will stay close to my heart and serve as a core motivator as I embark on my next chapter at the frontier of genomic medicines.

8. REFERENCES

1. Sung CH, Chuang JZ. The cell biology of vision. *J Cell Biol.* 2010;190(6):953-963.
2. Cremers FPM, Boon CJF, Bujakowska K, Zeitz C. Special Issue Introduction: Inherited Retinal Disease: Novel Candidate Genes, Genotype-Phenotype Correlations, and Inheritance Models. *Genes (Basel).* 2018;9(4).
3. Hu ML, Edwards TL, O'Hare F, et al. Gene therapy for inherited retinal diseases: progress and possibilities. *Clin Exp Optom.* 2021;104(4):444-454.
4. Olivares-González L, Velasco S, Campillo I, Rodrigo R. Retinal Inflammation, Cell Death and Inherited Retinal Dystrophies. *Int J Mol Sci.* 2021;22(4).
5. Cehajic-Kapetanovic J, Birtel J, McClements ME, et al. Clinical and Molecular Characterization of PROM1-Related Retinal Degeneration. *JAMA Network Open.* 2019;2(6):e195752-e195752.
6. Nanda A, McClements ME, Clouston P, Shanks ME, MacLaren RE. The Location of Exon 4 Mutations in RP1 Raises Challenges for Genetic Counseling and Gene Therapy. *Am J Ophthalmol.* 2019;202:23-29.
7. Thompson JA, De Roach JN, McLaren TL, Lamey TM. A Mini-Review: Leber Congenital Amaurosis: Identification of Disease-Causing Variants and Personalised Therapies. *Adv Exp Med Biol.* 2018;1074:265-271.
8. Jolly JK, Bridge H, MacLaren RE. Outcome Measures Used in Ocular Gene Therapy Trials: A Scoping Review of Current Practice. *Front Pharmacol.* 2019;10:1076-1076.
9. Naylor A, Hopkins A, Hudson N, Campbell M. Tight Junctions of the Outer Blood Retina Barrier. *Int J Mol Sci.* 2019;21(1).

10. Amato A, Arrigo A, Aragona E, et al. Gene Therapy in Inherited Retinal Diseases: An Update on Current State of the Art. *Front Med (Lausanne).* 2021;8:750586.

11. McClements ME, MacLaren RE. Gene therapy for retinal disease. *Transl Res.* 2013;161(4):241-254.

12. Li C, Samulski RJ. Engineering adeno-associated virus vectors for gene therapy. *Nature Reviews Genetics.* 2020;21(4):255-272.

13. Samulski RJ, Muzyczka N. AAV-Mediated Gene Therapy for Research and Therapeutic Purposes. *Annual Review of Virology.* 2014;1(1):427-451.

14. Wang D, Tai PWL, Gao G. Adeno-associated virus vector as a platform for gene therapy delivery. *Nat Rev Drug Discov.* 2019;18(5):358-378.

15. Bartel MA, Weinstein JR, Schaffer DV. Directed evolution of novel adeno-associated viruses for therapeutic gene delivery. *Gene Ther.* 2012;19(6):694-700.

16. Dalkara D, Byrne LC, Klimczak RR, et al. In vivo-directed evolution of a new adeno-associated virus for therapeutic outer retinal gene delivery from the vitreous. *Sci Transl Med.* 2013;5(189):189ra176.

17. Jang JH, Koerber JT, Kim JS, et al. An evolved adeno-associated viral variant enhances gene delivery and gene targeting in neural stem cells. *Mol Ther.* 2011;19(4):667-675.

18. Klimczak RR, Koerber JT, Dalkara D, Flannery JG, Schaffer DV. A novel adeno-associated viral variant for efficient and selective intravitreal transduction of rat Müller cells. *PLoS One.* 2009;4(10):e7467.

19. Perabo L, Endell J, King S, et al. Combinatorial engineering of a gene therapy vector: directed evolution of adeno-associated virus. *J Gene Med.* 2006;8(2):155-162.

20. Russell DW, Hirata RK. Human gene targeting by viral vectors. *Nat Genet.* 1998;18(4):325-330.

21. Bainbridge JWB, Mehat MS, Sundaram V, et al. Long-Term Effect of Gene Therapy on Leber's Congenital Amaurosis. *New England Journal of Medicine.* 2015;372(20):1887-1897.

22. Russell S, Bennett J, Wellman JA, et al. Efficacy and safety of voretigene neparvovec (AAV2-hRPE65v2) in patients with RPE65-mediated inherited retinal dystrophy: a randomised, controlled, open-label, phase 3 trial. *Lancet.* 2017;390(10097):849-860.

23. Xue K, Jolly JK, Barnard AR, et al. Beneficial effects on vision in patients undergoing retinal gene therapy for choroideremia. *Nat Med.* 2018;24(10):1507-1512.

24. Cehajic-Kapetanovic J, Xue K, Martinez-Fernandez de la Camara C, et al. Initial results from a first-in-human gene therapy trial on X-linked retinitis pigmentosa caused by mutations in RPGR. *Nat Med.* 2020;26(3):354-359.

25. Dreismann AK, McClements ME, Barnard AR, et al. Functional expression of complement factor I following AAV-mediated gene delivery in the retina of mice and human cells. *Gene Therapy.* 2021;28(5):265-276.

26. Guimaraes TACd, Georgiou M, Bainbridge JWB, Michaelides M. Gene therapy for neovascular age-related macular degeneration: rationale, clinical trials and future directions. *British Journal of Ophthalmology.* 2021;105(2):151-157.

27. Moore NA, Bracha P, Hussain RM, Morral N, Ciulla TA. Gene therapy for age-related macular degeneration. *Expert Opin Biol Ther.* 2017;17(10):1235-1244.

28. Ochakovski GA, Bartz-Schmidt KU, Fischer MD. Retinal Gene Therapy: Surgical Vector Delivery in the Translation to Clinical Trials. *Front Neurosci.* 2017;11:174.

29. Xue K, Groppe M, Salvetti AP, MacLaren RE. Technique of retinal gene therapy: delivery of viral vector into the subretinal space. *Eye (Lond).* 2017;31(9):1308-1316.

30. Barnard AR, Groppe M, MacLaren RE. Gene therapy for choroideremia using an adeno-associated viral (AAV) vector. *Cold Spring Harb Perspect Med.* 2014;5(3):a017293.

31. Bujakowska KM, Comander J. Moving Towards PDE6A Gene Supplementation Therapy. *JAMA Ophthalmol.* 2020;138(12):1251-1252.

32. Pang J-j, Boye SL, Kumar A, et al. AAV-Mediated Gene Therapy for Retinal Degeneration in the rd10 Mouse Containing a Recessive PDEβ Mutation. *Investigative Ophthalmology & Visual Science.* 2008;49(10):4278-4283.

33. Pang JJ, Lei L, Dai X, et al. AAV-mediated gene therapy in mouse models of recessive retinal degeneration. *Curr Mol Med.* 2012;12(3):316-330.

34. Choi VW, Bigelow CE, McGee TL, et al. AAV-mediated RLBP1 gene therapy improves the rate of dark adaptation in Rlbp1 knockout mice. *Mol Ther Methods Clin Dev.* 2015;2:15022.

35. Cukras C, Wiley HE, Jeffrey BG, et al. Retinal AAV8-RS1 Gene Therapy for X-Linked Retinoschisis: Initial Findings from a Phase I/IIa Trial by Intravitreal Delivery. *Mol Ther.* 2018;26(9):2282-2294.

36. Wang J-H, Hickey D, McClements ME, Colgan T, Edwards T. Validation of in vitro gene therapy for Bietti crystalline dystrophy. *Investigative Ophthalmology & Visual Science.* 2019;60(9):3420-3420.

37. Wang J-H, Lidgerwood GE, Daniszewski M, et al. AAV2-mediated gene therapy for Bietti crystalline dystrophy provides functional CYP4V2 in multiple relevant cell models. *Scientific Reports.* 2022;12(1):9525.

38. Reichel FF, Michalakis S, Wilhelm B, et al. Three-year results of phase I retinal gene therapy trial for CNGA3-mutated achromatopsia: results of a non randomised controlled trial. *Br J Ophthalmol.* 2022;106(11):1567-1572.

39. Carvalho LS, Xu J, Pearson RA, et al. Long-term and age-dependent restoration of visual function in a mouse model of CNGB3-associated achromatopsia following gene therapy. *Hum Mol Genet.* 2011;20(16):3161-3175.

40. McClements ME, Barnard AR, Singh MS, et al. An AAV Dual Vector Strategy Ameliorates the Stargardt Phenotype in Adult Abca4(-/-) Mice. *Hum Gene Ther.* 2019;30(5):590-600.

41. McClements ME, Barnard AR, Charbel Issa P, MacLaren RE. Assessment of AAV Dual Vector Safety in the Abca4−/− Mouse Model of Stargardt Disease. *Translational Vision Science & Technology.* 2020;9(7):20-20.

42. Binley K, Widdowson P, Loader J, et al. Transduction of photoreceptors with equine infectious anemia virus lentiviral vectors: safety and biodistribution of StarGen for Stargardt disease. *Invest Ophthalmol Vis Sci.* 2013;54(6):4061-4071.

43. Kong J, Kim SR, Binley K, et al. Correction of the disease phenotype in the mouse model of Stargardt disease by lentiviral gene therapy. *Gene Ther.* 2008;15(19):1311-1320.

44. Wheway G, Douglas A, Baralle D, Guillot E. Mutation spectrum of PRPF31, genotype-phenotype correlation in retinitis pigmentosa, and opportunities for therapy. *Exp Eye Res.* 2020;192:107950.

45. Price BA, Sandoval IM, Chan F, et al. Rhodopsin gene expression determines rod outer segment size and rod cell resistance to a dominant-negative neurodegeneration mutant. *PLoS One.* 2012;7(11):e49889.

46. Haeri M, Knox BE. Rhodopsin mutant P23H destabilizes rod photoreceptor disk membranes. *PLoS One.* 2012;7(1):e30101.

47. Orlans HO, Barnard AR, Patrício MI, McClements ME, MacLaren RE. Effect of AAV-Mediated Rhodopsin Gene Augmentation on Retinal Degeneration Caused by the Dominant P23H Rhodopsin Mutation in a Knock-In Murine Model. *Hum Gene Ther.* 2020;31(13-14):730-742.

48. Cideciyan AV, Sudharsan R, Dufour VL, et al. Mutation-independent rhodopsin gene therapy by knockdown and replacement with a single AAV vector. *Proc Natl Acad Sci U S A.* 2018;115(36):E8547-e8556.

49. Cremers FPM, Lee W, Collin RWJ, Allikmets R. Clinical spectrum, genetic complexity and therapeutic approaches for retinal disease caused by ABCA4 mutations. *Prog Retin Eye Res.* 2020:100861.

50. Gaj T, Gersbach CA, Barbas CF, 3rd. ZFN, TALEN, and CRISPR/Cas-based methods for genome engineering. *Trends Biotechnol.* 2013;31(7):397-405.

51. Li H, Yang Y, Hong W, Huang M, Wu M, Zhao X. Applications of genome editing technology in the targeted therapy of human diseases: mechanisms, advances and prospects. *Signal Transduction and Targeted Therapy.* 2020;5(1):1.

52. Deltcheva E, Chylinski K, Sharma CM, et al. CRISPR RNA maturation by trans-encoded small RNA and host factor RNase III. *Nature.* 2011;471(7340):602-607.

53. Doudna JA, Charpentier E. The new frontier of genome engineering with CRISPR-Cas9. *Science.* 2014;346(6213):1258096.

54. Jinek M, Chylinski K, Fonfara I, Hauer M, Doudna JA, Charpentier E. A programmable dual-RNA-guided DNA endonuclease in adaptive bacterial immunity. *Science.* 2012;337(6096):816-821.

55. Mali P, Yang L, Esvelt KM, et al. RNA-Guided Human Genome Engineering via Cas9. *Science.* 2013;339(6121):823-826.

56. Garneau JE, Dupuis M-È, Villion M, et al. The CRISPR/Cas bacterial immune system cleaves bacteriophage and plasmid DNA. *Nature.* 2010;468(7320):67-71.

57. Ishino Y, Shinagawa H, Makino K, Amemura M, Nakata A. Nucleotide sequence of the iap gene, responsible for alkaline phosphatase isozyme conversion in Escherichia coli, and identification of the gene product. *J Bacteriol.* 1987;169(12):5429-5433.

58. Mojica FJ, Díez-Villaseñor C, García-Martínez J, Soria E. Intervening sequences of regularly spaced prokaryotic repeats derive from foreign genetic elements. *J Mol Evol.* 2005;60(2):174-182.

59. Pourcel C, Salvignol G, Vergnaud G. CRISPR elements in Yersinia pestis acquire new repeats by preferential uptake of bacteriophage DNA, and provide additional tools for evolutionary studies. *Microbiology (Reading).* 2005;151(Pt 3):653-663.

60. Barrangou R, Fremaux C, Deveau H, et al. CRISPR provides acquired resistance against viruses in prokaryotes. *Science.* 2007;315(5819):1709-1712.

61. Gasiunas G, Barrangou R, Horvath P, Siksnys V. Cas9-crRNA ribonucleoprotein complex mediates specific DNA cleavage for adaptive immunity in bacteria. *Proc Natl Acad Sci U S A.* 2012;109(39):E2579-2586.

62. Cong L, Ran FA, Cox D, et al. Multiplex genome engineering using CRISPR/Cas systems. *Science.* 2013;339(6121):819-823.

63. Mali P, Yang L, Esvelt KM, et al. RNA-guided human genome engineering via Cas9. *Science.* 2013;339(6121):823-826.

64. Hidalgo-Cantabrana C, Barrangou R. Characterization and applications of Type I CRISPR-Cas systems. *Biochemical Society Transactions.* 2020;48(1):15-23.

65. Chylinski K, Makarova KS, Charpentier E, Koonin EV. Classification and evolution of type II CRISPR-Cas systems. *Nucleic Acids Res.* 2014;42(10):6091-6105.

66. Rouet P, Smih F, Jasin M. Introduction of double-strand breaks into the genome of mouse cells by expression of a rare-cutting endonuclease. *Molecular and cellular biology.* 1994;14(12):8096-8106.

67. Mao Z, Bozzella M, Seluanov A, Gorbunova V. Comparison of nonhomologous end joining and homologous recombination in human cells. *DNA Repair (Amst).* 2008;7(10):1765-1771.

68. Ran FA, Hsu PD, Wright J, Agarwala V, Scott DA, Zhang F. Genome engineering using the CRISPR-Cas9 system. *Nat Protoc.* 2013;8(11):2281-2308.

69. Sansbury BM, Hewes AM, Kmiec EB. Understanding the diversity of genetic outcomes from CRISPR-Cas generated homology-directed repair. *Communications Biology.* 2019;2(1):458.

70. Su T, Liu F, Gu P, et al. A CRISPR-Cas9 Assisted Non-Homologous End-Joining Strategy for One-step Engineering of Bacterial Genome. *Scientific Reports.* 2016;6(1):37895.

71. Song B, Yang S, Hwang GH, Yu J, Bae S. Analysis of NHEJ-Based DNA Repair after CRISPR-Mediated DNA Cleavage. *Int J Mol Sci.* 2021;22(12).

72. Gallagher DN, Haber JE. Repair of a Site-Specific DNA Cleavage: Old-School Lessons for Cas9-Mediated Gene Editing. *ACS Chem Biol.* 2018;13(2):397-405.

73. Shams F, Bayat H, Mohammadian O, et al. Advance trends in targeting homology-directed repair for accurate gene editing: An inclusive review of small molecules and modified CRISPR-Cas9 systems. *Bioimpacts.* 2022;12(4):371-391.

74. Sun W, Liu H, Yin W, Qiao J, Zhao X, Liu Y. Strategies for Enhancing the Homology-Directed Repair Efficiency of CRISPR-Cas Systems. *Crispr j.* 2022;5(1):7-18.

75. Mao Z, Bozzella M, Seluanov A, Gorbunova V. Comparison of nonhomologous end joining and homologous recombination in human cells. *DNA repair.* 2008;7(10):1765-1771.

76. Nami F, Basiri M, Satarian L, Curtiss C, Baharvand H, Verfaillie C. Strategies for in vivo genome editing in nondividing cells. *Trends in biotechnology.* 2018;36(8):770-786.

77. Bassuk AG, Zheng A, Li Y, Tsang SH, Mahajan VB. Precision Medicine: Genetic Repair of Retinitis Pigmentosa in Patient-Derived Stem Cells. *Sci Rep.* 2016;6:19969.

78. Bohrer LR, Wiley LA, Burnight ER, et al. Correction of NR2E3 Associated Enhanced S-cone Syndrome Patient-specific iPSCs using CRISPR-Cas9. *Genes (Basel).* 2019;10(4).

79. Deng WL, Gao ML, Lei XL, et al. Gene Correction Reverses Ciliopathy and Photoreceptor Loss in iPSC-Derived Retinal Organoids from Retinitis Pigmentosa Patients. *Stem Cell Reports.* 2018;10(4):1267-1281.

80. Burnight ER, Gupta M, Wiley LA, et al. Using CRISPR-Cas9 to Generate Gene-Corrected Autologous iPSCs for the Treatment of Inherited Retinal Degeneration. *Mol Ther.* 2017;25(9):1999-2013.

81. Vagni P, Perlini LE, Chenais NAL, et al. Gene Editing Preserves Visual Functions in a Mouse Model of Retinal Degeneration. *Front Neurosci.* 2019;13:945.

82. Sanjurjo-Soriano C, Erkilic N, Baux D, et al. Genome Editing in Patient iPSCs Corrects the Most Prevalent USH2A Mutations and Reveals Intriguing Mutant mRNA Expression Profiles. *Mol Ther Methods Clin Dev.* 2020;17:156-173.

83. Cai Y, Cheng T, Yao Y, et al. In vivo genome editing rescues photoreceptor degeneration via a Cas9/RecA-mediated homology-directed repair pathway. *Sci Adv.* 2019;5(4):eaav3335.

84. Suzuki K, Tsunekawa Y, Hernandez-Benitez R, et al. In vivo genome editing via CRISPR/Cas9 mediated homology-independent targeted integration. *Nature.* 2016;540(7631):144-149.

85. Bakondi B, Lv W, Lu B, et al. In Vivo CRISPR/Cas9 Gene Editing Corrects Retinal Dystrophy in the S334ter-3 Rat Model of Autosomal Dominant Retinitis Pigmentosa. *Mol Ther.* 2016;24(3):556-563.

86. Giannelli SG, Luoni M, Castoldi V, et al. Cas9/sgRNA selective targeting of the P23H Rhodopsin mutant allele for treating retinitis pigmentosa by intravitreal AAV9.PHP.B-based delivery. *Hum Mol Genet.* 2018;27(5):761-779.

87. Li P, Kleinstiver BP, Leon MY, et al. Allele-Specific CRISPR-Cas9 Genome Editing of the Single-Base P23H Mutation for Rhodopsin-Associated Dominant Retinitis Pigmentosa. *Crispr j.* 2018;1(1):55-64.

88. Tsai YT, Wu WH, Lee TT, et al. Clustered Regularly Interspaced Short Palindromic Repeats-Based Genome Surgery for the Treatment of Autosomal Dominant Retinitis Pigmentosa. *Ophthalmology.* 2018;125(9):1421-1430.

89. McCullough KT, Boye SL, Fajardo D, et al. Somatic Gene Editing of GUCY2D by AAV-CRISPR/Cas9 Alters Retinal Structure and Function in Mouse and Macaque. *Hum Gene Ther.* 2019;30(5):571-589.

90. Maeder ML, Stefanidakis M, Wilson CJ, et al. Development of a gene-editing approach to restore vision loss in Leber congenital amaurosis type 10. *Nat Med.* 2019;25(2):229-233.

91. Latella MC, Di Salvo MT, Cocchiarella F, et al. In vivo Editing of the Human Mutant Rhodopsin Gene by Electroporation of Plasmid-based CRISPR/Cas9 in the Mouse Retina. *Mol Ther Nucleic Acids.* 2016;5(11):e389.

92. Kim E, Koo T, Park SW, et al. In vivo genome editing with a small Cas9 orthologue derived from Campylobacter jejuni. *Nat Commun.* 2017;8:14500.

93. Nguyen Tran MT, Mohd Khalid MKN, Wang Q, et al. Engineering domain-inlaid SaCas9 adenine base editors with reduced RNA off-targets and increased on-target DNA editing. *Nat Commun.* 2020;11(1):4871.

94. Suh S, Choi EH, Leinonen H, et al. Restoration of visual function in adult mice with an inherited retinal disease via adenine base editing. *Nat Biomed Eng.* 2020.

95. Moreno AM, Fu X, Zhu J, et al. In Situ Gene Therapy via AAV-CRISPR-Cas9-Mediated Targeted Gene Regulation. *Mol Ther.* 2018;26(7):1818-1827.

96. Komor AC, Badran AH, Liu DR. CRISPR-Based Technologies for the Manipulation of Eukaryotic Genomes. *Cell.* 2017;168(1-2):20-36.

97. Nishida K, Arazoe T, Yachie N, et al. Targeted nucleotide editing using hybrid prokaryotic and vertebrate adaptive immune systems. *Science.* 2016;353(6305).

98. Anzalone AV, Randolph PB, Davis JR, et al. Search-and-replace genome editing without double-strand breaks or donor DNA. *Nature.* 2019;576(7785):149-157.

99. Yeh W-H, Chiang H, Rees HA, Edge AS, Liu DR. In vivo base editing of post-mitotic sensory cells. *Nature communications.* 2018;9(1):1-10.

100. Gaudelli NM, Komor AC, Rees HA, et al. Programmable base editing of A• T to G• C in genomic DNA without DNA cleavage. *Nature.* 2017;551(7681):464-471.

101. Komor AC, Kim YB, Packer MS, Zuris JA, Liu DR. Programmable editing of a target base in genomic DNA without double-stranded DNA cleavage. *Nature.* 2016;533(7603):420-424.

102. Kantor A, McClements ME, MacLaren RE. CRISPR-Cas9 DNA Base-Editing and Prime-Editing. *Int J Mol Sci.* 2020;21(17).

103. Kurt IC, Zhou R, Iyer S, et al. CRISPR C-to-G base editors for inducing targeted DNA transversions in human cells. *Nature Biotechnology.* 2020:1-6.

104. Zhang X, Zhu B, Chen L, et al. Dual base editor catalyzes both cytosine and adenine base conversions in human cells. *Nature Biotechnology.* 2020:1-5.

105. Sakata RC, Ishiguro S, Mori H, et al. Base editors for simultaneous introduction of C-to-T and A-to-G mutations. *Nature Biotechnology.* 2020:1-5.

106. Grünewald J, Zhou R, Lareau CA, et al. A dual-deaminase CRISPR base editor enables concurrent adenine and cytosine editing. *Nature Biotechnology.* 2020:1-4.

107. Komor AC, Kim YB, Packer MS, Zuris JA, Liu DR. Programmable editing of a target base in genomic DNA without double-stranded DNA cleavage. *Nature.* 2016;533(7603):420-424.

108. Krokan HE, Bjørås M. Base excision repair. *Cold Spring Harbor perspectives in biology.* 2013;5(4):a012583.

109. Kunz C, Saito Y, Schär P. DNA Repair in mammalian cells: Mismatched repair: variations on a theme. *Cell Mol Life Sci.* 2009;66(6):1021-1038.

110. Kim YB, Komor AC, Levy JM, Packer MS, Zhao KT, Liu DR. Increasing the genome-targeting scope and precision of base editing with engineered Cas9-cytidine deaminase fusions. *Nature biotechnology.* 2017;35(4):371.

111. Bhattacharyya S, Soniat MM, Walker D, Jang S, Finkelstein IJ, Harshey RM. Phage Mu Gam protein promotes NHEJ in concert with Escherichia coli ligase. *Proceedings of the National Academy of Sciences.* 2018;115(50):E11614-E11622.

112. Komor AC, Zhao KT, Packer MS, et al. Improved base excision repair inhibition and bacteriophage Mu Gam protein yields C:G-to-T:A base editors with higher efficiency and product purity. *Sci Adv.* 2017;3(8):eaao4774.

113. Shee C, Cox BD, Gu F, et al. Engineered proteins detect spontaneous DNA breakage in human and bacterial cells. *Elife.* 2013;2:e01222.

114. Koblan LW, Doman JL, Wilson C, et al. Improving cytidine and adenine base editors by expression optimization and ancestral reconstruction. *Nature biotechnology.* 2018;36(9):843-846.

115. Nishida K, Arazoe T, Yachie N, et al. Targeted nucleotide editing using hybrid prokaryotic and vertebrate adaptive immune systems. *Science.* 2016;353(6305):aaf8729.

116. Thuronyi BW, Koblan LW, Levy JM, et al. Continuous evolution of base editors with expanded target compatibility and improved activity. *Nature biotechnology.* 2019;37(9):1070-1079.

117. Kleinstiver BP, Prew MS, Tsai SQ, et al. Engineered CRISPR-Cas9 nucleases with altered PAM specificities. *Nature.* 2015;523(7561):481-485.

118. Lee CM, Cradick TJ, Bao G. The Neisseria meningitidis CRISPR-Cas9 System Enables Specific Genome Editing in Mammalian Cells. *Mol Ther.* 2016;24(3):645-654.

119. Müller M, Lee CM, Gasiunas G, et al. Streptococcus thermophilus CRISPR-Cas9 Systems Enable Specific Editing of the Human Genome. *Mol Ther.* 2016;24(3):636-644.

120. Zetsche B, Gootenberg JS, Abudayyeh OO, et al. Cpf1 is a single RNA-guided endonuclease of a class 2 CRISPR-Cas system. *Cell.* 2015;163(3):759-771.

121. Alsøe L, Sarno A, Carracedo S, et al. Uracil accumulation and mutagenesis dominated by cytosine deamination in CpG dinucleotides in mice lacking UNG and SMUG1. *Scientific reports.* 2017;7(1):1-14.

122. Gaudelli NM, Komor AC, Rees HA, et al. Programmable base editing of A•T to G•C in genomic DNA without DNA cleavage. *Nature.* 2017;551(7681):464-471.

123. Huang TP, Zhao KT, Miller SM, et al. Circularly permuted and PAM-modified Cas9 variants broaden the targeting scope of base editors. *Nat Biotechnol.* 2019;37(6):626-631.

124. Yang L, Zhang X, Wang L, et al. Increasing targeting scope of adenosine base editors in mouse and rat embryos through fusion of TadA deaminase with Cas9 variants. *Protein Cell.* 2018;9(9):814-819.

125. Losey HC, Ruthenburg AJ, Verdine GL. Crystal structure of Staphylococcus aureus tRNA adenosine deaminase TadA in complex with RNA. *Nat Struct Mol Biol.* 2006;13(2):153-159.

126. Zuo E, Sun Y, Wei W, et al. Cytosine base editor generates substantial off-target single-nucleotide variants in mouse embryos. *Science.* 2019;364(6437):289-292.

127. Richter MF, Zhao KT, Eton E, et al. Phage-assisted evolution of an adenine base editor with improved Cas domain compatibility and activity. *Nature Biotechnology.* 2020:1-9.

128. Anzalone AV, Randolph PB, Davis JR, et al. Search-and-replace genome editing without double-strand breaks or donor DNA. *Nature.* 2019;576(7785):149-157.

129. Hosfield DJ, Mol CD, Shen B, Tainer JA. Structure of the DNA repair and replication endonuclease and exonuclease FEN-1: coupling DNA and PCNA binding to FEN-1 activity. *Cell.* 1998;95(1):135-146.

130. Liang P, Sun H, Sun Y, et al. Effective gene editing by high-fidelity base editor 2 in mouse zygotes. *Protein & Cell.* 2017;8(8):601-611.

131. Lee HK, Willi M, Miller SM, et al. Targeting fidelity of adenine and cytosine base editors in mouse embryos. *Nat Commun.* 2018;9(1):4804.

132. Rees HA, Komor AC, Yeh WH, et al. Improving the DNA specificity and applicability of base editing through protein engineering and protein delivery. *Nat Commun.* 2017;8:15790.

133. Kim K, Ryu SM, Kim ST, et al. Highly efficient RNA-guided base editing in mouse embryos. *Nat Biotechnol.* 2017;35(5):435-437.

134. Billon P, Bryant EE, Joseph SA, et al. CRISPR-Mediated Base Editing Enables Efficient Disruption of Eukaryotic Genes through Induction of STOP Codons. *Mol Cell.* 2017;67(6):1068-1079.e1064.

135. Kuscu C, Parlak M, Tufan T, et al. CRISPR-STOP: gene silencing through base-editing-induced nonsense mutations. *Nature Methods.* 2017;14(7):710-712.

136. Zhang Y, Qin W, Lu X, et al. Programmable base editing of zebrafish genome using a modified CRISPR-Cas9 system. *Nat Commun.* 2017;8(1):118.

137. Chadwick AC, Wang X, Musunuru K. In Vivo Base Editing of PCSK9 (Proprotein Convertase Subtilisin/Kexin Type 9) as a Therapeutic Alternative to Genome Editing. *Arterioscler Thromb Vasc Biol.* 2017;37(9):1741-1747.

138. Gehrke JM, Cervantes O, Clement MK, et al. An APOBEC3A-Cas9 base editor with minimized bystander and off-target activities. *Nature biotechnology.* 2018;36(10):977.

139. Hu JH, Miller SM, Geurts MH, et al. Evolved Cas9 variants with broad PAM compatibility and high DNA specificity. *Nature.* 2018;556(7699):57-63.

140. Liu Z, Chen M, Chen S, et al. Highly efficient RNA-guided base editing in rabbit. *Nature Communications.* 2018;9(1):2717.

141. Rossidis AC, Stratigis JD, Chadwick AC, et al. In utero CRISPR-mediated therapeutic editing of metabolic genes. *Nature medicine.* 2018;24(10):1513-1518.

142. Gapinske M, Luu A, Winter J, et al. CRISPR-SKIP: programmable gene splicing with single base editors. *Genome biology.* 2018;19(1):107.

143. Yeh WH, Chiang H, Rees HA, Edge ASB, Liu DR. In vivo base editing of post-mitotic sensory cells. *Nat Commun.* 2018;9(1):2184.

144. Zafra MP, Schatoff EM, Katti A, et al. Optimized base editors enable efficient editing in cells, organoids and mice. *Nature Biotechnology.* 2018;36(9):888-893.

145. Gehrke JM, Cervantes O, Clement MK, et al. An APOBEC3A-Cas9 base editor with minimized bystander and off-target activities. *Nature Biotechnology.* 2018;36(10):977-982.

146. Wang X, Li J, Wang Y, et al. Efficient base editing in methylated regions with a human APOBEC3A-Cas9 fusion. *Nature Biotechnology.* 2018;36(10):946-949.

147. Chatterjee P, Jakimo N, Jacobson JM. Minimal PAM specificity of a highly similar SpCas9 ortholog. *Science Advances.* 2018;4(10):eaau0766.

148. Lee JK, Jeong E, Lee J, et al. Directed evolution of CRISPR-Cas9 to increase its specificity. *Nature Communications.* 2018;9(1):3048.

149. Chatterjee P, Lee J, Nip L, et al. A Cas9 with PAM recognition for adenine dinucleotides. *Nature Communications.* 2020;11(1):2474.

150. Nishimasu H, Shi X, Ishiguro S, et al. Engineered CRISPR-Cas9 nuclease with expanded targeting space. *Science.* 2018;361(6408):1259-1262.

151. Tanaka S, Yoshioka S, Nishida K, Hosokawa H, Kakizuka A, Maegawa S. In vivo targeted single-nucleotide editing in zebrafish. *Scientific Reports.* 2018;8(1):11423.

152. Hess GT, Frésard L, Han K, et al. Directed evolution using dCas9-targeted somatic hypermutation in mammalian cells. *Nature methods.* 2016;13(12):1036.

153. Ma Y, Zhang J, Yin W, Zhang Z, Song Y, Chang X. Targeted AID-mediated mutagenesis (TAM) enables efficient genomic diversification in mammalian cells. *Nature methods.* 2016;13(12):1029-1035.

154. Jiang W, Feng S, Huang S, et al. BE-PLUS: a new base editing tool with broadened editing window and enhanced fidelity. *Cell Research.* 2018;28(8):855-861.

155. Li X, Wang Y, Liu Y, et al. Base editing with a Cpf1–cytidine deaminase fusion. *Nature Biotechnology.* 2018;36(4):324-327.

156. Qin W, Lu X, Liu Y, Bai H, Li S, Lin S. Precise A•T to G•C base editing in the zebrafish genome. *BMC Biology.* 2018;16(1):139.

157. Nishikura K. A-to-I editing of coding and non-coding RNAs by ADARs. *Nat Rev Mol Cell Biol.* 2016;17(2):83-96.

158. Fry LE, Peddle CF, Barnard AR, McClements ME, MacLaren RE. RNA editing as a therapeutic approach for retinal gene therapy requiring long coding sequences. *Int J Mol Sci.* 2020;21(3).

159. Gilbert LA, Horlbeck MA, Adamson B, et al. Genome-Scale CRISPR-Mediated Control of Gene Repression and Activation. *Cell.* 2014;159(3):647-661.

160. Radzisheuskaya A, Shlyueva D, Müller I, Helin K. Optimizing sgRNA position markedly improves the efficiency of CRISPR/dCas9-mediated transcriptional repression. *Nucleic Acids Res.* 2016;44(18):e141.

161. Grimm D, Wang L, Lee JS, et al. Argonaute proteins are key determinants of RNAi efficacy, toxicity, and persistence in the adult mouse liver. *J Clin Invest.* 2010;120(9):3106-3119.

162. Jackson AL, Burchard J, Schelter J, et al. Widespread siRNA "off-target" transcript silencing mediated by seed region sequence complementarity. *Rna.* 2006;12(7):1179-1187.

163. Kanasty RL, Whitehead KA, Vegas AJ, Anderson DG. Action and reaction: the biological response to siRNA and its delivery vehicles. *Mol Ther.* 2012;20(3):513-524.

164. Shalem O, Sanjana NE, Zhang F. High-throughput functional genomics using CRISPR-Cas9. *Nat Rev Genet.* 2015;16(5):299-311.

165. Choo Y, Sánchez-García I, Klug A. In vivo repression by a site-specific DNA-binding protein designed against an oncogenic sequence. *Nature.* 1994;372(6507):642-645.

166. Larson MH, Gilbert LA, Wang X, Lim WA, Weissman JS, Qi LS. CRISPR interference (CRISPRi) for sequence-specific control of gene expression. *Nat Protoc.* 2013;8(11):2180-2196.

167. Li Y, Jiang Y, Chen H, et al. Modular construction of mammalian gene circuits using TALE transcriptional repressors. *Nat Chem Biol.* 2015;11(3):207-213.

168. Qi LS, Larson MH, Gilbert LA, et al. Repurposing CRISPR as an RNA-guided platform for sequence-specific control of gene expression. *Cell.* 2013;152(5):1173-1183.

169. Garriga-Canut M, Agustín-Pavón C, Herrmann F, et al. Synthetic zinc finger repressors reduce mutant huntingtin expression in the brain of R6/2 mice. *Proc Natl Acad Sci U S A.* 2012;109(45):E3136-3145.

170. Gilbert LA, Larson MH, Morsut L, et al. CRISPR-mediated modular RNA-guided regulation of transcription in eukaryotes. *Cell.* 2013;154(2):442-451.

171. Kearns NA, Pham H, Tabak B, et al. Functional annotation of native enhancers with a Cas9-histone demethylase fusion. *Nat Methods.* 2015;12(5):401-403.

172. Snowden AW, Gregory PD, Case CC, Pabo CO. Gene-specific targeting of H3K9 methylation is sufficient for initiating repression in vivo. *Curr Biol.* 2002;12(24):2159-2166.

173. Beerli RR, Segal DJ, Dreier B, Barbas CF, 3rd. Toward controlling gene expression at will: specific regulation of the erbB-2/HER-2 promoter by using polydactyl zinc finger proteins constructed from modular building blocks. *Proc Natl Acad Sci U S A.* 1998;95(25):14628-14633.

174. Cong L, Zhou R, Kuo YC, Cunniff M, Zhang F. Comprehensive interrogation of natural TALE DNA-binding modules and transcriptional repressor domains. *Nat Commun.* 2012;3:968.

175. Lawrence M, Daujat S, Schneider R. Lateral Thinking: How Histone Modifications Regulate Gene Expression. *Trends Genet.* 2016;32(1):42-56.

176. Friedman JR, Fredericks WJ, Jensen DE, et al. KAP-1, a novel corepressor for the highly conserved KRAB repression domain. *Genes Dev.* 1996;10(16):2067-2078.

177. Kim SS, Chen YM, O'Leary E, Witzgall R, Vidal M, Bonventre JV. A novel member of the RING finger family, KRIP-1, associates with the KRAB-A transcriptional repressor domain of zinc finger proteins. *Proc Natl Acad Sci U S A.* 1996;93(26):15299-15304.

178. Moosmann P, Georgiev O, Le Douarin B, Bourquin JP, Schaffner W. Transcriptional repression by RING finger protein TIF1 beta that interacts with the KRAB repressor domain of KOX1. *Nucleic Acids Res.* 1996;24(24):4859-4867.

179. Chung JY, Ain QU, Song Y, Yong SB, Kim YH. Targeted delivery of CRISPR interference system against Fabp4 to white adipocytes ameliorates obesity, inflammation, hepatic steatosis, and insulin resistance. *Genome Res.* 2019;29(9):1442-1452.

180. Thakore PI, Kwon JB, Nelson CE, et al. RNA-guided transcriptional silencing in vivo with S. aureus CRISPR-Cas9 repressors. *Nat Commun.* 2018;9(1):1674.

181. Burnight ER, Wiley LA, Drack AV, et al. CEP290 gene transfer rescues Leber congenital amaurosis cellular phenotype. *Gene Ther.* 2014;21(7):662-672.

182. Seo S, Mullins RF, Dumitrescu AV, et al. Subretinal gene therapy of mice with Bardet-Biedl syndrome type 1. *Invest Ophthalmol Vis Sci.* 2013;54(9):6118-6132.

183. Olsson JE, Gordon JW, Pawlyk BS, et al. Transgenic mice with a rhodopsin mutation (Pro23His): a mouse model of autosomal dominant retinitis pigmentosa. *Neuron.* 1992;9(5):815-830.

184. Hsu MN, Chang YH, Truong VA, Lai PL, Nguyen TKN, Hu YC. CRISPR technologies for stem cell engineering and regenerative medicine. *Biotechnol Adv.* 2019;37(8):107447.

185. Larouche J, Aguilar CA. New Technologies To Enhance In Vivo Reprogramming for Regenerative Medicine. *Trends Biotechnol.* 2019;37(6):604-617.

186. Maeder ML, Linder SJ, Cascio VM, Fu Y, Ho QH, Joung JK. CRISPR RNA-guided activation of endogenous human genes. *Nat Methods.* 2013;10(10):977-979.

187. Balboa D, Weltner J, Eurola S, Trokovic R, Wartiovaara K, Otonkoski T. Conditionally Stabilized dCas9 Activator for Controlling Gene Expression in Human Cell Reprogramming and Differentiation. *Stem Cell Reports.* 2015;5(3):448-459.

188. Beerli RR, Dreier B, Barbas CF, 3rd. Positive and negative regulation of endogenous genes by designed transcription factors. *Proc Natl Acad Sci U S A.* 2000;97(4):1495-1500.

189. Konermann S, Brigham MD, Trevino AE, et al. Genome-scale transcriptional activation by an engineered CRISPR-Cas9 complex. *Nature.* 2015;517(7536):583-588.

190. Maeder ML, Linder SJ, Reyon D, et al. Robust, synergistic regulation of human gene expression using TALE activators. *Nat Methods.* 2013;10(3):243-245.

191. Mali P, Aach J, Stranges PB, et al. CAS9 transcriptional activators for target specificity screening and paired nickases for cooperative genome engineering. *Nat Biotechnol.* 2013;31(9):833-838.

192. Perez-Pinera P, Ousterout DG, Brunger JM, et al. Synergistic and tunable human gene activation by combinations of synthetic transcription factors. *Nat Methods.* 2013;10(3):239-242.

193. Zhang F, Cong L, Lodato S, Kosuri S, Church GM, Arlotta P. Efficient construction of sequence-specific TAL effectors for modulating mammalian transcription. *Nat Biotechnol.* 2011;29(2):149-153.

194. Cheng AW, Wang H, Yang H, et al. Multiplexed activation of endogenous genes by CRISPR-on, an RNA-guided transcriptional activator system. *Cell Res.* 2013;23(10):1163-1171.

195. Farzadfard F, Perli SD, Lu TK. Tunable and multifunctional eukaryotic transcription factors based on CRISPR/Cas. *ACS Synth Biol.* 2013;2(10):604-613.

196. Perez-Pinera P, Kocak DD, Vockley CM, et al. RNA-guided gene activation by CRISPR-Cas9-based transcription factors. *Nat Methods.* 2013;10(10):973-976.

197. Chavez A, Tuttle M, Pruitt BW, et al. Comparison of Cas9 activators in multiple species. *Nat Methods.* 2016;13(7):563-567.

198. Tanenbaum ME, Gilbert LA, Qi LS, Weissman JS, Vale RD. A protein-tagging system for signal amplification in gene expression and fluorescence imaging. *Cell.* 2014;159(3):635-646.

199. Konermann S, Lotfy P, Brideau NJ, Oki J, Shokhirev MN, Hsu PD. Transcriptome Engineering with RNA-Targeting Type VI-D CRISPR Effectors. *Cell.* 2018;173(3):665-676.e614.

200. Lau CH, Suh Y. In vivo epigenome editing and transcriptional modulation using CRISPR technology. *Transgenic Res.* 2018;27(6):489-509.

201. Liu XS, Wu H, Ji X, et al. Editing DNA Methylation in the Mammalian Genome. *Cell.* 2016;167(1):233-247.e217.

202. Bordet T, Behar-Cohen F. Ocular gene therapies in clinical practice: viral vectors and nonviral alternatives. *Drug Discov Today.* 2019;24(8):1685-1693.

203. Gillmore JD, Gane E, Taubel J, et al. CRISPR-Cas9 in vivo gene editing for transthyretin amyloidosis. *New England Journal of Medicine.* 2021;385(6):493-502.

204. Maier MA, Jayaraman M, Matsuda S, et al. Biodegradable lipids enabling rapidly eliminated lipid nanoparticles for systemic delivery of RNAi therapeutics. *Molecular Therapy.* 2013;21(8):1570-1578.

205. Witzigmann D, Kulkarni JA, Leung J, Chen S, Cullis PR, van der Meel R. Lipid nanoparticle technology for therapeutic gene regulation in the liver. *Advanced drug delivery reviews.* 2020;159:344-363.

206. Li L, He ZY, Wei XW, Gao GP, Wei YQ. Challenges in CRISPR/CAS9 Delivery: Potential Roles of Nonviral Vectors. *Hum Gene Ther.* 2015;26(7):452-462.

207. Li SD, Huang L. Non-viral is superior to viral gene delivery. *J Control Release.* 2007;123(3):181-183.

208. Pack DW, Hoffman AS, Pun S, Stayton PS. Design and development of polymers for gene delivery. *Nat Rev Drug Discov.* 2005;4(7):581-593.

209. Davis ME. Non-viral gene delivery systems. *Curr Opin Biotechnol.* 2002;13(2):128-131.

210. Kim S, Kim D, Cho SW, Kim J, Kim JS. Highly efficient RNA-guided genome editing in human cells via delivery of purified Cas9 ribonucleoproteins. *Genome Res.* 2014;24(6):1012-1019.

211. Mintzer MA, Simanek EE. Nonviral vectors for gene delivery. *Chem Rev.* 2009;109(2):259-302.

212. Veres A, Gosis BS, Ding Q, et al. Low incidence of off-target mutations in individual CRISPR-Cas9 and TALEN targeted human stem cell clones detected by whole-genome sequencing. *Cell Stem Cell.* 2014;15(1):27-30.

213. Wang H, Yang H, Shivalila CS, et al. One-step generation of mice carrying mutations in multiple genes by CRISPR/Cas-mediated genome engineering. *Cell.* 2013;153(4):910-918.

214. Eoh J, Gu L. Biomaterials as vectors for the delivery of CRISPR-Cas9. *Biomater Sci.* 2019;7(4):1240-1261.

215. Wei T, Cheng Q, Min YL, Olson EN, Siegwart DJ. Systemic nanoparticle delivery of CRISPR-Cas9 ribonucleoproteins for effective tissue specific genome editing. *Nat Commun.* 2020;11(1):3232.

216. Wang HX, Song Z, Lao YH, et al. Nonviral gene editing via CRISPR/Cas9 delivery by membrane-disruptive and endosomolytic helical polypeptide. *Proc Natl Acad Sci U S A.* 2018;115(19):4903-4908.

217. Charbel Issa P, MacLaren RE. Non-viral retinal gene therapy: a review. *Clin Exp Ophthalmol.* 2012;40(1):39-47.

218. Johnson LN, Cashman SM, Read SP, Kumar-Singh R. Cell penetrating peptide POD mediates delivery of recombinant proteins to retina, cornea and skin. *Vision Res.* 2010;50(7):686-697.

219. Leaderer D, Cashman SM, Kumar-Singh R. G-quartet oligonucleotide mediated delivery of proteins into photoreceptors and retinal pigment epithelium via intravitreal injection. *Exp Eye Res.* 2016;145:380-392.

220. Cai X, Nash Z, Conley SM, Fliesler SJ, Cooper MJ, Naash MI. A partial structural and functional rescue of a retinitis pigmentosa model with compacted DNA nanoparticles. *PLoS One.* 2009;4(4):e5290.

221. Cai X, Conley SM, Nash Z, Fliesler SJ, Cooper MJ, Naash MI. Gene delivery to mitotic and postmitotic photoreceptors via compacted DNA nanoparticles results in improved phenotype in a mouse model of retinitis pigmentosa. *Faseb j.* 2010;24(4):1178-1191.

222. Ding XQ, Quiambao AB, Fitzgerald JB, Cooper MJ, Conley SM, Naash MI. Ocular delivery of compacted DNA-nanoparticles does not elicit toxicity in the mouse retina. *PLoS One.* 2009;4(10):e7410.

223. Han Z, Conley SM, Makkia RS, Cooper MJ, Naash MI. DNA nanoparticle-mediated ABCA4 delivery rescues Stargardt dystrophy in mice. *J Clin Invest.* 2012;122(9):3221-3226.

224. Han Z, Banworth MJ, Makkia R, et al. Genomic DNA nanoparticles rescue rhodopsin-associated retinitis pigmentosa phenotype. *Faseb j.* 2015;29(6):2535-2544.

225. Agudelo D, Carter S, Velimirovic M, et al. Versatile and robust genome editing with Streptococcus thermophilus CRISPR1-Cas9. *Genome Res.* 2020;30(1):107-117.

226. Edraki A, Mir A, Ibraheim R, et al. A Compact, High-Accuracy Cas9 with a Dinucleotide PAM for In Vivo Genome Editing. *Mol Cell.* 2019;73(4):714-726.e714.

227. Hu Z, Wang S, Zhang C, et al. A compact Cas9 ortholog from Staphylococcus Auricularis (SauriCas9) expands the DNA targeting scope. *PLoS Biol.* 2020;18(3):e3000686.

228. Ibraheim R, Song CQ, Mir A, Amrani N, Xue W, Sontheimer EJ. All-in-one adeno-associated virus delivery and genome editing by Neisseria meningitidis Cas9 in vivo. *Genome Biol.* 2018;19(1):137.

229. Ran FA, Cong L, Yan WX, et al. In vivo genome editing using Staphylococcus aureus Cas9. *Nature.* 2015;520(7546):186-191.

230. Wang D, Zhang F, Gao G. CRISPR-Based Therapeutic Genome Editing: Strategies and In Vivo Delivery by AAV Vectors. *Cell.* 2020;181(1):136-150.

231. De Caneva A, Porro F, Bortolussi G, et al. Coupling AAV-mediated promoterless gene targeting to SaCas9 nuclease to efficiently correct liver metabolic diseases. *JCI insight.* 2019;4(15).

232. Nishiyama J, Mikuni T, Yasuda R. Virus-Mediated Genome Editing via Homology-Directed Repair in Mitotic and Postmitotic Cells in Mammalian Brain. *Neuron.* 2017;96(4):755-768.e755.

233. Yang Y, Wang L, Bell P, et al. A dual AAV system enables the Cas9-mediated correction of a metabolic liver disease in newborn mice. *Nat Biotechnol.* 2016;34(3):334-338.

234. Hinderer C, Katz N, Buza EL, et al. Severe Toxicity in Nonhuman Primates and Piglets Following High-Dose Intravenous Administration of an Adeno-Associated Virus Vector Expressing Human SMN. *Hum Gene Ther.* 2018;29(3):285-298.

235. Wang L, Smith J, Breton C, et al. Meganuclease targeting of PCSK9 in macaque liver leads to stable reduction in serum cholesterol. *Nat Biotechnol.* 2018;36(8):717-725.

236. Wilson JM, Flotte TR. Moving Forward After Two Deaths in a Gene Therapy Trial of Myotubular Myopathy. *Hum Gene Ther.* 2020;31(13-14):695-696.

237. Esvelt KM, Mali P, Braff JL, Moosburner M, Yaung SJ, Church GM. Orthogonal Cas9 proteins for RNA-guided gene regulation and editing. *Nat Methods.* 2013;10(11):1116-1121.

238. Hou Z, Zhang Y, Propson NE, et al. Efficient genome engineering in human pluripotent stem cells using Cas9 from Neisseria meningitidis. *Proc Natl Acad Sci U S A.* 2013;110(39):15644-15649.

239. Lee B, Lee K, Panda S, et al. Nanoparticle delivery of CRISPR into the brain rescues a mouse model of fragile X syndrome from exaggerated repetitive behaviours. *Nature Biomedical Engineering.* 2018;2(7):497-507.

240. Lee K, Conboy M, Park HM, et al. Nanoparticle delivery of Cas9 ribonucleoprotein and donor DNA in vivo induces homology-directed DNA repair. *Nature Biomedical Engineering.* 2017;1(11):889-901.

241. Trigueros S, B. Domènech E, Toulis V, Marfany G. In Vitro Gene Delivery in Retinal Pigment Epithelium Cells by Plasmid DNA-Wrapped Gold Nanoparticles. *Genes.* 2019;10(4):289.

242. Wakabayashi-Ito N, Nagata S. Characterization of the regulatory elements in the promoter of the human elongation factor-1 alpha gene. *J Biol Chem.* 1994;269(47):29831-29837.

243. Lu J, Wu T, Zhang B, et al. Types of nuclear localization signals and mechanisms of protein import into the nucleus. *Cell Communication and Signaling.* 2021;19(1):60.

244. Goodwin EC, Rottman FM. The 3'-flanking sequence of the bovine growth hormone gene contains novel elements required for efficient and accurate polyadenylation. *J Biol Chem.* 1992;267(23):16330-16334.

245. Isomura H, Stinski MF. The human cytomegalovirus major immediate-early enhancer determines the efficiency of immediate-early gene transcription and viral replication in permissive cells at low multiplicity of infection. *J Virol.* 2003;77(6):3602-3614.

246. Li SP, Feng JJ, Wang HG, Wang XF, Lv ZJ. [The effects of SV40 PolyA sequence and its AATAAA signal on upstream GFP gene expression and transcription termination]. *Yi Chuan.* 2012;34(1):113-119.

247. Xie H, Ge X, Yang F, et al. High-fidelity SaCas9 identified by directional screening in human cells. *PLoS Biol.* 2020;18(7):e3000747.

248. Lee K, Conboy M, Park HM, et al. Nanoparticle delivery of Cas9 ribonucleoprotein and donor DNA in vivo induces homology-directed DNA repair. *Nature biomedical engineering.* 2017;1(11):889-901.

249. Wang P, Zhang L, Zheng W, et al. Thermo-triggered Release of CRISPR-Cas9 System by Lipid-Encapsulated Gold Nanoparticles for Tumor Therapy. *Angew Chem Int Ed Engl.* 2018;57(6):1491-1496.

250. Trigueros S, Domènech EB, Toulis V, Marfany G. In Vitro Gene Delivery in Retinal Pigment Epithelium Cells by Plasmid DNA-Wrapped Gold Nanoparticles. *Genes (Basel).* 2019;10(4).

251. Lim BJ, Berkeley RF, Debelouchina GT. Fused Split Inteins: Tools for Introducing Multiple Protein Modifications. *Methods Mol Biol.* 2020;2133:163-181.

252. Tornabene P, Trapani I, Centrulo M, et al. Inclusion of a degron reduces levels of undesired inteins after AAV-mediated protein trans-splicing in the retina. *Molecular Therapy - Methods & Clinical Development.* 2021;23:448-459.

253. Pausch P, Al-Shayeb B, Bisom-Rapp E, et al. CRISPR-CasΦ from huge phages is a hypercompact genome editor. *Science.* 2020;369(6501):333-337.

254. Yan WX, Hunnewell P, Alfonse LE, et al. Functionally diverse type V CRISPR-Cas systems. *Science.* 2019;363(6422):88-91.

255. Aliaga Goltsman DS, Alexander LM, Devoto AE, et al. Novel Type V-A CRISPR Effectors Are Active Nucleases with Expanded Targeting Capabilities. *Crispr j.* 2020;3(6):454-461.

256. Burstein D, Harrington LB, Strutt SC, et al. New CRISPR-Cas systems from uncultivated microbes. *Nature.* 2017;542(7640):237-241.

257. Jiang Y, Tang R, Duncan B, et al. Direct cytosolic delivery of siRNA using nanoparticle-stabilized nanocapsules. *Angew Chem Int Ed Engl.* 2015;54(2):506-510.

258. Anzalone AV, Koblan LW, Liu DR. Genome editing with CRISPR–Cas nucleases, base editors, transposases and prime editors. *Nature biotechnology.* 2020;38(7):824-844.

259. Doman JL, Raguram A, Newby GA, Liu DR. Evaluation and minimization of Cas9-independent off-target DNA editing by cytosine base editors. *Nature biotechnology.* 2020;38(5):620-628.

260. Schoenmaker L, Witzigmann D, Kulkarni JA, et al. mRNA-lipid nanoparticle COVID-19 vaccines: Structure and stability. *International Journal of Pharmaceutics.* 2021;601:120586.

261. Kim K, Park SW, Kim JH, et al. Genome surgery using Cas9 ribonucleoproteins for the treatment of age-related macular degeneration. *Genome research.* 2017;27(3):419-426.

262. Huu VAN, Luo J, Zhu J, et al. Light-responsive nanoparticle depot to control release of a small molecule angiogenesis inhibitor in the posterior segment of the eye. *Journal of Controlled Release.* 2015;200:71-77.

263. Asteriti S, Dal Cortivo G, Pontelli V, Cangiano L, Buffelli M, Dell'Orco D. Effective delivery of recombinant proteins to rod photoreceptors via lipid nanovesicles. *Biochemical and biophysical research communications.* 2015;461(4):665-670.

264. Benedicto I, Lehmann GL, Ginsberg M, et al. Concerted regulation of retinal pigment epithelium basement membrane and barrier function by angiocrine factors. *Nature communications.* 2017;8(1):1-12.

265. Yeagle P. Modulation of membrane function by cholesterol. *Biochimie.* 1991;73(10):1303-1310.

266. Albert AD, Boesze-Battaglia K. The role of cholesterol in rod outer segment membranes. *Progress in lipid research.* 2005;44(2-3):99-124.

267. Wong RW. New Activities of the Nuclear Pore Complexes. *Cells.* 2021;10(8).

268. Freitas N, Cunha C. Mechanisms and signals for the nuclear import of proteins. *Curr Genomics.* 2009;10(8):550-557.

269. Lange A, Mills RE, Lange CJ, Stewart M, Devine SE, Corbett AH. Classical Nuclear Localization Signals: Definition, Function, and Interaction with Importin α*. *Journal of Biological Chemistry.* 2007;282(8):5101-5105.

270. Bai H, Lester GMS, Petishnok LC, Dean DA. Cytoplasmic transport and nuclear import of plasmid DNA. *Biosci Rep.* 2017;37(6).

271. Darquet A, Cameron B, Wils P, Scherman D, Crouzet J. A new DNA vehicle for nonviral gene delivery: supercoiled minicircle. *Gene therapy.* 1997;4(12):1341-1349.

272. Kay MA, He C-Y, Chen Z-Y. A robust system for production of minicircle DNA vectors. *Nature biotechnology.* 2010;28(12):1287-1289.

273. Jia F, Wilson KD, Sun N, et al. A nonviral minicircle vector for deriving human iPS cells. *Nature methods.* 2010;7(3):197-199.

274. Li L, Dimitriadis EK, Yang Y, et al. Production and Characterization of Novel Recombinant Adeno-Associated Virus Replicative-Form Genomes: A Eukaryotic Source of DNA for Gene Transfer. *PLOS ONE.* 2013;8(8):e69879.

275. Konermann S, Brigham MD, Trevino A, et al. Optical control of mammalian endogenous transcription and epigenetic states. *Nature.* 2013;500(7463):472-476.

276. Thakore PI, Black JB, Hilton IB, Gersbach CA. Editing the epigenome: technologies for programmable transcription and epigenetic modulation. *Nat Methods.* 2016;13(2):127-137.

277. Chavez A, Scheiman J, Vora S, et al. Highly efficient Cas9-mediated transcriptional programming. *Nat Methods.* 2015;12(4):326-328.

278. Zalatan JG, Lee ME, Almeida R, et al. Engineering complex synthetic transcriptional programs with CRISPR RNA scaffolds. *Cell.* 2015;160(1-2):339-350.

279. Nuñez JK, Chen J, Pommier GC, et al. Genome-wide programmable transcriptional memory by CRISPR-based epigenome editing. *Cell.* 2021;184(9):2503-2519.e2517.

280. O'Geen H, Tomkova M, Combs JA, Tilley EK, Segal David J. Determinants of heritable gene silencing for KRAB-dCas9 + DNMT3 and Ezh2-dCas9 + DNMT3 hit-and-run epigenome editing. *Nucleic Acids Research.* 2022;50(6):3239-3253.

281. Schep R, Brinkman EK, Leemans C, et al. Impact of chromatin context on Cas9-induced DNA double-strand break repair pathway balance. *Mol Cell.* 2021;81(10):2216-2230.e2210.

282. Yeo NC, Chavez A, Lance-Byrne A, et al. An enhanced CRISPR repressor for targeted mammalian gene regulation. *Nat Methods.* 2018;15(8):611-616.

283. Jones PL, Veenstra GJ, Wade PA, et al. Methylated DNA and MeCP2 recruit histone deacetylase to repress transcription. *Nat Genet.* 1998;19(2):187-191.

284. Nan X, Ng HH, Johnson CA, et al. Transcriptional repression by the methyl-CpG-binding protein MeCP2 involves a histone deacetylase complex. *Nature.* 1998;393(6683):386-389.

285. Corish P, Tyler-Smith C. Attenuation of green florescent protein half-life in mammalian cells. *Protein Engineering, Design and Selection.* 1999;12(12):1035-1040.

286. Kitsera N, Khobta A, Epe B. Destabilized green florescent protein detects rapid removal of transcription blocks after genotoxic exposure. *Biotechniques.* 2007;43(2):222-227.

287. Nan X, Campoy FJ, Bird A. MeCP2 is a transcriptional repressor with abundant binding sites in genomic chromatin. *Cell.* 1997;88(4):471-481.

288. Kokura K, Kaul SC, Wadhwa R, et al. The Ski protein family is required for MeCP2-mediated transcriptional repression. *J Biol Chem.* 2001;276(36):34115-34121.

289. Kaludov NK, Wolffe AP. MeCP2 driven transcriptional repression in vitro: selectivity for methylated DNA, action at a distance and contacts with the basal transcription machinery. *Nucleic Acids Res.* 2000;28(9):1921-1928.

290. Kimura H, Shiota K. Methyl-CpG-binding protein, MeCP2, is a target molecule for maintenance DNA methyltransferase, Dnmt1. *Journal of Biological Chemistry.* 2003;278(7):4806-4812.

291. Jolly JK, Bridge H, MacLaren RE. Outcome Measures Used in Ocular Gene Therapy Trials: A Scoping Review of Current Practice. *Front Pharmacol.* 2019;10:1076.

292. Montana CL, Kolesnikov AV, Shen SQ, Myers CA, Kefalov VJ, Corbo JC. Reprogramming of adult rod photoreceptors prevents retinal degeneration. *Proc Natl Acad Sci U S A.* 2013;110(5):1732-1737.

293. Cheng H, Khanna H, Oh EC, Hicks D, Mitton KP, Swaroop A. Photoreceptor-specific nuclear receptor NR2E3 functions as a transcriptional activator in rod photoreceptors. *Hum Mol Genet.* 2004;13(15):1563-1575.

294. Singh MS, Park SS, Albini TA, et al. Retinal stem cell transplantation: Balancing safety and potential. *Prog Retin Eye Res.* 2020;75:100779.

295. Eiraku M, Takata N, Ishibashi H, et al. Self-organizing optic-cup morphogenesis in three-dimensional culture. *Nature.* 2011;472(7341):51-56.

296. Chichagova V, Hilgen G, Ghareeb A, et al. Human iPSC differentiation to retinal organoids in response to IGF1 and BMP4 activation is line- and method-dependent. *Stem Cells.* 2020;38(2):195-201.

297. Zhong X, Gutierrez C, Xue T, et al. Generation of three-dimensional retinal tissue with functional photoreceptors from human iPSCs. *Nat Commun.* 2014;5:4047.

298. Hallam D, Hilgen G, Dorgau B, et al. Human-Induced Pluripotent Stem Cells Generate Light Responsive Retinal Organoids with Variable and Nutrient-Dependent Efficiency. *Stem Cells.* 2018;36(10):1535-1551.

299. Chichagova V, Dorgau B, Felemban M, Georgiou M, Armstrong L, Lako M. Differentiation of Retinal Organoids from Human Pluripotent Stem Cells. *Curr Protoc Stem Cell Biol.* 2019;50(1):e95.

300. Reichman S, Slembrouck A, Gagliardi G, et al. Generation of Storable Retinal Organoids and Retinal Pigmented Epithelium from Adherent Human iPS Cells in Xeno-Free and Feeder-Free Conditions. *Stem Cells.* 2017;35(5):1176-1188.

301. Farjo Q, Jackson AU, Xu J, et al. Molecular characterization of the murine neural retina leucine zipper gene, Nrl. *Genomics.* 1993;18(2):216-222.

302. Kautzmann MA, Kim DS, Felder-Schmittbuhl MP, Swaroop A. Combinatorial regulation of photoreceptor differentiation factor, neural retina leucine zipper gene NRL, revealed by in vivo promoter analysis. *J Biol Chem.* 2011;286(32):28247-28255.

303. Mears AJ, Kondo M, Swain PK, et al. Nrl is required for rod photoreceptor development. *Nat Genet.* 2001;29(4):447-452.

304. Oh EC, Khan N, Novelli E, Khanna H, Strettoi E, Swaroop A. Transformation of cone precursors to functional rod photoreceptors by bZIP transcription factor NRL. *Proc Natl Acad Sci U S A.* 2007;104(5):1679-1684.

305. Rehemtulla A, Warwar R, Kumar R, Ji X, Zack DJ, Swaroop A. The basic motif-leucine zipper transcription factor Nrl can positively regulate rhodopsin gene expression. *Proc Natl Acad Sci U S A.* 1996;93(1):191-195.

306. Swain PK, Hicks D, Mears AJ, et al. Multiple phosphorylated isoforms of NRL are expressed in rod photoreceptors. *J Biol Chem.* 2001;276(39):36824-36830.

307. Roger JE, Ranganath K, Zhao L, et al. Preservation of cone photoreceptors after a rapid yet transient degeneration and remodeling in cone-only Nrl-/- mouse retina. *J Neurosci.* 2012;32(2):528-541.

308. Bessant DA, Holder GE, Fitzke FW, Payne AM, Bhattacharya SS, Bird AC. Phenotype of retinitis pigmentosa associated with the Ser50Thr mutation in the NRL gene. *Arch Ophthalmol.* 2003;121(6):793-802.

309. Bessant DA, Payne AM, Mitton KP, et al. A mutation in NRL is associated with autosomal dominant retinitis pigmentosa. *Nat Genet.* 1999;21(4):355-356.

310. Bessant DA, Payne AM, Plant C, Bird AC, Swaroop A, Bhattacharya SS. NRL S50T mutation and the importance of 'founder effects' in inherited retinal dystrophies. *Eur J Hum Genet.* 2000;8(10):783-787.

311. DeAngelis MM, Grimsby JL, Sandberg MA, Berson EL, Dryja TP. Novel mutations in the NRL gene and associated clinical findings in patients with dominant retinitis pigmentosa. *Arch Ophthalmol.* 2002;120(3):369-375.

312. Martinez-Gimeno M, Maseras M, Baiget M, et al. Mutations P51U and G122E in retinal transcription factor NRL associated with autosomal dominant and sporadic retinitis pigmentosa. *Hum Mutat.* 2001;17(6):520.

313. Kanda A, Friedman JS, Nishiguchi KM, Swaroop A. Retinopathy mutations in the bZIP protein NRL alter phosphorylation and transcriptional activity. *Hum Mutat.* 2007;28(6):589-598.

314. Bessant DAR, Holder GE, Fitzke FW, Payne AM, Bhattacharya SS, Bird AC. Phenotype of Retinitis Pigmentosa Associated With the Ser50Thr Mutation in the NRL Gene. *Archives of Ophthalmology.* 2003;121(6):793-802.

315. Littink KW, Stappers PTY, Riemslag FCC, et al. Correction: Littink, K. W.; et al. Autosomal Recessive NRL Mutations in Patients with Enhanced S-Cone Syndrome. Genes 2018, 9, 68. *Genes (Basel).* 2018;9(3).

316. Nishiguchi KM, Friedman JS, Sandberg MA, Swaroop A, Berson EL, Dryja TP. Recessive NRL mutations in patients with clumped pigmentary retinal degeneration and relative preservation of blue cone function. *Proc Natl Acad Sci U S A.* 2004;101(51):17819-17824.

317. Wright AF, Reddick AC, Schwartz SB, et al. Mutation analysis of NR2E3 and NRL genes in Enhanced S Cone Syndrome. *Hum Mutat.* 2004;24(5):439.

318. Botta S, Marrocco E, de Prisco N, et al. Rhodopsin targeted transcriptional silencing by DNA-binding. *Elife.* 2016;5:e12242.

319. Jiang L, Zhang H, Dizhoor AM, et al. Long-term RNA interference gene therapy in a dominant retinitis pigmentosa mouse model. *Proc Natl Acad Sci U S A.* 2011;108(45):18476-18481.

320. LaVail MM, Yasumura D, Matthes MT, et al. Ribozyme rescue of photoreceptor cells in P23H transgenic rats: long-term survival and late-stage therapy. *Proc Natl Acad Sci U S A.* 2000;97(21):11488-11493.

321. Mussolino C, Sanges D, Marrocco E, et al. Zinc-finger-based transcriptional repression of rhodopsin in a model of dominant retinitis pigmentosa. *EMBO Mol Med.* 2011;3(3):118-128.

322. Zhu J, Ming C, Fu X, et al. Gene and mutation independent therapy via CRISPR-Cas9 mediated cellular reprogramming in rod photoreceptors. *Cell Res.* 2017;27(6):830-833.

323. Kim JW, Yang HJ, Oel AP, et al. Recruitment of Rod Photoreceptors from Short-Wavelength-Sensitive Cones during the Evolution of Nocturnal Vision in Mammals. *Dev Cell.* 2016;37(6):520-532.

324. Curcio CA, Sloan KR, Kalina RE, Hendrickson AE. Human photoreceptor topography. *J Comp Neurol.* 1990;292(4):497-523.

325. Rothova A, Suttorp-van Schulten MS, Frits Treffers W, Kijlstra A. Causes and frequency of blindness in patients with intraocular inflammatory disease. *Br J Ophthalmol.* 1996;80(4):332-336.

326. Toral MA, Charlesworth CT, Ng B, et al. Investigation of Cas9 antibodies in the human eye. *Nat Commun.* 2022;13(1):1053.

327. Reichel FF, Dauletbekov DL, Klein R, et al. AAV8 Can Induce Innate and Adaptive Immune Response in the Primate Eye. *Mol Ther.* 2017;25(12):2648-2660.

328. Timmers AM, Newmark JA, Turunen HT, et al. Ocular Inflammatory Response to Intravitreal Injection of Adeno-Associated Virus Vector: Relative Contribution of Genome and Capsid. *Hum Gene Ther.* 2020;31(1-2):80-89.

329. Halldorsson BV, Eggertsson HP, Moore KHS, et al. The sequences of 150,119 genomes in the UK Biobank. *Nature.* 2022;607(7920):732-740.

330. Chavez A, Scheiman J, Vora S, et al. Highly efficient Cas9-mediated transcriptional programming. *Nature methods.* 2015;12(4):326-328.

331. Chakraborty S, Ji H, Kabadi AM, Gersbach CA, Christoforou N, Leong KW. A CRISPR/Cas9-based system for reprogramming cell lineage specification. *Stem cell reports.* 2014;3(6):940-947.

332. Wei S, Zou Q, Lai S, et al. Conversion of embryonic stem cells into extraembryonic lineages by CRISPR-mediated activators. *Scientific reports.* 2016;6(1):1-11.

333. Black JB, Adler AF, Wang H-G, et al. Targeted epigenetic remodeling of endogenous loci by CRISPR/Cas9-based transcriptional activators directly converts fibroblasts to neuronal cells. *Cell stem cell.* 2016;19(3):406-414.

334. Gemberling MP, Siklenka K, Rodriguez E, et al. Transgenic mice for in vivo epigenome editing with CRISPR-based systems. *Nature Methods.* 2021;18(8):965-974.

335. Zeitler B, Froelich S, Marlen K, et al. Allele-selective transcriptional repression of mutant HTT for the treatment of Huntington's disease. *Nature medicine.* 2019;25(7):1131-1142.

336. Rees HA, Liu DR. Base editing: precision chemistry on the genome and transcriptome of living cells. *Nature Reviews Genetics.* 2018;19(12):770-788.

337. Richter MF, Zhao KT, Eton E, et al. Phage-assisted evolution of an adenine base editor with improved Cas domain compatibility and activity. *Nature Biotechnology.* 2020;38(7):883-891.

338. Nguyen Tran MT, Mohd Khalid MKN, Wang Q, et al. Engineering domain-inlaid SaCas9 adenine base editors with reduced RNA off-targets and increased on-target DNA editing. *Nature Communications.* 2020;11(1):4871.

339. Kleinstiver BP, Prew MS, Tsai SQ, et al. Broadening the targeting range of Staphylococcus aureus CRISPR-Cas9 by modifying PAM recognition. *Nat Biotechnol.* 2015;33(12):1293-1298.

340. Yuen CTL, Thean DGL, Chan BKC, et al. High-fidelity KKH variant of Staphylococcus aureus Cas9 nucleases with improved base mismatch discrimination. *Nucleic Acids Research.* 2022;50(3):1650-1660.

341. Baba M, Kakue R, Leucht C, et al. Further increase in thermostability of Moloney murine leukemia virus reverse transcriptase by mutational combination. *Protein Engineering, Design and Selection.* 2017;30(8):551-557.

342. Das D, Georgiadis MM. The crystal structure of the monomeric reverse transcriptase from Moloney murine leukemia virus. *Structure.* 2004;12(5):819-829.

343. Gerard GF, Fox DK, Nathan M, D'Alessio JM. Reverse transcriptase. The use of cloned Moloney murine leukemia virus reverse transcriptase to synthesize DNA from RNA. *Mol Biotechnol.* 1997;8(1):61-77.

344. Kotewicz ML, Sampson CM, D'Alessio JM, Gerard GF. Isolation of cloned Moloney murine leukemia virus reverse transcriptase lacking ribonuclease H activity. *Nucleic Acids Res.* 1988;16(1):265-277.

345. Chow RD, Chen JS, Shen J, Chen S. A web tool for the design of prime-editing guide RNAs. *Nat Biomed Eng.* 2021;5(2):190-194.

346. Santos AC, Chiola S, Yang G, Shcheglovitov A, Park S. Secreted Reporter Assay Enables Quantitative and Longitudinal Monitoring of Neuronal Activity. *eNeuro.* 2021;8(5).

347. Wider D, Picard D. Secreted dual reporter assay with Gaussia luciferase and the red fluorescent protein mCherry. *PLoS One.* 2017;12(12):e0189403.

348. McGrath E, Shin H, Zhang L, et al. Targeting specificity of APOBEC-based cytosine base editor in human iPSCs determined by whole genome sequencing. *Nat Commun.* 2019;10(1):5353.

349. Beißel C, Neumann B, Uhse S, Hampe I, Karki P, Krebber H. Translation termination depends on the sequential ribosomal entry of eRF1 and eRF3. *Nucleic Acids Res.* 2019;47(9):4798-4813.

350. Chavatte L, Frolova L, Kisselev L, Favre A. The polypeptide chain release factor eRF1 specifically contacts the s4UGA stop codon located in the A site of eukaryotic ribosomes. *European Journal of Biochemistry.* 2001;268(10):2896-2904.

351. Tang X, Zhu Y, Baker SL, et al. Structural basis of suppression of host translation termination by Moloney Murine Leukemia Virus. *Nat Commun.* 2016;7:12070.

352. Ryu S-M, Koo T, Kim K, et al. Adenine base editing in mouse embryos and an adult mouse model of Duchenne muscular dystrophy. *Nature biotechnology.* 2018;36(6):536.

353. Song C-Q, Jiang T, Richter M, et al. Adenine base editing in an adult mouse model of tyrosinaemia. *Nature biomedical engineering.* 2020;4(1):125-130.

354. Villiger L, Grisch-Chan HM, Lindsay H, et al. Treatment of a metabolic liver disease by in vivo genome base editing in adult mice. *Nat Med.* 2018;24(10):1519-1525.

355. Hirano H, Gootenberg JS, Horii T, et al. Structure and Engineering of Francisella novicida Cas9. *Cell.* 2016;164(5):950-961.

356. Zhou C, Zhang M, Wei Y, et al. Highly efficient base editing in human tripronuclear zygotes. *Protein & cell.* 2017;8(10):772-775.

357. Chamberlain K, Riyad JM, Weber T. Expressing transgenes that exceed the packaging capacity of adeno-associated virus capsids. *Human gene therapy methods.* 2016;27(1):1-12.

358. Wu Z, Yang H, Colosi P. Effect of genome size on AAV vector packaging. *Molecular Therapy.* 2010;18(1):80-86.

359. Stone EM, Andorf JL, Whitmore SS, et al. Clinically focused molecular investigation of 1000 consecutive families with inherited retinal disease. *Ophthalmology.* 2017;124(9):1314-1331.

360. Barrett B, Kerns S, Kevany B, Padegimas L. Dual AAV vector strategy for expression of large genes targeted for Stargardt disease gene therapy development. *Investigative Ophthalmology & Visual Science.* 2021;62(8):1484-1484.

361. Carvalho LS, Turunen HT, Wassmer SJ, et al. Evaluating Efficiencies of Dual AAV Approaches for Retinal Targeting. *Frontiers in Neuroscience.* 2017;11.

362. McClements ME, Barnard AR, Charbel Issa P, MacLaren RE. Assessment of AAV Dual Vector Safety in theAbca4(-/-) Mouse Model of Stargardt Disease. *Transl Vis Sci Technol.* 2020;9(7):20.

363. McClements ME, Barnard AR, Singh MS, et al. An AAV dual vector strategy ameliorates the Stargardt phenotype in adult Abca4−/− mice. *Human gene therapy.* 2019;30(5):590-600.

364. Prelich G. Gene overexpression: uses, mechanisms, and interpretation. *Genetics.* 2012;190(3):841-854.

365. Herskowitz I. Functional inactivation of genes by dominant negative mutations. *Nature.* 1987;329(6136):219-222.

366. Smith I, Greenside PG, Natoli T, et al. Evaluation of RNAi and CRISPR technologies by large-scale gene expression profiling in the Connectivity Map. *PLoS biology.* 2017;15(11):e2003213.

367. Jackson AL, Linsley PS. Recognizing and avoiding siRNA off-target effects for target identification and therapeutic application. *Nat Rev Drug Discov.* 2010;9(1):57-67.

368. Adli M. The CRISPR tool kit for genome editing and beyond. *Nature communications.* 2018;9(1):1-13.

369. Ferrari S, Di Iorio E, Barbaro V, Ponzin D, S Sorrentino F, Parmeggiani F. Retinitis pigmentosa: genes and disease mechanisms. *Current genomics.* 2011;12(4):238-249.

370. Dryja TP, McGee TL, Hahn LB, et al. Mutations within the rhodopsin gene in patients with autosomal dominant retinitis pigmentosa. *New England Journal of Medicine.* 1990;323(19):1302-1307.

371. Bidou L, Allamand V, Rousset J-P, Namy O. Sense from nonsense: therapies for premature stop codon diseases. *Trends in molecular medicine.* 2012;18(11):679-688.

372. Cooper DN, Bacolla A, Férec C, Vasquez KM, Kehrer-Sawatzki H, Chen JM. On the sequence-directed nature of human gene mutation: the role of genomic architecture and the local DNA sequence environment in mediating gene mutations underlying human inherited disease. *Human mutation.* 2011;32(10):1075-1099.

373. Krawczak M, Ball EV, Fenton I, et al. Human gene mutation database—a biomedical information and research resource. *Human mutation.* 2000;15(1):45-51.

374. Lee C, Jo DH, Hwang G-H, et al. CRISPR-pass: Gene rescue of nonsense mutations using adenine base editors. *Molecular Therapy.* 2019;27(8):1364-1371.

375. Krawczak M, Reiss J, Cooper DN. The mutational spectrum of single base-pair substitutions in mRNA splice junctions of human genes: causes and consequences. *Human genetics.* 1992;90(1-2):41-54.

376. Shu X, Black GC, Rice JM, et al. RPGR mutation analysis and disease: an update. *Hum Mutat.* 2007;28(4):322-328.

377. Yuan J, Ma Y, Huang T, et al. Genetic modulation of RNA splicing with a CRISPR-guided cytidine deaminase. *Molecular cell.* 2018;72(2):380-394. e387.

378. den Hollander AI, Koenekoop RK, Yzer S, et al. Mutations in the CEP290 (NPHP6) gene are a frequent cause of Leber congenital amaurosis. *Am J Hum Genet.* 2006;79(3):556-561.

379. Drivas TG, Bennett J. CEP290 and the primary cilium. *Retinal Degenerative Diseases.* 2014:519-525.

380. Fu Y, Foden JA, Khayter C, et al. High-frequency off-target mutagenesis induced by CRISPR-Cas nucleases in human cells. *Nat Biotechnol.* 2013;31(9):822-826.

381. Abadi S, Yan WX, Amar D, Mayrose I. A machine learning approach for predicting CRISPR-Cas9 cleavage efficiencies and patterns underlying its mechanism of action. *PLoS Comput Biol.* 2017;13(10):e1005807.

382. Listgarten J, Weinstein M, Kleinstiver BP, et al. Prediction of off-target activities for the end-to-end design of CRISPR guide RNAs. *Nat Biomed Eng.* 2018;2(1):38-47.

383. Liu G, Zhang Y, Zhang T. Computational approaches for effective CRISPR guide RNA design and evaluation. *Comput Struct Biotechnol J.* 2020;18:35-44.

384. Wang Y, Wang M, Zheng T, et al. Specificity profiling of CRISPR system reveals greatly enhanced off-target gene editing. *Scientific Reports.* 2020;10(1):2269.

385. Tsai SQ, Zheng Z, Nguyen NT, et al. GUIDE-seq enables genome-wide profiling of off-target cleavage by CRISPR-Cas nucleases. *Nat Biotechnol.* 2015;33(2):187-197.

386. Kim D, Kim S, Kim S, Park J, Kim JS. Genome-wide target specificities of CRISPR-Cas9 nucleases revealed by multiplex Digenome-seq. *Genome Res.* 2016;26(3):406-415.

387. Tsai SQ, Nguyen NT, Malagon-Lopez J, Topkar VV, Aryee MJ, Joung JK. CIRCLE-seq: a highly sensitive in vitro screen for genome-wide CRISPR-Cas9 nuclease off-targets. *Nat Methods.* 2017;14(6):607-614.

388. Wienert B, Wyman SK, Richardson CD, et al. Unbiased detection of CRISPR off-targets in vivo using DISCOVER-Seq. *Science.* 2019;364(6437):286-289.

389. Simhadri VL, McGill J, McMahon S, Wang J, Jiang H, Sauna ZE. Prevalence of Pre-existing Antibodies to CRISPR-Associated Nuclease Cas9 in the USA Population. *Mol Ther Methods Clin Dev.* 2018;10:105-112.

390. Charlesworth CT, Deshpande PS, Dever DP, et al. Identification of preexisting adaptive immunity to Cas9 proteins in humans. *Nat Med.* 2019;25(2):249-254.

391. Vakulskas CA, Dever DP, Rettig GR, et al. A high-fidelity Cas9 mutant delivered as a ribonucleoprotein complex enables efficient gene editing in human hematopoietic stem and progenitor cells. *Nat Med.* 2018;24(8):1216-1224.

392. Rabinowitz R, Offen D. Single-Base Resolution: Increasing the Specificity of the CRISPR-Cas System in Gene Editing. *Molecular Therapy.* 2021;29(3):937-948.

393. Kocak DD, Josephs EA, Bhandarkar V, Adkar SS, Kwon JB, Gersbach CA. Increasing the specificity of CRISPR systems with engineered RNA secondary structures. *Nat Biotechnol.* 2019;37(6):657-666.

394. Cho SW, Kim S, Kim Y, et al. Analysis of off-target effects of CRISPR/Cas-derived RNA-guided endonucleases and nickases. *Genome research.* 2014;24(1):132-141.

395. Fu Y, Sander JD, Reyon D, Cascio VM, Joung JK. Improving CRISPR-Cas nuclease specificity using truncated guide RNAs. *Nature biotechnology.* 2014;32(3):279-284.

396. Mader S, White JH. A steroid-inducible promoter for the controlled overexpression of cloned genes in eukaryotic cells. *Proc Natl Acad Sci U S A.* 1993;90(12):5603-5607.

397. Gangopadhyay SA, Cox KJ, Manna D, et al. Precision Control of CRISPR-Cas9 Using Small Molecules and Light. *Biochemistry.* 2019;58(4):234-244.

398. Aubrey BJ, Kelly GL, Kueh AJ, et al. An inducible lentiviral guide RNA platform enables the identification of tumor-essential genes and tumor-promoting mutations in vivo. *Cell Rep.* 2015;10(8):1422-1432.

399. Dow LE, Fisher J, O'Rourke KP, et al. Inducible in vivo genome editing with CRISPR-Cas9. *Nat Biotechnol.* 2015;33(4):390-394.

400. Davis KM, Pattanayak V, Thompson DB, Zuris JA, Liu DR. Small molecule-triggered Cas9 protein with improved genome-editing specificity. *Nat Chem Biol.* 2015;11(5):316-318.

401. Oakes BL, Nadler DC, Flamholz A, et al. Profiling of engineering hotspots identifies an allosteric CRISPR-Cas9 switch. *Nat Biotechnol.* 2016;34(6):646-651.

402. Zhang J, Chen L, Zhang J, Wang Y. Drug Inducible CRISPR/Cas Systems. *Comput Struct Biotechnol J.* 2019;17:1171-1177.

403. Li A, Lee CM, Hurley AE, et al. A Self-Deleting AAV-CRISPR System for In Vivo Genome Editing. *Mol Ther Methods Clin Dev.* 2019;12:111-122.

404. Merienne N, Vachey G, de Longprez L, et al. The Self-Inactivating KamiCas9 System for the Editing of CNS Disease Genes. *Cell Rep.* 2017;20(12):2980-2991.

405. Petris G, Casini A, Montagna C, et al. Hit and go CAS9 delivered through a lentiviral based self-limiting circuit. *Nat Commun.* 2017;8:15334.

406. Collias D, Beisel CL. CRISPR technologies and the search for the PAM-free nuclease. *Nature Communications.* 2021;12(1):555.

407. Gleditzsch D, Pausch P, Müller-Esparza H, et al. PAM identification by CRISPR-Cas effector complexes: diversified mechanisms and structures. *RNA Biol.* 2019;16(4):504-517.

408. Hu Y, Chen Y, Xu J, et al. Metagenomic discovery of novel CRISPR-Cas13 systems. *Cell Discovery.* 2022;8(1):107.

409. Shmakov S, Abudayyeh OO, Makarova KS, et al. Discovery and Functional Characterization of Diverse Class 2 CRISPR-Cas Systems. *Mol Cell.* 2015;60(3):385-397.

410. York A. Mining for CRISPR–Cas. *Nature Reviews Microbiology.* 2017;15(3):133-133.

411. Anders C, Bargsten K, Jinek M. Structural Plasticity of PAM Recognition by Engineered Variants of the RNA-Guided Endonuclease Cas9. *Mol Cell.* 2016;61(6):895-902.

412. Hirano S, Nishimasu H, Ishitani R, Nureki O. Structural Basis for the Altered PAM Specificities of Engineered CRISPR-Cas9. *Mol Cell.* 2016;61(6):886-894.

413. Walton RT, Christie KA, Whittaker MN, Kleinstiver BP. Unconstrained genome targeting with near-PAMless engineered CRISPR-Cas9 variants. *Science.* 2020;368(6488):290-296.

414. Slaymaker IM, Gao L, Zetsche B, Scott DA, Yan WX, Zhang F. Rationally engineered Cas9 nucleases with improved specificity. *Science.* 2016;351(6268):84-88.

415. Kocak DD, Josephs EA, Bhandarkar V, Adkar SS, Kwon JB, Gersbach CA. Increasing the specificity of CRISPR systems with engineered RNA secondary structures. *Nature biotechnology.* 2019;37(6):657-666.

416. Cho SW, Kim S, Kim Y, et al. Analysis of off-target effects of CRISPR/Cas-derived RNA-guided endonucleases and nickases. *Genome Res.* 2014;24(1):132-141.

417. Fu Y, Sander JD, Reyon D, Cascio VM, Joung JK. Improving CRISPR-Cas nuclease specificity using truncated guide RNAs. *Nat Biotechnol.* 2014;32(3):279-284.

418. Lin S, Staahl BT, Alla RK, Doudna JA. Enhanced homology-directed human genome engineering by controlled timing of CRISPR/Cas9 delivery. *Elife.* 2014;3:e04766.

419. Liao H-K, Hatanaka F, Araoka T, et al. In vivo target gene activation via CRISPR/Cas9-mediated trans-epigenetic modulation. *Cell.* 2017;171(7):1495-1507. e1415.

420. Sahillioglu AC, Schumacher TN. Safety switches for adoptive cell therapy. *Current Opinion in Immunology.* 2022;74:190-198.

421. Zhou W, Brown W, Bardhan A, Tsang M, Deiters A. Optical Control of Base Editing and Transcription through Light-Activated Guide RNA. *ChemPhotoChem.* 2021;5(11):984-988.

422. Chappell J, Westbrook A, Verosloff M, Lucks JB. Computational design of small transcription activating RNAs for versatile and dynamic gene regulation. *Nat Commun.* 2017;8(1):1051.

423. Ferry QR, Lyutova R, Fulga TA. Rational design of inducible CRISPR guide RNAs for de novo assembly of transcriptional programs. *Nat Commun.* 2017;8:14633.

424. Campa CC, Weisbach NR, Santinha AJ, Incarnato D, Platt RJ. Multiplexed genome engineering by Cas12a and CRISPR arrays encoded on single transcripts. *Nature Methods.* 2019;16(9):887-893.

425. Tak YE, Kleinstiver BP, Nuñez JK, et al. Inducible and multiplex gene regulation using CRISPR–Cpf1-based transcription factors. *Nature methods.* 2017;14(12):1163-1166.

426. Arbab M, Shen MW, Mok B, et al. Determinants of Base Editing Outcomes from Target Library Analysis and Machine Learning. *Cell.* 2020;182(2):463-480.e430.

427. Marquart KF, Allam A, Janjuha S, et al. Predicting base editing outcomes with an attention-based deep learning algorithm trained on high-throughput target library screens. *Nat Commun.* 2021;12(1):5114.

428. Chen C, Ji W, Niu Y. Primate Organoids and Gene-Editing Technologies toward Next-Generation Biomedical Research. *Trends Biotechnol.* 2021;39(12):1332-1342.

429. Kim J, Koo BK, Knoblich JA. Human organoids: model systems for human biology and medicine. *Nat Rev Mol Cell Biol.* 2020;21(10):571-584.

430. Manafi N, Shokri F, Achberger K, et al. Organoids and organ chips in ophthalmology. *Ocul Surf.* 2021;19:1-15.

431. Luo C, Lancaster MA, Castanon R, Nery JR, Knoblich JA, Ecker JR. Cerebral Organoids Recapitulate Epigenomic Signatures of the Human Fetal Brain. *Cell Rep.* 2016;17(12):3369-3384.

9. APPENDIX

i. List of key plasmids

Plasmids

Source	Cloning Plasmid	Description
Addgene	Plasmid #71666	pdCas9-DNMT3A-EGFP
	Plasmid #71685	pdCas9-DNMT3A-EGFP (ANV)
	Plasmid #62988	pSpCas9(BB)-2A-Puro (PX459) V2.0
	Plasmid #89753	pU6-Cj-sgRNA
	Plasmid #107035	pX551-CMV-CjCas9
	Plasmid #61591	pX601-AAV-CMV::NLS-SaCas9-NLS-3xHA-bGHpA;U6::BsaI-sgRNA
	Plasmid #110821	dCas9-KRAB-MeCP2
	Plasmid #122610	pBT280 (evoFERNY-BE4max)
	Plasmid #132775	pCMV-PE2
	Plasmid #132777	pU6-pegRNA-GG-acceptor
	Plasmid #132778	pU6-Sp-pegRNA-HEK3_CTT_ins
	Plasmid #35672	psiCHECK-2
	Plasmid #138489	ABE8e
	Plasmid #138500	SaABE8e
	Plasmid #138502	SaKKH-ABE8e
	Plasmid #138495	ABE8e (TadA-8e V106W)
	Plasmid #112095	pCMV_ABEmax
	Plasmid #119814	SaABEmax
	Plasmid #135367	nSaCas9 D126 miniABEMax V82G
	Plasmid #106219	AAV CMV-dSaCas9-KRAB-bGHpA
	Plasmid #25328	DNMT3A
	Plasmid #110821	dCas9-KRAB-MeCP2
Gift from C Peddle	pCP-S (-108 to +46)	PDE6B(short)-DsRed
	pCP-L (-163 to +46)	PDE6B(long)-DsRed
Gift from M McClements	pUF6.1	RHOKpr.GFP.pA
	Plasmid #112864	pAAV2/8 Y733F (AAV capsid)
	Plasmid #112867	pAdDeltaF6 (AAV Helper Plasmid)

PlasmidFactory	PF435	pDP5 plasmid
	pAK-01	AAV-EFS-SpCas9-bGH-U6-gRNA
	pAK-02	AAV-EFS-SaSas9-bGH-U6-gRNA
	pAK-03	AAV-CMV-SaCas9-bGH-U6-gRNA
	pAK-04	AAV-EFS-SaSas9-SV40-U6-gRNA
	pAK-05	EFS-dSaCas9-KRAB-U6-sagRNA
	pAK-06	EFS-dCjCas9-KRAB-U6-cjgRNA
Generated	pAK-07	EFS-dSaCas9-MeCP2-U6-sagRNA
	pAK-08	EFS-dCjCas9-MeCP2-U6-cjgRNA
	pAK-09	EFS-dSaCas9-KRAB-MeCP2-U6-sagRNA
	pAK-10	EFS-dCjCas9-KRAB-MeCP2-U6-cjgRNA
	pAK-11	EFS-dSaCas9-DNMT3A-U6-sagRNA
	pAK-12	EFS-dCjCas9-DNMT3A-U6-cjgRNA
	pAK-13	GRK1-dSaCas9-KRAB-U6-sagRNA
	pAK-14	PDE6B (short) -dSaCas9-KRAB-U6-sagRNA
	pAK-15	GRK1-dSaCas9-MeCP2-U6-sagRNA
	pAK-16	GRK1-dSaCas9-KRAB-MeCP2-U6-sagRNA
	pAK-17	AAV-GRK1-SaSas9-bGH-U6-gRNA
	pAK-18	EFS-EvoFERNY-nSaCas9-UGI-U6-sagRNA
	pAK-19	EFS-EvoFERNY-nCjCas9-UGI-U6-sagRNA
	pAK-20	U6-gRNA-DsRed
	pAK-21	EFS-SaCas9-ABE8e
	pAK-22	EFS-SaCas9-ABE8e-U6-gRNA
	pAK-23	CMV-SpCas9-MMLV-RT (aa0-aa540)
	pAK-24	CMV-SpCas9-MMLV-RT (aa0-aa465)
	pAK-25	CMV-SpCas9-MMLV-RT (aa201-aa671)
	pAK-26	CMV-SpCas9-MMLV-RT (aa73-aa392)

ii. List of gRNA sequences

gRNA Sequences

Cas9 development & optimization

gRNA-Cj1-GFP/R1 5′	CACCGggtggcatcgccctcgccctcg
gRNA-Cj1-GFP/L1 5′	AAACcgagggcgagggcgatgccaccC
gRNA-Cj2-GFP/R2 5′	CACCGcatgcccgaaggctacgtccag
gRNA-Cj2-GFP/L2 5′	AAACctggacgtagccttcgggcatgC

gRNA-Cj3-GFP/R3 5'	CACCGccgcgccgaggtgaagttcgag
gRNA-Cj3-GFP/L3 5′	AAACctcgaacttcacctcggcgcggC
gRNA-Sp-to-matchCj1GFP/R1 5′	CACCGggcatcgccctcgccctcgc
gRNA-Sp-to-matchCj1GFP/L1 5′	AAACgcgagggcgagggcgatgccC
gRNA-Sp-to-matchCj2GFP/R2 5′	CACCGcatgcccgaaggctacgtcc
gRNA-Sp-to-matchCj2GFP/L2 5′	AAACggacgtagccttcgggcatgC
gRNA-Sp-to-matchCj3GFP/R3 5′	CACCGcgcgccgaggtgaagttcga
gRNA-Sp-to-matchCj3GFP/L3 5′	AAACtcgaacttcacctcggcgcgC
gRNA-Sa1-GFP/R1 5′	CACCGaagggcgaggagctgttcac
gRNA-Sa1-GFP/L1 5′	AAACgtgaacagctcctcgcccttC
gRNA-Sa2-GFP/R2 5′	CACCGcaacatcctggggcacaagc
gRNA-Sa2-GFP/L2 5′	AAACgcttgtgccccaggatgttgC
gRNA-Sa3-GFP/R3 5′	CACCGacgtcgccgtccagctcgac
gRNA-Sa3-GFP/L3 5′	AAACgtcgagctggacggcgacgtC
gRNA-Sp-to-matchSa3GFP/R3 5′	CACCGgccgtccagctcgaccagga
gRNA-Sp-to-matchSa3GFP/L3 5′	AAACtcctggtcgagctggacggcC

dGFP screening (epigenetic editing)	
SaCas-toCMV-gRNA1-R	caccggtggatagcggtttgactcac
SaCas-toCMV-gRNA1-L	aaacgtgagtcaaaccgctatccacc
SaCas-toCMV-gRNA2-R	caccgccccattgacgcaaatgggc
SaCas-toCMV-gRNA2-L	aaacgcccatttgcgtcaatggggc
CjCas-toCMV-gRNA1-R	CACCGattgacgtcaatgggagtttgt
CjCas-toCMV-gRNA1-L	AAACacaaactcccattgacgtcaatC
CjCas-toCMV-gRNA2-R	CACCGcattgacgcaaatgggcggtag
CjCas-toCMV-gRNA2-L	AAACctaccgcccatttgcgtcaatgC

NRL screening (epigenetic editing)	
CjCas9-grna4/R	CACCgctgggaacgcgtatatgtctc
CjCas9-grna4/L	AAACgagacatatacgcgttcccagc

SaCas9-grna4/R	CACCGcgtatatgtctcCTTGacac
SaCas9-grna4/L	AAACgtgtCAAGgagacatatacgC
CjCas9-grna3/R	CACCGaccccaaacaccacccctccat
CjCas9-grna3/L	AAACatggaggggtggtgtttggggtC
SaCas9-grna3/R	CACCGccccaaacaccacccctcca
SaCas9-grna3/L	AAACtggaggggtggtgtttggggC
CjCas9-grna2/R	CACCGctgtgcccacagccccttgttc
CjCas9-grna2/L	AAACaacaaggggctgtgggcacagC
SaCas9-grna2/R	CACCGtgcccacagcccccttgttc
SaCas9-grna2/L	AAACgaacaaggggctgtgggcaC
CjCas9-grna1/R	CACCGacgtagtcactgtcagaaccAG
CjCas9-grna1/L	AAACCTggttctgacagtgactacgtC
SaCas9-grna1/R	CACCGacgtagtcactgtcagaacc
SaCas9-grna1/L	AAACggttctgacagtgactacgtC

gRNAs with homology to human and mouse NRL

NRLgRNA-1R	CACCGggacaggtttaaacatctcc
NRLgRNA-1L	AAACggagatgtttaaacctgtccC
NRLgRNA-2R	CACCGagaggtgttaggggattagg
NRLgRNA-2L	AAACcctaatcccctaacacctctC
NRLgRNA-3R	CACCGggctgtgggcacagagccca
NRLgRNA-3L	AAACtgggctctgtgcccacagccC
NRLgRNA-4R	CACCGccagacaggcacagcttccc
NRLgRNA-4L	AAACgggaagctgtgcctgtctggC

NRL screening (PsiCHECK2)

Oligo1-R1	ctagctgaggatgggctgggaacgcgtatatgtctcCTTGacacggagt
Oligo1-L1	CTagactccgtgtCAAGgagacatatacgcgttcccagcccatcctcag
Oligo1-R2	ctAgCagaattgtgtTTCCatggaggggtggtgtttggggtcaacatggct
Oligo1-L2	ctagagccatgttgaccccaaacaccacccctccatGGAAacacaattctG
Oligo1-R3	ctagcagtgtcctctgggctctgtgcccacagccccttgttcTGAATacagggt
Oligo1-L3	ctagaccctgtATTCAgaacaaggggctgtgggcacagagcccagaggacactg
Oligo1-R4	ctagctgtgccTTTCTggttctgacagtgactacgtcatctctgccattacgaatt

Oligo1-L4	ctagaattcgtaatggcagagatgacgtagtcactgtcagaaccAGAAAggcacag
Human and mouse NRL screening (PsiCHECK2)	
gRNA1NRLhm-R	CTAGCcagcttcggacaggtttaaacatctccttggataattcagctctaagaggtgttaggggattaggctgaaT
gRNA1NRLhm-L	CTAGAttcagcctaatcccctaacacctcttagagctgaattatccaaggagatgtttaaacctgtccgaagctgG
gRNA2NRLhm-R	CTAGCgaatgcccttgggctctgtgcccacagccccctcttcagtctcctggggaagctgtgcctgtctggctctggcacT
gRNA2NRLhm-L	CTAGAgtgccagagccagacaggcacagcttcccaggagactgaagaggggctgtgggcacagagcccaaagggcattcG
ABE gRNA screening (HEK293-ABE)	
SaABE1-R	CACCGaagggcTaggagctgttcac
SaABE1-L	AAACgtgaacagctcctAgcccttC
SaABE2-R	CACCGagggcTaggagctgttcaccgg
SaABE2-L	AAACccggtgaacagctcctAgccctC
CBE gRNA screening (HEK293-CBE)	
SaCBE1-R	CACCGccaccaCggtgagcaaTggcg
SaCBE1-L	AAACcgccAttgctcaccGtggtgC
SaCBE2-R	CACCGccaccaCggtgagcaaTggcg
SaCBE2-L	AAACccaccaCggtgagcaaTggcgC
ABE gRNA screening (*mUsh2a*-W3947X)	
ABE1-18bp-R	CACCGtagtccacaatacagacc
ABE1-18bp-L	AAACggtctgtattgtggactaC
ABE1-19bp-R	CACCGgtagtccacaatacagacc
ABE1-19bp-L	AAACggtctgtattgtggactacC
ABE1-20bp-R	CACCGcgtagtccacaatacagacc
ABE1-20bp-L	AAACggtctgtattgtggactacgC
ABE1-21bp-R	CACCGccgtagtccacaatacagacc
ABE1-21bp-L	AAACggtctgtattgtggactacggC
ABE1-22bp-R	CACCGcccgtagtccacaatacagacc
ABE1-22bp-L	AAACggtctgtattgtggactacgggC

ABE2-19bp-R	CACCGtagtccacaatacagaccc
ABE2-19bp-L	AAACgggtctgtattgtggactaC
ABE2-20bp-R	CACCGgtagtccacaatacagaccc
ABE2-20bp-L	AAACgggtctgtattgtggactacC
ABE2-21bp-R	CACCGcgtagtccacaatacagaccc
ABE2-21bp-L	AAACgggtctgtattgtggactacgC
ABE2-22bp-R	CACCGccgtagtccacaatacagaccc
ABE2-22bp-L	AAACgggtctgtattgtggactacggC
ABE3KKH-18bp-R	CACCGggtggacagcccgtagtc
ABE3KKH-18bp-L	AAACgactacgggctgtccaccC
mUsh2a-W3947X (Luciferase assay)	CTG GAG TTT ACT GAT ACA GGC ACT CTG CGG CCT TTT ACA CTG TAT GAG TAC CGG GTG AGA GCC TGG AAC TCC CAG GGT GCA GTG GAC AGC CCG TAG TCC ACA ATA CAG ACC CTG GAA GCC CCA CCT CGT GGC CTC CCA GCA CCA CGG GTT CAA GCC ACC AGT GCT CAT TCA GCC ATG CTA AAC TGG ACA GAG CCA
hUSH2A-W3955X (Luciferase assay)	GCC CTT GAA TTT ATG GAT GAA GGA GAC ACC CTG AGG CCT TTC ACA CTC TAC GAA TAT CGG GTC AGA GCC TGT AAC TCC AAG GGT TCA GTG GAG AGT CTG TAG TCA TTA ACA CAA ACT CTG GAA GCT CCA CCT CAA GAT TTT CCA GCT CCT TGG GCT CAA GCC ACG AGT GCT CAT TCA GTT CTG TTG AAT TGG ACA AAG
Prime editing gRNA and pegRNA design (ligated into Addgene #132777)	
sgRNA-R	caccgAGGTCTGTATTGTGGACTACgttttaga
sgRNA-L	tagctctaaaacGTAGTCCACAATACAGACCTc
Scaff-R	GCTAGAAATAGCAAGTTAAAATAAGGCTAGTCC GTTATCAACTTGAAAAAGTGGCACCGAGTCG
Scaff-L	GCACCGACTCGGTGCCACTTTTTCAAGTTGATAA CGGACTAGCCTTATTTTAACTTGCTATTTC
Extens-R	gtgcTGGACAGCCCGTGGTCCACAATACAGAC
Extens-L	aaaaGTCTGTATTGTGGACCACGGGCTGTCCA
PE3_nicksgRNA-R	caccgCTTTTACACTGTATGAGTAC
PE3_nicksgRNA-L	aaacGTACTCATACAGTGTAAAAGc

PE3b_nicksgRNA-R	caccgAGGGTGCAGTGGACAGCCCG
PE3b_nicksgRNA-L	aaacCGGGCTGTCCACTGCACCCTc
Candidate primary editing sgRNAs	
sgRNAantisenseCut113	AGGTCTGTATTGTGGACTAC
sgRNAantisenseCut114	CAGGTCTGTATTGTGGACTA
sgRNAantisenseCut121	GGGCTTCCAGGTCTGTATTG
Candidate secondary nicking sgRNAs (for PE3)	
SecondnicksgRNACut109	AGGGTGCAGTGGACAGCCCG
SecondnicksgRNACut67	CTTTTACACTGTATGAGTAC
SecondnicksgRNACut68	TTTTACACTGTATGAGTACC

iii. Key sequencing and PCR primers

Key sequencing and PCR primers

Key sequencing primers	U6/R1	gcctatttcccatgattcctt
	U6/L1:	aaaactgcaaactacccaagaa
	EFS-NC/R1	tgatccggtgcctagagaag
	EFS-NC/L1	ggagccagtacacgacatca
	CjCas9/R	gcaaactaccagagtgtgg
	CjCas9/R1	catcaatgaggataagaagg
	F1ori/R	cgatttcggcctattggtta
	F1ori/L	taaccaataggccgaaatcg
	AMPp/R	ccgctcatgagacaataacc
	ori/R	ggtggtttgtttgccggatc
	SaCas9/R	gaccagcgactacgtgaaag
	SaCas9/R1	gaagcttcatccagagcatc
	SaCas9/R2	gagatcgaaaccgagcagg
	SaCas9- Cterm/R	caggatcattaagacaatcg
	BGHpA-L (PE)	gatggctggcaactagaagg
	SpCas9-C-R (PE)	gatcgacctgtctcagctg
AAV helper plasmid sequencing	pAD_F1	gcgcattcagcaggccg
	pAD_F2	gacgctcaagtcagag
	pAD_F3	ctgacgctcagtggaac

AAV helper plasmid sequencing	pAD_F4	ctccgatcgttgtc
	pAD_F5	gacagcttatcatcg
	pAD_F5a	ttcgctacttggagccact
	pAD_F6a	cttggttatgccggtactgc
	pAD_F7	tgaccgaggagctgt
	pAD_F8	tacaatggccggact
	pAD_F9	atgacactacgacca
	pAD_F10	cagttactgtgctga
	pAD_F11	tcttgggcaatgtatg
	pAD_F12	taggaaccatagccttg
	pAD_F13	gtactgctatcggtg
	pAD_F14	gcaaggaggtgctgctg
	pAD_F15	caagcgaggagctcac
	pAD_F16	gatcgcagagacctg
	pAD_F17	gtctgacacctcttcg
	pAD_F18	agaccgtcaccgctca
	pAD_F19	atctccgggtcagca
	pAD_F20	tgggctcgcatgtgccgt
	pAD_F21	cggatgaggcggcgtatc
	pAD_F22	cagaggtgacctacaagc
	pAD_F23	cgacttcaagatatc
	pAD_F24	gctacggcgcaggagtg
	pAD_F25	cggcatcacctggatgtc
	pAD_R	acagtcagccttaccagta
	pAD_Ra	tcaaacatgtctgcgggt
AAV8(Y733F) RepCap plasmid sequencing	Cap2 FW1	atggctgccgatggtta
	Cap8 FW1	tggctgccgatggttatct
	Cap8 FW2	ttccagaccctcaacctctcg
	Cap8 FW3	acggctacctaacactca
	Cap8 FW4	atcctggcatcgctatggca
	Cap8 FW5	actacaaatctacaagtgtgga
	Cap8 RC1	caggtttcagcgcccaccac
	Rep2 Fw1	agaagctgcagcgcga
	Rep2 Fw2	tgcggcctccaactcgcggt
	Rep2 FW3	gccgtctggatcatgact
	Rep2 RC1	ctcccattccttctc
	Rep2 RC2	acgtgcatgtggaagta
	RepCap FW1	cgtctatcagggcgat
	RepCap FW2	acctgtcgtgccagctgc
	RepCap FW3	actatcgtcttgagtcca

	RepCap FW4	atctggccccagtgctgca
	RepCap FW5	aggatcttaccgctgttga
PCR primers		
Site-directed mutagenesis	H559A R	ggagatcgacGCcatctatccgtatagcag
	H559A L	agcattttctcgtcctgc
	D8A R	cctcgctttcgCcatcggaatctctag
	D8A L	atgcgggcggacgcttc
	dCjCas9PmlI/R (stop codon removal)	ctaagtccgggatgctgactagc
	dCjCas9BglII/L (stop codon removal)	cacagatctaatgaaaacaaagatGttttattgCatGctAagc
	dSaCas9BamHI-KpnI oligo-R (stop codon removal)	GATCCTcAAATAAAAGATCTTTGTTTTCATTAGATCTGTGTGTTGGTTTTTTGTGTGCggCCggtac
	dSaCas9BamHI-KpnI oligo-L (stop codon removal)	cGGccGCACACAAAAAACCAACACACAGATCTAATGAAAACAAAGATCTTTTATTTgAG
Epigenetic editing cloning	CjCas9 R	agcgcgaggattttaagaaaagccccaa
	CjCas9 F	cgaagcgtccgcccgcatcctcgctt
	SphI-gensc R (KRAB MeCP2)	CTATAGGGCGAATTGAAGGAAGG
	SphI-gensc L (KRAB MeCP2)	GAAAGCGGGCAGTGAAAGG
	KRABonlySapI-R	gggagaagagccctcggagggatcccccaagaaaaaacgcaaggtgtgaaataaaaCatctttgttttcatta
	KRABonlyAarI-L	gatctaatgaaaacaaagatGttttatttcacaccttgcgtttttttcttgggggatccctccgagggctcttct
	MeCP2onlySphI-R	cgggggatcctcg
	MeCP2onlyAarI-L	cctccgaggatcccccgCatG
	KRABonlyAarI-R	gagggtgtgcaggtggagggttcccccaagaaaaaacgcaaggtgtgag
	KRABonlyBamHI-L	gatcctcacaccttgcgtttttttcttgggggaaccctccacctgcacac
	KRABonlyAarI-R	gagggtgtgcaggtggagggttcccccaagaaaaaacgcaaggtgtgag
	KRABonlyBamHI-L	gatcctcacaccttgcgtttttttcttgggggaaccctccacctgcacac
	MeCP2onlyBstEII-R	gtgaccggaggtggttcg

Prime editor cloning	MeCP2onlyAarI-L	cctccgaaccacctccg
	dCas9only-1R5′	gtgacccccaagaaaaaacgcaaggtgtgag
	dCas9only-1L5′	gatcctcacaccttgcgttttttcttgggg
	Del 1 AgeI-AgeI oligo/R	ccggtgGGGggaTctcccaagaagaagaggaaagtcGG GTCTcatcatcaccatcaccatTAAa
	Del 1 oligo/L	ccggtTTAatggtgatggtgatgatgAGACCCgactttc ctcttcttcttgggagAtccCCCca
	Del 2 BamHI-BamHI oligo/R	GATCCAGGGCTCGAGGGAG
	Del 2 oligo/L	GATCCTCCCTCGAGCCCTG
	Del 3 BstEII-PmeI oligo/R	gtgaccgagcccaagaagaagaggaaagtcggtcatcatcac catcaccattgagttt
	Del 3 oligo/L	aaactcaatggtgatggtgatgatgaccgactttcctcttcttctt gggctcg
	Del 4 PC2Kpn/R	cacatacagagactgttggac
	Del 4 oligo/L	tttggacaggtaggTcacc
IDT gBlocks gene fragments		
Cloning gene fragments	Kozak sequence, 3xFLAG, SV40 NLS (2x)	ACCGGTGCCACCATGGACTACAAAGAC CATGACGGTGATTATAAAGATCATGACA TAGATTACAAGGATGACGATGACAAGG GTGGATCGCCAAAGAAAAAGAGGAAAG TCGCCCCAAAGAAGAAGCGGAAGGTCG GTATCCACGGAGTCCCAGCAGCCAAGC
	KRAB-MeCP2	GGAACTACATCCTGGGCCTGGCCATCGG CATCACCAGCGTGGGCTACGGCATCATC GACTACGAGACACGGGACGTGATCGAT GCTTAGCATGCGGGGGATCCCGGACACT GGTGACCTTCAAGGATGTATTTGTGGAC TTCACCAGGGAGGAGTGGAAGCTGCTGG ACACTGCTCAGCAGATCGTGTACAGAAA TGTGATGCTGGAGAACTATAAGAACCTG GTTTCCTTGGGTTATCAGCTTACTAAGCC AGATGTGATCCTCCGGTTGGAGAAGGGA GAAGAGCCCTCGGGAGGTGGTTCGGGA GGTGGTTCGGAGGGTGTGCAGGTGAAAA GGGTCCTGGAGAAAAGTCCTGGGAAGCT CCTTGTCAAGATGCCTTTTCAAACTTCGC CAGGGGGCAAGGCTGAGGGGGGTGGGG

		CCACCACATCCACCCAGGTCATGGTGAT CAAACGCCCCGGCAGGAAGCGAAAAGC TGAGGCCGACCCTCAGGCCATTCCCAAG AAACGGGGCCGAAAGCCGGGGAGTGTG GTGGCAGCCGCTGCCGCCGAGGCCAAA AAGAAAGCCGTGAAGGAGTCTTCTATCC GATCTGTGCAGGAGACCGTACTCCCCAT CAAGAAGCGCAAGACCCGGGAGGGATC CCCCAAGAAAAAACGCAAGGTGTGAAA TAAAACATCTTTGTTTTCATTAGATCT
qPCR primers		
AAV Titration	GRK1qPCR1_FW	GTACCGGGCCCCAGAAGCCTG
	GRK1qPCR1_RV	GGCTGACACAGCACCAGGCTA
	GRK1qPCR2_FW	AAATCAATTGGGGCCCCAGAAGCCTG
	GRK1qPCR2_RV	AAATaccggtCCCGGGGCTGACA
	PDE6BqPCR1_FW	GTAGGAGTGAGTCAGCTGACC
	PDE6BqPCR1_RV	CTGGAGACGCTGCTGCTC
	U6qPCR1_FW	CGATACAAGGCTGTTAGAGAGATA
	U6qPCR1_RV	AAACTGCAAACTACCCAAGAAA
Y79 / WERI-Rb-1	gRNA-NRLtoHuman-1R	caccgCAGGTTTAAACATCTCCT
	gRNA-NRLtoHuman-1L	aaacAGGAGATGTTTAAACCTGc
	gRNA-NRLtoHuman-2R	caccgAGGCGATTAGGCTGAAAATGT
	gRNA-NRLtoHuman-2L	aaacACATTTTCAGCCTAATCGCCTc
	rtPCRtoNRL-Exon-2R	gcactgaccacatcctctcg
	rtPCRtoNRL-Exon-3L	cattctggagctgggctgg
	rtPCRtoNRL-Exon-3R	Cccatggctactacccag
	rtPCRtoNRL-Exon-4L	gcacagacatcgagaCcag
TaqMan assays		
Human	hGAPDH	Hs01064292_g1
	hNRL	Hs01007657_m1

Mouse	hNR2E3	Hs00183915_m1
	hPDE6B	Hs01557860_m1
	hARR3	Hs01020134_m1
	hOPN1SW	Hs00181790_m1
	hCRX	Hs00230899_m1
	mGAPDH	Mm99999915_g1
	mARR3	Mm00504628_m1
	mNR2E3	Mm00443299_m1
	mNrl	Mm00476550_m1
Custom Assays	sgRNA.Scaffold	AAACAAGGCAAAATGC
	SaCas9.Probe	ATCGAGAAGATCAAGCTGC

iv. Sequences of key plasmid elements

Sequences of key plasmid elements	
EF-1 Alpha Short (EFS) promoter	GGGCAGAGCGCACATCGCCCACAGTCCCCGAGAAGTTGGG GGGAGGGGTCGGCAATTGATCCGGTGCCTAGAGAAGGTGG CGCGGGGTAAACTGGGAAAGTGATGTCGTGTACTGGCTCC GCCTTTTTCCCGAGGGTGGGGGAGAACCGTATATAAGTGCA GTAGTCGCCGTGAACGTTCTTTTTCGCAACGGGTTTGCCGCC AGAACACA
Human cytomegalovirus (CMV) promoter	GTGATGCGGTTTTGGCAGTACATCAATGGGCGTGGATAGCGG TTTGACTCACGGGGATTTCCAAGTCTCCACCCCATTGACGTC AATGGGAGTTTGTTTTGGCACCAAAATCAACGGGACTTTCCA AAATGTCGTAACAACTCCGCCCCATTGACGCAAATGGGCGG TAGGCGTGTACGGTGGGAGGTCTATATAAGCAGAGC TCTCTGGCTAACTA
GRK1 -112/+87 promoter	GGGCCCCAGAAGCCTGGTGGTTGTTTGTCCTTCTCAGGGGAA AAGTGAGGCGGCCCCTTGGAGGAAGGGGCCGGGCAGAATG ATCTAATCGGATTCCAAGCAGCTCAGGGGATTGTCTTTTTCTA GCACCTTCTTGCCACTCCTAAGCGTCCTCCGTGACCCCGGCT GGGATTTAGCCTGGTGCTGTGTCAGCCCCGGG
Human U6 (hU6) promoter	GAGGGCCTATTTCCCATGATTCCTTCATATTTGCATATACGA TACAAGGCTGTTAGAGAGATAATTGGAATTAATTTGACTGT AAACACAAAGATATTAGTACAAAATACGTGACGTAGAAAGT AATAATTTCTTGGGTAGTTTGCAGTTTTAAAATTATGTTTTA

	AAATGGACTATCATATGCTTACCGTAACTTGAAAGTATTTCG ATTTCTTGGCTTTATATATCTTGTGGAAAGGAC
PDE6B -108/+46 promoter	GTCTGAGGAGAGGGAGCGCAGGCCCCCATTTGTAGGAGTGA GTCAGCTGACCCGCCCCCGGGGTTCCTAATCTCACTAAGAAA GACTTTGCTGATGACAGGGTTTCCTGGGAGTCCATGCGTGCC TGGAGCAGCAGCGTCTCCAGGGACAGGCA
PDE6B -163/+46 promoter	CTCCCAGCCTTCATTCCACAGGGTCTGGTTTTCCTGGAAGGT GGGAAGTCCCAGGGTCTGAGGAGAGGGAGCGCAGGCCCCC ATTGTAGGAGTGAGTCAGCTGACCCGCCCCCGGGGTTCCTAA TCTCACTAAGAAAGACTTTGCTGATGACAGGGTTTCCTGGGA GTCCATGCGTGCCTGGAGCAGC AGCGTCTCCAGGGACAGGCAA
bGH PolyA	CTGTGCCTTCTAGTTGCCAGCCATCTGTTGTTTGCCCCTCCC CCGTGCCTTCCTTGACCCTGGAAGGTGCCACTCCCACTGTCC TTTCCTAATAAAATGAGGAAATTGCATCGCATTGTCTGAGT AGGTGTCATTCTATTCTGGGGGGTGGGGTGGGGCAGGAC AGCAAGGGGGAGGATTGGGAAGACAATAGCAGGCATGCT GGGGATGCGGTGGGCTCTATGG
SV40 PolyA	TAAGATACATTGATGAGTTTGGACAAACCACAACTAGAATG CAGTGAAAAAAATGCTTTATTTGTGAAATTTGTGATGCTAT TGCTTTATTTGTAACCATTATAAGCTGCAATAAACAAGTT
SV40 NLS	CCAAAGAAAAAGAGGAAAGTC
SpCas9	ATGGACAAGAAGTACTCCATTGGGCTCGATATCGGCACAAA CAGCGTCGGCTGGGCCGTCATTACGGACGAGTACAAGGTGC CGAGCAAAAAATTCAAAGTTCTGGGCAATACCGATCGCCAC AGCATAAAGAAGAACCTCATTGGCGCCCTCCTGTTCGACTCC GGGGAGACGGCCGAAGCCACGCGGCTCAAAAGAACAGCAC GGCGCAGATATACCCGCAGAAAGAATCGGATCTGCTACCTG CAGGAGATCTTTAGTAATGAGATGGCTAAGGTGGATGACTCT TTCTTCCATAGGCTGGAGGAGTCCTTTTTGGTGGAGGAGGAT AAAAAGCACGAGCGCCACCCAATCTTTGGCAATATCGTGGA CGAGGTGGCGTACCATGAAAAGTACCCAACCATATATCATC TGAGGAAGAAGCTTGTAGACAGTACTGATAAGGCTGACTTG CGGTTGATCTATCTCGCGCTGGCGCATATGATCAAATTTCGG GGACACTTCCTCATCGAGGGGGACCTGAACCCAGACAACAG CGATGTCGACAAACTCTTTATCCAACTGGTTCAGACTTACAA TCAGCTTTTCGAAGAGAACCCGATCAACGCATCCGGAGTTG ACGCCAAAGCAATCCTGAGCGCTAGGCTGTCCAAATCCCGG CGGCTCGAAAACCTCATCGCACAGCTCCCTGGGGAGAAGAA

	GAACGGCCTGTTTGGTAATCTTATCGCCCTGTCACTCGGGCT GACCCCCAACTTTAAATCTAACTTCGACCTGGCCGAAGATGC CAAGCTTCAACTGAGCAAAGACACCTACGATGATGATCTCG ACAATCTGCTGGCCCAGATCGGCGACCAGTACGCAGACCTT TTTTTGGCGGCAAAGAACCTGTCAGACGCCATTCTGCTGAGT GATATTCTGCGAGTGAACACGGAGATCACCAAAGCTCCGCT GAGCGCTAGTATGATCAAGCGCTATGATGAGCACCACCAAG ACTTGACTTTGCTGAAGGCCCTTGTCAGACAGCAACTGCCTG AGAAGTACAAGGAAATTTTCTTCGATCAGTCTAAAAATGGCT ACGCCGGATACATTGACGGCGGAGCAAGCCAGGAGGAATTT TACAAATTTATTAAGCCCATCTTGGAAAAAATGGACGGCAC CGAGGAGCTGCTGGTAAAGCTTAACAGAGAAGATCTGTTGC GCAAACAGCGCACTTTCGACAATGGAAGCATCCCCCACCAG ATTCACCTGGGCGAACTGCACGCTATCCTCAGGCGGCAAGA GGATTTCTACCCCTTTTTGAAAGATAACAGGGAAAAGATTGA GAAAATCCTCACATTTCGGATACCCTACTATGTAGGCCCCCT CGCCCGGGGAAATTCCAGATTCGCGTGGATGACTCGCAAAT CAGAAGAGACCATCACTCCCTGGAACTTCGAGGAAGTCGTG GATAAGGGGGCCTCTGCCCAGTCCTTCATCGAAAGGATGAC TAACTTTGATAAAAATCTGCCTAACGAAAAGGTGCTTCCTAA ACACTCTCTGCTGTACGAGTACTTCACAGTTTATAACGAGCT CACCAAGGTCAAATACGTCACAGAAGGGATGAGAAAGCCA GCATTCCTGTCTGGAGAGCAGAAGAAAGCTATCGTGGACCT CCTCTTCAAGACGAACCGGAAAGTTACCGTGAAACAGCTCA AAGAAGACTATTTCAAAAAGATTGAATGTTTCGACTCTGTTG AAATCAGCGGAGTGGAGGATCGCTTCAACGCATCCCTGGGA ACGTATCACGATCTCCTGAAAATCATTAAAGACAAGGACTT CCTGGACAATGAGGAGAACGAGGACATTCTTGAGGACATTG TCCTCACCCTTACGTTGTTTGAAGATAGGGAGATGATTGAAG AACGCTTGAAAACTTACGCTCATCTCTTCGACGACAAAGTCA TGAAACAGCTCAAGAGGCGCCGATATACAGGATGGGGGCG GCTGTCAAGAAAACTGATCAATGGGATCCGAGACAAGCAGA GTGGAAAGACAATCCTGGATTTTCTTAAGTCCGATGGATTTG CCAACCGGAACTTCATGCAGTTGATCCATGATGACTCTCTCA CCTTTAAGGAGGACATCCAGAAAGCACAAGTTTCTGGCCAG GGGGACAGTCTTCACGAGCACATCGCTAATCTTGCAGGTAG CCCAGCTATCAAAAAGGGAATACTGCAGACCGTTAAGGTCG TGGATGAACTCGTCAAAGTAATGGGAAGGCATAAGCCCGAG AATATCGTTATCGAGATGGCCCGAGAGAACCAAACTACCCA

	GAAGGGACAGAAGAACAGTAGGGAAAGGATGAAGAGGATT GAAGAGGGTATAAAAGAACTGGGGTCCCAAATCCTTAAGGA ACACCCAGTTGAAAACACCCAGCTTCAGAATGAGAAGCTCT ACCTGTACTACCTGCAGAACGGCAGGGACATGTACGTGGAT CAGGAACTGGACATCAATCGGCTCTCCGACTACGACGTGGA TCATATCGTGCCCCAGTCTTTTCTCAAAGATGATTCTATTGAT AATAAAGTGTTGACAAGATCCGATAAAAATAGAGGGAAGA GTGATAACGTCCCCTCAGAAGAAGTTGTCAAGAAAATGAAA AATTATTGGCGGCAGCTGCTGAACGCCAAACTGATCACACA ACGGAAGTTCGATAATCTGACTAAGGCTGAACGAGGTGGCC TGTCTGAGTTGGATAAAGCCGGCTTCATCAAAAGGCAGCTTG TTGAGACACGCCAGATCACCAAGCACGTGGCCCAAATTCTC GATTCACGCATGAACACCAAGTACGATGAAAATGACAAACT GATTCGAGAGGTGAAAGTTATTACTCTGAAGTCTAAGCTGGT CTCAGATTTCAGAAAGGACTTTCAGTTTTATAAGGTGAGAGA GATCAACAATTACCACCATGCGCATGATGCCTACCTGAATGC AGTGGTAGGCACTGCACTTATCAAAAAATATCCCAAGCTTG AATCTGAATTTGTTTACGGAGACTATAAAGTGTACGATGTTA GGAAAATGATCGCAAAGTCTGAGCAGGAAATAGGCAAGGC CACCGCTAAGTACTTCTTTTACAGCAATATTATGAATTTTTTC AAGACCGAGATTACACTGGCCAATGGAGAGATTCGGAAGCG ACCACTTATCGAAACAAACGGAGAAACAGGAGAAATCGTGT GGGACAAGGGTAGGGATTTCGCGACAGTCCGGAAGGTCCTG TCCATGCCGCAGGTGAACATCGTTAAAAAGACCGAAGTACA GACCGGAGGCTTCTCCAAGGAAAGTATCCTCCCGAAAAGGA ACAGCGACAAGCTGATCGCACGCAAAAAAGATTGGGACCC CAAGAAATACGGCGGATTCGATTCTCCTACAGTCGCTTACAG TGTACTGGTTGTGGCCAAAGTGGAGAAAGGGAAGTCTAAAA AACTCAAAAGCGTCAAGGAACTGCTGGGCATCACAATCATG GAGCGATCAAGCTTCGAAAAAAACCCCATCGACTTTCTCGA GGCGAAAGGATATAAAGAGGTCAAAAAAGACCTCATCATTA AGCTTCCCAAGTACTCTCTCTTTGAGCTTGAAAACGGCCGGA AACGAATGCTCGCTAGTGCGGGCGAGCTGCAGAAAGGTAAC GAGCTGGCACTGCCCTCTAAATACGTTAATTTCTTGTATCTGG CCAGCCACTATGAAAAGCTCAAAGGGTCTCCCGAAGATAAT GAGCAGAAGCAGCTGTTCGTGGAACAACACAAACACTACCT TGATGAGATCATCGAGCAAATAAGCGAATTCTCCAAAAGAG TGATCCTCGCCGACGCTAACCTCGATAAGGTGCTTTCTGCTT ACAATAAGCACAGGGATAAGCCCATCAGGGAGCAGGCAGA

	AAACATTATCCACTTGTTTACTCTGACCAACTTGGGCGCGCC TGCAGCCTTCAAGTACTTCGACACCACCATAGACAGAAAGC GGTACACCTCTACAAAGGAGGTCCTGGACGCCACACTGATT CATCAGTCAATTACGGGGCTCTATGAAACAAGAATCGACCT CTCTCAGCTCGGTGGAGAC
SaCas9	AAGCGGAACTACATCCTGGGCCTGGACATCGGCATCACCAG CGTGGGCTACGGCATCATCGACTACGAGACACGGGACGTGA TCGATGCCGGCGTGCGGCTGTTCAAAGAGGCCAACGTGGAA AACAACGAGGGCAGGCGGAGCAAGAGAGGCGCCAGAAGG CTGAAGCGGCGGAGGCGGCATAGAATCCAGAGAGTGAAGA AGCTGCTGTTCGACTACAACCTGCTGACCGACCACAGCGAG CTGAGCGGCATCAACCCCTACGAGGCCAGAGTGAAGGGCCT GAGCCAGAAGCTGAGCGAGGAAGAGTTCTCTGCCGCCCTGC TGCACCTGGCCAAGAGAAGAGGCGTGCACAACGTGAACGA GGTGGAAGAGGACACCGGCAACGAGCTGTCCACCAAAGAG CAGATCAGCCGGAACAGCAAGGCCCTGGAAGAGAAATACG TGGCCGAACTGCAGCTGGAACGGCTGAAGAAAGACGGCGA AGTGCGGGGCAGCATCAACAGATTCAAGACCAGCGACTACG TGAAAGAAGCCAAACAGCTGCTGAAGGTGCAGAAGGCCTA CCACCAGCTGGACCAGAGCTTCATCGACACCTACATCGACC TGCTGGAAACCCGGCGGACCTACTATGAGGGACCTGGCGAG GGCAGCCCCTTCGGCTGGAAGGACATCAAAGAATGGTACGA GATGCTGATGGGCCACTGCACCTACTTCCCCGAGGAACTGCG GAGCGTGAAGTACGCCTACAACGCCGACCTGTACAACGCCC TGAACGACCTGAACAATCTCGTGATCACCAGGGACGAGAAC GAGAAGCTGGAATATTACGAGAAGTTCCAGATCATCGAGAA CGTGTTCAAGCAGAAGAAGAAGCCCACCCTGAAGCAGATCG CCAAAGAAATCCTCGTGAACGAAGAGGATATTAAGGGCTAC AGAGTGACCAGCACCGGCAAGCCCGAGTTCACCAACCTGAA GGTGTACCACGACATCAAGGACATTACCGCCCGGAAAGAGA TTATTGAGAACGCCGAGCTGCTGGATCAGATTGCCAAGATCC TGACCATCTACCAGAGCAGCGAGGACATCCAGGAAGAACTG ACCAATCTGAACTCCGAGCTGACCCAGGAAGAGATCGAGCA GATCTCTAATCTGAAGGGCTATACCGGCACCCACAACCTGA GCCTGAAGGCCATCAACCTGATCCTGGACGAGCTGTGGCAC ACCAACGACAACCAGATCGCTATCTTCAACCGGCTGAAGCT GGTGCCCAAGAAGGTGGACCTGTCCCAGCAGAAAGAGATCC CCACCACCCTGGTGGACGACTTCATCCTGAGCCCCGTCGTGA AGAGAAGCTTCATCCAGAGCATCAAAGTGATCAACGCCATC

	ATCAAGAAGTACGGCCTGCCCAACGACATCATTATCGAGCT GGCCCGCGAGAAGAACTCCAAGGACGCCCAGAAAATGATC AACGAGATGCAGAAGCGGAACCGGCAGACCAACGAGCGGA TCGAGGAAATCATCCGGACCACCGGCAAAGAGAACGCCAA GTACCTGATCGAGAAGATCAAGCTGCACGACATGCAGGAAG GCAAGTGCCTGTACAGCCTGGAAGCCATCCCTCTGGAAGAT CTGCTGAACAACCCCTTCAACTATGAGGTGGACCACATCATC CCCAGAAGCGTGTCCTTCGACAACAGCTTCAACAACAAGGT GCTCGTGAAGCAGGAAGAAAACAGCAAGAAGGGCAACCGG ACCCCATTCCAGTACCTGAGCAGCAGCGACAGCAAGATCAG CTACGAAACCTTCAAGAAGCACATCCTGAATCTGGCCAAGG GCAAGGGCAGAATCAGCAAGACCAAGAAAGAGTATCTGCT GGAAGAACGGGACATCAACAGGTTCTCCGTGCAGAAAGACT TCATCAACCGGAACCTGGTGGATACCAGATACGCCACCAGA GGCCTGATGAACCTGCTGCGGAGCTACTTCAGAGTGAACAA CCTGGACGTGAAAGTGAAGTCCATCAATGGCGGCTTCACCA GCTTTCTGCGGCGGAAGTGGAAGTTTAAGAAAGAGCGGAAC AAGGGGTACAAGCACCACGCCGAGGACGCCCTGATCATTGC CAACGCCGATTTCATCTTCAAAGAGTGGAAGAAACTGGACA AGGCCAAAAAAGTGATGGAAAACCAGATGTTCGAGGAAAA GCAGGCCGAGAGCATGCCCGAGATCGAAACCGAGCAGGAG TACAAAGAGATCTTCATCACCCCCCACCAGATCAAGCACAT TAAGGACTTCAAGGACTACAAGTACAGCCACCGGGTGGACA AGAAGCCTAATAGAGAGCTGATTAACGACACCCTGTACTCC ACCCGGAAGGACGACAAGGGCAACACCCTGATCGTGAACA ATCTGAACGGCCTGTACGACAAGGACAATGACAAGCTGAAA AAGCTGATCAACAAGAGCCCCGAAAAGCTGCTGATGTACCA CCACGACCCCCAGACCTACCAGAAACTGAAGCTGATTATGG AACAGTACGGCGACGAGAAGAATCCCCTGTACAAGTACTAC GAGGAAACCGGGAACTACCTGACCAAGTACTCCAAAAAGG ACAACGGCCCCGTGATCAAGAAGATTAAGTATTACGGCAAC AAACTGAACGCCCATCTGGACATCACCGACGACTACCCCAA CAGCAGAAACAAGGTCGTGAAGCTGTCCCTGAAGCCCTACA GATTCGACGTGTACCTGGACAATGGCGTGTACAAGTTCGTGA CCGTGAAGAATCTGGATGTGATCAAAAAAGAAAACTACTAC GAAGTGAATAGCAAGTGCTATGAGGAAGCTAAGAAGCTGA AGAAGATCAGCAACCAGGCCGAGTTTATCGCCTCCTTCTACA ACAACGATCTGATCAAGATCAACGGCGAGCTGTATAGAGTG ATCGGCGTGAACAACGACCTGCTGAACCGGATCGAAGTGAA

	CATGATCGACATCACCTACCGCGAGTACCTGGAAAACATGA ACGACAAGAGGCCCCCCAGGATCATTAAGACAATCGCCTCC AAGACCCAGAGCATTAAGAAGTACAGCACAGACATTCTGGG CAACCTGTATGAAGTGAAATCTAAGAAGCACCCTCAGATCA TCAAAAAGGGC
CjCas9	GCCCGCATCCTCGCTTTCGACATCGGAATCTCTAGTATCGGA TGGGCCTTCTCTGAAAACGACGAACTGAAAGACTGCGGCGT GAGAATCTTCACAAAGGTTGAAAACCCTAAAACAGGCGAGT CTTTAGCTCTGCCACGTAGGTTGGCCCGCTCCGCCCGAAAAA GGCTGGCTCGGCGGAAGGCTCGCCTCAACCACTTGAAGCAT TTGATAGCTAATGAGTTCAAACTGAACTACGAAGATTACCA GTCCTTCGACGAGTCATTGGCAAAAGCCTACAAAGGCAGCC TTATCAGTCCTTATGAGTTGAGATTTCGCGCACTCAACGAAC TGCTTTCTAAGCAAGACTTTGCTAGGGTCATTCTGCACATCG CAAAACGGCGAGGTTATGACGATATCAAGAACTCCGACGAT AAAGAAAAGGGAGCCATTCTCAAGGCGATCAAACAGAATG AGGAAAAATTGGCAAACTACCAGAGTGTGGGCGAGTATCTG TATAAAGAGTATTTCCAGAAGTTTAAGGAAAACAGCAAGGA GTTTACAAACGTCAGAAATAAAAAGGAGTCTTACGAGAGAT GCATCGCGCAGTCATTCCTCAAAGATGAGCTGAAGCTGATAT TTAAGAAGCAACGCGAATTTGGTTTCTCATTCTCTAAGAAGT TCGAAGAGGAGGTTCTTTCCGTGGCGTTTTACAAGAGGGCGC TCAAAGACTTCTCCCACCTGGTTGGTAACTGTAGTTTCTTCAC GGATGAGAAGCGAGCTCCCAAAAATTCTCCCCTGGCTTTCAT GTTTGTTGCCCTGACTCGGATCATTAACCTGCTGAACAACCT GAAAAATACTGAAGGGATCTTGTATACGAAGGACGACCTAA ATGCACTCCTGAATGAAGTGCTCAAAAACGGAACTCTAACC TATAAACAGACCAAGAAATTACTGGGGCTCTCTGACGACTA CGAGTTCAAGGGCGAGAAGGGTACTTATTTTATCGAATTCAA AAAGTATAAGGAGTTCATTAAAGCATTGGGGGAACACAACC TCAGCCAGGACGATCTCAATGAAATTGCCAAGGACATCACG CTGATTAAAGACGAGATAAAACTGAAAAAGGCACTGGCCA AGTATGACCTCAACCAGAACCAGATCGACTCTCTGTCCAAG CTGGAGTTCAAAGACCACCTAAACATATCCTTCAAAGCCCTG AAACTGGTCACCCCTCTAATGCTCGAAGGAAAAAAATACGA CGAGGCGTGTAATGAACTGAATCTTAAGGTGGCCATCAATG AGGATAAGAAGGACTTTCTTCCAGCCTTTAACGAGACATATT ACAAAGACGAGGTCACAAACCCGGTTGTGCTGAGGGCCATA AAAGAGTATCGGAAGGTTCTGAATGCCCTCCTGAAGAAGTA

	CGGCAAAGTGCACAAAATAAATATCGAATTGGCTAGGGAGG TGGGGAAGAACCATTCTCAGCGAGCAAAGATCGAGAAAGA GCAGAATGAGAACTACAAAGCCAAGAAAGACGCCGAACTG GAGTGCGAAAAGCTGGGGCTTAAAATAAACAGTAAAAACA TCCTGAAATTAAGATTGTTCAAAGAGCAAAAGGAGTTTTGCG CCTACTCAGGGGAAAAAATCAAAATATCAGACCTGCAGGAC GAGAAAATGCTGGAGATCGACCACATCTATCCGTATAGCAG GTCATTTGACGATTCCTACATGAACAAAGTGCTTGTGTTTAC CAAACAGAACCAAGAAAAGCTGAACCAAACCCCCTTTGAG GCTTTCGGAAACGACTCAGCCAAGTGGCAGAAAATCGAAGT CCTAGCCAAGAATCTGCCTACAAAAAAACAAAAGAGGATTC TTGATAAGAACTATAAGGACAAGGAACAGAAAAACTTTAAA GACAGGAACCTGAATGACACGAGGTACATTGCGCGACTGGT TCTAAACTATACCAAAGACTACCTGGATTTCCTCCCTCTGAG CGACGACGAGAATACTAAACTGAATGATACCCAGAAAGGCT CAAAGGTCCACGTTGAGGCTAAGTCCGGGATGCTGACTAGC GCCCTCCGCCACACGTGGGGCTTCAGCGCCAAAGATCGGAA TAATCATCTTCATCACGCTATTGATGCAGTAATCATAGCCTA CGCTAACAACAGCATCGTGAAAGCCTTCTCCGATTTCAAGA AAGAACAGGAGTCTAATAGCGCCGAGTTGTACGCCAAGAAA ATTTCCGAATTGGACTATAAAAATAAGAGAAAATTCTTCGA ACCCTTCTCCGGGTTTCGCCAAAAGGTCTTAGATAAGATCGA CGAGATTTTCGTTTCCAAGCCCGAAAGAAAAAAGCCTTCAG GGGCACTGCACGAAGAGACATTCCGCAAGGAAGAGGAATTT TACCAATCTTACGGTGGTAAAGAGGGAGTTCTGAAGGCTCTG GAGCTTGGGAAGATCCGCAAGGTAAACGGGAAAATCGTGA AAAACGGGGACATGTTCAGGGTGGATATCTTCAAGCACAAA AAGACCAACAAGTTCTACGCAGTACCCATCTACACTATGGA TTTCGCTTTAAAGGTTCTCCCAAATAAGGCGGTGGCTCGATC GAAGAAAGGAGAGATCAAGGACTGGATCTTAATGGATGAA AATTACGAGTTTTGCTTCTCGCTCTACAAAGATAGCCTGATTC TGATCCAGACAAAAGACATGCAGGAACCAGAATTTGTTTAT TATAACGCCTTCACGAGCAGTACAGTGTCCCTGATTGTGAGC AAGCATGATAACAAGTTCGAGACTCTGTCTAAGAATCAGAA AATCCTTTTCAAGAACGCCAACGAGAAGGAGGTCATCGCAA AGTCAATTGGCATCCAAAACCTGAAGGTGTTCGAGAAATAC ATAGTGTCCGCACTCGGTGAAGTAACTAAAGCCGAATTTCG ACAGCGCGAGGATTTTAAGAAA

KRAB	AGAACACTGGTTACGTTCAAGGACGTGTTTGTGGACTTTACA CGTGAGGAGTGGAAATTGCTGGATACTGCGCAACAAATTGT GTATCGAAATGTCATGCTTGAGAATTACAAGAACCTCGTCAG TCTCGGATACCAGTTGACGAAACCGGATGTGATCCTTAGGCT CGAAAAGGGGGAAGAACCTTGGCTGGTA
MeCP2 TRD (George Church)	GTGCAGGTGAAAAGGGTGCTGGAAAAATCCCCCGGCAAACT CCTCGTGAAGATGCCCTTCCAGGCTTCCCCTGGCGGAAAAGG TGAAGGGGGTGGCGCAACCACATCTGCCCAGGTCATGGTCA TCAAGCGACCTGGAAGGAAAAGAAAGGCCGAGGCTGACCC TCAGGCCATTCCAAAGAAACGGGGACGCAAGCCAGGGTCCG TGGTCGCAGCTGCAGCAGCTGAGGCTAAGAAAAAGGCAGTG AAGGAAAGCTCCATCCGCAGTGTGCAGGAGACTGTCCTGCC CATCAAGAAGAGGAAGACTAGGGAGACCGTGTCCATCGAG GTCAAAGAAGTGGTCAAGCCCCTGCTCGTGTCCACCCTGGGC GAAAAATCTGGAAAGGGGCTCAAAACATGCAAGTCACCTGG ACGGAAAAGCAAGGAGTCTAGTCCAAAGGGGCGCTCAAGC TCCGCTTCTAGTCCCCCTAAAAAGGAACACCATCACCATCAC CATCACGCCGAGTCTCCTAAGGCTCCTATGCCACTGCTCCCA CCACCTCCACCACCTGAGCCACAGTCAAGCGAAGACCCCAT CAGCCCACCCGAGCCTCAGGATCTGTCCTCTAGTATTTGCAA AGAGGAAAAGATGCCCAGAGCAGGCAGCCTGGAGAGTGAT GGCTGTCCAAAAGAACCCGCCAAGACCCAGCCTATGGTGGC AGCCGCTGCAACTACCACCACAACCACAACTACCACAGTGG CCGAAAAATACAAGCATCGCGGCGAGGGCGAACGAAAGGA CATTGTGTCAAGCTCCATGCCCAGACCTAACCGGGAGGAAC CAGTCGATAGTAGGACACCCGTGACTGAGAGAGTCTCA
MeCP2 TRD (Designed)	GAGGGTGTGCAGGTGAAAAGGGTCCTGGAGAAAAGTCCTGG GAAGCTCCTTGTCAAGATGCCTTTTCAAACTTCGCCAGGGGG CAAGGCTGAGGGGGGTGGGGCCACCACATCCACCCAGGTCA TGGTGATCAAACGCCCCGGCAGGAAGCGAAAAGCTGAGGC CGACCCTCAGGCCATTCCCAAGAAACGGGGCCGAAAGCCGG GGAGTGTGGTGGCAGCCGCTGCCGCCGAGGCCAAAAAGAA AGCCGTGAAGGAGTCTTCTATCCGATCTGTGCAGGAGACCGT ACTCCCCATCAAGAAGCGCAAGACCCGG
DNMT3A	CCCTCCCGGCTCCAGATGTTCTTCGCTAATAACCACGACCAG GAATTTGACCCTCCAAAGGTTTACCCACCTGTCCCAGCTGAG AAGAGGAAGCCCATCCGGGTGCTGTCTCTCTTTGATGGAATC GCTACAGGGCTCCTGGTGCTGAAGGACTTGGGCATTCAGGTG GACCGCTACATTGCCTCGGAGGTGTGTGAGGACTCCATCACG

	GTGGGCATGGTGCGGCACCAGGGGAAGATCATGTACGTCGG GGACGTCCGCAGCGTCACACAGAAGCATATCCAGGAGTGGG GCCCATTCGATCTGGTGATTGGGGGCAGTCCCTGCAATGACC TCTCCATCGTCAACCCTGCTCGCAAGGGCCTCTACGAGGGCA CTGGCCGGCTCTTCTTTGAGTTCTACCGCCTCCTGCATGATGC GCGGCCCAAGGAGGGAGATGATCGCCCCTTCTTCTGGCTCTT TGAGAATGTGGTGGCCATGGGCGTTAGTGACAAGAGGGACA TCTCGCGATTTCTCGAGTCCAACCCTGTGATGATTGATGCCA AAGAAGTGTCAGCTGCACACAGGGCCCGCTACTTCTGGGGT AACCTTCCCGGTATGAACAGGCCGTTGGCATCCACTGTGAAT GATAAGCTGGAGCTGCAGGAGTGTCTGGAGCATGGCAGGAT AGCCAAGTTCAGCAAAGTGAGGACCATTACTACGAGGTCAA ACTCCATAAAGCAGGGCAAAGACCAGCATTTTCCTGTGTTCA TGAATGAGAAAGAGGACATCTTATGGTGCACTGAAATGGAA AGGGTATTTGGTTTCCCAGTCCACTATACTGACGTCTCCAAC ATGAGCCGCTTGGCGAGGCAGAGACTGCTGGGCCGGTCATG GAGCGTGCCAGTCATCCGCCACCTCTTCGCTCCGCTGAAGGA GTATTTTGCGTGA
ABEmax	TCTGAAGTCGAGTTTAGCCACGAGTATTGGATGAGGCACGC ACTGACCCTGGCAAAGCGAGCATGGGATGAAAGAGAAGTC CCCGTGGGCGCCGTGCTGGTGCACAACAATAGAGTGATCGG AGAGGGATGGAACAGGCCAATCGGCCGCCACGACCCTACC GCACACGCAGAGATCATGGCACTGAGGCAGGGAGGCCTGGT CATGCAGAATTACCGCCTGATCGATGCCACCCTGTATGTGAC ACTGGAGCCATGCGTGATGTGCGCAGGAGCAATGATCCACA GCAGGATCGGAAGAGTGGTGTTCGGAGCACGGGACGCCAA GACCGGCGCAGCAGGCTCCCTGATGGATGTGCTGCACCACC CCGGCATGAACCACCGGGTGGAGATCACAGAGGGAATCCTG GCAGACGAGTGCGCCGCCCTGCTGAGCGATTTCTTTAGAATG CGGAGACAGGAGATCAAGGCCCAGAAGAAGGCACAGAGCT CCACCGACTCTGGAGGATCTAGCGGAGGATCCTCTGGAAGC GAGACACCAGGCACAAGCGAGTCCGCCACACCAGAGAGCT CCGGCGGCTCCTCCGGAGGATCCTCTGAGGTGGAGTTTTCCC ACGAGTACTGGATGAGACATGCCCTGACCCTGGCCAAGAGG GCACGCGATGAGAGGGAGGTGCCTGTGGGAGCCGTGCTGGT GCTGAACAATAGAGTGATCGGCGAGGGCTGGAACAGAGCC ATCGGCCTGCACGACCCAACAGCCCATGCCGAAATTATGGC CCTGAGACAGGGCGGCCTGGTCATGCAGAACTACAGACTGA TTGACGCCACCCTGTACGTGACATTCGAGCCTTGCGTGATGT

	GCGCCGGCGCCATGATCCACTCTAGGATCGGCCGCGTGGTGT TTGGCGTGAGGAACGCAAAAACCGGCGCCGCAGGCTCCCTG ATGGACGTGCTGCACTACCCCGGCATGAATCACCGCGTCGA AATTACCGAGGGAATCCTGGCAGATGAATGTGCCGCCCTGC TGTGCTATTTCTTTCGGATGCCTAGACAGGTGTTCAATGCTCA GAAGAAGGCCCAGAGCTCCACCGACTCCGGAGGATCTAGCG GAGGCTCCTCTGGCTCTGAGACACCTGGCACAAGCGAGAGC GCAACACCTGAAAGCAGCGGGGGCAGCAGCGGGGGGTCA
ABE8e	TCTGAGGTGGAGTTTTCCCACGAGTACTGGATGAGACATGCC CTGACCCTGGCCAAGAGGGCACGGGATGAGAGGGAGGTGC CTGTGGGAGCCGTGCTGGTGCTGAACAATAGAGTGATCGGC GAGGGCTGGAACAGAGCCATCGGCCTGCACGACCCAACAG CCCATGCCGAAATTATGGCCCTGAGACAGGGCGGCCTGGTC ATGCAGAACTACAGACTGATTGACGCCACCCTGTACGTGAC ATTCGAGCCTTGCGTGATGTGCGCCGGCGCCATGATCCACTC TAGGATCGGCCGCGTGGTGTTTGGCGTGAGGAACTCAAAAA GAGGCGCCGCAGGCTCCCTGATGAACGTGCTGAACTACCCC GGCATGAATCACCGCGTCGAAATTACCGAGGGAATCCTGGC AGATGAATGTGCCGCCCTGCTGTGCGATTTCTATCGGATGCC TAGACAGGTGTTCAATGCTCAGAAGAAGGCCCAGAGCTCCA TCAACTCCGGAGGATCTAGCGGAGGCTCCTCTGGCTCTGAGA CACCTGGCACAAGCGAGAGCGCAACACCTGAAAGCAGCGG GGGCAGCAGCGGGGGGTCA
BE4max	AGCAGTGAAACCGGACCAGTGGCAGTGGACCCAACCCTGAG GAGACGGATTGAGCCCCATGAATTTGAAGTGTTCTTTGACCC AAGGGAGCTGAGGAAGGAGACATGCCTGCTGTACGAGATCA AGTGGGGCACAAGCCACAAGATCTGGCGCCACAGCTCCAAG AACACCACAAAGCACGTGGAAGTGAATTTCATCGAGAAGTT TACCTCCGAGCGGCACTTCTGCCCCTCTACCAGCTGTTCCATC ACATGGTTTCTGTCTTGGAGCCCTTGCGGCGAGTGTTCCAAG GCCATCACCGAGTTCCTGTCTCAGCACCCTAACGTGACCCTG GTCATCTACGTGGCCCGGCTGTATCACCACATGGACCAGCAG AACAGGCAGGGCCTGCGCGATCTGGTGAATTCTGGCGTGAC CATCCAGATCATGACAGCCCCAGAGTACGACTATTGCTGGC GGAACTTCGTGAATTATCCACCTGGCAAGGAGGCACACTGG CCAAGATACCCACCCCTGTGGATGAAGCTGTATGCACTGGA GCTGCACGCAGGAATCCTGGGCCTGCCTCCATGTCTGAATAT CCTGCGGAGAAAGCAGCCCCAGCTGACATTTTTCACCATTGC TCTGCAGTCTTGTCACTATCAGCGGCTGCCTCCTCATATTCTG

	TGGGCTACAGGCCTGAAGTCTGGAGGATCTAGCGGAGGATC CTCTGGCAGCGAGACACCAGGAACAAGCGAGTCAGCAACA CCAGAGAGCAGTGGCGGCAGCAGCGGCGGCAGC
evoFERNY BE4max	AGTTTTGAGAGGAACTACGACCCCCGGGAGCTGAGAAAGGA GACATACCTGCTGTATGAGATCAAGTGGGGCAAGTCCGGCA AGCTGTGGAGGCACTGGTGCCAGAACAATCGCACACAGCAC GCCGAGGTGTACTTCCTGGAGAACATCTTTAATGCCCGGAGA TTCAATCCATCTACCCACTGTAGCATCACATGGTATCTGAGC TGGTCCCCCTGCGCCGAGTGTTCTCAGAAGATCGTGGATTTC CTGAAGGAGCACCCTAACGTGAATCTGGAGATCTATGTGGC CCGGCTGTACTATCCAGAGAACGAGAGGAATAGGCAGGGCC TGCGGGATCTGGTGAATTCCGGCGTGACCATCAGAATCATGG ACCTGCCAGATTACAACTATTGCTGGAAGACCTTCGTGAGCG ATCAGGGAGGCGACGAGGATTACTGGCCAGGACACTTCGCC CCTTGGATCAAGCAGTATAGCCTGAAGCTGTCTGGCGGATCT AGCGGAGGATCCTCTGGCAGCGAGACACCAGGAACAAGCG AGTCAGCAACACCAGAGAGCAGTGGCGGCAGCAGCGGCGG CAGC
M-MLV RT (WT)	TCTGGAGGATCTAGCGGAGGATCCTCTGGCAGCGAGACACC AGGAACAAGCGAGTCAGCAACACCAGAGAGCAGTGGCGGC AGCAGCGGCGGCAGCAGCACCCTAAATATAGAAGATGAGT ATCGGCTACATGAGACCTCAAAAGAGCCAGATGTTTCTCTAG GGTCCACATGGCTGTCTGATTTTCCTCAGGCCTGGGCGGAAA CCGGGGGCATGGGACTGGCAGTTCGCCAAGCTCCTCTGATC ATACCTCTGAAAGCAACCTCTACCCCCGTGTCCATAAAACA ATACCCCATGTCACAAGAAGCCAGACTGGGGATCAAGCCCC ACATACAGAGACTGTTGGACCAGGGAATACTGGTACCCTGC CAGTCCCCCTGGAACACGCCCCTGCTACCCGTTAAGAAACC AGGGACTAATGATTATAGGCCTGTCCAGGATCTGAGAGAAG TCAACAAGCGGGTGGAAGACATCCACCCCACCGTGCCCAAC CCTTACAACCTCTTGAGCGGGCTCCCACCGTCCCACCAGTGG TACACTGTGCTTGATTTAAAGGATGCCTTTTTCTGCCTGAGAC TCCACCCCACCAGTCAGCCTCTCTTCGCCTTTGAGTGGAGAG ATCCAGAGATGGGAATCTCAGGACAATTGACCTGGACCAGA CTCCCACAGGGTTTCAAAAACAGTCCCACCCTGTTTAATGAG GCACTGCACAGAGACCTAGCAGACTTCCGGATCCAGCACCC AGACTTGATCCTGCTACAGTACGTGGATGACTTACTGCTGGC CGCCACTTCTGAGCTAGACTGCCAACAAGGTACTCGGGCCCT GTTACAAACCCTAGGGAACCTCGGGTATCGGGCCTCGGCCA

	AGAAAGCCCAAATTTGCCAGAAACAGGTCAAGTATCTGGGG TATCTTCTAAAAGAGGGTCAGAGATGGCTGACTGAGGCCAG AAAAGAGACTGTGATGGGGCAGCCTACTCCGAAGACCCCTC GACAACTAAGGGAGTTCCTAGGGAAGGCAGGCTTCTGTCGC CTCTTCATCCCTGGGTTTGCAGAAATGGCAGCCCCCCTGTAC CCTCTCACCAAACCGGGGACTCTGTTTAATTGGGGCCCAGAC CAACAAAAGGCCTATCAAGAAATCAAGCAAGCTCTTCTAAC TGCCCCAGCCCTGGGGTTGCCAGATTTGACTAAGCCCTTTGA ACTCTTTGTCGACGAGAAGCAGGGCTACGCCAAAGGTGTCC TAACGCAAAAACTGGGACCTTGGCGTCGGCCGGTGGCCTAC CTGTCCAAAAAGCTAGACCCAGTAGCAGCTGGGTGGCCCCC TTGCCTACGGATGGTAGCAGCCATTGCCGTACTGACAAAGG ATGCAGGCAAGCTAACCATGGGACAGCCACTAGTCATTCTG GCCCCCCATGCAGTAGAGGCACTAGTCAAACAACCCCCCGA CCGCTGGCTTTCCAACGCCCGGATGACTCACTATCAGGCCTT GCTTTTGGACACGGACCGGGTCCAGTTCGGACCGGTGGTAGC CCTGAACCCGGCTACGCTGCTCCCACTGCCTGAGGAAGGGC TGCAACACAACTGCCTTGATATCCTGGCCGAAGCCCACGGA ACCCGACCCGACCTAACGGACCAGCCGCTCCCAGACGCCGA CCACACCTGGTACACGGATGGAAGCAGTCTCTTACAAGAGG GACAGCGTAAGGCGGGAGCTGCGGTGACCACCGAGACCGA GGTAATCTGGGCTAAAGCCCTGCCAGCCGGGACATCCGCTC AGCGGGCTGAACTGATAGCACTCACCCAGGCCCTAAAGATG GCAGAAGGTAAGAAGCTAAATGTTTATACTGATAGCCGTTAT GCTTTTGCTACTGCCCATATCCATGGAGAAATATACAGAAGG CGTGGGTGGCTCACATCAGAAGGCAAAGAGATCAAAAATA AAGACGAGATCTTGGCCCTACTAAAAGCCCTCTTTCTGCCCA AAAGACTTAGCATAATCCATTGTCCAGGACATCAAAAGGGA CACAGCGCCGAGGCTAGAGGCAACCGGATGGCTGACCAAG CGGCCCGAAAGGCAGCCATCACAGAGACTCCAGACACCTCT ACCCTCCTCATAGAAAATTCATCACCCTCTGGCGGCTCAAAA AGAACCGCCGACGGCAGCGAATTCGAG

v. List of key resources

Software and algorithms

NCBI Blast	
pegFinder	Yale University (Chen lab)

CRISPick (GPP sgRNA Design)	Broad Institute (Zhang lab)
GlobPlot 2.3	Nucleic Acid Res 2003 - Vol. 31, No.13
PSIPRED	UCL Bioinformatics Group
Clustal Omega	EMBL-EBI
ICM-Browser	Molsoft LLC
CFX Maestro	Bio-Rad Laboratories
FIJI	NIH
Geneious	Biomatters
SnapGene	Insightful Science
Prism 9	GraphPad
HEYEX	Heidelberg
Image Studio	LI-COR
MARS Data Analysis	BMG Labtech
NEBuilder Assembly Tool	NEB
Omega Reader Control	BMG Labtech
RStudio	RStudio
Microsoft Office (Excel, PPT)	Microsoft
Primer3	ELIXIR

cSLO Mean Grey Value Macro

ImageJ macro used to measure the grey value of the superior and inferior retina on cSLA images taken using the blue auto fluorescence channel.

```
//#### DEFINE FUNCTIONS ####
//Each measurement consists of two functions - one to check the folder and
only process .tif, and one to measure the MGV
//--SUPERIOR MGV MEASUREMENT—
function processFolder_supMGV(input) {
list = getFileList(input);
      for (i = 0; i <list.length; i++) {
            if(endsWith(list[i], ".tif"))
                  processFile_supMGV(input, list[i]);
                  }
}
function processFile_supMGV(input, file) {
            print("Measuring Superior MGV: " + input + file);
            open(input+list[i]);
```

```
                run("Gaussian Blur...", "sigma=3");
                //Selection of superior half circle
                run("Specify...", "width=1336 height=1080 x=100 y=100 oval"); {
                        if (selectionType!=1)
                           exit("Elliptical selection required");
                        getBoundingRect(x, y, width, height);
                        midy = y + height/2;
                        getSelectionCoordinates(sx, sy);
                        for (i=0; i<sy.length; i++) {
                           if (sy[i]>midy) sy[i] = midy;
                        }
                        makeSelection(3, sx, sy);
                     }
                run("Measure");
                close();
                        }
//--SUPERIOR MGV MEASUREMENT--
function processFolder_infMGV(input) {
list = getFileList(input);
      for (i = 0; i <list.length; i++) {
                if(endsWith(list[i], ".tif"))
                        processFile_infMGV(input, list[i]);
                        }
}
function processFile_infMGV(input, file) {
                print("Measuring Inferior MGV: " + input + file);
                open(input+list[i]);
                run("Gaussian Blur...", "sigma=3");
                run("Specify...", "width=1336 height=1080 x=100 y=356 oval");
                        {
                           if (selectionType!=1)
                              exit("Elliptical selection required");
                           getBoundingRect(x, y, width, height);
                           midy = y + height/2;
                           getSelectionCoordinates(sx, sy);
                           for (i=0; i<sy.length; i++) {
                              if (sy[i]<midy) sy[i] = midy;
                           }
                           makeSelection(3, sx, sy);
                        }
```

```
                run("Measure");
                close();
                        }
//--360 BAND --
function processFolder_bandMGV(input) {
list = getFileList(input);
      for (i = 0; i <list.length; i++) {
                if(endsWith(list[i], ".tif"))
                        processFile_bandMGV(input, list[i]);
                        }
}
function processFile_bandMGV(input, file) {
                print("Measuring Band MGV: " + input + file);
                open(input+list[i]);
                run("Gaussian Blur...", "sigma=3");
                run("Specify...", "width=600 height=600 x=468 y=468 oval
constrain");
                run("Make Band...", "band=2.65");
                run("Measure")
                close();                        }
```

vi. Published manuscripts, book chapters, & presentations

Published Manuscripts

Salman, A., **Kantor, A.,** McClements, M. E., Marfany, G., Trigueros, S., & MacLaren, R. E. (2022). Non-Viral Delivery of CRISPR/Cas Cargo to the Retina Using Nanoparticles: Current Possibilities, Challenges, and Limitations. *Pharmaceutics*, *14*(9), 1842. https://doi.org/10.3390/pharmaceutics14091842

Han, R. C., Fry, L. E., **Kantor, A.,** McClements, M. E., Xue, K., & MacLaren, R. E. (2021). Is subretinal AAV gene replacement still the only viable treatment option for choroideremia?. *Expert opinion on orphan drugs*, *9*(1), 13–24. https://doi.org/10.1080/21678707.2021.1882300

Quinn, J., Musa, A., **Kantor, A.,** McClements, M. E., Cehajic-Kapetanovic, J., MacLaren, R. E., & Xue, K. (2021). Genome-Editing Strategies for Treating Human Retinal

Degenerations. *Human gene therapy*, *32*(5-6), 247–259. https://doi.org/10.1089/hum.2020.231

Kantor, A., McClements, M. E., & MacLaren, R. E. (2020). CRISPR-Cas9 DNA Base-Editing and Prime-Editing. *International journal of molecular sciences*, *21*(17), 6240. https://doi.org/10.3390/ijms21176240

Gemberling, M. P., Siklenka, K., Rodriguez, E., Tonn-Eisinger, K. R., Barrera, A., Liu, F., **Kantor, A.,** Li, L., Cigliola, V., Hazlett, M. F., Williams, C. A., Bartelt, L. C., Madigan, V. J., Bodle, J. C., Daniels, H., Rouse, D. C., Hilton, I. B., Asokan, A., Ciofani, M., Poss, K. D., … Gersbach, C. A. (2021). Transgenic mice for *in vivo* epigenome editing with CRISPR-based systems. *Nature methods*, *18*(8), 965–974. https://doi.org/10.1038/s41592-021-01207-2

Book Chapters

Kantor, A., McClements, M. E., Peddle, C. F., Fry, L. E., Salman, A., Cehajic-Kapetanovic, J., Xue, K., & MacLaren, R. E. (2021). CRISPR genome engineering for retinal diseases. *Progress in molecular biology and translational science*, *182*, 29–79. https://doi.org/10.1016/bs.pmbts.2021.01.024

Presentations

Development of dCas-repressor fusions for targeted epigenetic editing in patient-derived 3D retinal organoids. Genome Engineering: Frontiers of CRISPR-Cas. Cold Spring Harbor Laboratory New York 2022. Oral presentation.

Development of CRISPR-Cas9 repressors for targeted epigenome editing of inherited retinal degenerations. Oxford Ophthalmological Congress 2022. Poster presentation.

Development of dCas-repressor fusions for targeted epigenetic editing. Genome Engineering Oxford (Virtual). Seminar held by the University of Oxford, Oxford, UK. 2022. Oral presentation (Co-organizer).

Development of CRISPR-Cas9 repressors for targeted epigenome editing in patient derived retinal organoids. Association for Research in Vision and Ophthalmology Annual Meeting 2022, Denver. Poster Presentation.

Development of minimal PE variant with enhanced prime editing *in vitro*. Genome Engineering Oxford (Virtual). Seminar held by the University of Oxford, Oxford, UK. 2021.

Development of all-in-one dCas9 repressors for targeted transcriptional repression *in vitro*. Genome Engineering: Frontiers of CRISPR-Cas. Cold Spring Harbor Laboratory New York (Virtual Meeting) 2021. Poster presentation.

Comparison of Cas9 orthologues for gene suppression activity. Genome Engineering: Frontiers of CRISPR-Cas. Cold Spring Harbor Laboratory New York (Virtual Meeting) 2020. Poster presentation.

Comparison of Cas9 orthologues for gene suppression activity. American Society for Cell and Gene Therapy (Virtual Meeting) 2020. Poster Presentation.